University of Southampton

Faculty of Medicine

School of Human Development and Health

Ultra High Density Mapping and Ablation Biophysics of Diseased Human Myocardium

by

Dr Alexander Philip Bates MA MB BChir MRCP

ORCID ID = 0000-0001-5517-1964

Thesis for the Degree of Doctor of Philosophy

December 2023

University of Southampton

Abstract

Faculty of Medicine

School of Human Development and Health

Thesis for the Degree of Doctor of Philosophy

Ultra High Density Mapping and Ablation Biophysics of Diseased Human Myocardium

By

Dr Alexander Philip Bates MA MB BChir MRCP

Atrial fibrillation (AF) is a cardiac arrhythmia with a prevalence in the United Kingdom of approximately 1.5 million people. Patients with AF can suffer debilitating symptoms including palpitations, breathlessness, and fatigue. Furthermore, they are at increased risk of other life changing conditions such as stroke, heart failure and dementia. Ventricular tachycardia (VT) is a life-threatening cardiac arrhythmia that most commonly occurs due to structural heart disease. During an episode of VT, patients can suffer with palpitations, pre-syncope, syncope, chest pains, breathlessness and ultimately may deteriorate into ventricular fibrillation and death.

When medical therapy fails for these arrhythmias, a treatment option is radiofrequency catheter ablation (RFCA). RFCA is an invasive procedure where a set of lesions applied to the myocardium using RF energy to inhibit recurrence of the arrhythmia. The procedure is aided by the creation of a 3D electroanatomical map (3D EAM), which integrates anatomy with electrophysiological parameters detailing the perceived underlying degree of fibrosis. During ablation itself, the development of the lesion can be monitored using biophysical feedback, that being either drops (Δ) in impedance (local [LI] or generator [GI]) or electrogram amplitude. Alternatively, an

accumulating scoring system known as Ablation Index (AI) based upon pre-determined ablation inputs known to affect lesion size such as power, duration and contact force can be used.

However, there are still several unknowns in RFCA. Firstly, as histology is not readily available, fibrosis is represented on 3D EAMs using an electrical surrogate, typically bipolar voltage amplitude. Despite widespread use of values representing dense scar and diseased tissue, these values have never been histologically validated. Secondly, novel ultra-high-density mapping systems have not yet been used to confirm the relationship of atrial fibrosis with progression of AF, between atria or cardiac rhythms (sinus rhythm vs AF) that have been described by lower density systems. Thirdly, pre-ablation factors that affect ΔLI and their relative importance have yet to be fully elucidated. Fourthly, the interaction of catheter contact force (CF) on tissue LI is unknown. Finally, the effect of ventricular tissue fibrosis on biophysical feedback during radiofrequency ablation in the human heart is uninvestigated.

In this thesis, I seek to shed some light onto these unknowns. In Chapter 3, I document a study where electrical surrogates of atrial fibrosis (bipolar voltage and LI) are assessed in a physiological manner using pacing thresholds. Based on this work, new thresholds for dense scar and diseased tissue are suggested. This is followed in Chapter 4, where the differences in tissue voltages and surface area of scar between rhythm, atria and AF type are explored using an ultra-high-density 3D EAM and these new scar thresholds. In Chapter 5, the interaction of catheter CF and resting tissue LI is studied using a catheter that integrates both technologies. Chapter 6 then proceeds to examine the effect and interactions of different ablation parameters that affect ΔLI for two different LI measuring catheters. Finally in Chapter 7, the effect of endocardial ventricular fibrosis on the relationship between GI and AI is investigated. Values of AI that do not provide additional biophysical changes on average are presented.

In conclusion, I find that current values used to determine atrial fibrosis can be improved. There is considerable interaction between CF and resting tissue LI, which alongside other ablation parameters can affect ΔLI. Lastly, endocardial ventricular fibrosis significantly effects biophysical feedback during RFCA. Ultimately, I hope these findings can be used by interventional electrophysiologists across the world to improve and guide their ablation procedures, enable them to optimise every ablation lesion they deliver and aid patients in being arrhythmia free for as long as possible.

Table of Contents

Table of Tables

Table of Figures

Research Thesis: Declaration of Authorship

Print name: Dr Alexander Philip Bates

Title of thesis: Ultra High Density Mapping and Ablation Biophysics of Diseased Human Myocardium

I declare that this thesis and the work presented in it are my own and has been generated by me as the result of my own original research.

I confirm that:

1. This work was done wholly or mainly while in candidature for a research degree at this University;
2. Where any part of this thesis has previously been submitted for a degree or any other qualification at this University or any other institution, this has been clearly stated;
3. Where I have consulted the published work of others, this is always clearly attributed;
4. Where I have quoted from the work of others, the source is always given. With the exception of such quotations, this thesis is entirely my own work;
5. I have acknowledged all main sources of help;
6. Where the thesis is based on work done by myself jointly with others, I have made clear exactly what was done by others and what I have contributed myself;
7. Parts of this work have been published as:-

Publications, Presentations and Abstracts

Chapter 3

Highest Scoring Abstracts Oral Presentation at Heart Rhythm Congress 2022, Birmingham, UK

AP Bates, JR Paisey, A Yue, P Banks, PR Roberts, W Ullah, Redefining atrial scar: analysis using pacing thresholds, electrogram amplitudes and local impedance. Can we improve on 0.05 and 0.5mV? European Journal of Arrhythmia & Electrophysiology. 2022;8(Suppl. 1):abstr23.

https://www.touchcardio.com/atrial-fibrillation/journal-articles/23-redefining-atrial-scar-an-analysis-using-pacing-thresholds-electrogram-amplitudes-and-local-impedance-can-we-improve-on-0-05-and-0-5mv/

ePoster Presentation at European Heart Rhythm Association Conference 2023, Barcelona, Spain

AP Bates, JR Paisey, A Yue, P Banks, PR Roberts, W Ullah, Refinement of Voltage-Based Atrial Scar Assessment Using Pacing Thresholds and Local Impedance.

Chapter 4

Oral Presentation at Heart Rhythm Congress 2022, Birmingham, UK

AP Bates, JR Paisey, A Yue, P Banks, PR Roberts, W Ullah, Assessment of scar between atria, rhythms and atrial fibrillation types. Does ultra-high-density mapping offer new insights? European Journal of Arrhythmia & Electrophysiology. 2022;8(Suppl. 1):abstr30.

https://www.touchcardio.com/atrial-fibrillation/journal-articles/30-assessment-of-scar-between-atria-rhythms-and-atrial-fibrillation-types-does-ultra-high-density-mapping-offer-new-insights/

ePoster Presentation at European Heart Rhythm Association Conference 2023, Barcelona, Spain

AP Bates, JR Paisey, A Yue, P Banks, PR Roberts, W Ullah, Comparison of Voltages Between Atria, Rhythms and Atrial Fibrillation Types: Does Ultra High Density Mapping Offer New Insights?

Publication in Journal of Interventional Cardiovascular Electrophysiology

AP Bates, JR Paisey, A Yue, P Banks, PR Roberts, W Ullah, Comparison of voltages between atria: differences in sinus rhythm and atrial fibrillation. J Interv Card Electrophysiol (2023).

J Interv Card Electrophysiol. 2023 Oct 24. doi: 10.1007/s10840-023-01671-0. Epub ahead of print. PMID: 37875609.

Chapter 5

ePoster Presentation at European Heart Rhythm Association Conference 2023, Barcelona, Spain

AP Bates, JR Paisey, A Yue, P Banks, PR Roberts, W Ullah, Determinants of Left Atrial Local Impedance: Relationships with Contact Force, Atrial Fibrosis and Rhythm

Chapter 6

Oral Presentation at Heart Rhythm Congress 2022, Birmingham, UK

AP Bates, JR Paisey, A Yue, P Banks, PR Roberts, W Ullah, A local impedance-based comparison of IntellaNav MiFi and Stablepoint catheters. European Journal of Arrhythmia & Electrophysiology. 2022;8(Suppl. 1):abstr41.

https://www.touchcardio.com/atrial-fibrillation/journal-articles/41-a-local-impedance-based-comparison-of-intellanav-mifi-and-stablepoint-catheters/

Chapter 7

Poster Presentation at European Heart Rhythm Association Conference 2022, Copenhagen, Denmark

A Bates, JR Paisey, A Yue, P Banks, PR Roberts, W Ullah, Establishing safe, effective ablation in the diseased human ventricle: an analysis of generator impedance and electrogram attenuation, EP Europace, Volume 24, Issue Supplement_1, May 2022, euac053.353,

https://doi.org/10.1093/europace/euac053.353

Moderated Poster Presentation at Heart Rhythm Congress 2022, Birmingham, UK

AP Bates, JR Paisey, A Yue, P Banks, PR Roberts, W Ullah, Radiofrequency ablation of the diseased human left ventricle: biophysical and electrogram based analysis, European Journal of Arrhythmia & Electrophysiology. 2022;8(Suppl. 1):abstr54.

https://www.touchcardio.com/arrhythmia/journal-articles/54-radiofrequency-ablation-of-the-diseased-human-left-ventricle-biophysical-and-electrogram-based-analysis/

Publication in Journal of the American College of Cardiology: Clinical Electrophysiology

Bates A, Paisey J, Yue A, *et al*. Radiofrequency Ablation of the Diseased Human Left Ventricle. J Am Coll Cardiol EP. In press

JACC Clin Electrophysiol. 2023 Mar;9(3):330-340. doi: 10.1016/j.jacep.2022.10.001. Epub 2022 Oct 10. PMID: 36371330.

Signature: Date: 19/12/2023

Acknowledgements

Many people who have supported, assisted and guided me throughout my research and in compilation of this thesis.

First and foremost, my thanks go to all of the patients who consented to participate in this research. Through prolonging their procedures for a brief period of time, I was able to collect data that I hope will have meaningful impact on the field and improve procedures for others in the future.

Several representatives from industry have assisted me on this journey. Both Boston Scientific and Biosense Webster provided grants for this research. In particular I wish to acknowledge Jon Toms, Mariana Mota, and Kirsty Rough who ensured my data collection and export was as smooth a process as could be. Neill Townshend, who provided me with training on the Rhythmia mapping system and Tobias Oesterlein for showing me the best ways to process the data.

My thanks to the cardiac rhythm management team at University Hospital Southampton, particularly Phil Banks, Claire Newbery, Osian Nixon and Jordan Evans, whose patience in the catheter lab, and experience with the mapping systems (and by the end, my research protocols) was greatly appreciated. Similarly, to the research team, Lisa Fletcher, Sarah Earles and Bibi Greenwood who have supported and advised me throughout, particularly with the administrative side of research.

The electrophysiologists at University Hospital Southampton, Dr John Paisey, Dr Arthur Yue and Professor Paul Roberts have been nothing but supportive throughout my research. They have helped me focus on the clinical implications of my work and prevented me going down rabbit holes. When asking them if they would mind performing a research procedure, without hesitation the answer has always been yes.

I am extremely grateful to my main supervisor Dr Waqas Ullah, who had the faith to appoint me to this post and has been my main source of inspiration and guidance throughout my candidacy. He has dedicated a huge amount of time to this research from developing our projects, obtaining grants, performing procedures, reviewing manuscripts again and again, and encouraging me to learn skills that will benefit me throughout my career as a clinician.

My most sincere thanks to my family. To my Mum and Dad for their unwavering support and encouragement on my endeavours in studying medicine. And finally, to my wife Suzanne, and children Matthew and Madeleine, who support and motivate me every day, and to whom this work is dedicated.

Definitions and Abbreviations

%ΔGI	Percentage generator impedance drop
ΔGI	Generator impedance drop
ΔLI	Local impedance drop
ΔLI5s	Local impedance drop at 5 seconds
3D EAM	3 dimensional electroanatomical mapping
AC	Alternating current
ACEi	Angiotensin converting enzyme inhibitor
AF	Atrial fibrillation
AI	Ablation index
ANOVA	Analysis of variance
ANS	Autonomic nervous system
ARB	Angiotensin receptor blocker
AUROC	Area under receiver operator curve
AVN	Atrio-ventricular node
AVNRT	Atrio-ventricular nodal re-entrant tachycardia
AVRT	Atrio-ventricular re-entrant tachycardia
Bpm	Beats per minute
CAMKII	Calcium / calmodulin dependent protein kinase II
CF	Contact force
CFAE	Complex fractionated atrial electrogram
CFV	Contact force variability
CPVT	Catecholaminergic polymorphic ventricular tachycardia

CRT	Cardiac resynchronisation therapy
CRT-D	Cardiac resynchronisation therapy defibrillator
CRT-P	Cardiac resynchronisation therapy pacemaker
DAD	Delayed after depolarisation
DC	Direct current
DCCV	Direct current cardioversion
DE MRI	Delayed enhancement magnetic resonance imaging
DOAC	Direct oral anti-coagulant
EA	Electrically active (area of myocardium)
EAD	Early after depolarisation
EBI	Electrode blood interface
ECG	Electrocardiogram
EGM	Electrogram
EI	Electrically inert (area of myocardium)
ETI	Electrode tissue interface
FACM	Fibrotic atrial cardiomyopathy
FIRM	Focal impulse and rotor modulation
FTI	Force time integral
g	grams
GI	Generator impedance
GLMM	Generalized linear mixed model
gs	Gram * seconds
HCN	Hyperpolarisation activated cyclic nucleotide gated channel
ICD	Implantable cardiac defibrillator

I-LVM	Combined intermediate – low voltage myocardium
IVM	Intermediate voltage myocardium
LA	Left atrium
LAT	Local activation time
LBBB	Left bundle branch block
LGE	Late gadolinium enhancement
LI	Local impedance
LIr	Referenced local impedance
LTCC	L-type calcium channel
LV	Left ventricle
LVA	Low voltage area
LVEF	Left ventricular ejection fraction
LVM	Low voltage myocardium
mA	Milliamps
maLVA	Mildly affected low voltage area
MANOVA	Multivariate analysis of variance
MI	Myocardial infarction
MiFi	IntellaNav MiFi ablation catheter
MRA	Mineralocorticoid receptor antagonist
MRI	Magnetic resonance imaging
mV	Millivolts
NCX	Sodium calcium exchanger
NHS	National Health Service
NVM	Normal voltage myocardium

^{o}C	Degrees centigrade
PA	Partially active (area of myocardium)
PAF	Paroxysmal atrial fibrillation
PEA	Pulseless electrical activity
PeAF	Persistent atrial fibrillation
PES	Programmed electrical stimulation
PKA	Protein kinase A
PKC	Protein kinase C
PLB	Phospholambin
PNS	Parasympathetic nervous system
PT	Pacing threshold
PVC	Premature ventricular complex
PVI	Pulmonary vein isolation
RA	Right atrium
RAAS	Renin angiotensin aldosterone system
RF	Radiofrequency
RFA	Radiofrequency ablation
RMCorr	Repeated measures correlation
RNA	Ribonucleic acid
ROC	Receiver operator curve
RV	Right ventricle
RVOT	Right ventricular outflow tract
RyR2	Ryanodine receptor 2
S	Seconds

SAN	Sinoatrial node
SCD	Sudden cardiac death
SERCA2a	Sarco / endoplasmic reticulum calcium ATPase 2a
SNS	Sympathetic nervous system
SP	IntellaNav Stablepoint ablation catheter
SR	Sinus rhythm
ST	Smart Touch ablation catheter
STSF	Smart Touch Surround Flow ablation catheter
UK	United Kingdom
VF	Ventricular fibrillation
VT	Ventricular tachycardia
W	Watts
WACA	Wide antral circumferential ablation
Z_A	Resistance at the electrode interface
Z_B	Resistance of the body tissue
Z_{DE}	Resistance at the tissue about the dispersive electrode
Z_{EBI}	Resistance of the electrode blood interface
Z_{ETI}	Resistance of the electrode tissue interface
Ω	Ohms

Chapter 1 Introduction

1.1 Historical Perspective

Our knowledge of the pathophysiology of cardiac arrhythmias has accelerated across the last 100 years. However, its foundations were built through millennia of study.

1.1.1 Atrial Fibrillation

The earliest description of a pathology that could be atrial fibrillation (AF) is found in the Yellow Emperor's Classic of Internal Medicine by Huang Ti Ching Su Wen who ruled over China 4500 years ago[1]. It is commented:

> *"When the pulse is irregular and tremulous, and beats occur at intervals then the impulse of life fades. When the pulse is slender (smaller than feeble but still perceptible, thin like silk thread) then the impulse of life is small."*

Sphygmology, the art of feeling the pulse and its interpretation, occurred across several dynasties. Chinese, Indian, and Greek physicians all practiced sphygmology in different guises. The foremost of which was Galen (131 – 200 AD) who authored multiple books on the topic. Interestingly, several of his descriptions could easily be translated into arrhythmia we know today, including one of "pulse inequality," which matches closely to AF[2].

Moving forward to 1628, William Harvey, best known as the first physician to accurately describe the circulatory system, also described fibrillation of the auricles of dying animals[3]. An observation replicated by Jean Baptiste de Senac in his 'Traite de la structure du coeur, de son action et de ses maladies,' perhaps the first ever cardiology textbook[3,4]. This was then linked in the 19th century to pathology. A pulse irregularity was noticed in combination with mitral stenosis by Robert Adams and then Etienne Marey who published a pulse tracing of such a patient[1].

It was at the start of the 20th century and the development of the electrocardiogram (ECG) by William Einthoven where our modern understanding of AF begins. His contemporary and collaborator Sir Thomas Lewis pushed this forward noticing on several ECGs:

"A number of irregular waves apart from the ventricular curve. They are more clearly defined in diastole[5]."

He also describes paroxysmal cases of 'pulsus irregularis' where the irregularity of the 'V-curve' (the modern day QRS complex) vanishes alongside the irregular waves. He thus concludes:

"[The paroxysms] are therefore due to a temporary and disorderly action of some part of the heart wall."

Before commenting that:

"Cardiographic curves give no evidence of such disordered action in the ventricle and fibrillation of the auricle yields curves which are identical in every respect."

Thereby deducing that pulsus irregularis is due to auricular fibrillation[5].

Lewis' later experiments were able to better define auricular fibrillation as:

"Conspicuous and continuous oscillations of varying forms and dimensions of auricular origin."

This is a fairly poetic yet accurate description of what we know as atrial fibrillation today[6].

In the 20th century, mechanisms underlying AF were discovered. Experiments by Scherf suggested an ectopic focus could trigger AF following its induction by injecting aconitine into canine atria. This effect could then be reversed by cooling[7]. Moe and Abildskov were then able to sustain AF in canine experiments. From their observations they noticed:

"Irregular wavefronts becoming fractionated and dividing about islets or strands of refractory tissue. Each daughter wavelet can be considered as independent offspring."

This would become what is known today as the multiple wavelet hypothesis[8].

Attention was then drawn to therapy for AF. Ventricular rate control with digitalis was noted in 1935. Electrical cardioversion was developed in the late 1960s[9] before the advent of anti-arrhythmic medication and stroke prevention with anticoagulation in the 1980s[10]. Surgical procedures such as the Cox-MAZE were developed from 1987[11]. Finally, catheter ablation following the discovery of pulmonary vein foci as initiators for AF arose from the late 1990s[1,12].

1.1.2 Ventricular Tachycardia

The first electrocardiographic description of ventricular tachycardia (VT) was given by Sir Thomas Lewis in 1909. In a patient with exertional shortness of breath, precordial pain, palpitations, and dropsy, he was able to document ventricular bigeminy:

"…the patient is subject of extra-systole and that at times the premature beats alternate with the regular beats."

Before describing VT:

"The patient not only shows single and alternating extrasystoles, but they may also appear in groups."

Lewis's case report showed an electrocardiogram with 3 successive extrasystoles, and also comments on up to 11[13]. He deduced they were ventricular in origin from their higher rate and dissociation from atrial activity, which interestingly one of the most useful criteria to diagnose VT on an ECG today[14].

Lewis was then able to relate VT to ischaemic heart disease in an experimental dog model. By ligating the right or left anterior descending arteries, he found an increased number of ventricular extrasystoles occurring before a paroxysmal tachycardia which could degenerate into ventricular fibrillation (VF) and death. He once again deduced the tachycardia to be ventricular in origin on ECG traces, being separate to the slower atrial rhythm and lacking in response to vagal stimulation[15].

The first ECG criteria for VT were developed by Robinson and Herrman in 1921[16]. The criteria included:

1. Rapid succession of ventricular complexes;
2. Abnormal in form;
3. Independent to atrial complexes; and
4. Related ventricular extrasystoles occurring before or after the paroxysm.

Rosenberg, Dressler and Roseler also noted the merger of conducted atrial and premature ventricular complexes forming a fusion beat as a characteristic of the tachycardia[17,18].

For treatment of VT, in 1922 RW Scott discovered quinidine could terminate and prevent episodes[19]. By noting an increase in coupling gap between premature ventricular beats he correctly deduced quinidine increased the refractoriness of the ventricle. Quinidine then formed the mainstay of treatment for VT until the 1950s when procainamide was developed as a chemical substitute for procaine. Procaine had been found to decrease ventricular extrasystoles when applied to the epicardium during cardiac surgery[20]. However, it caused significant central nervous system toxicity making it unusable in a conscious patient. Lidocaine was then developed

and used clinically in the 1960s[21]. Familiar medications today such as beta-blockers and amiodarone were subsequently developed and used clinically from the late 1960s and 1970s respectively[22,23].

Defibrillation was found to terminate VT refractory to medication in 1956 by Zoll[24]. The technique was refined by Lown including the use of direct current (DC) and synchronisation to the R wave, effectively giving rise to DC cardioversion[25,26]. Ultimately this resulted in the development and implantation of the first cardiac defibrillators (ICD) in the 1980s which are commonplace in cardiac practice today[27].

Successful use of overdrive pacing to treat persistent VT was shown by Heiman and Helwig[28]. This technique had previously been shown to prevent ventricular arrhythmias in patients with atrioventricular block and post cardiac surgery[29,30]. This concept would later give rise to anti-tachycardic pacing seen on modern ICDs.

Surgery for VT began with aneurysmectomy in 1959[31] but was associated with high mortality and poor arrhythmic freedom[32]. The more focal and electrophysiologically guided subendocardial resection evolved across the 1970s[33]. However, this was then superseded by catheter ablation, a technique refined across the last 35 years and has become the mainstay of treatment for medication refractory paroxysmal VT in modern times[34].

1.2 Background and Burden

1.2.1 Atrial Fibrillation

Current international guidelines define AF as:

"A supraventricular tachyarrhythmia with uncoordinated atrial electrical activation and consequently ineffective atrial contraction[35]."

AF is diagnosed through an ECG with 3 characteristics, (Figure 1-1)[35]:

1. Irregularly irregular RR intervals (when atrioventricular conduction is not impaired);
2. Absence of distinct repeating p-waves;
3. Irregular atrial activations (f-waves).

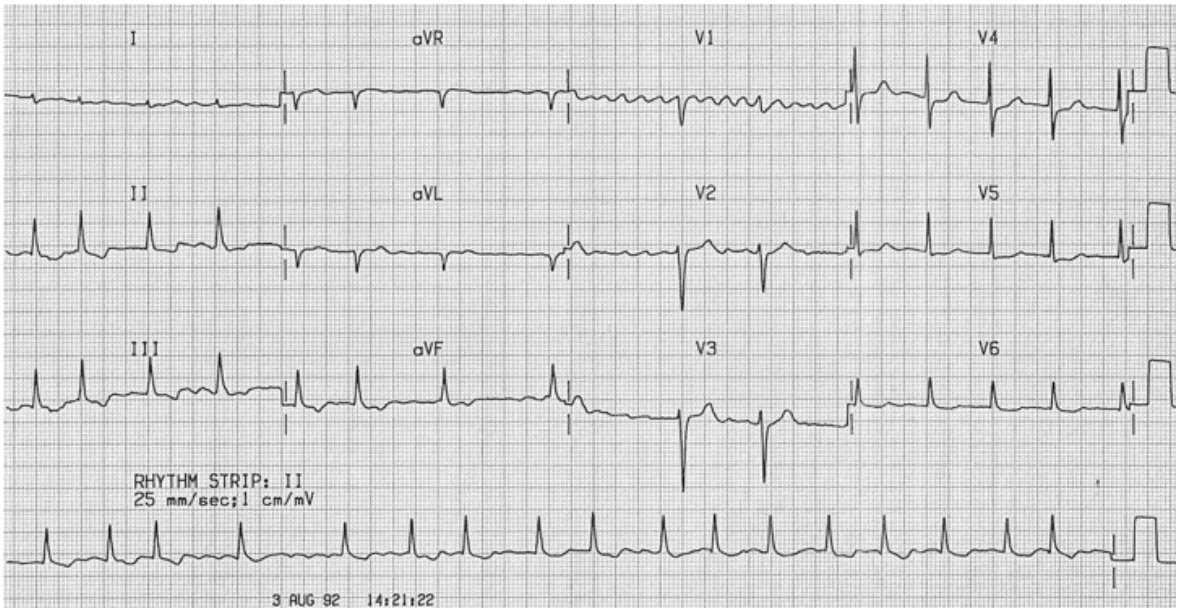

Figure 1-1 *A 12 lead ECG demonstrating AF.*
The intervals between QRS complexes are irregularly irregular and the normal p wave symbolising atrial depolarisation is replaced with a chaotic electrical baseline best seen in V1.

Consensus agreements define an episode of AF lasting 30 seconds as diagnostic[36]. AF is then divided into 4 subtypes dependent upon the timeframe of episodes, presence of self-termination of episodes and the management strategy adopted, (Table 1.1).

Table 1.1 *Classification of Atrial Fibrillation*

Type of Atrial Fibrillation	Definition
Paroxysmal	Spontaneous termination of AF in less than 7 days
Persistent	AF lasting greater than 7 days, even if reverted medically
Long standing persistent	AF lasting greater than 1 year, but a rhythm control strategy is being pursued
Permanent	Acceptance that AF will be present chronically and rhythm strategy abandoned

1.2.1.1 Symptoms

Patient symptoms are variable in character and perception. For some patients, AF is completely asymptomatic and diagnosed co-incidentally; others describe combinations of palpitations, dyspnoea, chest pain, dizziness, tiredness, weakness, and exertional intolerance. There also appears to be a psychological role in patient experience of symptoms, as increased symptom burden has been linked with depressed mood irrespective of the frequency of AF seen on prolonged ECG monitoring[37].

1.2.1.2 Quality of Life

Patients with AF report a diminished quality of life using validated questionnaires, an effect that improves with treatment. Indeed, the severity of this should not be underestimated, as the assessed impairment on quality of is similar to that reported by patients suffering with heart failure or myocardial infarction (MI)[38-40].

1.2.1.3 Mortality

AF is an independent risk factor for mortality as shown in the Framingham Heart Study (1998) with an odds ratio of 1.5 and 1.9 for men and women respectively. In a large Swedish registry, similar figures were obtained and a significant increase in mortality was noted regardless of age. Furthermore, the younger a patient is the greater risk to life AF poses[41,42].

1.2.1.4 Association with Other Diseases

AF increases risk of stroke. The loss of electro-mechanical coupling within the atria results in increased risk of thrombus forming in the left atrial appendage. Embolisation from this appendage then results in stroke. A 5-fold increase is seen accounting for other risk factors[43]. Registries in Canada and Scotland showed AF to increase stroke risk 2-fold for men and 5-fold for women[44,45]. As one ages, the cause of stroke is more likely to be AF, increasing from 1.5% for those 50-59 years to 23.5% at 80-89 years[46].

AF increases risk of dementia by 30% regardless of subtype. A recent meta-analysis shows this to be independent of stroke[47]. Mechanisms here are postulated to be an increase in silent cerebral ischaemia from sub-clinical micro emboli, cerebral microbleeds, and potential intermittent cerebral hypoperfusion due to irregular RR intervals and loss of atrial systole[47]. Interestingly the number of silent cerebral ischaemic events shown on magnetic resonance imaging (MRI) appears to be consistent with the burden of AF reflecting their increased number in patients with persistent over paroxysmal AF. Furthermore, AF has been shown to correlate with cognitive impairment[48].

AF increases risk of sudden death 2-fold compared to controls with similar concomitant co-morbidities. This relative risk continued to be present in patients with hypertrophic cardiomyopathy, coronary artery disease and heart failure, whilst tripling the risk in patients with Brugada syndrome[49].

AF increases risk of heart failure. The relationship of AF with heart failure is complex. Both conditions are known to predispose and exacerbate one another[50-52]. Interestingly, if one develops AF before heart failure the mortality risk is greater than the converse[53].

1.2.1.5 Epidemiology

Large numbers of patients suffer with AF. In 2020 Public Health England estimated the prevalence of AF to be 2.5% of the population, approximately 1.5 million people[54]. However, reflecting AF is often an asymptomatic disease, the true prevalence is likely to be higher. AF prevalence increases with age, (Table 1.2) and shows a male preponderance of 1.2 : 1[55]. The

incidence of AF is 120 000 – 215 000 cases annually. Going forward, the estimated European prevalence in 2030 is 2.7 - 3.3%. This equates to 14 – 17 million new patients, 280 000 – 340 000 additional strokes and 3.5 – 4 million further hospitalisations. The increasing prevalence of AF reflects our ageing population, better chronic disease treatment and increased availability of diagnostics[55].

Table 1.2 *Prevalence of Atrial Fibrillation with Age*

Age	Prevalence
< 49 years	0.12 – 0.16%
60 – 70 years	3.7 – 4.2%
> 80 years	10 – 17%

The large numbers of patients suffering AF reflects an endemic disease. The increased mortality, hospitalisation and number of diseases associated with AF highlights the urgency of its treatment.

1.2.1.6 Economics

The financial, societal, and emotional costs of AF are large. In 1995 the cost of AF to the NHS was £243.9 million. This is 0.62% of all NHS expenditure. By the year 2000 this had increased to £459 million, 0.88% of NHS expenditure[56]. However, this was only the direct cost of AF, and did not include AF as a secondary diagnosis, for example admission due to an associated stroke. Additionally, these numbers are now over 20 years old and were also taken before the use of modern anticoagulants and the widespread use of catheter ablation. Slightly more recently in 2004 in Europe, the estimated cost per patient per year was between £1500 – 3200[57].

AF is strongly associated with stroke. The societal cost of every stroke is extensive. The Stroke Association calculates in the first year following a stroke the cost to society is £45 409 and £24 778 is subsequent years[58]. However, the majority of this is the value of care contributed by informal unpaid family members and carers which reflects the large burden the disease places upon society and individual families. The overall cost of stroke per year to the UK is £25.6 Billion.

Since, AF is responsible for up to 23% of strokes in patients >80 years, these numbers reflect the substantial social and economic effect of the disease.

1.2.2 Ventricular Tachycardia

The modern definition of VT is:

1. 3 or more consecutive beats originating from the ventricle;
2. Independent of atrial or atrioventricular node (AVN) conduction;
3. At a rate greater than 100 beats per minute (bpm), (Figure 1-2).

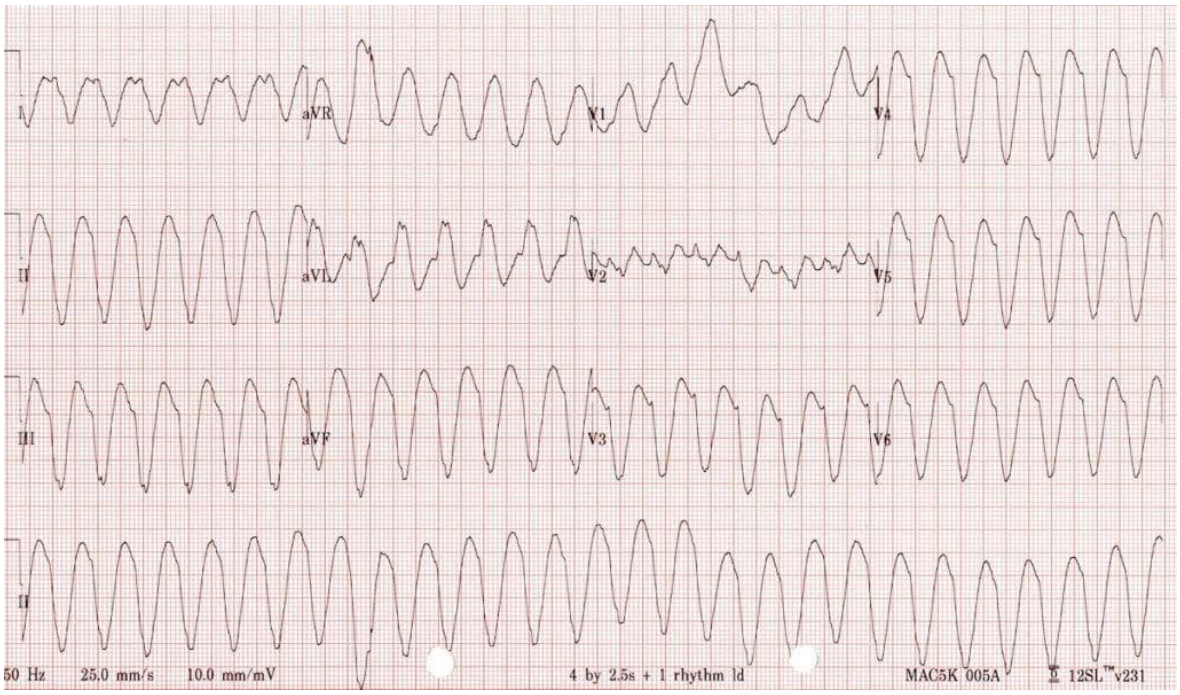

Figure 1-2 *A 12 lead ECG demonstrating VT.*
Every QRS complex in the ECG is broad with regular intervals in between. The ventricular rate is tachycardic at approximately 162bpm

However, VT can be categorised in several different ways based upon clinical characteristics, ECG morphology and underlying mechanism. Indeed, in an international consensus document published by the Heart Rhythm Society in 2020, 25 different definitions were provided[34].

The pathology underlying VT is different to AF. Whereas AF is perhaps best described as a primary condition that is associated with other diagnoses, VT is an arrhythmia seen more commonly secondary to other disease processes.

1.2.2.1 Symptoms

Patient experience of VT varies depends on the clinical characteristics of the arrhythmia and the presence of underlying structural cardiac disease. In general, symptoms include palpitations, pre-syncope, syncope, chest pain, shortness of breath, and weakness. Cerebral symptoms (syncope, pre-syncope) occur more significantly with ventricular rates greater than 200bpm and in patients with pre-existing heart failure[59]. VT also has the potential to deteriorate to VF and cause sudden cardiac death (SCD)[60]. For patients with an ICD, anti-tachycardic pacing and defibrillation can be severely debilitating, commonly causing palpitations and chest pain.

1.2.2.2 Quality of Life

For those specifically undergoing ablation for VT, validated health related quality of life questionnaires EQ5D and SF-36 show a lower baseline score compared to the healthy population[61-63]. Patients who had experienced multiple shocks from their ICD also report reduced quality of life, anxiety, psychosocial problems and concerns regarding complications[64].

1.2.2.3 Mortality

Diagnosing VT specifically as the primary reason for death is impractical as it is often secondary to another disease process, for example, myocardial infarction. Also, due to the rapid deterioration seen, achieving a confirmatory ECG is often challenging. To establish a mortality rate from ventricular tachyarrhythmias overall, we can use retrospective and observational reports of sudden cardiac death as a surrogate. However, this introduces errors as the true causes of SCD are not known and could have been caused by any terminal rhythm. With this in mind, the incidence of SCD reported across studies in North America and Europe is 50 – 100 per 100 000 years in the general population[65-67].

1.2.2.4 Causes of Ventricular Tachycardia

Several pathological processes can cause VT, with distinct differences in disease associations between younger (< 35 years) and older patients being seen.

In younger patients, channelopathies, cardiomyopathy, myocarditis, substance abuse and sudden unexplained death predominate[68]. Thankfully these conditions are rare and the incidence of SCD in the young is reported as 1.8 – 2.3 per 100 000 person years[69-71].

In older patients, the main causes of SCD are ischaemic heart disease, valvular heart disease and heart failure[34]. Consequently, with the large prevalence of these conditions, SCD is also more common, with a sub-study of the VALIANT study showing risk of SCD as 1.4% in the first month following MI, before falling to 0.14% per month after 2 years. Those with a reduced left ventricular ejection fraction (< 30%) had even higher risk, at 2.3% in the first month and 0.25% at 2 years[72].

1.2.2.5 Economics

The direct and indirect costs of VT to society is difficult to substantiate. No specific cost analysis has been undertaken taking into account the entirety of care required for VT. This would include the variety of presentations to healthcare services VT can cause, (for example, outpatient appointments, emergency department attendance, out of hospital cardiac arrest), plus the various treatment modalities, (medication, implantable defibrillators, ablation procedures), and their follow up. Furthermore, one could include the societal effect of sudden cardiac deaths and unexplained cardiac arrests potentially caused by ventricular tachyarrhythmias.

Analyses have been performed on the cost effectiveness of implantable defibrillators, with a 2007 analysis from the UK, Italy, France and Germany showing annual total expenditure of €493 million[73]. Overall, ICDs have been found to be cost effective, globally for secondary prevention[74], and specifically for primary prevention in the UK delivering a 5 to 1 return on investment[75].

A sub-study of the VANISH trial evaluating the cost effectiveness of catheter ablation for VT against escalation in anti-arrhythmic drug therapy, found greater quality adjusted life years, (1.63 vs 1.49) for the ablation group at the expense of extra cost, ($65 126 vs $60 269)[76].

1.3 Cardiac Anatomy and Physiology

1.3.1 Cardiac Anatomy

To understand the pathophysiology of AF or VT and the treatment options for them, an understanding of normal cardiac anatomy and electrophysiology is required.

The heart is divided into 4 chambers, 2 upper chambers known as the atria and 2 lower chambers known as the ventricles. The right and left atria function as filling chambers receiving low pressure blood from the systemic and pulmonary circulations respectively. Blood then flows into the ventricles and is pumped around the lungs and body at higher pressure. Due to the difference in function between the atria and ventricles, their structure is different with the atria being thin walled and compliant, whilst the ventricles are thick and muscular. Both the atria and ventricular walls are composed of 3 layers – the inner endocardium, the middle myocardium and the outer epicardium.

1.3.1.1 Right Atrium

The right atrium (RA) accepts blood from 3 inlets, the superior vena cava, the inferior vena cava and the coronary sinus. Its outlet is via the inferolateral tricuspid valve into the right ventricle. The endocardium of the RA is muscular and separated from the left atrium (LA) by thin layer known as the interatrial septum.

1.3.1.2 Left Atrium

The LA accepts blood from 4 pulmonary veins though anatomical variants of 3 and 5 do exist. Its outlet is via the mitral valve into the left ventricle. In contrast to the RA, the endocardium of the left is much smoother and extends into the pulmonary veins. The

myocardium of the LA then also extends into the veins before tapering like the sleeves of a shirt. This is of particular note, as these muscular sleeves are a common site of atrial ectopy.

Also of note in the LA, is a thin tubular structure which arises from the left inferolateral wall. This is the left atrial appendage, a common source of thrombo-emboli in AF.

1.3.1.3 Right Ventricle

The right ventricle (RV) is triangular in shape longitudinally, and when cut in cross section will appear crescentic due to the higher pressure of the left ventricle (LV) upon the inter-ventricular septum. It accepts blood from the RA via the tricuspid valve at its base. It has coarse trabeculae forming its endocardium before becoming smoother at the sub-pulmonary infundibulum just below its outlet, the pulmonary valve.

The RV is thin walled compared to the LV, being 3-5mm thick on its most muscular free wall and consequently supplies a lower pressure to the pulmonary circulation[77].

1.3.1.4 Left Ventricle

The LV is a cone shaped, muscular chamber that receives blood from the LA via the mitral valve. Its outlet is through the aortic valve into the aorta. It has thin trabeculations composing its endocardium at its apical segments before these become thicker and smoother moving towards its outflow tract. At its thickest the LV wall can measure up to 15mm in normal hearts, and larger under pathological processes resulting in hypertrophy (e.g. hypertensive heart disease, aortic stenosis, hypertrophic cardiomyopathy)[78].

1.3.2 Electrical Anatomy

The heart is a unique organ having its own intrinsic electrical system. Cardiac conduction initiates in a specialised area of tissue known as the sino-atrial node (SAN). This is situated at the junction of the superior vena cava and right atrium. It is crescentic in shape and extends down inferolaterally and diffusely into the crista terminalis[79,80]. The specialised cells of the SAN initiate

depolarisation, generating an electrical signal which propagates around the RA, before travelling to the LA by Bachmann's bundle, the coronary sinus musculature and interatrial muscular bundles. It is unable to conduct directly to the ventricle due to electrically inert tissue formed by the annuli of the mitral and tricuspid valves.

The electrical impulse reaches the AVN, a second specialised area of conduction tissue situated at the base of the right atrium within the triangle of Koch. This triangle is an area delineated by the septal leaflet of the tricuspid valve, the coronary sinus and the tendon of Tordaro. At the AVN, a conduction delay occurs allowing blood to flow from atria to ventricles.

Electrical conduction then continues down the Bundle of His before dividing into the left and right bundle branches and subdividing into smaller subendocardial Purkinje fibres. Having the function to provide cardiac output to the rest of the body, the left ventricular myocardium is much thicker and larger than that of the right. Co-ordination of contraction of apex before base is important to optimise cardiac output. The structure of the ventricular electrical system supplies this with conduction purely within nervous tissue (rather than muscular bundles seen in the atria), insulation from underlying muscular tissue, and a specialised moderator band to the distant RV free wall. Rapid depolarisation can then occur across the entire ventricular tissue in 80 – 120ms.

1.3.3 Cardiac Electrophysiology

The initiation and propagation of cardiac conduction is complex. Precise cellular mechanisms occur within specialised tissues throughout the heart each related to a specific role. The subtle differences are reflected in the changes in action potential morphology and presence of specific ion channels and pumps present within these tissues. These particular ion channels and pumps allow certain components of the electrical system to function as initiators as well as propagators of conduction.

1.3.3.1 Initiation of Cardiac Conduction

During normal sinus rhythm, the SAN initiates cardiac conduction. To achieve this, it raises the voltage across its cell membrane formed by the concentrations of intra- and extra-cellular ions. This voltage is known as its membrane potential. A slow leak of sodium and

potassium ions through hyperpolarised activated cyclic nucleotide gated channels (HCN) causes a current across the cell membrane. This is known as the 'funny current.' It causes a rise in membrane potential from -90mV to between -50mV to -20mV resulting in opening of voltage gated calcium channels. This causes a rapid influx of calcium and a rapid rise in membrane potential up to +25mV. In the SAN, repolarisation occurs following the closure of HCN channels, and the voltage gated sodium and calcium channels. Potassium channels open allowing an efflux out of the cell, lowering the membrane potential to baseline.

1.3.3.2 Propagation of Cardiac Conduction

The rise in membrane potential in the SAN allows propagation across its cells through the sequential activation of adjacent voltage gated channels. Propagation then spreads from cell to cell through organelles known as connexins or gap junctions.

When the propagating current moves to tissue outside the SAN, the subcellular mechanism of conduction changes and is broken down into 5 phases, (Table 1.3 and Figure 1-3).

Table 1.3 *The Phases of the Cardiac Action Potential*

Phase	Description
Phase 0	Rapid depolarisation occurs via the opening of voltage gated sodium channels rather than a slow leak. Voltage peaks at 50mV.
Phase 1	Voltage gated sodium channels close. Specialised potassium channels open lowering voltage slightly and creating a 'notch' of the action potential.
Phase 2	The action potential is held in a depolarised state by a slow influx of calcium through L-type calcium channels holding the membrane potential high. This is known as the 'plateau phase.' Of note the influx of calcium also causes cardiac contraction by binding to ryanodine receptors.
Phase 3	The calcium influx slowly tails off allowing an efflux of potassium to repolarise the cardiac myocyte. Action potential falls to starting voltage of -90mV.
Phase 4	Following repolarisation, ion pumps function to restore sodium and potassium to their original levels.

The length of each of these phases depends on the function of the particular tissue. For example, ventricular myocytes have prolonged phase 2 allowing a greater influx of calcium to generate more powerful cardiac contraction, and to lengthen their refractory period preventing arrhythmia. Atrial myocytes have a shorter phase 2 with less efflux of calcium giving a shorter refractory period and allowing for greater responsiveness to humoral and autonomic stimuli. These subcellular mechanisms propagate throughout the heart, from the atria to AVN and into the ventricles.

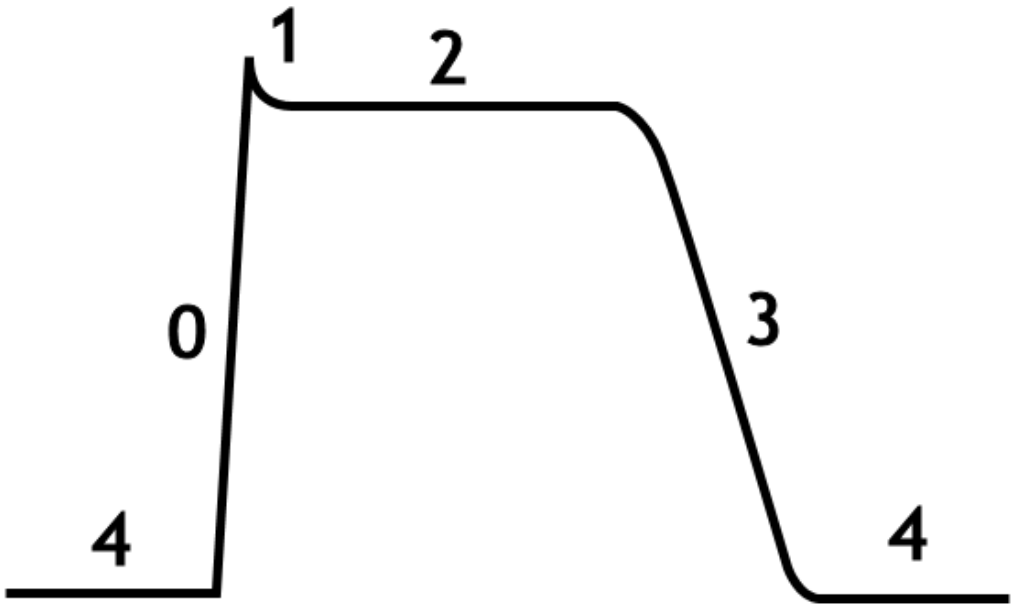

Figure 1-3 *Phases of the action potential within a ventricular myocyte.*

1.3.3.3 The Refractory Period

Following depolarisation, the myocardium cannot depolarise again until its ionic mechanisms are reset. This is the refractory period. The refractory period is divided into 2 parts, absolute and relative. The absolute refractory period occurs between phases 0 – 2. Here the membrane potential is raised, the voltage gated sodium channels have opened (Phase 0) or have now closed but are locked down preventing re-opening (Phases 1-2). As the myocyte repolarises in phase 3, these sodium channels are capable of opening again. At this time a relative refractory period is in place, where the myocyte can depolarise, but it requires a more potent signal to do so.

In the atria, the refractory period is just under 200ms[81]. In the ventricles the refractory period is approximately 250ms[82].

1.4 Pathophysiology of Cardiac Arrhythmias

1.4.1 The Mechanisms of Arrhythmia

Mechanisms of arrhythmia are divided into abnormal impulse formation and re-entry. These in themselves are further subdivided depending on the underlying ionic mechanisms triggering and maintaining the arrhythmia, (Figure 1-4).

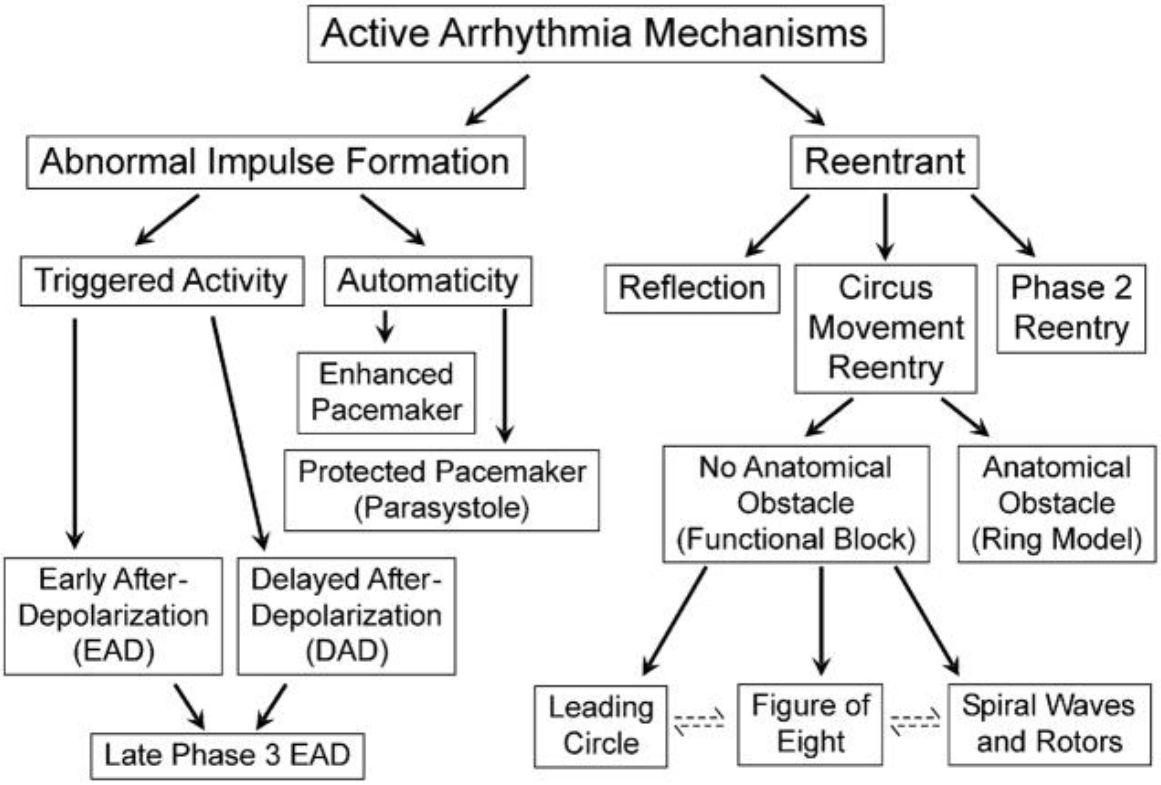

Figure 1-4 *Mechanisms of arrhythmia*

Reproduced from Antzelevitch C et al (2011)[83] with permission from Elsevier.

1.4.1.1 Increased Automaticity

As the initiator of cardiac conduction, changes in the automaticity of the SAN will correspondingly affect heart rate. This is typically a physiological response to neurohumoral

factors, for example, sympathetic activity seen with exercise. However, increased automaticity at sites outside of the SAN can result in arrhythmias.

Aside from the SAN, other cardiac tissues are able to function as pacemakers. These include the atria, the AVN, the His bundle and Purkinje fibres, all of which can initiate conduction but do so at sequentially lower heart rates. For example, the atria at 40-50bpm, the AVN at 30-50bpm and Purkinje fibres at 20-40bpm. Operating as secondary pacemakers, they are constantly reset by the more dominant, higher rate pacemaker of the SAN. However, in pathological circumstances such as ischaemia, digitalis toxicity, catecholamine excess, or raised extracellular potassium a secondary pacemaker can develop automaticity with higher rate than the SAN, effectively becoming the dominant pacemaker. The mechanism of this is through raising the maximum diastolic potential, that is the lowest voltage of the action potential within phase 4. This effectively decreases the time to reach the threshold for activation of voltage gated sodium channels, initiating phase 0 and depolarisation. When a secondary pacemaker becomes dominant due to its enhanced automaticity, a tachyarrhythmia can result, for example an accelerated junctional tachycardia, a focal atrial tachycardia or in the context of ischaemia, potentially VT.

1.4.1.2 Triggered Activity

Triggered activity is the premature activation of cardiac tissue caused by oscillations in membrane potential during the action potential. These oscillations are known as afterdepolarisations and divided into early (EADs), occurring in phase 2 or 3, i.e. prior to repolarisation,[84] and delayed (DADs), occurring in phase 4, i.e. after repolarisation[85] (Figure 1-5). When the EAD or DAD is large enough to reach the threshold potential to cause voltage gated sodium channels to open, triggered activity occurs and results in an extrasystole. Furthermore, having triggered activity itself can precipitate further afterdepolarisations and if these also reach threshold potential, further triggered activity occurs, effectively setting up a recurring cycle and a tachyarrhythmia.

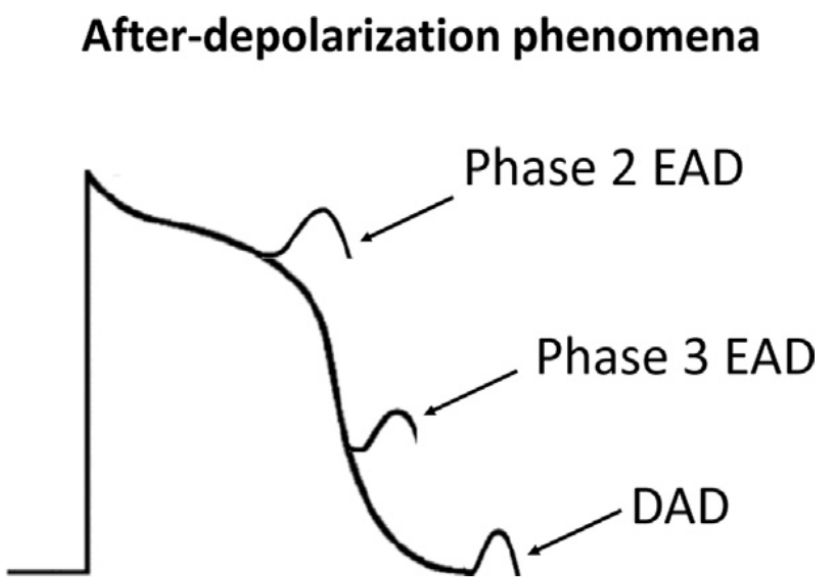

Figure 1-5 *The types and timings of afterdepolarisations.*
With appropriate timing and the potency of the afterdepolarisation, a new action potential can be triggered.
Reproduced from Tse G (2016)[86] with permission from Elsevier.

EADs typically occur with prolongation of the action potential. Here, the inward current across the myocyte membrane outweighs the outward current. This can be caused by an increase in the inward sodium current (I_{Na}), the inward calcium current (I_{Ca})[87], increased activity of the sodium-calcium exchanger (I_{NCX})[88], a decrease in the outward potassium currents (I_{to}, I_{Kr}, I_{Ks}, I_{K1}) or a combination of the above.

Consequently, any pathophysiology or medication that affects these currents can precipitate EADs. Common examples include electrolyte abnormalities (hypokalaemia, hypocalcaemia, hypomagnesaemia), hypoxia, catecholamine excess, acidosis, bradycardia, long QT syndrome and class I and III antiarrhythmics. If the EAD is large enough an action potential will be triggered.

DADs occur in the presence of high intracellular calcium load. The high calcium concentration causes further spontaneous calcium increases through opening of calcium currents

(I_{NCX}, I_{CLCA}, I_{NS}), collectively known as the transient inward current (I_{TI})[89]. The presence of high levels of catecholamines can also raise intracellular calcium levels through leak from ryanodine 2 receptors (RyR2) in the sarcoplasmic reticulum, a mechanism particularly seen with catecholaminergic polymorphic ventricular tachycardia (CPVT)[90]. The further calcium increase causes the sodium calcium exchanger (NCX) to activate, moving sodium into the cell, raising the membrane potential to rise giving a DAD. If this reaches threshold triggered activity is generated. Examples giving rise to DADs include digitalis toxicity[91], CPVT[92], LV hypertrophy[93], heart failure[94], and ischaemia[95].

1.4.1.3 Re-Entry

Re-entry occurs due to the failure of the action potential to extinguish itself. In the presence of anatomical or electrophysiological abnormalities, re-activation of an area of myocardium that has recovered from its refractory period takes place. In most circumstances this starts a self-sustaining loop of propagation and repetitive excitation of the heart. However, it can also generate triggered activity causing further arrhythmias.

To initiate and sustain, re-entrant rhythms require[96]:

1. Myocardial substrate with susceptible electrophysiological properties;
2. An area of block which the arrhythmia can propagate around;
3. Unidirectional conduction block;
4. A critical tissue mass that is large enough for a site to recover from refractoriness and be depolarised again to sustain the rhythm;
5. A trigger to initiate the rhythm.

Re-entry can be classified into anatomical and functional categories.

1.4.1.3.1 Anatomical Re-entry

Anatomical re-entry involves circus movement around an obstacle. A wave of depolarisation followed by a wave of repolarisation travels around this obstacle. The obstacle

could be microscopic such as fibrosis (as seen in ischaemic cardiomyopathy), fibro-fatty infiltration (as seen in arrhythmogenic cardiomyopathy), or the AVN (as seen in atrio-ventricular node re-entrant tachycardia (AVNRT)). It can also be macroscopic, circling around anatomical features such as accessory pathways (as seen in atrio-ventricular re-entrant tachycardia, (AVRT)), or the cavo-tricuspid isthmus and atriotomy scars (such as different types of atrial flutter). As the depolarisation wave reaches its starting point having completed a revolution, it will begin a second revolution if the repolarisation wave has left this site.

For anatomical re-entry to sustain, the duration of the circuit to complete a single revolution must be longer than the absolute refractory period, (Figure 1-6). Otherwise, it will collide with inexcitable tissue and extinguish. For this to occur, either the anatomical object must be sufficiently large for the wave of depolarisation to propagate around, or its conduction velocity must be slowed at a stage within the circuit.

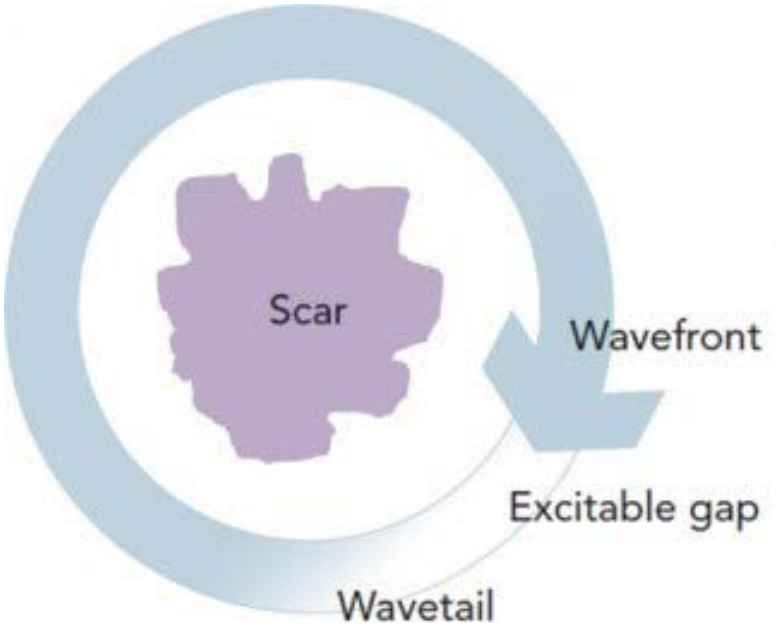

Figure 1-6 *Anatomical re-entry*
A wave of depolarisation (arrowhead) travels around the obstacle, returning to its starting point after repolarisation and the refractory period (arrow tail) has completed. Hence, the starting point can be depolarised again, allowing for a re-entrant arrhythmia to be setup.
Reproduced from Waks J et al (2014)[97] with permission from Radcliffe.

1.4.1.3.2 Functional Re-entry

Functional re-entry concepts include the leading circle model, spiral and scroll waves, reflection, and phase 2 re-entry. With functional re-entry concepts, it is useful to think of the activation of tissue as a wave depolarisation, after which the tissue is refractory. This is then followed by a wave of repolarisation, where the tissue has left the absolute refractory period and the tissue can be re-excited.

1.4.1.3.2.1 Leading Circle Model

The leading circle model was first described by Allisie *et al* in 1977[98]. In their study, a premature extra stimulation of rabbit left atrial tissue gave rise to a wave of excitation. Due to electrophysiological heterogeneity within the tissue, the wave propagated only in a direction where tissue had recovered from its absolute refractory period. Furthermore, it did so with decreased conduction velocity. With this decreased conduction velocity, the excitation wave could return to its site of origin, and having fully repolarised, commence a re-entrant circuit (Figure 1-7). As there is no structural obstacle within the centre of this circuit, depolarisation could occur with inward, centripetal waves into it and outward, centrifugal waves away from it. The centripetal waves could then develop a further smaller re-entrant circle, to the point where depolarisation immediately followed the absolute refractory period with no excitable gap in-between. The time period for this circuit would be precisely the time of the refractory period. The distance or wavelength of the circuit would be equal to the product of conduction velocity and absolute refractory period. Any circuit outside of this would be abolished by depolarisation of its excitation gap from the shorter time framed 'leading circle,' and any depolarisation wave within the circle would collide with refractory tissue, extinguishing it. Through electrode measurements, Allisie *et al* found the core of the leading circle was inexcitable, being consistently above depolarisation threshold values. This is a phenomenon caused by the multiple short centripetal wavelets constantly depolarising, repolarising and colliding within the core.

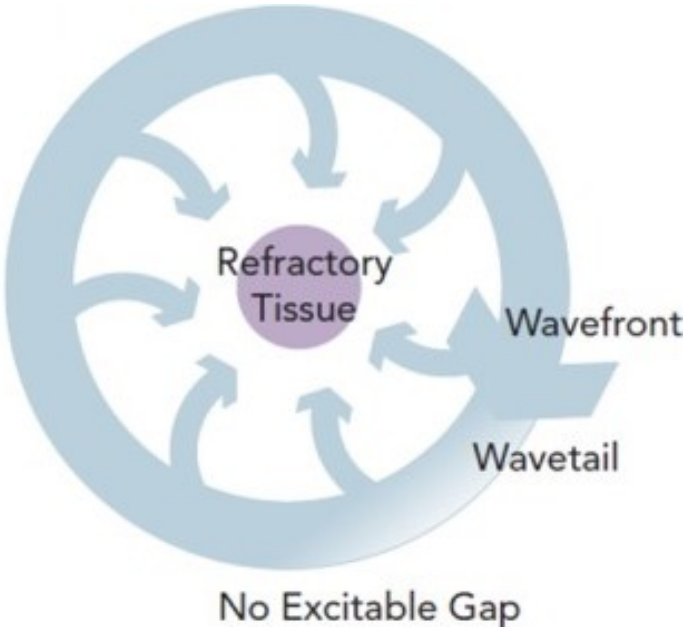

Figure 1-7 *Leading circle model*
A wave of depolarisation travels around a central core of tissue that is constantly depolarised by centripetal waves. The depolarisation wave follows the repolarisation wave so closely that there is no excitable gap between them.
Reproduced from Waks J et al (2014)[97] with permission from Radcliffe

Although the leading circle concept was well demonstrated in an animal model,[99,100] it was inconsistent with the clinical effectiveness of certain anti-arrhythmic medications. For example, sodium channel blockers such as flecainide shorten the refractory period, decreasing the wavelength and distance of tissue required to maintain re-entry. This ought to act to stabilise the arrhythmia, requiring a smaller tissue mass to sustain and allowing other potential circuits to begin. This is the opposite to what is noted clinically, where flecainide can be used to chemically cardiovert a patient in AF or VT. Furthermore, the leading circle concept has not been demonstrated by numerical or high-density mapping studies[101].

1.4.1.3.2.2 Spiral Wave Concept

The spiral wave concept has gained significant traction since its first description in models and experimentally the early 1990s[102,103]. The concept is of a rotational two-dimensional wave of excitation emitted from a self-organising source of functional re-entrant activity. This source is termed a rotor and has a core of excitable tissue but remains unexcited as waves propagate around it[103]. The three-dimensional equivalent of this is a scroll wave.

A spiral wave initiates in the presence of an inexcitable anatomical (e.g., scar), or functional obstacle (e.g., electrophysiological heterogeneity). Triggered by a pre-mature stimulus, the excitation wave adjacent to the obstacle moves past it and then meanders around it like an eddy current in a river. Provided the curvature of this 'eddy current' is stable, a re-entrant circuit can be set up detached from this obstacle, centred around a functional core, and having a spinning spiral wavefront rotating around it[89]. To add to its complexity, a rotor does not necessarily stay static in the myocardium but can drift. This can lead to break up of the waves as they collide and degeneration into fibrillation[96], (Figure 1-8).

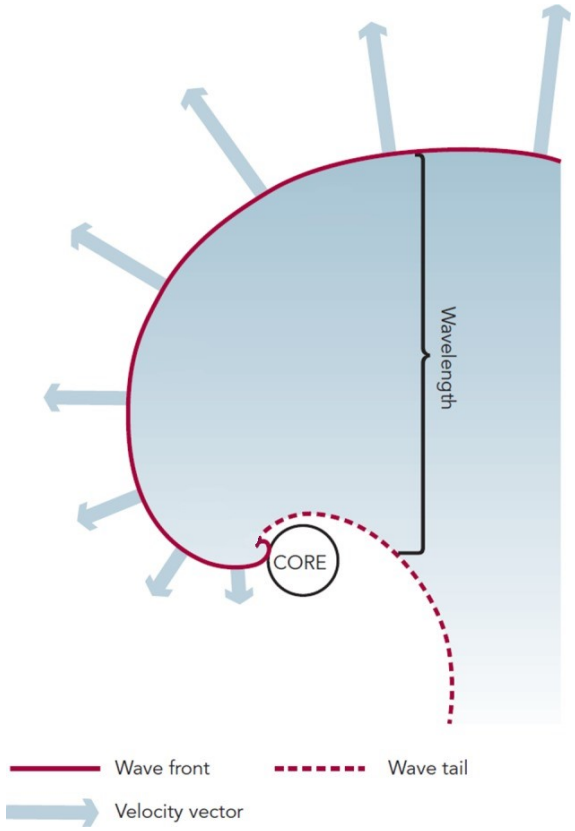

Figure 1-8 *Diagrammatic representation of a spiral wave or rotor*
The wavefront moves anti-clockwise around the core starting a spiral of depolarisation.
Reproduced from Waks J et al (2014)[97] with permission from Radcliffe

The concept has been demonstrated clinically on specialised mapping systems, and provides explanation for AF, VF and both monomorphic and polymorphic VT. Treating rotors with ablation with specialised systems currently also looks promising. However, rotors cannot yet be demonstrated on current isochronal mapping systems[104,105].

1.4.1.3.2.3 Reflection

Reflection is a phenomenon that does not involve circus re-entry. Here, a central inexcitable gap exists between two normally conductive areas. When an action potential propagates through the first area and meets the gap it terminates. However, as the gap is small, passive electrotonic current is able to spread to the second area and initiate further depolarisation. This in turn then sends passive electrotonic current back through the inexcitable gap to the first section, effectively reflecting the initial action potential[106]. This mechanism has been suggested to underlie ventricular bigeminy[89].

1.4.1.3.2.4 Phase 2 Re-entry

Phase 2 re-entry also does not rely on circus movement but heterogeneity of action potential durations between adjacent areas of myocardium.[107] A typical example is between the endo- and epicardium. Differences in the transient outward current (I_{to}) result in a longer action potential duration in the endocardium. In circumstances including high intracellular calcium, ischaemia and use of sodium channel blockers (e.g. flecainide), the endocardial action potential duration is further prolonged[108]. If the adjacent epicardium in this time has repolarised, the high membrane potential still present in phase 2 in the endocardium can trigger an extrasystole. This mechanism has been associated with the initiation of polymorphic VT in Brugada Syndrome[109].

1.4.2 Factors Involved in the Genesis and Maintenance of Atrial Fibrillation

AF arrhythmogenesis and maintenance is a complex interaction of factors occurring across genetic, structural and electrophysiological levels which shall be discussed. Although the research into this area is highly detailed, the relative timing of each of these pathological changes to one another is yet to be fully understood. Expert consensus guidelines state:

"It is generally believed that a degree of structural remodelling must predate electrical remodelling."

However, the degree of structural remodelling that is required to initiate or maintain AF is not known, nor progress from paroxysmal to persistent forms[101]. Additionally, the presence of AF has been shown to perpetuate these factors. This also demonstrates why long-standing forms of AF have poorer response rates to ablation as the atria reach a figurative structural and electrophysiological point of no return.

1.4.2.1 Genetics

As of 2018, 134 genetic loci have been associated with increased AF risk[110]. The majority of these code for either ion channel subunits or associated transcription factors, however their individual relationship to the arrhythmogenesis of AF is often unclear. It is postulated several will cause changes in action potential duration resulting in a decrease in the refractory period. The first specific gene identified with increased AF risk was KCNQ1, seen in a family with hereditary persistent AF in Shanghai. KCNQ1 codes for the α subunit of the potassium ion channel handling the current I_{Ks}. Its mutation allowed a 'gain in function' of the channel with resultant earlier repolarisation, reduced refractory period and providing electrophysiological substrate for re-entry[111].

1.4.2.2 Intracellular Calcium Dysregulation

Intracellular calcium dysregulation contributes to AF arrhythmogenesis by providing triggers via DADs. However, its downstream effects also contribute to electrical and structural remodelling processes providing substrate necessary to maintain AF.

Physiologically, calcium enters a myocyte via L-type calcium channels (LTCC) during phase 2 of the action potential. This triggers calcium release via RyR2 receptors within the sarcoplasmic reticulum and inducing myofilament contraction. Calcium is returned to the sarcoplasmic reticulum via a calcium ATPase pump (SERCA2a). Activity of SERCA2a is controlled by an inhibitor, phosphalamban (PLB). Following an adrenergic response, both RyR2 and PLB are phosphorylated by calcium calmodulin dependent protein kinase (CaMKII) and protein kinase A (PKA) respectively. This results in an increased probability of activation of RyR2, raising the intracellular calcium load, whilst the dissociation of PLB from SERCA2a allows greater calcium return to the sarcoplasmic reticulum. Effectively, this increases cellular-sarcoplasmic reticulum calcium turnover providing an appropriate chronotropic and inotropic myocardial response[112].

In AF there is constant atrial depolarisation, raising intracellular calcium levels chronically. Hyperphosphorylation by CaMKII causes RyR2 hypersensitivity and consequent greater calcium leak from the sarcoplasmic reticulum for corresponding intracellular levels[113,114]. Furthermore, CaMKII itself is upregulated. Indeed, in patients with long standing AF, CaMKII expression is enhanced 40% +/- 15% and RyR2 phosphorylation 110% +/- 53%[114]. In response to the raised intracellular calcium load, a myocyte uses other mechanisms to remove it. NCX expression is increased, exchanging 3 sodium ions for a single calcium ion and resulting in greater I_{NCX} for any given intracellular concentration of calcium. The increase in I_{NCX} results in DADs and the potential for triggered activity. Clinically, the importance of calcium dysregulation and specifically the role of RyR2 is seen with CPVT, a genetic condition with RyR2 mutations where an increased incidence of AF is documented[115].

1.4.2.3 Electrical Remodelling

Numerous changes in the expression of ion channels and connexins are associated with AF.

1.4.2.3.1 Downregulation of L-Type Calcium Channels

Alongside the increased expression of NCX, downregulation of LTCC has been shown with long standing AF. In a canine model, tachy-pacing of the atria resulted in a rise in intracellular calcium levels. Activation of the calcineurin/NFAT signalling pathway resulted in downregulation of genes CACNA1C and CACNAB2, coding for α and β subunits of the LTCC[116]. As LTCC are responsible for the phase 2 plateau of the cardiac action potential, their decreased expression results in reduced action potential duration and refractory period favouring the formation of re-entrant waves. This is a finding also shown in humans with long standing AF[117].

1.4.2.3.2 Upregulation of Inward Rectifier Potassium Channels

I_{K1} is the main inward rectifier potassium current responsible for repolarisation of the myocyte during phase 3 of the action potential and determines its baseline resting potential. Raised intracellular calcium levels activate pathways that decrease levels of inhibitory micro RNAs miR-26[118] and miR-1[119]. This consequently increases the expression of gene KCNJ2, coding for Kir 2.1, a subunit of the inward rectifier potassium channel[120]. This increases $I_{K1.}$ Indeed, in samples

from the LA of patients undergoing cardiac surgery with AF showed a reduction of 86% in miR-1 compared to those in sinus rhythm (SR), with an associated significant rise in Kir2.1 mRNA and I_{K1} current density[119].

The increase in I_{K1} shortens action potential duration providing electrophysiological substrate for re-entry.

1.4.2.3.3 Upregulation of Constitutive Acetylcholine Activated Potassium Channels

Further inward rectifier current is supplied by the G protein, acetylcholine activated potassium channel, I_{KAch}. Physiologically used to deliver a negative chronotropic response to vagal activity in the SAN, I_{KAch} channels also exist throughout the atria and conducting system. In AF the agonist activation of I_{KAch} decreases, however a constitutive form of the channel is formed known as I_{KAchC}. This is driven by phosphorylation from a change in protein kinase C (PKC) isoform from PKCα to PKCε as demonstrated in canine model of atrial tachycardia remodelling at 400bpm[121,122]. The upregulation of I_{KAchC} decreases action potential duration.

1.4.2.3.4 Upregulation of Small Conductance Calcium Activated Potassium Channels

Genes KCNN1, KCNN2 and KCNN3 encoding for small conductance calcium activated potassium channels have also been found to be upregulated in AF and in the presence of raised intracellular calcium[123]. Their action in maintaining of AF is believed also to be via reduction in action potential duration.

1.4.2.3.5 Gap Junction Remodelling

Gap junctions linking atrial myocytes include connexin 40, (gene GJA5) and connexin 43 (gene GJA1). It is felt that a combination of reduction in connexins and their lateralisation contributes to a fall in conduction velocity, heterogenous conduction between myocyte strands and disorganised conduction promoting re-entry. Consequently, numerous studies involving human and animal models have been conducted to examine changes in the expression and distribution of connexins with AF[124]. However, there are contradictory results even in similar models. For example, two studies used human right atrial tissue with long standing persistent AF.

One group found an increase in connexin 40 expression but no change in connexin 43[125]. In contrast, the second group found a decrease in both forms of connexin[126]. Interestingly, there is a consistency in results for distribution of connexins – with a greater lateralisation being found in AF over SR[124].

1.4.2.4 Structural Remodelling

Alongside molecular changes allowing for triggers and electrophysiological substrate for maintenance of AF, structural changes in the atria must occur to support the propagation of the arrhythmia. This is formed firstly by having atrial dilatation to the point of allowing arrhythmic re-entry, a concept described in section 1.4.1.3 and demonstrated with the correlation of LA diameter >4.5cm with AF persistence and recurrence[127]. Secondly, through the presence of atrial fibrosis.

Fibrosis is a maladaptation to injury, which in the case of the atria is a result of raised atrial pressures. Fibrosis provides structural substrate for AF through its electrically inert nature. Interruption of myocyte bundle continuity, creating local conduction disturbances and zig-zag style propagation causes a decrease in conduction velocity across the atria and the potential for electrical micro re-entry.

The creation of atrial fibrosis on a molecular level occurs via two pathways. The first is via calcium dysregulation within pre-existing fibroblasts. Increased atrial pressures result in atrial stretch channels TRPM7, SAC, and TRPC3/6/7 opening, increasing intracellular calcium load[128]. The raised calcium level then promotes fibroblast proliferation and differentiation into myofibroblasts[129]. The second route sees the increased expression of pro-inflammatory mediators such as angiotensin II and TGFβ. Through membrane bound receptors, these mediators activate pathways such as the cleaving of PIP_3 to IP_3 and DAG which releases calcium from endoplasmic reticulum stores, and opens the stretch mediated calcium channels mentioned before. Consequently, this pathways further upregulates pro-fibrotic genes, fibroblast proliferation and differentiation[128].

Although the development of atrial fibrosis on a molecular level is becoming clearer, how different clinical factors affect its genesis is uncertain. It would seem logical that individual risk

factors for AF would correlate with the presence of atrial fibrosis. Indeed, in experimental animal models, hypertension[130], obesity[131,132], obstructive sleep apnea[132,133], diabetes[134], and heart failure[135] have all been found to be associated with atrial fibrosis[136]. However, in humans the evidence is less clear, with one study using delayed enhancement MRI (DE MRI) finding the severity of LA fibrosis in patients with AF to be independent of cardiovascular risk factors[137]. A similar finding was demonstrated in an autopsy study between patients with and without AF. Although patients with AF had 3 to 5-fold greater LA fibrosis, the CHA_2DS_2-VASc score between the two groups were similar, (3.8 +/- 1.8 in AF patients, 4.3 +/- 1.9 in no AF patients)[138].

So, although there is experimental evidence for risk factors giving rise to LA fibrosis, this has not translated to humans clinically. This gives rise to a second notion, that perhaps AF itself could perpetuate fibrosis, that is the concept of 'AF begets AF.' Although this concept may be true with regards to electrical remodelling, the evidence for structural remodelling is less clear. For example, if AF itself perpetuated the development of fibrosis, one would expect a regression or plateau in LA fibrosis with maintenance of SR. That is, a process of reverse remodelling. Reverse remodelling has been demonstrated in patients with AF secondary to mitral stenosis following commissurotomy. Atrial voltage amplitude used as a surrogate for fibrosis on electroanatomical voltage mapping was shown to increase at 6 months postoperatively[139]. However, this condition is the exception and not the rule. Patients with lone AF following ablation show a further decrease in mean voltage amplitude across their LA despite elimination of AF[140].

This gives rise to a third concept - a progressive fibrotic bi-atrial cardiomyopathy (FACM), a primary condition that progresses independent of cardiovascular risk factors or the presence of AF[141]. With time, FACM gives the structural substrate required to initiate and maintain AF. Furthermore, FACM has been linked to other arrhythmia including atrial tachycardia and sinus node disease[142,143].

1.4.2.5 Autonomic Nervous System Remodelling

The autonomic nervous system (ANS) is capable of regulating the bioelectricity of the atria in response to a stimulus. Thus, it stands to reason that alterations in its function are capable of affecting AF initiation and maintenance. Interestingly this involves both sympathetic and parasympathetic pathways.

The sympathetic nervous system contributes through adrenergic effects. Activation of cardiac G-protein linked β adrenoceptors leads to activation of protein kinase A, phosphorylation of RyR2, and PLB. Overstimulation of this pathway leads to calcium dysregulation as described in Section 1.4.2.2. Parasympathetic pathways involve the cholinergic stimulation of muscarinic M_2 receptors, activating the I_{KACh} channels and reducing action potential duration as described in Section 1.4.2.3.3.[144]

With long standing AF, ANS remodelling is seen with increased sympathetic and parasympathetic nerve densities in canine models[145-147] and sympathetic hyperinnervation and nerve 'twigs' in humans[148,149]. Interestingly, although individual hyperstimulation of either side of the ANS can induce AF,[150] it is simultaneous stimulation that are more likely to trigger the onset of atrial arrhythmia[151].

Ganglionic plexi are clusters of ANS nerves located in the epicardial fat pads. Four are positioned at the left atrial-pulmonary vein junctions[152]. Stimulation of ganglionic plexi via injection of a parasympathomimetic or rapid pacing increases ectopy at the pulmonary veins and can provide an effective trigger to initiate AF[147,153]. This has led to ganglionic plexi becoming an ablation target, particularly for patients believed to have a vagal trigger for paroxysmal AF[154].

1.4.3 Mechanisms of Atrial Fibrillation

Multiple hypotheses exist for the underlying mechanism of AF which have been conceived and developed over the last 100 years. They involve focal discharges, macro- and micro- re-entrant mechanisms and complex interactions between myocardial layers. Each hypothesis has a considerable evidence base, and reflecting the complex nature of AF, and the compatibility of hypotheses with each other, their concomitant existence of them seems plausible if not extremely likely.

1.4.3.1 Ectopic Focus Firing

Scherf *et al* demonstrated AF could be initiated through ectopic focus firing using aconitine in an ovine model[7]. This theory was then supported by Haïssaguerre *et al* who noted ectopic pulmonary vein firing could trigger AF and successful abolition with focal pulmonary vein ablation and later pulmonary vein isolation could prevent AF[12,155]. Later, further ectopic foci were identified at other sites including (but not limited to) the superior vena cava, the ligament of Marshall, across the atria, coronary sinus, and crista terminalis[156].

1.4.3.2 Multiple Wavelet Hypothesis

The multiple wavelet hypothesis is the presence of multiple co-existing independent waves of depolarisation which weave through non-refractory atrial tissue. The description of the multiple wavelet hypothesis for fibrillatory conduction was first described by Garrey in 1914[157]. Mo and Abildskov applied this concept to AF, describing the:

"…spread of an irregular wavefront which becomes fractionated as it divides about islands or strands of refractory tissue[8]."

They noted the persistence of AF depended on the number of wavelets present, that being a greater number had less chance of merging, creating a universally refractory state, and terminating the arrhythmia. In turn, the number of wavelets present was dependent on the atrial mass, their conduction velocity and the refractory period of the tissue[8]. The existence of the multiple wavelet hypothesis was further evidenced by computer models[158], and intra-operative epicardial electrophysiological studies demonstrating the presence of multiple macro re-entrant circuits with pacing induced AF[159,160].

1.4.3.3 Spiral Waves and Rotors

The concept of spiral waves and rotors developed from computer models in the early 1990s[161]. Rotors have been demonstrated in humans with AF using advanced electrophysiological mapping systems called focal impulse and rotor modulation (FIRM)[162]. Rotors are able to meander through the atria, degenerating the spiral wave into fibrillatory conduction, or they can

be found to anchor to specific areas, typically a border between healthy and fibrotic tissue, which could provide a source similar to an ectopic focus[163,164].

1.4.3.4 Endocardial – Epicardial Re-entry

To add a literal dimension of complexity to AF mechanisms, detailed combined epi- and endocardial mapping studies have revealed the arrhythmia can propagate through myocardial layers[165-167]. These studies reveal that both layers have asynchronous activation patterns. With this, any bridging conduction tissue gives the potential for activation to travel between myocardial layers – known as a breakthrough wave. Additionally, this gives the theoretical possibility of re-entry, whereby a breakthrough wave travels from one layer to another by one bridge and returns via another.[168]

One small study noted breakthrough in 65% of all focal fibrillation waves[166]. Furthermore, in patients with long standing persistent AF the number of identified transmural breakthrough waves is 4-fold higher than those with acutely induced AF[167]. The ability of fibrillation waves to transverse myocardial layers, and evidence that the epi- and endocardium have asynchronous activation patterns means AF needs to be understood as a 3-dimensional arrhythmia.

1.4.4 Factors Involved in the Genesis and Maintenance of Ventricular Tachycardia

The causes of VT can be divided into structural, familial, and idiopathic, illustrated in Table 1.4.

Table 1.4 *Causes of Ventricular Tachycardia*

Category	Sub-category	Disease
Structural	Fibrosis	Ischaemic heart disease Hypertrophic cardiomyopathy Dilated cardiomyopathy Infiltrative heart disease Arrhythmogenic cardiomyopathy Myocarditis Congenital heart disease
	Non-fibrotic	Congenital heart disease Bundle branch re-entry Valvular heart disease
	Interventional	Surgical treatment of congenital heart disease
Electrophysiological	Congenital	Brugada syndrome Long / short QT syndrome Catecholaminergic polymorphic VT Early repolarisation syndrome
	Acquired	Electrolyte disorders Medications / Toxins
Idiopathic		Local VT (e.g. outflow tract) Fascicular VT

Reflecting this considerable number of disorders, the mechanisms underlying VT can vary significantly between patients. However, fundamentally the arrhythmic mechanisms for VT of increased automaticity, triggered activity, and re-entry remain the same.

1.4.4.1 Genetics

Several genetic mutations and associated syndromes are linked to ventricular arrhythmogenesis.

Some mutations result in the malfunction of ion channel subunits affecting action potential duration, refractoriness, and conduction velocity. Consequently, by providing electrophysiological

heterogeneity across the myocardium, a patient is pre-disposed to functional re-entry. An example here is Brugada Syndrome, which currently has associated 20 genes. The most common of which is SCN5A, which codes for the α-subunit of the sodium channel carrying I_{Na}. Indeed, as of 2010, 293 individual mutations in SCN5a had been identified[169].

Other mutations involve the generation of anatomical obstacles, particularly in the form of fibrosis, again predisposing to re-entry. An example here would be arrhythmogenic cardiomyopathy, where mutations in desmosome proteins lead to myocyte apoptosis and fibro-fatty infiltration. As of 2016, 11 genes have been identified that result in an arrhythmogenic cardiomyopathy phenotype, the most common being PKP2[170].

Finally, single nucleotide polymorphisms in genes coding for G-protein subunits have also been identified in association with SCD in patients receiving a primary prevention ICD[171].

1.4.4.2 Intracellular Calcium Dysregulation

Raised intracellular calcium levels can trigger and maintain ventricular arrhythmia via EADs and DADs as described in Section 1.4.2.2. Different aetiologies of VT have separate ways in which calcium dysregulation occurs.

CPVT provides increased intracellular calcium through leak of RyR2 due to a genetic mutation[172]. Long QT syndrome type 8, has a mutation in CACNA1C encoding a subunit of LTCC, increasing $I_{Ca\text{-}L}$ and the inflow of calcium during phase 2[173].

In heart failure multiple changes occur. There is upregulation[174] and increased activity[175] of NCX[176], downregulation of SERCA2a[177] and decreased PLB phosphorylation[178], resulting in decreased uptake of calcium back into the sarcoplasmic reticulum. Additionally, CAMKIIδc isoform is upregulated, modulating RyR2 and further affecting calcium levels[179].

1.4.4.3 Electrical Remodelling

Similar to AF, pathological electrical remodelling occurs in ventricular myocytes which predisposes to arrhythmia. However, in contrast, due to the secondary nature of VT, there are subtle differences in the electrical remodelling processes between pathologies. As the two most common causes of ventricular arrhythmia, myocardial infarction and heart failure shall be discussed.

1.4.4.3.1 Acute Myocardial Infarction

As the most common cause of sudden cardiac death[180], MI induced acute electrical remodelling has been extensively researched. The experimental evidence here is based upon animal models. However, there are limitations to be noted, with differences in species used, and experimental conditions, (e.g. methods of inducing MI, or how the heart is perfused). Furthermore, the rapid electrical changes that occur make measurements of specific ions, molecules or currents challenging to the point of impossibility[181]. Presently, precise mechanisms have not been fully elucidated. To combat these difficulties, computer simulations of the changing electrophysiological properties are used, with the acceptance that their data input is from incomplete animal models[182].

However, what is clear is heterogeneity in electrophysiological properties gives rise to the substrate for re-entry, the development of VT and potential deterioration to VF.

Electrical remodelling seen with MI proceeds through three phases, acute (less than 1 hour), subacute (less than 72 hours) and chronic[183]. Current research[182] shows the following ionic changes occur acutely:

1. Raised intracellular sodium and calcium;
2. Raised extracellular potassium;
3. Decreased intracellular ATP and pH;
4. Decreased extracellular sodium.

Computer simulations show these changes are caused by a combination of inhibition of the Na^+/K^+ ATPase pump, increased activation of I_{KATP} and a new ischaemia activated sodium current I_{NaS}[181].

Consequently, changes in action potential morphology begin to take place. Increased extracellular potassium raises the phase 4 resting potential from -85mV to -60mV and gives a slow recovery of sodium channels from inactivation extending the effective refractory period[181]. A decrease in I_{Na} from inactivation of sodium channels and a reduced transmembrane gradient results in a slow phase 0 upstroke which is biphasic due to I_{NaS}[184]. Reduced phase 0 upstroke decreases action potential amplitude[185]. Hypoxic inhibition of the transient outward potassium current I_{to} eliminates the classic phase 1 notch[186]. A decrease in $I_{Ca\text{-}L}$ shortens the phase 2 plateau phase, leads rapidly into phase 3 repolarisation which is accelerated by ischaemia activated $I_{K\text{-}ATP}$, and further reduces the action potential amplitude and duration, (Figure 1-9)[183].

Figure 1-9 *Action potential morphology changes with acute myocardial infarction Reproduced from Rodriguez et al (2006)[182] with permission from Wiley.*

With progression of the infarction, myocytes within the ischaemic zone eventually become unresponsive due to anoxia. The acute electrical remodelling occurs at different rates across the infarction, giving rise to electrophysiological heterogeneity within, and in layers from the sub-endocardium to the sub-epicardium[182]. These differences in action potential duration, effective refractory period and conduction velocity are particularly notable at the scar/infarction border zone and leaves the substrate required for re-entry to begin following an extra stimulus[187].

After 72 hours, myocyte necrosis from the infarction is gradually resorbed and replaced with collagen. This forms a scar surrounded by a border zone with altered electrophysiological properties. At this time, animal studies show upregulation of I_{KAS}[188] and downregulation of $I_{Ca\text{-}L}$[189-

[191] which results in an earlier and faster repolarisation with a decrease in action potential duration.

However, as time progresses electrophysiological properties further evolve with eventual normalisation of action potential duration. In a canine model, at two weeks the I_{to} current begins to return, giving the action potential its classic phase 1 notch. By 2 months this process has fully remodelled. $I_{Ca\text{-}L}$ is dampened at 2 weeks and is compensated by increased T-type calcium currents ($I_{Ca\text{-}T}$) returning a phase 2 plateau[189,190]. At 2 months, $I_{Ca\text{-}L}$ remains abnormal however the plateau normalises suggesting compensation from other transmembrane currents. The phase 4 resting potential, action potential amplitude, and phase 1 upstroke velocity return to normal by 2 weeks[189,192].

1.4.4.3.2 Heart Failure

In contrast to MI, heart failure provides the triggers and substrate for ventricular arrhythmia through electrical remodelling that prolongs the action potential duration, (Figure 1-10). Initially this prolongation is compensatory, increasing contractile strength and lowering heart rate to maximise cardiac output[177,193]. However, as the disease progresses, these changes become maladaptive, setting up the required electrical heterogeneity for VT.

Electrical remodelling in heart failure occurs through a combination of:

1. Decreased outward potassium currents, (I_{to}, I_{Kir});
2. Increased inward sodium currents (I_{NaL});
3. Alteration in calcium current kinetics, ($I_{Ca\text{-}L}$);
4. Increase in the activity of NCX.

Regarding potassium currents, animal studies with tachycardic pacing induced heart failure show a downregulation of the Kv4.3 gene[177]. Coding for a potassium channel subunit, Kv4.3 downregulation results in a decreased I_{to}, prolonging phase 1 of the cardiac action potential. Downregulation of the inward rectifier current (I_{K1})[175], and the delayed rectifier current, (K_s), further delays repolarisation in phase 3, increasing the chances of EADs.

Changes of I_{Na} in phase 0 of the cardiac action potential in heart failure are unclear with studies showing variable results. No change, increased and reduced conductance have all been reported[194]. However, there is more consistency with the late sodium current, I_{NaL}, which is increased and has a delay in inactivation. As this inward current flows during phase 2, it extends action potential duration increasing EADs[195].

Intracellular calcium regulation is abnormal in heart failure as described in Section 1.4.4.2, and associated with this are alterations in $I_{Ca\text{-}L}$. However, the exact changes in $I_{Ca\text{-}L}$ have not been fully elucidated, with studies showing both a decrease and no change at all. Interestingly, it appears L-type calcium channel membrane density is decreased, but an increase in phosphorylation increases their opening probability compensating for this[196,197].

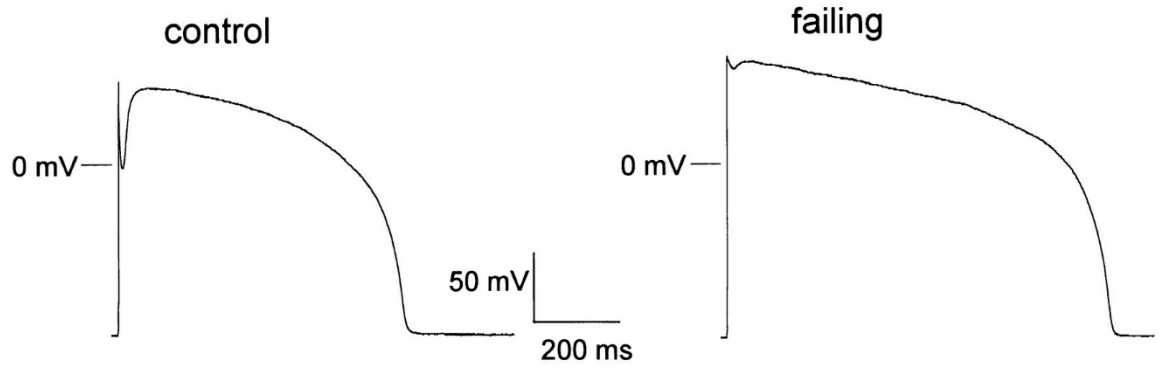

Figure 1-10 *Action potential morphology changes with heart failure.*
Electrical remodelling results in a larger action potential with a greater duration.
Reproduced from Kaab et al (1996)[198] with permission from Wolters Kluwer.

As mentioned above, an increase in action potential duration can be a compensatory process for those with heart failure. However as with MI, changes in the electrophysiological properties creates increased heterogeneity across the myocardium which sets up the required substrate for re-entry. This is also seen across myocardial layers, with prolongation of action potential duration seen in the endocardium and mid-myocardium over the epicardium.[199]

1.4.4.3.3 Gap Junction Remodelling

Similar gap junction remodelling processes are seen with ventricular arrhythmias regardless of aetiology. Heterogenous changes in connexin expression, density and distribution all occur. Similar to the atria, connexin 43 is the most common gap junction. Connexin 43 is downregulated by up to 50% in animal models with heart failure,[200,201] and are decreased in number and size in healed canine infarctions[202]. Furthermore, expression was found to be lower in the subepicardium compared to mid-myocardium or subendocardium, effectively decoupling myocardial layers and accentuating differences in conduction velocity between them[201]. Dephosphorylation of connexin 43 in rabbit and human hearts with heart failure also impairs their conductance and further decouples adjacent ventricular myocytes[203]. Redistribution of connexin 43 away from intercalated discs in a process termed lateralisation is seen in both heart failure and myocardial infarction[204-206]. Interestingly however, this is not associated with an increase in transverse conduction velocity, suggesting the function of these gap junctions is also impaired[207]. The electrophysiological alterations caused by lateralisation of gap junctions are associated with re-entry and increased probability of ventricular arrhythmia.[208]

1.4.4.4 Structural Remodelling

Alongside electrical remodelling, ventricular fibrosis provides the necessary substrate for re-entry.

The most common way fibrosis is formed is following MI. Through a complex interaction of inflammatory cytokines, myocardial necrosis is resorbed and followed by the deposition of a collagen-3 based matrix with proliferation of myofibroblasts forming a fibrotic scar. As weeks and months pass the scar matures and contracts as collagen-3 is replaced by collagen-1[209].

However, the formation of fibrosis is also seen in a wide variety of cardiac conditions including hypertrophic cardiomyopathy, dilated cardiomyopathy, cardiac sarcoid, arrhythmogenic cardiomyopathy, myocarditis and congenital heart disease[210].

Within areas of fibrosis, surviving myofibril bundles exist and via adjacent connections can transverse the entirety of the scar. The connections between the myofibrils are not orderly or

efficient, instead viable connections weave from one end to the other. Consequently, and in combination with the electrical remodelling noted above, conduction through the scar occurs slowly and weaves as a zigzag[211]. Furthermore, areas of fibrosis can have multiple entry exit points, resulting in multiple VT morphologies that can occur from one scar.

Myocardial fibrosis also shows different patterns depending upon the aetiology. For example, following myocardial infarction fibrosis is typically focal, in a coronary artery territory, and sub-endocardial reflecting the focus of the anoxic insult. Myocarditis on the other hand shows patchy diffuse scar which is focused in the mid-myocardium or sub-epicardium. Sarcoidosis generates multiple islands of fibrosis spread across the sub-epicardium and sub-endocardium[210].

For risk stratification for ventricular arrhythmias in the presence of fibrosis, studies have consistently shown the increase in scar extent, heterogeneity, border zone size, number, and location all increase the incidence of ventricular arrhythmias and mortality, regardless of aetiology[212-217].

From an interventional standpoint, knowing the anatomy of ventricular scar has become increasingly important, as it can affect the requirement for therapy with an ICD, and planning ventricular ablation strategy.

1.4.4.5 Autonomic Nervous System Remodelling

Alterations in autonomic nervous system anatomy and function are seen in patients with ventricular arrhythmias. Augmented sympathetic nervous system (SNS) activity is pro-arrhythmic, whilst parasympathetic nervous system (PNS) activity is anti-arrhythmic[218].

Following acute MI, increased SNS activity[219,220] and denervation at the site of the infarction occurs[221,222]. Increased SNS activity raises local catecholamine levels whilst denervation results in increased adrenergic sensitivity[221,223]. This combination provides triggers through EADs and DADs, whilst providing substrate by reducing local action potential durations and widening electrophysiological heterogeneity[224]. Illustrating the clinical importance of this, when assessing

patients with ischaemic cardiomyopathy by positron emission tomography, the degree of sympathetic denervation was seen to correlate with the incidence of ventricular arrhythmias and appropriate ICD therapy[225].

Following denervation, peripheral neurons respond by attempting to regrow, forming nerve sprouts which hyperinnervate the area, particularly at scar border zones[226]. This hyperinnervation is associated with greater ventricular arrhythmias both following MI and in heart failure[227].

Elevation in neurotransmitters are seen, with increased neuropeptide Y and noradrenaline levels[228-230]. Acetylcholine release from parasympathetic neurons is inhibited by the action of these hormones, tilting the autonomic balance towards the SNS[231]. In heart failure, downregulation of α_2 receptors peripherally relaxes the negative feedback cycle that inhibits noradrenaline release, further raising noradrenaline levels[232].

PNS dysfunction is also seen post MI. Decreased parasympathetic afferent neurotransmission from aortic and carotid baroceptors decreases vagal tone and is associated with greater risk of arrhythmia[233].

1.4.4.6 Altered Renin-Angiotensin-Aldosterone System Activation

Finally, alterations in the renin-angiotensin-aldosterone (RAAS) can influence the creation of substrate and triggers for ventricular arrhythmias. Decreased cardiac output, either from heart failure or MI results in activation of RAAS, increasing systemic levels of angiotensin 2 and aldosterone. Angiotensin 2 increases release of noradrenaline[234] and is pro-arrhythmic through renal loss of potassium and magnesium. Aldosterone is associated with interstitial fibrosis and cardiac hypertrophy, contributing to the arrhythmic substrate[235].

Endothelin 1, a vasoconstrictor, has also been found to be increased in decompensated heart failure[236]. Elevated levels of endothelin-1 have been shown to correlate with incidence of VT in animal studies[237,238].

1.4.5 Mechanisms of Ventricular Tachycardia

1.4.5.1 Re-Entry

VT is most commonly caused by re-entry about a structural abnormality. Typically, this abnormality is the border zone of an area of fibrosis but could be a congenital defect or iatrogenic from surgical intervention. In order to explain the mechanism of initiation of VT, long standing ventricular fibrosis in ischaemic cardiomyopathy is taken as an example.

A normal beat occurs. A wave of depolarisation followed by a wave of repolarisation flows through the ventricular myocardium. In reaching the area of fibrosis, the waves enter, slow down and weave through the fibrosis via surviving strands of tissue[211]. Meanwhile the rest of the normal myocardium depolarises and repolarises. Due to multiple potential exits within the fibrosis, the waves also enter on the other side, colliding with the propagation moving slowly through and terminating it.

A perfectly timed premature ventricular extrastimulus then occurs. This travels through the ventricles in all areas that have repolarised, such as the normal myocardium, but not through areas that are still refractory, such as the original entrance into the fibrosis which has altered electrophysiological properties. However, it can enter through another non-refractory entrance, and weave through the fibrosis as before. This time there is no extrastimulus (or normal stimulus for that matter), and the myocardium is electrically quiescent, compensating for the previous premature beat. During this time, the extrastimulus wave of depolarisation emerges from the fibrosis. If the tissue at its exit has repolarised, it will be depolarised once again. This new depolarisation can then travel through any repolarised myocardial tissue, including back to the entrance to the area of fibrosis it entered from. Consequently, setting up a re-entry circuit about an anatomical object resulting in VT.

It should be mentioned that this is one mechanism of setting up re-entry with VT. A vital component is electrophysiological heterogeneity that causes spatial dispersion of conduction velocity and refractoriness. Re-entry circuitry is highly complex, particularly when involving large, or islands of fibrosis with multiple potential entrances, exits and pathways.

VT can also occur via functional re-entry and the development of rotors. If anatomically stable these rotors generate monomorphic VT, whilst if they wander their waves can collide, degenerating into VF[34].

1.4.5.2 Other Mechanisms

Other mechanisms of VT are associated with particular aetiologies. These include increased automaticity, for example, from Purkinje cells in the subacute phase of MI, or self-perpetuating triggered activity from EADs or DADs, for example, idiopathic right ventricular outflow tract (RVOT) VT or long QT syndrome[182].

1.5 Treatment

1.5.1 Atrial Fibrillation

There are two key decisions to make between clinician and patient in the treatment of AF. The first and most important is to decide whether to commence anticoagulation or not. The second is to decide which strategy to adopt, rate or rhythm control.

1.5.1.1 Anticoagulation

Until recently the only prognostic intervention for AF was anticoagulation[239,240]. Previously this was achieved with warfarin, but more recently direct oral anticoagulants (DOAC) have been prescribed. Indeed, in March 2018 prescriptions of direct oral anticoagulants in the UK superseded warfarin for the first time. As of July 2020, there are 1.15 million active prescriptions for DOACs, and 461 000 for warfarin[241]. Apixaban and Edoxaban both showed superiority to warfarin for stroke, embolism and mortality with lower major bleeding rates[242,243]. Dabigatran also showed superiority to warfarin for stroke and embolism without significant difference in mortality or bleeding rates[244]. Rivaroxaban showed non-inferiority to warfarin[245]. Patients are anticoagulated in the absence of contraindications and if their risk of stroke is greater than that of a life-threatening bleed. This is weighed up clinically by a physician and assisted by scoring systems such as CHA_2DS_2-VASc[246] and HASBLED[247].

Alongside anticoagulation, modifiable risk factors contributing to AF are addressed. Abstinence from alcohol, weight loss, adequate exercise, and optimisation of co-morbidities are all advised in international guidelines[35,248].

1.5.1.2 Rate vs Rhythm Control

The next step in AF management is to decide upon a rate or rhythm control strategy.

Rate control involves accepting permanent AF and lowering a patient's ventricular rate to < 110bpm[35,249]. Rate control is achieved through medication, usually via a beta blocker, calcium channel blocker, or digoxin. Alternatively, rate control can be achieved through implantation of a permanent pacing device and disconnecting atrioventricular conduction through an AVN ablation.

Rhythm control involves restoring and maintaining sinus rhythm using antiarrhythmic medication, DC cardioversion (DCCV), a Cox-MAZE procedure or catheter ablation. Anti-arrhythmic medication acts by blocking ion channels that affect the morphology of the cardiac action potential and therefore the refractory period[250]. This alteration interferes with the electrical substrate used to maintain AF with the aim of terminating it and/or maintaining SR.

DCCV acts by passing an external electrical current through the heart of a sedated patient to render the entire myocardium refractory, terminating AF (or any other arrhythmia), and allowing the SAN to restart normal conduction with SR. DCCV is used for patients with persistent AF, as by definition their AF is unable to terminate spontaneously.

A Cox-MAZE procedure is a surgical treatment which has evolved since its inception in 1987[11]. The current Cox-MAZE IV procedure involves performing bipolar radiofrequency ablation through atriotomies to the LA and RA, (Figure 1-11). In the LA, the pulmonary veins are isolated, whilst connecting roof, floor and mitral lines are created. In the RA, a superior to inferior vena cava line, two tricuspid valve lines, and a right atrial free wall lesion set is applied. Cryoablation is then also applied to the coronary sinus and the ends of the mitral and two tricuspid lines to minimise the risk of damage to the valve apparatus. The Cox-MAZE procedure allows for

transmission between SAN and AVN whilst isolating the most common sites of triggers for AF and disrupting potential anatomical re-entrant circuits[251].

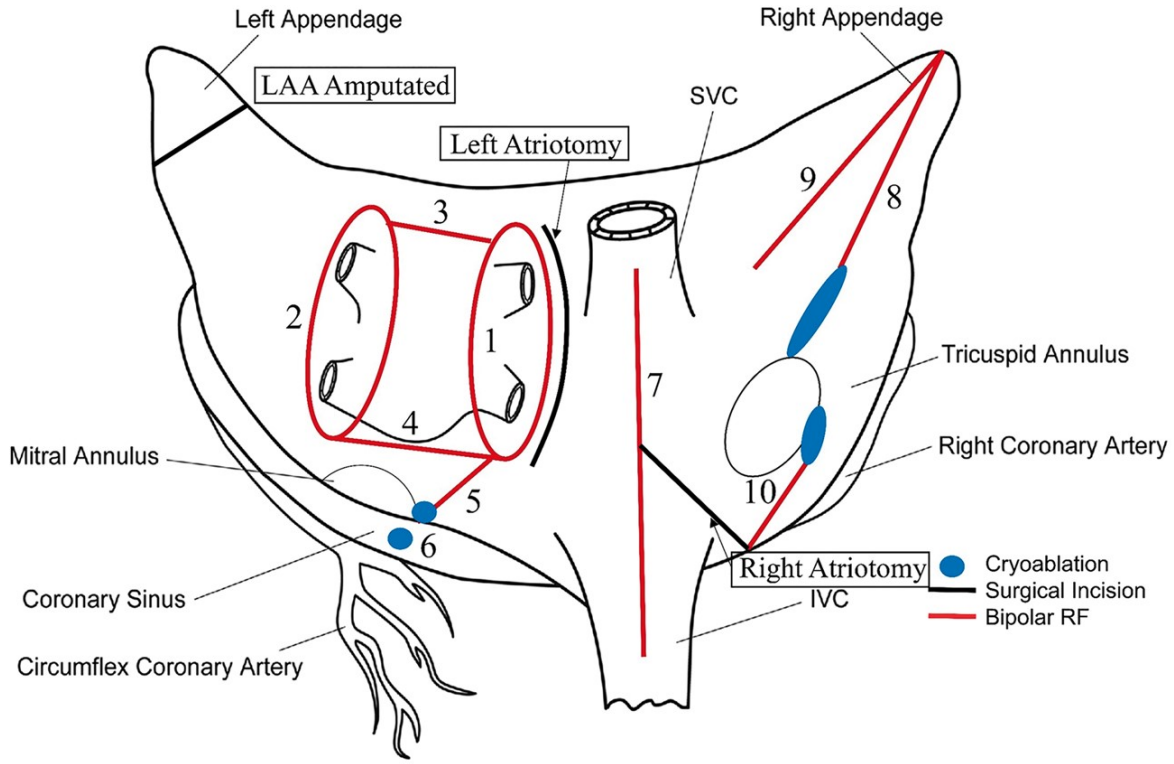

Figure 1-11 *The Cox-MAZE IV procedure lesion set.*
Reproduced from Ruaengsri C et al (2018)[251] and adapted from Lall S et al (2007)[252] with permission from Oxford University Press and Elsevier.

Although effective, the advent and advancement of interventional catheter ablation limits the indications to perform a Cox-MAZE procedure largely to patients with AF who are undergoing concomitant cardiac surgery for other reasons[35].

Until recently, deciding between a rate or rhythm control strategy was seen to be purely a decision based upon a patient's symptoms, as several smaller trials,[253-256] and then the landmark AFFIRM trial[257] comparing these strategies had shown no mortality benefit to rhythm control. Indeed, there were even significantly more hospitalisations and medication side effects necessitating withdrawal in the rhythm control arms. Furthermore, quality of life scores was comparable between arms in an AFFIRM sub-study[258].

However, post-publication on-treatment analyses of AFFIRM discovered the presence of SR was associated with a 47% lower risk of mortality. This however was offset by a 49% increase with the use of antiarrhythmic drugs[259]. This mortality improvement in the maintenance of SR was also seen in the DIAMOND study, independent of the use of dofetilide[260]. This was particularly seen in patients with reduced left ventricular systolic function[261,262]. Consequently, this was hypothesis generating that maintenance of SR could provide a prognostic as well as symptomatic advantage in subsets of patients.

Until September 2020, rhythm control for AF was a strategy for managing patients who are symptomatic despite adequate rate control. However, management recently became more complex with the publication of the EAST-AFNET4 trial which compared rhythm control (of any method), against usual care (rhythm control only if symptomatic after trial of rate control) for patients with early onset AF (<1 year)[263]. EAST-AFNET4 found that rhythm control was superior in improving a composite outcome of death, stroke or serious adverse events at 5 years, consequently, opening up the rate vs rhythm control discussion once again.

1.5.1.3 Catheter Ablation

Catheter ablation involves the delivery of energy to create lesions to modify or electrically isolate triggers or substrate of AF. The technology involved has evolved rapidly over the last 20 years.

Since the initial rate vs rhythm trials almost 20 years ago, catheter ablation has become widespread. Catheter ablation was used minimally for rhythm control in AFFIRM. By negating the potential use of anti-arrhythmic medications, catheter ablation was seen as an intervention that could show a mortality benefit for rhythm over rate control. However, interestingly in a large prospective trial the same findings have been found. The landmark CABANA trial showed no mortality benefit to catheter ablation against medical therapy for all comers with AF in its intention to treat analysis[264]. However, there was improvement in quality of life,[265,266] and specifically mortality benefit for those with heart failure, an effect that were then repeated in the CASTLE-AF[267] trial.

Consequently, reflecting the outcome of EAST AFNET4, and with the symptomatic and potential prognostic value of catheter ablation, the procedure will likely be fundamental in treatment plans for AF for years to come.

1.5.2 Ventricular Tachycardia

The treatment options for VT are ICDs, anti-arrhythmic medication and catheter ablation. For the purposes of this thesis, the treatment options are discussed in reference to scar-mediated VT, rather than idiopathic forms of VT.

1.5.2.1 Implantable Cardiac Defibrillators

In the treatment of ventricular arrhythmias, ICDs have the greatest amount of supporting evidence for both primary and secondary prevention.

In survivors of cardiac arrest secondary to ventricular arrhythmia, multiple large international randomised controlled trials have shown a mortality benefit for ICDs over antiarrhythmic therapy[268-270]. This is regardless of whether the aetiology is ischaemic or non-ischaemic. A meta-analysis of these trials demonstrated a 50% reduction in arrhythmic mortality and a 28% reduction in total mortality[271].

For primary prevention of ventricular arrhythmias, large trials have been conducted on patients suffering with symptomatic heart failure with reduced ejection fraction. In ischaemic cardiomyopathy the evidence for ICDs is clear, with a 60% reduction in sudden cardiac death seen in the ICD arm of SCD-HeFT,[272] and a 31% reduction in all cause death in MADIT II[273], compared to usual standard of care. In non-ischaemic cardiomyopathy, initial trial data was also supportive, even if the trial size was smaller. Both the DEFINITE trial[274] and the non-ischaemic arm of SCD-HeFT[272] showed a trend towards mortality reduction. However, the more up-to-date DANISH trial using modern medical and device therapy for heart failure showed no overall mortality benefit to prophylactic ICD implantation in non-ischaemic cardiomyopathy[275]. Interestingly though, there was a significant reduction in sudden cardiac death in the ICD group, suggesting a sub-group of patients within the trial may benefit from this therapy. The recently announced randomised controlled BRITISH trial will examine whether the presence of ventricular scar detected by MRI is

a deciding factor in whether patients with non-ischaemic cardiomyopathy would benefit from ICD implantation (ClinicalTrials.gov Identifier: NCT 05568069).

Although the evidence for ICDs is strong and they are undoubtedly the foundation of treatment for VT, one must bear in mind they are also associated with complications, with up to 20% of patients experiencing an inappropriate shock at a median of 5 years follow up[276]. Hence, appropriate patient selection and discussion is of utmost importance when considering ICD implantation.

1.5.2.2 Anti-Arrhythmic Medication

A drawback in using ICDs in the treatment of ventricular arrhythmia is that they are limited to being an abortive therapy, acting only when arrhythmia occurs and not in its prevention. Experiencing a shock from an ICD, regardless if appropriate or not, can be a traumatic experience, affects quality of life[277,278] and is associated with increased mortality[279,280]. Consequently, almost all patients with an ICD will be prescribed an anti-arrhythmic regardless of whether it is for primary or secondary prevention. Beta blockers are typically the first line anti-arrhythmic used, being well tolerated and having the added prognostic effect in MI[281-283], and heart failure[284-286].

In the era of ICDs, amiodarone has been shown not to confer a mortality benefit in patients with high risk of ventricular arrhythmia[272,287]. However, it is the most effective anti-arrhythmic currently available, reducing shocks from ICDs by 73% when used in combination with a beta blocker in the OPTIC study[288]. However, amiodarone is associated with multiple potentially irreversible side effects, limiting its clinical use. Indeed a 18.2% discontinuation rate was noted in OPTIC.

Sotalol is another antiarrhythmic shown to suppress shocks from ICDs,[288,289] albeit less effective than amiodarone. However, it has a similar patient intolerance rate to amiodarone. Interestingly, the d-isoform of sotalol was shown to increase mortality and ventricular arrhythmias in post MI patients with reduced ejection fraction in the SWORD trial.[290]

1.5.2.3 Catheter Ablation

Catheter ablation aims to suppress scar mediated VT through disrupting the arrhythmic circuitry vital to its maintenance.

Multiple randomised control trials have shown a morbidity benefit of VT ablation, decreasing the number of shocks patients receive from ICDs.[291-293] However, there was not a mortality benefit. The randomised VANISH trial[292] comparing VT ablation to escalation in anti-arrhythmic therapy interestingly showed a significant difference in the composite primary outcome, (mortality, VT storm and appropriate ICD shock >30 days post ablation) in favour of ablation for those patients receiving amiodarone. The difference between groups was driven mainly by fewer ICD shocks rather than mortality. Similarly, in the SMS trial (Substrate Modification Study), which randomised patients with ischaemic cardiomyopathy to an ICD plus VT ablation or ICD alone, a reduction in ICD therapies was seen in the ablation group, but no difference in mortality[294]. In this way, VT ablation can be seen as a palliative procedure, performed where patients are receiving ICD shocks despite optimisation of anti-arrhythmic medication and have consequently exhausted other therapeutic options.

Interestingly however, a recent trial has suggested that the timing of VT ablation may be important. The PARTITA trial investigated patients undergoing VT ablation after the first appropriate ICD shock versus standard of care[295]. The group undergoing VT ablation after the first shock were found to have a reduced risk of the composite outcome of mortality and heart failure admission, an effect mainly drive by the reduction in mortality.

This result may affect clinical care and guidelines in the future. Current international guidelines published before PARTITA recommend catheter ablation for those patients experiencing recurrent ICD shocks especially if they have failed anti-arrhythmic therapy[34,296].

1.6 Catheter Ablation

1.6.1 The Procedure

Cardiac catheter ablation is an interventional electrophysiological procedure performed in specialised cardiac laboratories whilst a patient is under general anaesthetic or conscious sedation.

For AF ablation, long catheters are inserted into the heart via the femoral vein. The LA is accessed by crossing the interatrial septum through a fluoroscopic or ultrasound guided puncture. The number of catheters used is dependent on the method of performing ablation, but typically involves a reference catheter being placed in the coronary sinus and an ablation catheter being inserted into the LA. If a 3D electroanatomical map is to be created a mapping catheter will also be used. Following this set up ablation can proceed accordingly.

For scar mediated VT ablation, the LV is accessed. For endocardial ablation the LV can be accessed in a similar way to AF ablation, via the interatrial septum to the LA and through the mitral valve into the LV. Alternatively, it can be accessed in a retrograde fashion via the femoral artery, the aorta and through the aortic valve. A reference catheter is placed in the RV, whilst mapping and ablation catheters are placed into the LV. If epicardial access is required, a delicate subxiphisternal puncture is performed into the pericardial space under fluoroscopic guidance. In modern VT ablation procedures, a 3D electroanatomical map is always created. Following this, ablation can then occur.

1.6.2 Energy Sources in Catheter Ablation

Several types of energy source can be used to perform catheter ablation. Each of these aims to cause necrosis and resulting fibrosis of the underlying tissue in order to render it electrically inert. Delivery methods of an energy source vary from system to system, with point-to-point catheter delivery and balloon devices being two of the most popular.

1.6.2.1 Radiofrequency Ablation

Unipolar radiofrequency ablation (RFA) has been the mainstay of electrophysiological therapy for 30 years. Before this time, successful treatment of supraventricular arrhythmias was performed with ablation administered through direct current. However, this was fraught with complications such as impaired left ventricular function and even cardiac rupture[297]. Cardiac clinical use of RFA was first reported in the successful treatment of Wolff-Parkinson-White syndrome in 1991[298]. It was then used safely and highly effectively on several supraventricular tachycardias including AVNRT, atrial tachycardia, atrial flutter and in performing AVN ablation[299].

With RFA, energy is emitted from an ablating catheter at the electrode tissue interface (ETI) as an alternating current (AC) of 350 – 700 kHz. The current flows to a large dispersive electrode as a skin patch typically on a patient's thigh, (Figure 1-12). At a typical ablation power of 30W, the RF energy causes damage at the ETI through resistive heating of the myocardium with a radius of approximately 1 mm. This heat conducts to adjacent tissues causing further damage completing the ablation lesion.

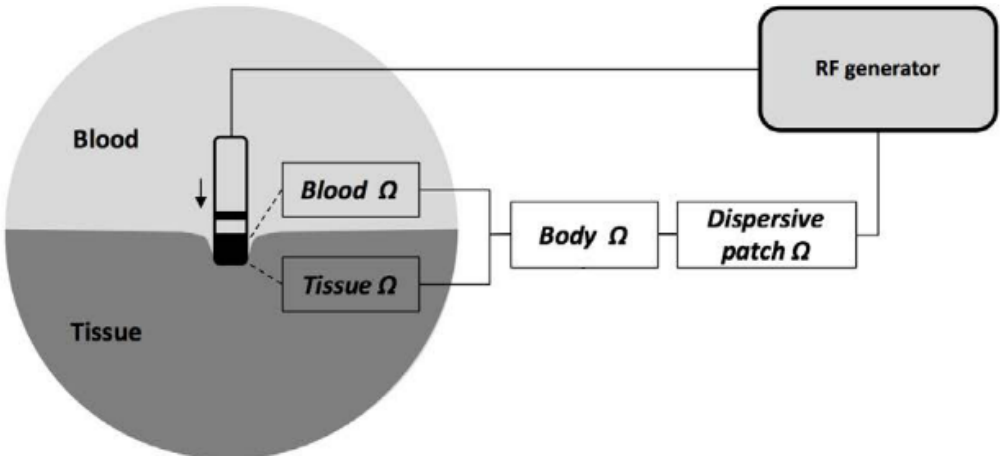

Figure 1-12 *Schematic representation of the electrical circuit in radiofrequency ablation. Adapted from Barkagan et al (2018)[300] with permission from Wolters Kluwer*

As ablation occurs and tissue temperature rises, cardiac myocytes go through a series of electrophysiological changes. At 45°C, marked depolarisation of the cell membrane occurs, followed by an increased rate of action potential rise before a fall in overall amplitude. Finally, irreversible loss of excitability of the cell occurs at temperatures greater than 50°C.[301]

Macroscopically, this results in a lesion with a pale necrotic core of coagulation necrosis surrounded by a haemorrhagic periphery. Microscopically, infiltration of inflammatory mononuclear cells and neutrophils are seen. Electron microscopy shows ultrastructural damage occurs up to 6 mm away from what is visible[302]. Chronically these lesions turn into a fibrous scar with granulation tissue, fat cells, cartilage and infiltrates[303,304].

Radiofrequency energy is most commonly applied in ablation via a single tip catheter, (Figure 1-13B). In combination with a detailed 3D electroanatomical map, using a single tip catheter allows an operator to be precise with their selection of sites to ablate, and allows tailored lesion sets to be delivered. This makes it ideal when performing ablation procedures that do not follow a standard workflow such as repeat AF ablation and VT ablation. Alternative methods of delivery include bipolar ablation, where current flows between two closely related rings forming a narrower, deeper lesion[305], or needle ablation where ablation occurs from a needle inserted within the myocardium itself in order to create deeper intramyocardial lesions[306].

Radiofrequency ablation allows an operator to vary power settings, contact force, and ablation duration can to levels desired and be changed from lesion to lesion. The disadvantage to this method is it tends to be slower[307,308], as each ablation requires time for conductive heating to occur to maximise lesion parameters, and each lesion is comparatively small being the width of the catheter (approximately 4-5mm). Furthermore, as the energy used to create an ablation lesion is from thermal heating, complications such as steam pops, tissue char and even fistulae to surrounding structures can occur.

1.6.2.2 Cryoablation

Cryoablation uses hypothermia at the catheter-tissue interface to create ablation lesions. As the tissue cools, cardiac myocytes slow their metabolism losing ion channel function leading to a fall in intracellular pH. The formation of ice crystals, initially extracellularly and then intracellularly at temperatures below -40^{o}C causes mechanical and then biochemical damage to cell organelles due to diffusion of solute ions. Microcirculatory damage also occurs with interruption of blood flow leading to tissue ischaemia. This destructive process is exacerbated during thawing, where ice crystals enlarge and amalgamate, and the damaged microcirculation

allows oedema and necrosis to occur. The result is irreversibly damaged tissue which progresses to electrically inert fibrosis[309].

Cryoablation is commonly used during de novo AF ablation procedures using a balloon delivery device, (Figure 1-13A)[307], however cryo-tip catheters are also available and are used for ablation of sites in close proximity to structures for which it is imperative no damage occurs, (e.g. the AVN). The advantages of cryoablation using balloon devices for de novo AF ablation include a large area of ablation can be administered in a single shot, they are tolerated by patients better generating less discomfort and procedures are shorter compared to RFA whilst maintaining comparable freedom from arrhythmia at long term follow up[307,308]. However, balloon ablation technology is unable to deliver a tailored lesion set similar to tip catheters, restricting its use largely to procedures within a standardised workflow.

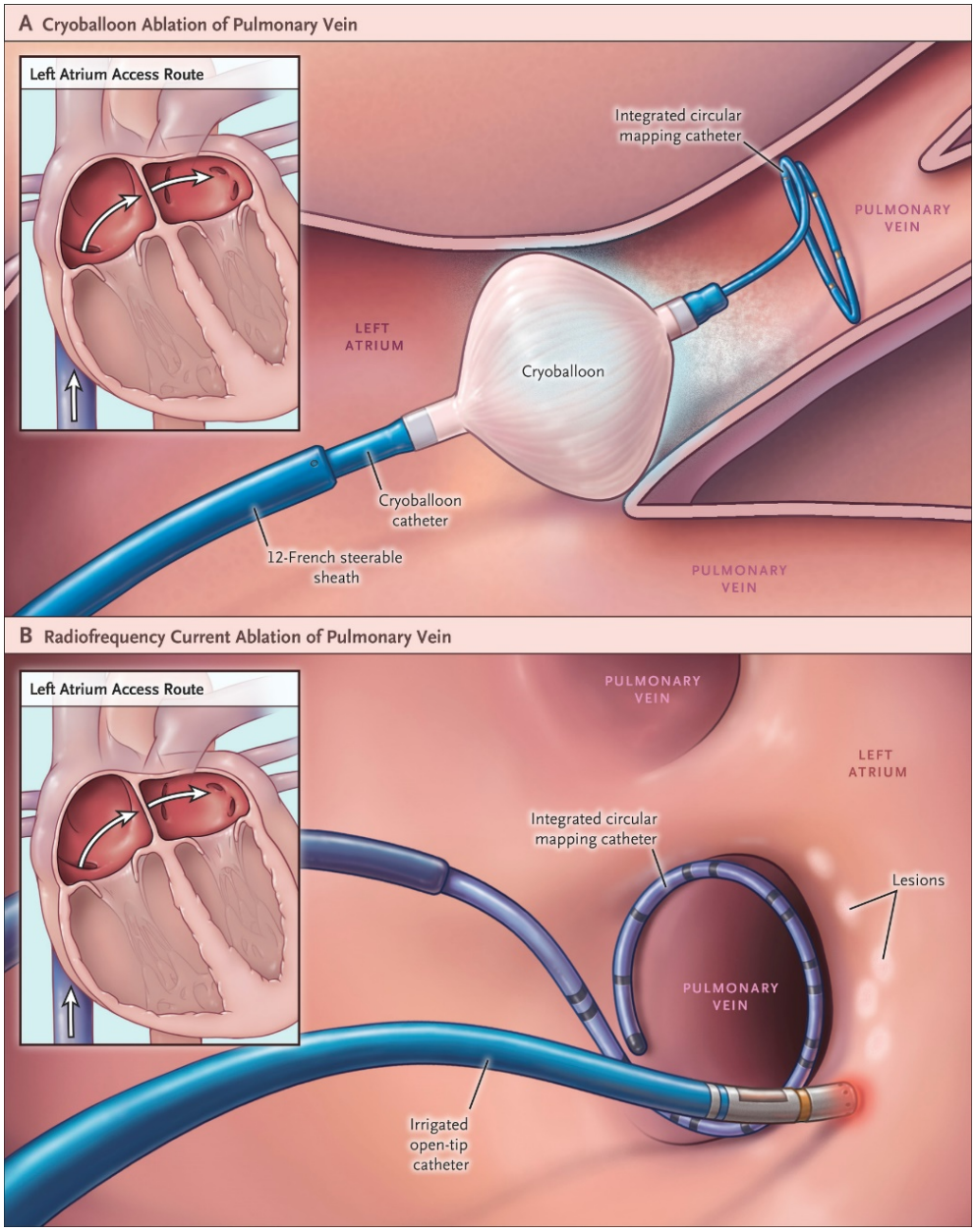

Figure 1-13 *Methods of delivering thermal energy to the left atrium.*

A = A cryoballoon is inserted into a pulmonary vein and inflated before cooling to temperatures as low as -75°C. The tissue in contact with the balloon is consequently damaged. Ideally, the circumference of the vein is in contact with the balloon, isolating the vein from the rest of the atrium in one 'freeze'

B = Radiofrequency ablation creating lesions on a point-by-point basis from the end of a catheter.

Reproduced with permission from Kuck et al (2016)[307], Copyright Massachusetts Medical Society.

1.6.2.3 Laser Energy

Laser is another energy source that uses a balloon catheter to deliver ablation lesions. Using a multi-electrode catheter, multiple overlapping administrations are undertaken until a circumferential lesion is completed. Randomised controlled trials have shown that laser balloons have comparable 1 year freedom from arrhythmia to RFA and cryoablation, but longer procedural times[310,311].

1.6.2.4 Pulsed Field Ablation

A new method of performing cardiac ablation that has recently come to market is pulsed field ablation. Using a multi-electrode catheter, pulse field ablation uses a train of high amplitude electrical pulses to create microscopic pores in the cardiac myocyte cell membrane in a process called electroporation. This results in cell death and fibrosis. Pulsed field ablation is an interesting development as it does not use thermal energy, effectively eliminating the side effects seen with these energy sources[312]. Furthermore, there appears to be tissue specificity to the electrical pulses. Usefully, cardiac myocytes have a low threshold to damage from electroporation, whilst neighbouring tissues such as the oesophagus are more resistant[313]. This allows for ablation to occur whilst minimising collateral damage to surrounding structures[314]. Early procedural results show promise for the effectiveness of pulsed field ablation in AF ablation whilst minimising complications[315].

1.6.3 Catheter Ablation for Atrial Fibrillation

1.6.3.1 Initial Attempts

Modern day techniques for catheter ablation for AF were first described by Michel Haissguerre *et al* in Bordeaux in 1998[12]. Using a multi-electrode catheter, the earliest electrical activity preceding AF (i.e. electrical activity triggering AF) was identified to originate 2 – 4cm inside the pulmonary veins in 94% of cases. Triggers were also found from both right and left atria. Following this finding, radiofrequency ablation was used to eliminate these areas. Although 67% of patients in the initial series required multiple procedures during their hospitalisation, the success of the procedure was marked with 62% of patients AF free and off anti-arrhythmic drugs at 8 month follow up. These results were replicated in other pioneering centres[316].

However, the long-term outcomes were less satisfactory, with freedom from AF documented in other '2nd wave' centres globally to be 33 – 66 % following ablation[317-319]. Furthermore, there were procedural difficulties. Some patients had inconsistent atrial ectopic firing and thus were unable to be mapped for accurate ablation. Some had multiple foci mapped and therefore a lack of clarity of where to ablate. Others could not be mapped as SR could not be sustained despite cardioversion from AF. Consequently, intention to treat analyses revealed success rates were even lower still at 23 – 28%[319,320].

The procedure was also associated with complications, including pulmonary vein stenosis rates shown on transoesophageal echocardiography as high as 42%[316,321]. Indeed, some patients required intervention with pulmonary vein balloon dilatation or stenting[318].

Procedure times were also particularly long with a mean duration documented of 7.5 hours[320]. Fluoroscopy times could also extend beyond 1 hour, delivering significant radiation doses to patients and staff[320,321].

1.6.3.2 Improvements in Technique

Refinement was needed to improve clinical outcomes from AF ablation and to decrease its complication rate and procedure time. To help accomplish these goals 3D electroanatomical mapping technology and new ablative techniques were developed contemporarily.

A new ablative technique by Pappone *et al*[155] looked not to treat the triggers of AF, but to isolate them. The pulmonary vein ostia were isolated by circular ablation lines known as a wide area circumferential ablation (WACA). This technique delivered ablation lesions in a point-by-point method to create a line effectively by 'joining the dots.' This avoided the pulmonary veins in their entirety, eliminating stenoses whilst having the added effect of capturing any extra triggers occurring from the pulmonary vein antra. The technique reported significant success with the initial study showing a freedom from AF rate of 85% at 9 month follow up and no pulmonary vein stenoses on trans-oesophageal echocardiography[155]. Although further techniques have been developed in the last 20 years, WACA and resultant pulmonary vein isolation (PVI) remains the cornerstone of AF ablation to this day[322] .

1.6.3.3 Techniques Beyond Pulmonary Vein Isolation

PVI is performed in AF ablation regardless of how progressed the disease has become within an individual. However, freedom from AF rates for persistent AF ablation have been consistently poorer than that for paroxysmal AF[323]. Successful persistent AF ablation has been shown to result in decreased symptoms, decreased hospitalisation, and improvement in left ventricle ejection fraction compared to medical therapy[324]. Consequently, there is great merit in seeking advancements in technique to improve outcomes with persistent AF ablation procedures.

Techniques in addition to PVI to treat persistent AF have often shown initial enthusiasm but then lost momentum. One such technique was the ablation of sites demonstrating complex fractionated atrial electrograms (CFAEs) which had a high success rate for freedom from arrhythmia in the primary research centre of 95%[325]. However, results could not be replicated in other centres and the large international multicentre STAR AF2 trial showed no additional benefit of CFAE ablation in addition to PVI[326]. This finding was repeated in the RASTA study[327] and the CHASE AF trial[328].

The addition of ablation lines to electrically disconnect areas of the LA associated with AF triggers such as the posterior wall have also not been found to be superior to PVI alone. In fact, in the STAR AF2 trial, patients receiving ablation lines had a significantly greater recurrence of atrial arrhythmias[326], a difference that was maintained even after repeat procedures. Stepwise ablation strategies involving both CFAEs and ablation lines in the LA and RA have also been found to be unsuccessful and in some ways inferior with an increase incidence of atrial arrhythmias[327] or increased fluoroscopy time compared to PVI alone[328].

Ablation of rotors has shown some success. However, this requires complex specialist equipment that is not widespread and integration with pre-procedural imaging. Initial studies have shown patients receiving ablation through all identified rotors had an 80% freedom from AF [104,105]. However, if a rotor source was missed this fell to 18.2%. Again, this complex system looked promising, but a 2018 meta-analysis[329] did not show any additional freedom from arrhythmia above PVI alone. Similarly, a recent randomised trial between rotor ablation and

standard of care in patients undergoing repeat procedures, showed comparable freedom from AF at 1 year[330].

1.6.3.4 Tailored Low Voltage Area Ablation

Left atrial fibrosis has been shown to be both a substrate[331,332] and trigger area[333] for AF. Consequently, the strategy of ablation or isolation of these areas has received increased attention. This strategy was first described by Rolf *et al* who performed tailored atrial substrate modification based upon low voltage areas (LVAs) as detected by a 3D electroanatomical map (EAM)[334,335]. This modification was mainly scar homogenisation, however if there was concern of collateral damage to other crucial structures (for example, the oesophagus or AVN), or creating isthmuses for potential re-entry, lines to electrically inert areas were also performed. At follow-up, freedom from AF for patients receiving this strategy was 70%. This compared to 27% for patients who were shown to have LVAs but underwent PVI alone. It was also comparable to the 62% success rate of patients who received PVI alone due to the absence of LVAs.

Box isolation of low voltage areas is another strategy described by Kottkamp *et al*[336]. In their study, 18 patients with persistent AF and LVAs received PVI with either anterior box isolation or posterior box isolation dependent on the position of their fibrosis. 13 further patients were found to have no LVAs and received PVI alone. AF free survival between these groups showed no significant difference after one, (72.2% [PVI plus box isolation for LVAs] vs 69.2% [PVI alone and no LVAs]) or multiple procedures (83.3% vs 84.6%).

A 2017 meta-analysis[337] of retrospective / observational studies of LVA guided AF ablation strategies showed a 70% freedom from atrial arrhythmias at 17 months. However, between the studies within this meta-analysis, there were inconsistencies in the definitions of LVA, the specific ablation strategy used, the mapped rhythm in 3D EAM, catheter electrode size and resolution, highlighting that despite a standardised workflow, tailored LVA ablation continued to show promise.

Further single centre studies continued to show results in favour of LVA guided ablation[338-344], before the prospective, multi-centre, randomised ERASE-AF trial provided the strongest evidence yet for its use. In 324 patients with persistent AF randomised to either PVI

plus LVA substrate modification or PVI alone, a significant difference in arrhythmic recurrence at 12 months was shown at 35% vs 50% respectively[345].

Consequently, tailored LVA ablation strategies are gaining traction with increasing levels of evidence signalling it should be used as standard of care when LVAs are present. It therefore stands to reasons that detecting and defining LVAs physiologically is of the utmost importance.

1.6.4 Catheter Ablation for Ventricular Tachycardia

1.6.4.1 Procedural Development

Catheter ablation for VT was innovated from a successful surgical procedure called subendocardial resection[346]. During this procedure performed for patients with ischaemic cardiomyopathy, the ventricular aneurysm and endocardial scar responsible for VT are resected. This was based on pre- and intra-operative electrogram recordings that demonstrated the border zone of the scar contained pre-systolic signals and therefore vital elements of the re-entrant circuitry. Although the procedure was successful, it suffered from a high operative mortality rate (5 – 15%)[347]. Therefore, in order to improve this figure and as the scar responsible for forming re-entrant circuits in ischaemic cardiomyopathy was known to be focussed in the endocardium, a logical next step was to develop an intervention using a percutaneous approach.

Radiofrequency catheter ablation for scar-mediated VT was first reported in 1993[348] with a success rate of 73% acutely and at 9 months follow up. Over the course of the next decade several advancements were made including in entrainment mapping to electrophysiologically define different sites of the re-entrant circuit[349], and substrate mapping with the advent of 3D EAM systems[350].

1.6.4.2 Mapping Strategies

Several different strategies to map VT during a procedure were refined including activation, entrainment, pace and substrate mapping. Traditionally, accurate mapping of the VT circuit and therefore a guide to optimal sites of ablation was achieved by activation and entrainment mapping.[351] However, both activation and entrainment mapping rely on a patient

being haemodynamically stable in VT, a feature present in as low as 10% of referred patients[348]. Furthermore, the VT circuits require electrical stability for the duration of mapping, and not to convert to a different circuit, or resolve spontaneously.

With this in mind, and the evolution of 3D EAM systems, substrate-based mapping and ablation have become the preferred strategy, being able to occur in underlying rhythm, or via endocardial pacing. Additionally, prospective randomised trials have shown substrate mapping to be superior to activation mapping in reducing VT recurrence, procedure time, fluoroscopy time, and intra-procedure defibrillation rates[352,353]. Finally, a recent meta-analysis of patients with haemodynamically stable VT undergoing ablation showed a statistically significant improved outcomes for substrate over standard mapping[354].

1.6.4.3 Ablation Strategies

The aim of VT ablation is to irreversibly damage the crucial components that form the re-entrant arrhythmic circuitry. Typically, this involves identifying the isthmus of delayed conduction within the ventricular scar and ablating at this site accordingly. However, in contrast to AF ablation where a workflow in WACA and PVI exists, in VT ablation, no standard ablation lesion set exists. Consequently, several different techniques exist for VT ablation[354]. These include linear lesions[355], scar homogenisation[356], scar dechannelling[357], abolition of late potentials[358,359], abolition of local abnormal ventricular activities[360], and core isolation[361]. The procedural endpoints for each of these techniques also varies making comparison of their efficacy challenging[354]. Indeed, no studies comparing VT substrate ablation strategies exist.

However, vital to all of these ablation strategies is the accurate identification of ventricular scar on a 3D EAM, therefore an operator is aware of the type of substrate they are ablating. Furthermore, knowledge of the progression of each administered ablation lesion to maximise its effect in disrupting VT circuitry is fundamental.

1.7 3D Electroanatomical Mapping

The successful treatment of cardiac arrhythmias using percutaneous methods logically lead to a desire to treat those with increasingly complex mechanisms. To achieve this, a novel imaging modality was necessary to visualise arrhythmic mechanisms, the underlying tissue substrate and the position of delivered ablation lesions. This would also help combat long procedure and fluoroscopy times.

The development of 3D EAM systems gave electrophysiologists the ability to associate intracardiac electrograms with an endocardial site for the first time. Their advantages for mapping and ablation of arrhythmia were quickly established. For the first time, an accurate, non-fluoroscopic visual representation of up-to-date intracardiac anatomy could be provided, alongside the ability to navigate this with multiple catheters. Complex arrhythmic mechanisms could be visualised, their sites of activation and propagation seen and their relationship to cardiac anatomy and scar understood. Areas of interest during mapping could be highlighted and returned to later with ease and without multiplane fluoroscopy. Appropriate sites for radiofrequency ablation could be identified with confidence. When ablating, a location could be labelled to avoid repeat applications and create effective lines to isolate arrhythmogenic substrate or triggers. Decreased fluoroscopy times were also beneficial to the patient and staff[362,363].

1.7.1 CARTO

The first 3D EAM system developed was CARTO[364] (Biosense, Inc. Israel [Pre-1998]), Biosense Webster Inc. Irvine, CA, USA).

1.7.1.1 Creating a 3D Electroanatomical Map

CARTO can detect the position of a catheter using an electromagnetic system. A locator pad is placed underneath the patient containing three coils each emitting an ultra-low magnetic field ($5 \times 10^{-6} \rightarrow 5 \times 10^{-5}$ Tesla). Using an external patch on the patient's skin as a reference, a magnetic field sensor at the tip of an invasive catheter detects the strength of each field. As distance from the coil can be correlated to the decaying strength of the magnetic field, the catheter position can be triangulated. CARTO is also able to interpret catheter orientation in

three planes – roll, pitch and yaw[350] therefore allowing an accurate position of the catheter to be displayed.

By manoeuvring the mapping catheter through the chamber of interest, CARTO can establish the intracardiac geometry and record any electrical activity at the sampled sites. The outer most points form the 'shell' – a representation of the endocardial surface. Upon the shell, electrogram voltage data is displayed for analysis. The amplitude of the electrograms collected when displayed form the electroanatomical voltage map.

The system also calculates the timing of each electrogram relative to a fiducial point. This is known as the local activation time (LAT). This fiducial point can be a stable intracardiac electrogram (for example, within the coronary sinus or the right ventricle) or from surface ECG. After multiple LAT points are taken, CARTO can display this as a colour coded map or play it a video to the operator.

1.7.1.2 Validation of CARTO

Use of CARTO was first published in 1997. In vitro and in vivo studies using a plexiglass block and swine respectively, found the system to be highly geometrically accurate and reproducible[350]. Furthermore, the LAT of intracardiac electrograms were validated using a traditional mapping catheter fluoroscopically placed next to the CARTO catheter. Here, the cross-correlation coefficient was 0.96[365].

The reproducibility and accuracy of the CARTO system extended to the delivery of ablation lesions. In a porcine model, following construction of a 3D EAM, an ablation lesion was delivered before the catheter was fully removed. The catheter was returned to the same position for a repeat lesion to be administered. On autopsy, these corresponding points were found to be closely matched, being 2.3 ± 0.5 mm to each other. Operators were also able to accurately create and measure an ablation line using up to 12 lesions[365]. This accuracy was repeated in AF by creating ablation lines in the left and right atria in goats[366]. CARTO was then used accurately in humans in for the first time in 1998[367].

1.7.1.3 CARTO3

Over the course of the last 20 years the CARTO system has had several technological upgrades. The current third generation system is CARTO3. CARTO3 has a more refined location system which also uses relative electrical current. 6 detection patches are placed on a patient, 3 on the chest and 3 on the back. A unique current frequency is emitted by each electrode on an intra-cardiac catheter. Each current's strength is then measured by every detection patch. Using the values returned and with knowledge of the unique frequency, CARTO3 can determine a precise location for each distinct electrode using a 'current ratio'. The locating abilities of CARTO3 uses a hybrid of these complimentary technologies[368] and found to be highly accurate in a phantom model[369].

Multielectrode mapping catheters have also been introduced. An example of this is the PENTARAY®, a flexible star shaped catheter with 5 splines and 22 electrodes of 1mm^2, (Figure 1-14) .

Figure 1-14 *The PENTARAY® catheter.*
Provided with permission from Biosense Webster, Inc.

Using the above technology, CARTO3 has advanced to where automated, swift, accurate electroanatomical mapping can occur. Electrograms and their geometric position are

automatically accepted using pre-specified criteria, negating the requirement for manual approval of every sampled point.

1.7.1.4 Ablation Catheters

Regarding ablation, the ThermoCool® SmartTouch Surround Flow™ (STSF) ablation catheter, also manufactured by Biosense Webster pairs with the CARTO3 system, (Figure 1-15). The STSF catheter obtains its name from an advanced irrigation system that uses 56 irrigation holes to make cooling more homogeneous whilst significantly minimising irrigation volume[370]. The STSF is a contact force sensing catheter with a 3.5mm tip linked to a precision spring. This allows for a small amount of electrode movement and emits a location reference signal, which is detected by a sensor on the shaft of the catheter. From this information, CARTO3 is then able to calculate the contact force exerted to a sensitivity of 1g and the catheter orientation which is then displayed on the CARTO3 screen alongside other parameters such as power, temperature, ablation index, electrograms and generator impedance data[371].

Figure 1-15 *The ThermoCool® SmartTouch Surround Flow™ (STSF) ablation catheter Provided with permission from Biosense Webster, Inc.*

1.7.2 Rhythmia

Rhythmia is a new ultra-high-density EAM system from Boston Scientific with first published clinical use in 2015[372].

Rhythmia works using a hybrid of technologies. The first applies magnetic location technology using a reference patch on the patient's back, ECG electrodes and sensors within its catheters. The second is impedance location technology which derives the electrical impedance of each individual electrode. From this, Rhythmia creates an anatomical impedance field. These two technologies operate synergistically and provide accuracy to less than 1 mm[373].

1.7.2.1 Creating a 3D Electroanatomical Map

To create its 3D EAM, Rhythmia uses a basket-shaped mapping catheter known as the Intellamap Orion, (Figure 1-16). The Orion catheter has a total of 64 electrodes spread across 8 flexible spines. The basket is flexible and can expand open to a diameter of 22 mm. Its electrodes are 2.5 mm apart and have an area of 0.4 mm^2 each[374]. Rhythmia creates its 3D anatomical shell similar to the CARTO system by using the outermost points collected from the position of the Orion and removing any points internal to them.

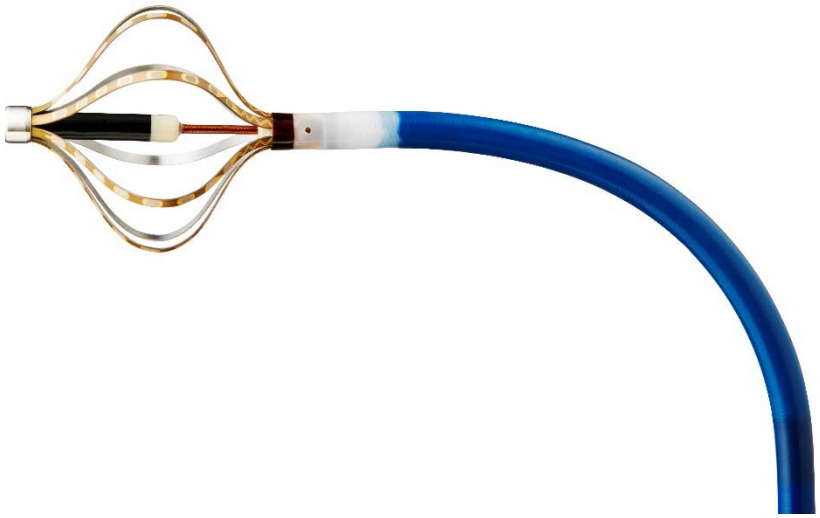

Figure 1-16 *The Intellamap Orion catheter*
Provided with permission by Boston Scientific

Electrogram data is integrated into the anatomical shell from the Orion electrodes provided they meet criteria defined within the system. Electrograms must be detected within a user-defined distance from the shell (typically 1-5 mm).

For an electroanatomical activation map, the timing of an electrogram is taken relative to a reference. This reference electrogram is typically from a stable intracardiac electrode such as a coronary sinus catheter. Electrograms for the activation map are only accepted by the system if they fulfil certain criteria that ensure the signal reproducibility and stability.

1.7.2.2 Ablation Catheters

Ablation catheters that pair with Rhythmia HDx include the IntellaNav MiFi™ OI, and IntellaNav Stablepoint™.

The MiFi catheter is a non-contact force sensing catheter with a 4.5mm tip which features 3 miniature electrodes. The miniature electrodes allow more detailed electrograms to be collected than a traditional catheter tip to distal ring electrode bipole when the catheter tip is placed against the myocardium, (Figure 1-17).

Figure 1-17 *The IntellaNav MiFi ablation catheter*
Provided with permission by Boston Scientific

The Stablepoint catheter is a contact force sensing catheter with a 4mm tip (Figure 1-18). A force sensing spring from the tip to the distal ring electrode exists in place of the 3 miniature electrodes and allows a contact force reading based upon spring dynamics[375,376]. Both the MiFi

and Stablepoint catheters measure a novel important parameter called local impedance which is discussed in detail in Chapter 1.10[376].

Figure 1-18 *The IntellaNav Stablepoint ablation catheter*
Provided with permission by Boston Scientific

1.7.2.3 Validation of Rhythmia

Rhythmia was first used in a canine model in 2012. The RA was mapped using automated acceptance criteria displaying a much higher number of electrograms than previously seen, (range 2197 – 12 412, median 4227). This gave the system an extremely high resolution of 2.6 mm. Furthermore, artificial areas of scar that were created via either surgical excision or epicardial radiofrequency ablation were successfully identified. Accuracy of ablation was also validated in this model by demonstrating electrical block following ablation between two areas of artificially created scar[374].

Rhythmia was then further validated in a porcine model through mapping of the RA and LV. In this study, the Orion catheter and automated acceptance of electrograms was compared to both the use of a conventional catheter and manual acceptance of electrograms. Rhythmia was able to accurately collect a significantly higher number of electrograms for both chambers than a conventional catheter or manual annotation and in a shorter time[373].

Rhythmia was first used clinically in human cases in 2015. The first case series presented 20 patients with a variety of arrhythmias, 7 atrial tachycardia, 8 AF, 3 VT, and 2 ventricular ectopic ablations. Once again, the system was able to develop a highly accurate map with a vast number of accepted electrograms in all cardiac chambers. Minimal manual correction was required with only 0.02% of points removed. The system was able to identify gaps in previous linear atrial

ablation lesions, channels of slow conduction in ventricular scar, identify the origin of ventricular ectopy, and successfully terminate these arrhythmias with ablation[372].

1.8 3D Electroanatomical Mapping in Atrial Fibrillation Ablation

AF is associated with the generation of atrial fibrosis. The progression of atrial fibrosis decreases the ability of the atria to conduct signal efficiently and forms the triggers and substrate necessary for the initiation and maintenance of AF. The presence and extent of LA fibrosis on 3D EAM is of the utmost importance as it provides prognostic information and can guide procedural strategy during ablation beyond PVI, (Section 1.6.3.4).

1.8.1 Left Atrial Fibrosis and Prognosis

The surface area of LA fibrosis demonstrated has been shown to relate to the progression of AF from paroxysmal to persistent to long-standing persistent types[334,335]. These studies were performed using manual review of electrograms and on lower density systems then currently in use.

Furthermore, the presence of LA fibrosis has been noted to affect the outcome of AF ablation. Verma *et al* showed using a circular mapping catheter and CARTO® that patients with low voltage areas (LVA, < 0.5mV) had a recurrence of AF of 57% vs 19% for those without, at a mean of 15.8 months follow up[377]. This difference was maintained even after repeat procedures with overall freedom from AF in patients with LVAs at 52% vs 90% without. Uni- and multivariate analyses found that detectable LVAs to be an independent and the most significant predictor of AF recurrence following ablation.

Studies using DE MRI to demonstrate atrial fibrosis also show a relationship between post-ablation AF recurrence and progression between AF types[137,378-380]. Of note, Oakes *et al* correlated the presence of LVAs on a 3D EAM to the atrial fibrosis shown on DE MRI helping to validate LVAs as a surrogate for atrial fibrosis[379].

1.8.2 Factors Affecting the Creation of a Voltage Map

Reflecting the prognostic and procedural implications endocardial substrate maps can confer, an understanding of the distinct factors affecting their creation is required.

To define myocardial fibrosis, 3D EAM systems use tissue voltage as a surrogate. For this purpose, most commonly the peak to trough amplitude of bipolar electrograms are used. The measured voltage amplitude on a 3D EAM can be affected by both tissue and non-tissue factors. The non-tissue factors include:

1. Catheter – tissue contact[381-383];
2. The orientation of the mapping catheter to the activation direction of the tissue[384];
3. The catheter electrode spacing between bipoles[385,386];
4. The catheter electrode size[387];
5. Electronic filtering[388].

It is important to minimise variation of these non-tissue factors to ensure the voltage represented on the map are consistent and accurate in reflecting the fibrosis in the underlying tissue[389]. Points 1 – 4 are largely operator dependent, from selection of the appropriate mapping system and catheters for a case, to influencing catheter manipulation and application of contact force.

Tissue factors include:

1. The mass of tissue capable of being depolarised;
2. The direction of tissue activation relative to the mapping catheter[384];
3. The strength of the source of underlying the rhythm[390]; and
4. The distance from the recording catheter to the depolarisation, (dependent on constant tissue contact force with the mapping catheter)[390].

Underlying fibrosis is a key element affecting the measured voltage considering these tissue factors. Increasing amounts of fibrosis decrease the volume of tissue being capable of

being depolarised, (Point 1), an effect also dependent on the chamber being mapped. Furthermore, the nature of fibrosis results in signal weaving its way through disorganised bundles of myofibrils which are constantly changing direction, and therefore decreasing the measured voltage (Point 2)[391]. This effect is also affected by the underlying cardiac rhythm, particularly the chaotic nature of AF versus organised SR, (Points 2 and 3)[392,393]. Fibrosis may also change the biomechanical response of tissue to contact force created by the mapping catheter, however, this is not well understood or investigated, (Point 4).

1.8.3 Defining Low Voltage Areas

For the reasons previously stated, knowing the presence, position, and extent of LVAs during an AF ablation procedure is crucial. Consequently, accurate definition of left atrial LVAs on a 3D EAM is imperative and specific values are therefore required. Throughout the electrophysiological literature, values of less than 0.05 mV and 0.5 mV have been used to determine dense (electrically inert) scar and abnormal low voltage tissue respectively[335,339,394-396]. However, curiously their level of validation is limited.

Ideally, validation of tissue voltage values to define atrial fibrosis would be done histologically. However, no studies performed in this way for native atrial fibrosis exist. A single atrial model of a porcine right atrium by Harrison *et al*[397] showed a decrease in tissue voltage following radiofrequency ablation from 3.3 mV pre-ablation to 0.6 mV post ablation acutely, and 0.3 mV chronically. These values correlated with a transmural injury assessed histologically.

In the absence of histological evidence, statistical approaches have also been used to define LVAs. Lin *et al* investigated the electrophysiological characteristics of 20 patients undergoing a left sided accessory pathway ablation as a control group to those with paroxysmal, persistent and chronic persistent AF[398]. Using a 95% cut off of all bipolar voltages, they determined 0.4 mV as the defining value for a LVA. However, they also found 95% of CFAEs existed in areas of tissue voltage less than 1.3 mV[398], suggesting electrophysiological abnormalities in higher values of tissue voltage. Using the same method, Saghy *et al* defined a LVA at less than 0.5mV using 9 patients undergoing ablation for left sided supraventricular tachycardias[399]. In contrast, Yagishita *et al* found a much higher value, with the bottom 5% of tissue voltages being below 1.46 mV in 6 patients undergoing left sided accessory pathway

ablation[400]. Differences were also noted between atrial walls, with the lowest region being the LA septum 1.17 mV.

Interestingly, when Yagishita et al used a 1.1mV cut off for a LVA, they found 43% of their study patients who would have not been classified as having a LVA would subsequently have been so[400]. These patients were found to have a significantly greater rate of AF recurrence and CFAE burden, again suggesting that tissue fibrosis and relevant electrophysiological abnormalities exist in a higher cut-off value than 0.5mV.

1.8.4 Pacing Thresholds

Another potential method to define the presence and extent of tissue fibrosis would be to examine its local pacing threshold. Those sites with increased amounts fibrosis would be hypothesised to have higher pacing threshold as the tissue requires an increased current to capture the stimulus. With dense fibrosis, the tissue would be expected to be electrically inert and therefore an immeasurable pacing threshold. Although this method was used in the initial study using CARTO® to define areas of dense scar less than 0.05 mV it has not been used in follow-up studies since[401]. However, endocardial pacing is commonly performed during ablation procedures to assess the efficacy of ablation lesions, for example when pacing WACA lines to examine for gaps. It also provides a useful physiological assessment of the underlying tissue, examining its inherent ability to conduct signal. Mapping an entire cardiac chamber using this method is not plausible, due to the significant time taken to perform each pacing threshold. Consequently, its use would be restricted to assisting to validating other surrogates for mapping tissue fibrosis.

1.8.5 The Effect of Cardiac Rhythm

The depicted substrate on 3D electroanatomical voltage maps has been shown to be dependent upon the underlying cardiac rhythm[392,393]. This poses the question of which rhythm to create a voltage map in to best depict the underlying fibrosis, SR or AF? Furthermore, if a patient is unable to maintain SR for the mapping procedure, is a voltage map created in AF an acceptable substitute?

One would expect that with the chaotic nature of signal propagation during AF that a lower voltage amplitude would be sampled at individual sites and globally compared to the highly organised conduction of SR. Indeed, statistical studies have also shown that patients with AF have a lower mean global LA tissue voltage than controls[398,400]. This reduction in mean tissue voltage progresses through types of AF from paroxysmal to persistent to chronic persistent[402-404].

To compare voltage maps between SR and AF, studies either take the mean tissue voltage for an anatomical area, or match electrograms that are less than 5 mm apart as validation for individual points[392,393]. Both of these methods show the amplitude of bipolar signals are consistently lower in AF compared to SR[392,393,405,406]. Interestingly, they have also been shown to vary between atrial walls in both SR and AF, suggesting values for normal and diseased tissue may vary for different anatomical sites[392,393,405-407].

Electrogram morphology has been shown to vary between AF and SR. Ndrepepa *et al*[406] found that 40% of corresponding electrograms switched from a normal morphology to fractionated when mapped in SR and then AF. Curiously, 19% of fractionated electrograms in SR obtained a normal morphology in AF. Teh *et al*[405] showed that the lower voltage of LA tissue whilst mapping in AF unsurprisingly resulted in an increased number of LVAs. However, when these LVAs were endocardially paced, their electrical characteristics returned to normal. This reflects the chaotic nature of signal conduction during AF and in combination with comparatively higher values for voltage amplitude seen in SR, this suggests 3D EAMs are best generated in the more reliable SR.

Regarding whether voltage maps generated in AF are consistent with those in SR, studies have found a weak linear correlation does exists. This is particularly the case if electrograms in both SR and AF are not fractionated[392,393], with progressively weaker correlations being seen if one or both of the compared electrograms are fractionated. This is of particular note, as with increasing fibrosis, increasing fractionation of electrograms occurs. This suggests whilst voltage maps created in AF may be representative of that in SR in healthy tissue, with increasing disease the map becomes less reliable.

Yagishita *et al* suggested that reflecting the weak but linear relationship between tissue voltages in AF and SR that different cut-offs could be used to define LVAs depending on which rhythm a voltage map was generated. Using a cut-off of 0.5 mV for SR, but 1.5 mV for AF, patients were found to have no difference in the number of low-voltage areas on their 3D EAMs[393].

The studies discussed above performed their analyses using manual acceptance of electrograms on lower density systems. Modern systems with automated acceptance criteria and ultra-high-density mapping catheters allow for the comparison between SR and AF and patients with paroxysmal and persistent AF to be re-investigated in far more thorough detail.

1.8.6 Mapping the Right Atrium

RA ablation as an adjunctive therapy for AF has been practised for greater than 20 years, including different ablation lines, CFAE ablation and involvement in stepwise ablation protocols[327,328,408-410]. Triggers for AF within the RA have been noted to occur mainly from the crista terminalis, superior vena cava or coronary sinus[334,411]. Interestingly, the tissue voltage at these sites were not found to be lower than that of control cases in contrast to the findings within the LA. Consequently, this suggests the RA triggers AF due to anatomical abnormalities rather than in association with LVAs[334]. However, using FIRM mapping 25% of rotors were identified in the RA and a recent study using an automated algorithm on CARTO3 found CFAEs and localised sources were evenly distributed across both atria[162,412]. Furthermore, remodelled substrate in the RA has been demonstrated in patients with paroxysmal AF triggered from the superior vena cava[413]. This suggests the RA holds the substrate necessary to maintain AF, and consequently mapping the RA may become of increased importance in the future.

1.8.7 Local Impedance Mapping

A different measurable electrical parameter which may prove to be a useful mapping surrogate in the future is local impedance (LI). Rather than measuring the electrical activity that passes through the tissue, LI measures its resistance, which can be sampled at any stage of the cardiac cycle. LI can currently only be measured by a tip catheter and is used largely as a method of gauging the progress of an ablation (as will be discussed in greater detail in section 1.10).

However, in proof-of-concept studies, LI has been shown to be able to differentiate between ablation lines and native tissue and identify gaps in WACA lines[414,415]. Furthermore, starting LI values are known to affect changes in LI with ablation[416,417]. As a potentially complimentary mapping variable to tissue voltage, developing values of LI that may represent underlying tissue fibrosis could be of great use. Furthermore, how the baseline tissue LI readings can be affected by operator dependent factors such as contact force and atrial rhythm is uninvestigated.

1.9 3D Electroanatomical Mapping for Ventricular Tachycardia Ablation

Scar-mediated VT is most commonly caused by re-entrant circuits about islands of electrically inert tissue. These circuits are formed and maintained by thin areas of delayed conduction known as isthmuses which form the target of VT ablation[418,419]. Most frequently these isthmuses are found in areas of dense congruent fibrosis originating from the endocardium secondary to ischaemic cardiomyopathy[211]. However, they may also be found throughout myocardial layers[420-422] as patchy fibrosis due to other disease processes such as reperfusion from acute MI[423,424], myocyte disarray in hypertrophic cardiomyopathy,[425,426] or desmosome mutations in arrhythmogenic cardiomyopathy[427].

Consequently, being able to visualise the substrate housing arrhythmic circuitry is vital for determining sites of ablation and planning appropriate strategy. Furthermore, the degree of fibrosis is known to affect the development of ablation lesions[428,429], and as VT ablation is essentially ablation of scar tissue, prior knowledge of the substrate being ablated is necessary to guide an operator on the ablation settings they may wish to use.

1.9.1 Defining Abnormal Ventricular Substrate

Similar to the atria, ventricular fibrosis is represented on a 3D EAM using voltage amplitude as a surrogate[430]. Bipolar voltage values of 0.5mV and 1.5mV are commonly used cut-offs in clinical practice to represent dense scar and diseased tissue respectively.

Histological studies undertaken to validate appropriate cut-offs have occurred in a porcine model and a single human subject[431,432]. In the porcine model, seven swine with left

anterior descending artery infarctions had bipolar voltage amplitudes measured in normal tissue, the centre of the infarction and the border zone, with significant differences seen between all three, (Infarct: 1.2 ± 0.5mV, Border: 2.8 ± 0.9mV, Normal: 5.1 ± 2.1mV). Furthermore, the area of infarction (< 1mV) and border zone (1 – 2mV) determined on CARTO corresponded closely with those seen on pathological specimens[432].

In the single human model, Deneke *et al* correlated histopathological findings with endocardial bipolar voltage readings on CARTO in a patient who had died from ischaemic cardiomyopathy having had a VT ablation seven days prior. Using predetermined tissue voltages for scar (<0.5 mV) and border zones (0.5 – 1.5 mV), they found those regions defined on CARTO to be congruent with histological fibrosis of greater than 80% of the myocardium and 20 – 80% respectively. Consequently, one can infer 0.5mV and 1.5mV are threshold values consistent with 'more' and 'less' extensive scarring, whilst also appreciating it is possible to have viable tissue <0.5 mV and some fibrosis >1.5 mV[431].

Statistical evaluation of bipolar tissue voltage has also occurred in humans[355]. Creating 3D EAMs on CARTO, Marchlinski *et al* studied six patients without structural heart disease undergoing ablation for haemodynamically unstable VT. They found 95% of all bipolar endocardial electrograms were >1.55mV in the LV with a mean voltage of 4.8 mV. They consequently established the value of >1.5 mV for normal tissue and <0.5 mV for dense scar. Interestingly, they note the value of 0.5 mV was arbitrarily chosen, yet it remains used clinically and throughout the electrophysiological literature today[353,357,433-437].

1.10 Radiofrequency Ablation

In AF ablation, the objective is to apply the smallest number of safe, transmural lesions to achieve PVI and isolate or eliminate other arrhythmogenic substrate. In VT ablation, it is to apply safe lesions deep enough to disrupt re-entrant circuitry. If procedural success is achieved, both will lead to significant relief from symptoms.

When undertaking radiofrequency ablation, every lesion administered should be optimised to obtain maximal dimensions whilst maintaining patient safety. To achieve this,

knowledge of the biophysics of lesion creation and the factors affecting it is fundamental. To assist this, having measurable, well-defined parameters that allow one to monitor lesion development and signal when ablation should be terminated is highly valuable.

1.10.1 Factors Affecting Ablation Lesion Creation

1.10.1.1 Temperature

Thermodynamic concepts determine the area of resistive heating is proportional to the square of the current density in the tissue. The current density will be supplied from the abating electrode and is determined by the power selected by the operator.

In 1989, Haines *et al* were able to demonstrate this proof of concept. Using a canine in vitro model, their study showed increasing the temperature at the electrode tissue interface (ETI) from 50 to 85°C correlated with larger ablation lesion depth and width. Furthermore, they showed tissue temperature fell with distance from the ablating electrode and was predictable in a hyperbolic thermodynamic model[438]. A similar finding was then demonstrated in vivo[439].

However, complications were seen with extreme catheter tip temperatures. Temperatures measuring greater than 100°C were associated with plasma boiling and resulted in tissue pops with shredding and the formation of coagulum coating the electrode, risking thromboembolic events and preventing the delivery of further ablation lesions[439].

Consequently, methods to cool the catheter tip whilst maintaining a high tissue temperature to maximise lesion size were developed. Nakagawa *et al* showed this could be achieved through use of a saline irrigated ablation catheter within an in vivo canine model[440]. Dorwarth *et al* also demonstrated this in a porcine model[441]. Both achieved ablation lesions with significantly greater depth and volume than non-irrigated catheters. Perhaps unsurprisingly, the rate of cooling irrigation was then shown to also affect lesion dimensions, with smaller surface diameter seen with increased flow[442].

Unfortunately, although irrigated catheters were providing greater ablation lesion volumes, they were also limited by complications at temperatures >100^{o}C, forming steam bubbles below the electrode. With a sudden pop, steam bubbles would burst forming a crater in the tissue and risking myocardial rupture[440].

Consequently, using modern irrigated RFA catheters, the power used must be carefully judged and a trade-off established between optimisation of ablation lesion size, and complications. In clinical practice, common RFA powers used are 30 – 50W, however extra high power, short duration strategies using 90W are under investigation[443,444].

1.10.1.2 Contact Force

As mentioned, the area of resistive heating in the myocardium is proportional to the square of the current density in the tissue. Furthermore, the current density itself is inversely proportional to the square of the distance from the ablation electrode to the tissue. Consequently, the area of resistive heating (and therefore ablation lesion volume) is inversely proportional to the distance of the ablating electrode to the tissue to the fourth power. This emphasises the importance of effective electrode tissue contact forming the ETI[445].

The role of tissue contact force (CF) was initially shown by Haines *et al* in 1991 using an in vitro canine model[446]. In their study, using a non-irrigated catheter, they administered ablation lesions in the RV at CF levels from 0 – 41g, whilst maintaining a constant ETI temperature of 80°C. Interestingly, there was a significant difference in lesion size between 0 g of force and 1 g, but no difference between 1 g and 40 g, suggesting the biggest effect is having tissue contact itself rather than excessive force. A similar finding was found by Peterson *et al* in their temperature controlled porcine ventricular model, where no difference was found in lesion size between 10 and 20 g of force[447]. Using a canine ventricular model, Avitall *et al* also found catheter contact causing tissue indentation of 3mm showed an increase in ablation lesion size compared to 0mm[448].

Similar to tissue temperature, complications were seen with increasing amounts of CF, with greater numbers of tissue pops demonstrated, particularly in combination with high power

delivery[448]. Irrigated catheters used with in vitro and in vivo canine models also demonstrated increased lesion dimensions with CF and complications when used in excess[449-451].

Despite the clear procedural and safety advantages of knowing tissue CF clinically, interestingly, for AF ablation no randomised control trial has been able to demonstrate improved arrhythmia free survival specifically with its presence compared to non-CF sensing catheters[452]. However, the largest prospective trial, (TOCCASTAR), demonstrated that if optimal contact force (>10g) was applied in 90% of lesions in patients undergoing PVI for paroxysmal AF, a greater freedom from atrial arrhythmia was seen[453], indicating that appropriate application of the technology is more important than its availability.

CF is also affected by cardiac rhythm, with studies showing less contact force variability (the difference between CF peaks and troughs) in AF over SR[454]. This is consistent with the dynamic nature of the atria in SR where cardiac contraction physically pushes against the catheter. In contrast, the chaotic contraction seen in AF actually provides a more consistent contact for the catheter. The degree of contact force variability has been shown to affect effective lesion delivery when judged by impedance drop in humans and histologically in a bovine model[389,455].

1.10.1.3 Electrode Size

In initial studies using non-irrigated catheters, increasing the ablation catheter diameter resulted in larger ablation lesion size[456]. However, the effect of this was limited, as beyond 8 mm, poor endocardial contact conferred by stiff, difficult to manoeuvre catheters resulted in smaller lesions being generated. Interestingly, newer irrigated catheters have been shown to deliver smaller lesions with larger diameter electrodes for a specified output voltage. This is due to greater current shunting through the electrode-blood interface rather than the ETI and consequently creating less tissue heating[457]. Today, the most commonly used ablation catheters have a 4mm diameter.

1.10.1.4 Electrode Orientation

The orientation of the ablation catheter to the myocardium affects the proportion of the ablating electrode making contact with the underlying tissue. The more of the electrode in contact, the more current will flow through the ETI rather than the electrode blood interface, therefore increasing current density, tissue heating and lesion size. With perpendicular orientation the tip of the electrode will form the majority of contact which is approximately 25% of the electrode surface area. Parallel contact has the side of the electrode in contact and is more dependent upon tissue characteristics, for example whether the electrode is wedged within trabeculae of the LV or sliding on the smooth surface of LA[458]. This means parallel orientation has the capability of having a greater proportion of electrode – tissue contact, but this contact tends to be less reliable[447,459].

1.10.1.5 Time of Delivery

During RFA, the area of resistive heating achieves a steady-state temperature rapidly. However, the area of conductive heating takes more time to achieve and produce the full lesion size. Haines *et al* showed lesion width and depth increased with ablation duration mono-exponentially, with a half-time of 7 to 10 seconds and eventually plateauing at 45-60 seconds[446].

Using an irrigated catheter with bovine in vitro and porcine in vivo models, Borne *et al* showed ablation lesion size continued to increase even further up to 90 seconds[460]. This suggests that prolonged ablation could offer benefits, particularly if the arrhythmic circuitry is set deeper within the myocardium.

Clinically, ablation lesion size cannot be monitored in real-time, however biophysical surrogates such as impedance are seen to drop, curve and plateau with ablation in a comparable manner to the mono-exponential models above. The plateau seen in ablation lesion size histologically and with clinical surrogates suggests there is an optimal time for ablation delivery where a lesion has maximised its dimensions and after which returns are minimal but risk complications[383].

1.10.1.6 Tissue Characteristics

As ablation lesions are most dependent upon conduction of heat, lesion size will be affected by the thermal conductivity of the tissue[461,462]. In healthy myocardium, uniformly and densely packed cardiomyocytes with minimal interstitial tissue allows for heat to be conducted evenly, forming well demarcated ablation lesions. In contrast, in scarred myocardium, a heterogenous pattern of damaged cardiomyocytes, collagen, and adipose tissue exists, which overall lowers the resistance of the tissue. Due to the lower resistance, uneven distribution of these tissue components and their varying heat capacitance, less tissue heating occurs, creating irregular scattered damage with ablation[428].

Tofig *et al* demonstrated this in a porcine ventricular model. 12 weeks following artificial induction of myocardial infarction, RFA lesions were applied to different areas of the ventricle reflecting their voltage amplitude on CARTO3®. Histological analysis revealed a significant and progressive decrease in lesion size from normal- (> 1.5mV), intermediate-, and low-voltage (< 0.5mV) myocardium[429].

Knowledge of the effect of RFA on ventricular scar is of the upmost importance in VT ablation. As the re-entrant circuits that form VT occur around islands of scar, their abolition requires heat to conduct through scar to reach the isthmuses responsible. No previous studies have examined the effects of ventricular scar on RFA in a clinical setting.

Surprisingly, there have been no histological studies investigating how scar affects ablation lesion dimensions specifically in the atrium. Although one can hypothesise that results would be similar to the ventricle, the interspersed, patchy nature of fibrosis seen in AF, is quite different to that seen in the ventricle. Consequently, the conductance of heat may occur in a more uniform and predictable way. Furthermore, the left atrium is a thin structure. This may mean that despite fibrosis being present, it may have a less significant role in affecting the development of a lesion as it can achieve transmurality before its dimensions have been fully maximised. However, with scar guided ablation strategies gaining traction its effect on scarred atrial tissue warrants further investigation.

1.10.2 Assessing Ablation Lesions Efficacy

Clinically, knowing an ablation lesion being delivered has been effective is of great importance, but it is also a challenge. During a procedure, we are unable to assess in real time the size of a lesion on histology, nor is it practical to monitor its development with advanced imaging techniques. Currently, our assessment of the efficacy of an ablation lesion occurs in two ways:

1) Hitting a target based on a scoring system that accumulates points during ablation; and / or
2) The biophysical feedback we receive during ablation.

1.10.2.1 Force Time Integral

Force time integral (FTI) is the cumulative product of contact force and time. During ablation, FTI continually increases based upon CF and time until a pre-determined target is reached. In clinical studies, FTI has been shown to be associated with transmural ablation lesions using validated electrogram criteria as a surrogate[463-465]. Additionally, lesions adjacent to gaps in WACA lines have been shown to have experienced a low FTI, suggesting they had inadequate CF, ablation duration or both.

Studies currently recommend an FTI of 400gs with a 20 g average contact force for each ablation lesion in paroxysmal AF[382,466,467]. In persistent AF, a slightly higher FTI is used, with 500gs being associated with a plateau in impedance drop[383].

There has been no work with FTI on the ventricle.

Although a useful marker in its simplicity, FTI does not account for one of the key factors known to be associated with ablation lesion size, the power delivered.

1.10.2.2 Ablation Index

Ablation index (AI) is a non-linear composite score of contact force, time and power. First validated with an in vivo dog model, AI was found to correlate with lesion dimensions in both atria and ventricles[468,469]. Das *et al* were first to demonstrate the utility of AI clinically. In their prospective study in patients with paroxysmal AF undergoing PVI, WACA lines were divided into segments and created with the operator blinded to AI. At follow up electrophysiological study at 2 months, segments with pulmonary vein reconnection were found to have a significantly lower minimum AI delivered within their set of lesions. Interestingly, certain segments of the WACA line were found to require greater AI to ensure isolation (>370 for posterior / inferior wall, and >480 for anterior wall / roof), indicating the applied AI needed to vary depending on anatomical location[467].

Prospective use of slightly higher AI values by the same research group (>400 and >550 respectively), was found to result in more successful first pass PVI, decreased acute pulmonary vein reconnection and clinical arrhythmia recurrence compared with lone contact force guided ablation[470]. This was then confirmed in a 2019 meta-analysis[471]. Outcomes were also found to extend to patients with persistent AF[472].

Regarding the ventricle, two studies have examined AI guided procedures on outflow tract premature ventricular complexes[473,474]. Casella *et al* retrospectively analysed 145 patients, finding a maximal AI cut-off of 550 was optimal for clinical success. Gasperetti *et al* prospectively enrolled 60 patients for AI guided ablation and compared them to propensity matched non-AI guided patients finding AI guided patients had improved arrhythmia free survival. However, these studies are quite different to the use of AI for scar mediated VT, reflecting a different anatomical site, arrhythmic mechanisms, and tissue characteristics. No studies examining the optimal AI required for scar mediated VT have been performed.

1.10.2.3 Electrogram Attenuation

Following ablation, the electrograms of the underlying tissue are altered, showing a decrease in amplitude and change in morphology. Otomo *et al* showed in an atrial porcine model that specific electrogram changes correlate with a transmural lesion[475].[475]. For a unipolar

electrogram, the elimination of any negative deflection was consistent with transmurality, whilst for a bipolar electrogram, an amplitude reduction of 80% is believed to be required[476].[476].

These criteria have subsequently been used to validate FTI and AI as methods of effective lesion delivery in clinical atrial ablation studies[382,463]. However, during a procedure the real-time review of multiple electrograms, noise from the ablation catheter and variation in catheter-tissue contact with cardiac movement makes real-time assessment of electrograms to confirm transmurality challenging.

Regarding the much thicker left ventricle, achieving a transmural lesion using RFA is not feasible, and consequently, electrogram changes are seen to a smaller degree. In a porcine model, Sapp *et al* demonstrated a 22% decrease in unipolar electrogram amplitude and 56% decrease in bipolar electrogram amplitude following ablation. However, these values correlated poorly with ablation lesion dimensions on post-mortem, suggesting that in the ventricle, whilst electrogram attenuation is reassuring, other methods are superior at assessing lesion delivery.

1.10.2.4 Change in Pacing Threshold

Following ablation, one would expect a rise in pacing threshold of the underlying tissue as it has been rendered electrically inert. This is particularly useful in the atrium, as transmural lesions would be expected to have no pacing capture at all. In the ventricle, as transmurality does not occur, a rise in threshold is reassuring that ablation has occurred, however the adequacy of the lesion is less certain.

In the atrium, Kosmidou *et al* showed in a porcine model that loss of bipolar pacing capture at 10mA was consistent with formation of a uniform transmural lesion in 79% of cases[477]. Clinically, Stephen *et al* showed pacing along a WACA line could accurately detect pulmonary vein reconnection gaps and guide further ablation, achieving a 95% PVI rate[478]. Furthermore, patients with absence of pacing capture on their WACA lines showed greater freedom from arrhythmia at 1- and 5-year follow-up, when compared to achievement of acute bidirectional block alone[479-481].

In the ventricle, Sapp *et al* demonstrated a 320% rise in pacing threshold occurs following ablation of healthy tissue[482]. Additionally, the rise in pacing threshold was predictive of ablation lesion volume.

1.10.2.5 Electrical Isolation

A simple assessment of ablation lesion efficacy is to test for bidirectional block across a line intending to isolate tissue. This confirms that the chain of lesions has achieved transmurality successfully and is used as a clinical endpoint when performing PVI in AF ablation. Although this method cannot assess individual ablation efficacy in real-time, it can be used retrospectively when examining for reconnection gaps in WACA lines by assessing the characteristics of ablation lesions either side of the gap. Indeed, several studies have used this method to investigate the efficacy of contact force[464-466], AI[467,470,472], and pacing capture[478,480,481] when performing PVI.

1.10.2.6 Programmed Electrical Stimulation

For VT ablation, testing the efficacy of a set of lesions can be tested by the non-inducibility of the arrhythmia at the end of the procedure[483].[483]. Being unable to induce VT at the end of a procedure is associated with a significantly lower risk of arrhythmic recurrence compared to inducible non-clinical VT (odds ratio 0.5) and clinical VT (odds ratio 0.1)[484]. However, like the PVI for AF ablation, programmed electrical stimulation is an assessment of overall effectiveness of the procedure and does not reflect the efficacy of an individual lesion whilst it being delivered.

1.10.2.7 Impedance Drop

Impedance is the total opposition to radiofrequency current flow and the inverse of conductivity[485]. During ablation, heating of tissue increases its conductivity and a corresponding drop in impedance occurs. This allows the impedance drop to act as a surrogate for local tissue heating. As it can be directly measured during ablation, impedance drop (ΔGI) can be used to assess the development of an ablation lesion in real time. This is a distinct advantage over other methods in assessing lesion efficacy, which rely upon either scores from input data, (AI, FTI), or can only be applied post-ablation, (electrogram attenuation, pacing thresholds, electrical isolation).

Clinical outcomes from AF ablation guided by ΔGI have been favourable. Reichlin *et al* demonstrated that by ensuring a ΔGI of 5Ω within 10 seconds for all their lesions resulted in 84% freedom from AF at 14 months follow-up[486]. Chintz *et al* noted on redo procedures, 89% of pulmonary vein reconnection sites were bordered by a prior ablation lesion with a ΔGI of less than 10Ω using a non-contact force sensing catheter[487]. Furthermore, reconnection was only seen in only 1.5% of circumstances if ablation points had a ΔGI of greater than 10Ω.

1.10.3 Impedance

1.10.3.1 Modelling the Ablation Circuit

To understand impedance drop one can simplify the ablation circuit as a lumped element model with three resistors in series connected by perfectly conducting wires, (Figure 1-19)[485].

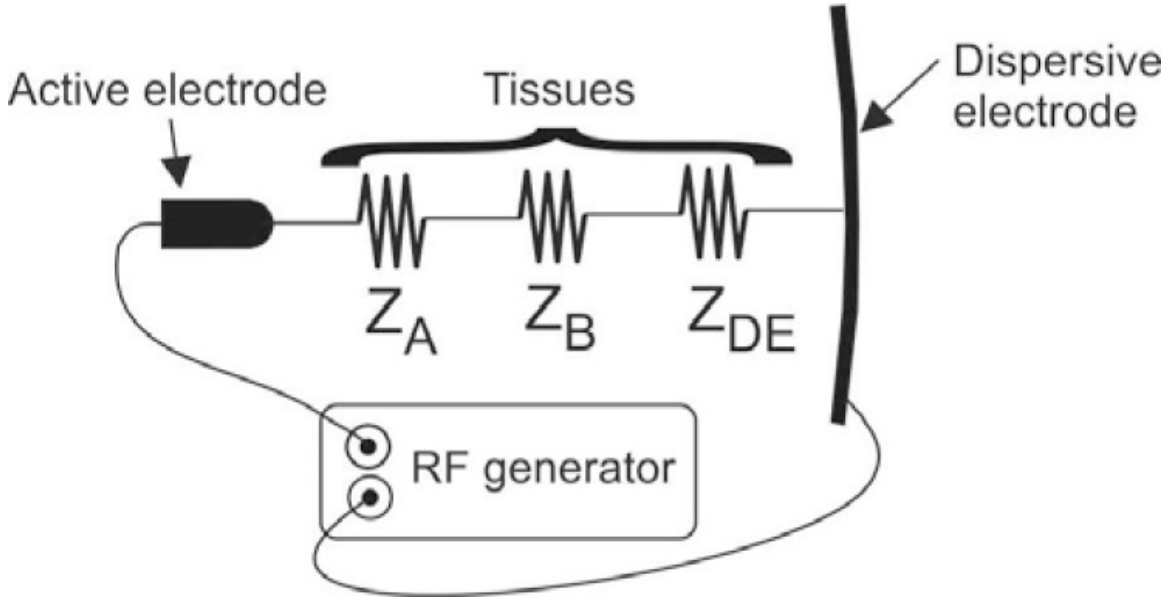

Figure 1-19 *The ablation circuit as a lumped element three resistor model*

Reproduced from Berjano E and d'Avila A (2013)[485], with permission from Bentham Open

These three resistors are:

Z_A The resistance at the interface of the electrode tip;

Z_B The resistance of body tissues *en route* to the dispersive electrode (lungs, blood vessels, air, adipose tissue); and

Z_{DE} The resistance of the tissue around the dispersive electrode (mainly keratinised epidermis at the skin patch).

As the electrode tip is in contact with both blood and myocardium which have varying resistances, Z_A is divided into two resistors in parallel. This is Z_{EBI} (electrode blood interface) and Z_{ETI} (electrode tissue interface). From a technical perspective, the total resistance at the electrode tip Z_A can be defined as:

$$Z_A = Z_{EBI} * Z_{ETI} / (Z_{EBI} + Z_{ETI})$$

This gives the circuit demonstrated in Figure 1-20:

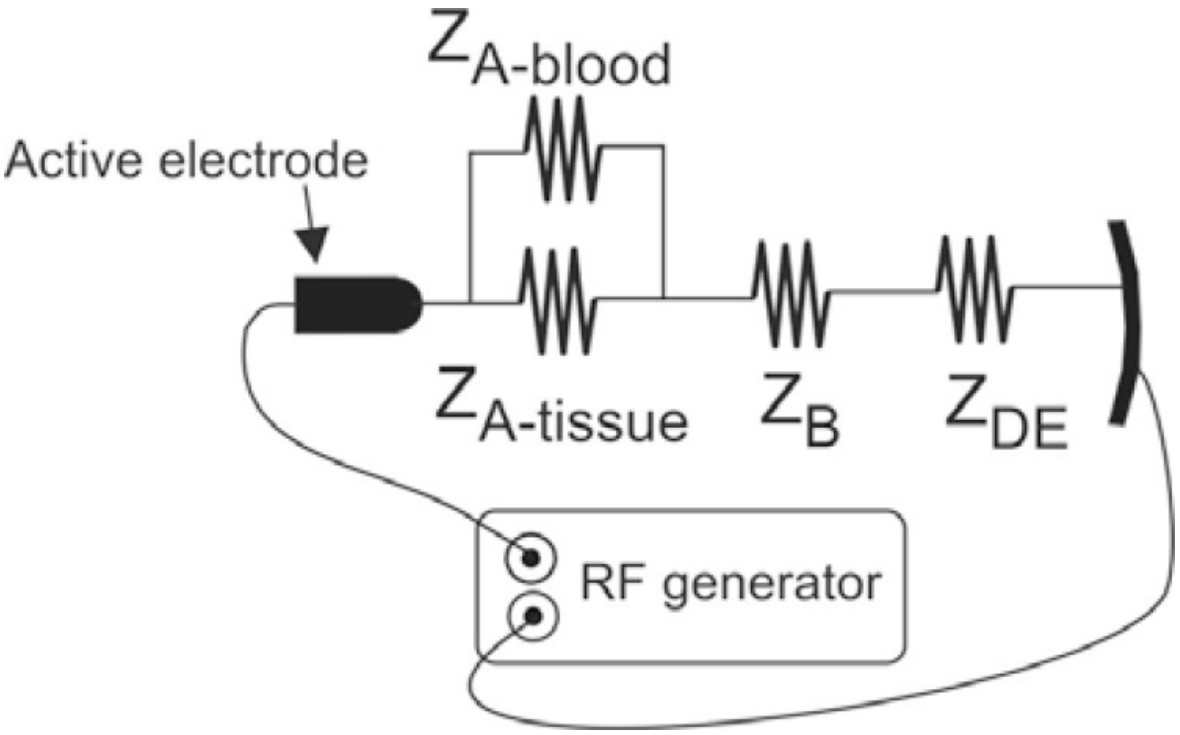

Figure 1-20 *The ablation circuit with Z_{EBI} and Z_{ETI} in parallel*

Reproduced from Berjano E and d'Avila A (2013)[485], with permission from Bentham Open

Clinically, the impedance of the ablation circuit can be measured in two ways. Firstly, the impedance of the whole circuit can be measured as a parameter called generator impedance (GI). GI by definition therefore is calculated as:

$$Generator\ Impedance = Z_A + Z_B + Z_{DE}$$

Secondly, recent technology has allowed Z_A to be measured independent of Z_B or Z_{DE}, known as local impedance (LI).

1.10.3.2 Impedance Drop with Ablation

Resistors convert electrical energy into heat. That heat spreads over the surface area of the resistor. When heat is able to alter the conductive properties of the resistor, it operates as a thermistor. During RF ablation, the surface areas of Z_B and Z_{DE} are large and therefore their heating effect is negligible, estimated to be 0.01°C for a 75 kg person[458]. Consequently, with no heating effect, Z_B or Z_{DE} do not act as thermistors. Thus, any significant changes in GI will be caused by changes at Z_A.

At Z_A, the tip of a 4mm electrode has a surface area of 27mm². This small surface area enables the tip to transfer focussed current to the myocardium when the circuit is activated. At the ablation site, the adjacent tissue experiences an area of high current density and heats. At the EBI, the heating effect is minimal due to the cooling effect of circulating blood. Thus, Z_{EBI} stays constant. At the ETI, the temperature of the tissue rises, resulting in a fall in Z_{ETI} and creating an ablation lesion.

With a fall in Z_{ETI} during ablation, Z_A will fall until a steady-state temperature in the tissue occurs and full lesion size is achieved[446]. At this stage, generator impedance will plateau indicating the lesion has reached its biophysical limit, (Figure 1-21).

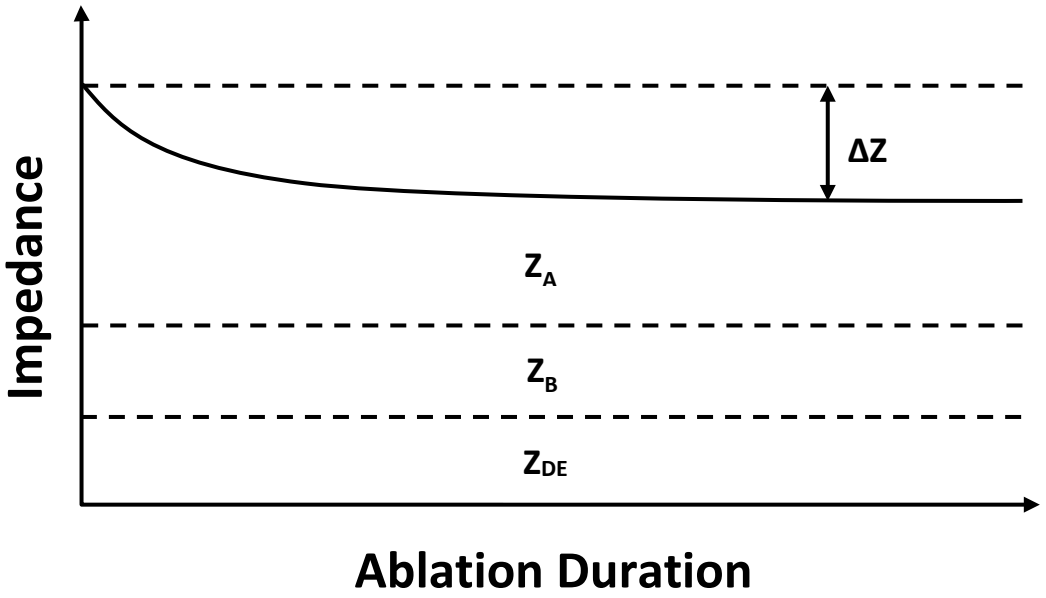

Figure 1-21 *Changes in the different components of impedance with ablation time*

Adapted from Berjano E and d'Avila A (2013)[485], with permission from Bentham Open

Consequently, a drop in GI (ΔGI) with ablation is representative of lesion development, whilst its plateau is indicative of its completion.

Unfortunately, the model above cannot be simply applied to an ablation procedure in clinical practice. GI sees variations within a patient in Z_B due to patient movement, breathing and different locations within the heart[488,489]. Furthermore, there are differences between patients, as Z_B is affected by surface area it is distributed, most reflected by a patient's BMI[485]. Consequently, GI can suffer from a significant amount of noise which is then filtered by a mapping system to present a clinically useful impedance curve[485].

1.10.3.3 Clinical Factors Affecting Generator Impedance Drop

In both pre-clinical and clinical settings, GI has been shown to be a useful surrogate for ablation lesion development and completion. In pre-clinical models, the maximum ΔGI achieved demonstrates a strong correlation with ablation lesion dimensions[300,429,448,490]. However, pre-clinical models possess the advantage of being able to control several variables that cannot be in

clinical practice. Consequently, it is important to understand the relationships of GI with other clinical factors.

1.10.3.3.1 Contact Force

The degree of CF has been shown to correlate with ΔGI in multiple clinical and experimental studies[448,451,488,491,492]. Furthermore, ΔGI has also been shown to plateau at different timeframes with different degrees of CF. In a canine model, Avitall *et al* found with good CF (1 - 3mm tissue indentation) GI plateaued at 40 seconds[448]. With minimal CF (electrode touching but 0mm indentation), ΔGI plateaued within a few seconds. A similar finding was noted clinically by De Bortoli *et al*, where 1 – 5 g of CF resulted in a ΔGI plateau at 10 seconds, compared with 6g – 30g which plateaued at 30 seconds[488]. These results are consistent with the seminal experimental findings by Haines who noted ablation lesions increased in size mono-exponentially with time and plateaued at a maximal size at 40 seconds[446]. These findings again suggest that having adequate rather than excessive CF is key in optimising ablation lesion development, and that ΔGI is a suitable surrogate in assessing this.

Due to cardiac contraction, maintaining catheter, and therefore CF stability is challenging. Consequently, CF will vary during ablation, and the degree of this (contact force variability, CFV) has been shown to negatively correlate with ΔGI. This finding is consistent with greater ΔGI being shown when atrial ablation is performed in AF over SR[389], where atrial contraction is essentially absent[389]. This is an interesting finding, as it raises the question of which atrial rhythm it would be more efficacious to perform ablation in. Along similar lines, the actual catheter drift within 3D space is also negatively correlated with ΔGI[389].

1.10.3.3.2 Ablation Index and Force Time Integral

To establish average values of AI and FTI for when ablation lesion completion occurs, the start of the ΔGI plateau has been used as a surrogate. This technique also allowed the average maximal ΔGI at this point to be calculated in the left atrium, which could be used by electrophysiologists as a guide to the progress of an individual ablation. Using the Thermocool SmartTouch catheter (Biosense Webster), Ullah *et al* found a ΔGI plateau at 7.5% in patients with persistent AF, consistent with a target FTI of 500gs[383]. With the same catheter, Hussain *et al* found a median ΔGI of 13.7Ω when using an AI target of between 400 – 550[470]. Using the

Thermocool SmartTouch Surround Flow catheter, a plateau of 184gs or 400AI was shown, a ΔGI of approximately 3.5%[493].

No studies have established average values of AI, FTI or maximal ΔGI corresponding to the ΔGI plateau in the left ventricle.

1.10.3.3.3 Tissue Characteristics

Similar to differences in ablation lesion size with ventricular fibrosis, differences in ΔGI have also been shown. In a porcine model, Tofig *et al* showed alongside creating smaller ablation lesions in areas of lower voltage amplitude, there was a corresponding decrease in ΔGI, with normal voltage myocardium showing a mean maximal ΔGI of 27Ω and low voltage myocardium 9Ω[429].

The effect of ventricular fibrosis on ΔGI has not been studied in a clinical setting.

1.10.3.4 Clinical Targets for Generator Impedance Drop

A precise value for the optimal maximal ΔGI has not been definitively established for clinical use in either the atrium or ventricle. Experimental ventricular models have noted a ΔGI greater than 15Ω is associated with tissue pops, clearly indicating an upper safety level to be avoided during ablation[448,494]. A 10Ω drop has been shown to be a reasonable target, delivering equal sized lesions to a 20Ω drop in a porcine model whilst minimising complications[494]. Furthermore, in the atrium, 10Ω has successfully eliminated accessory pathways clinically[495], and minimise pulmonary vein reconnection sites[487]. Using AI to guide AF ablation, Hussain *et* al found a mean maximal ΔGI of 13.7Ω delivered 83% arrhythmia freedom at 12 months[470].

However, due to variations in Z_B between patients, a specific value of 10Ω may be too low for some, but too high for others (e.g., due to variation in body surface areas) to achieve an effective ablation lesion. Consequently, a percentage drop from baseline has been suggested as a more all-encompassing target. For left atrial ablation, Ullah *et al* found the average maximal %ΔGI plateaued at 7.5% when ablating in AF and 6% when ablating in SR[383].

There is a paucity of clinical studies investigating clinical targets for ΔGI in the left ventricle. Bourke *et al* investigated changes in biophysical parameters in VT ablation lesions including a maximal ΔGI of 10Ω or greater[496]. However, the specific relationship of this ΔGI to a clinical endpoint such as late potential abolition or modification is not noted. No other clinical studies exist aiming to determine an optimal ΔGI in VT ablation, nor relationships to FTI, AI or EGM attenuation.

1.10.4 Local Impedance

Although GI is a useful biophysical parameter, its measurement is dependent on all parts of the ablation circuit. For an electrophysiologist, the measurement of interest in Z_A, in particular the impedance at the EBI. Recently, two ablation catheters (IntellaNav MiFi and IntellaNav Stablepoint from Boston Scientific®) have come to market capable of measuring Z_A or local impedance (LI) within the ablation circuit alone. Measuring LI is a promising development as it eliminates the inconsistencies that can be seen with Z_B and GI. Consequently, LI could act as a more accurate and sensitive surrogate for lesion development and completion than GI.

1.10.4.1 Measuring Local Impedance

Both the MiFi and Stablepoint catheters measure LI in a similar manner. A non-stimulatory alternating current of 5μA at 14.5Hkz flows between the catheter tip and a ring electrode (MiFi: proximal, Stablepoint: 2nd), creating an electrical field. The voltage of this field is passively measured in a separate circuit by the tip electrodes. Any electrical field distortions, (for example, by tissue), will affect the voltage within the field. Through Ohm's law, the LI can then be measured by the dividing the voltage by the supplied current. For the MiFi catheter, as current flows to the three miniature electrodes, three values are established with the highest being displayed to the operator[489]. For Stablepoint, the catheter tip possesses only a single electrode and thus one reading is generated and displayed[375]. Due to the difference in the generation of the electrical field, differences in LI are seen between the two catheters, with Stablepoint having relatively higher values than MiFi. This means that LI values generated by the two are not directly comparable.

1.10.4.2 Clinical Factors Affecting Baseline Local Impedance

The baseline LI is a measurement of Z_A, and consequently reflects the amount of ETI and EBI formed at the catheter tip. This means it is capable of reflecting tissue contact as ETI increases in place of EBI. However, it is also able to determine the underlying tissue health, as the resistance at through the myocardium will be affected by its intra- and extra-cellular composition. Both of these factors combined determine the baseline LI, a vital metric which can be used as a mapping parameter and is a key determinant of ΔLI.

1.10.4.2.1 Tissue Characteristics

Although clinical use of LI has only begun in recent years, initial studies exist from over 30 years ago. The ability of baseline LI to discern the underlying degree of fibrosis within ventricular myocardium was first established by Fallert *et al* in 1993[497]. Using an ovine model, epicardial LI measurements were taken pre- and post- MI, showing infarcted regions had a LI of 59% from baseline. Similar findings were published in later pre-clinical studies[498,499]. The pathophysiological reasoning behind the fall in LI is surmised to be due to the increase in extracellular space caused by necrosis and myocyte loss through which current can flow following infarction[497].

The use of LI in an ablation catheter (MiFi) was first examined by Sulkin *et al*[489]. Using porcine models, they noted LI was significantly lower in the blood pool compared to tissue contact, (median 67.6Ω vs 119.7Ω). A similar finding was noted by Garrott *et al* in the first study using the Stablepoint catheter, (mean 122Ω vs 220Ω [perpendicular tissue contact] or 207Ω [parallel])[375].

However, the effect of myocardial fibrosis on baseline LI has not been extensively examined and no histological studies exist to correlate the two. Using a computer model, Unger *et al* demonstrated a fall and recovery in LI when a virtual catheter approached and then passed over a linear ablation line[376]. Clinically, studies have used bipolar voltage amplitude as a surrogate for tissue health. Martin *et al* demonstrated an exponential relationship of bipolar voltage with baseline LI using the MiFi catheter[500]. Similar results were shown by Gunawardene *et al*[501]. However, as the MiFi catheter lacks CF technology, these studies could not control this variable, and data linking baseline LI to bipolar voltage using the Stablepoint catheter to control for this is lacking.

1.10.4.2.2 Contact Force

In addition to the difference in LI found between tissue contact and the blood pool, Sulkin *et al* also found LI increased with CF using the MiFi catheter[489]. Using an in vivo atrial canine model with the Stablepoint catheter, Gutbrod *et al* noted baseline LI increased with CF, but plateaued from 20g onwards[502]. A similar finding was noted by Matsuura *et al* in an ex vivo ventricular model[503].

This is an interesting finding, as it again suggests the catheter-tissue coupling can no longer be optimised above a certain CF level.

Curiously, these results do not translate clinically, where studies have shown single readings of baseline LI and CF taken pre-ablation have no correlation[417,504]. However, these studies do not consider the effect of the underlying tissue characteristics, which could affect these readings. Nor do they account for the underlying rhythm, and therefore contact force variability that affects GI readings. The interactions of baseline LI, atrial rhythm, CF, and bipolar voltage have therefore not been fully investigated.

1.10.4.3 Clinical Factors Affecting Local Impedance Drop

Maximal ΔGI has been shown in pre-clinical and clinical studies to be a useful surrogate for ablation lesion development and completion. However, by having a greater focus on the impedance changes at the electrode-tissue interface, ΔLI could be an even more effective surrogate. Pre-clinical studies suggest this is the case, as ΔLI correlates more closely with ablation lesion dimensions than ΔGI for both MiFi and Stablepoint catheters[375,489].

The effects of different clinical factors on ΔLI are similar to ΔGI, with the key factors outlined below.

1.10.4.3.1 Duration

The duration of an ablation is a key contributor to ΔLI and follows a similar relationship to that of ΔGI with a linear drop before plateauing when a steady state temperature has been reached[489].

1.10.4.3.2 Tissue Characteristics

When using LI, the underlying tissue can be characterised in two ways, using traditional bipolar voltage, or through the baseline LI. Although a degree of correlation between the two has been shown, their relationship to ΔLI within the atrium is different.

Segreti *et al* found no correlation between bipolar voltage and ΔLI when using the MiFi catheter[505]. This is an interesting finding as one would expect a blunted response similar to that demonstrated by ΔGI in the ventricle[429]. Investigation of this relationship using Stablepoint has not yet been undertaken.

In contrast, baseline LI has been shown to be a predictor of ΔLI in multiple studies for both catheters[416,417,501,504-506]. This finding is valuable, as it suggests that if baseline LI could be optimised prior to ablation, it could result in greater maximal ΔLI values achieved, and creation of a larger lesion.

1.10.4.3.3 Contact Force

Similar to ΔGI, pre-clinical studies show a positive correlation between ΔLI and CF[502,503,507]. Interestingly, Gutbrod *et al* and Matsuura *et al* both showed initial increases in ΔLI before a plateau at approximately 20g, a relationship that was also seen with ablation lesion dimensions[502,503]. This finding has translated clinically, with Solimene *et al* also noting a plateau from approximately 20g in the ΔLI-CF relationship[417,508]. However, when dividing CF into 5g categories, although significant, the actual difference seen between ΔLI values is small, (e.g., 5 – 9g: 22.2Ω vs 20 – 24g: 24.6 Ω). This suggests that although there is an effect of CF on ΔLI, the most important aspect is making contact and forming an adequate electrode-tissue coupling at a small level of CF.

Furthermore, for the studies above, the bivariate correlations seen between CF and ΔLI are weaker than that with baseline LI. This suggests that CF is a complimentary metric to baseline LI, being able to detect a tissue-catheter coupling regardless of underlying tissue characteristics, but perhaps not being the optimal parameter to predict ΔLI during ablation.

1.10.4.3.4 Power

In pre-clinical studies, for both catheters, significantly greater ΔLI and lesion dimensions have been shown with higher power ablation (50W vs 40W or 30W)[502,507,509,510]. Tsutsui *et al* noted that power had an interaction effect on the CF-ΔLI relationship, with progressively greater ΔLI from 30W to 40W to 50W[507]. Clinically, the effect of power on ΔLI has not been extensively investigated, mainly being controlled in studies investigating the effects of CF or ΔLI on ablation lesions adjacent to gaps in WACA or posterior wall isolation lines[417,504].

1.10.4.3.5 Location

Differences in ΔLI have been noted between atrial walls. In a prospective trial where operators were blinded to ΔLI, both the anterior-superior walls and the posterior-inferior walls were found to have similar ΔLI values, with the former being larger. Due to this they were combined when discerning targets of ΔLI to be used clinically[467].

The effect of these clinical factors upon ΔLI for both the MiFi and Stablepoint catheters have been well investigated in pre-clinical and clinical studies. However curiously, their relative effects on ΔLI in a multivariable analysis has not occurred. Similarly, a comparison of the ability of the two catheters to predict ΔLI from these factors has not been applied, but would be useful, particularly to view the benefits of adding CF technology to Stablepoint, in exchange for the three mini-electrodes.

1.10.4.4 Clinical Targets for Local Impedance Drop

Establishing a clinical target for ΔLI that indicates an effective ablation lesion is important to guide electrophysiologists performing ablation. This is particularly relevant during AF ablation,

where a ΔLI value with a strong positive predictive value for transmurality is necessary to ensure effective PVI.

In the first study using Rhythmia and the MiFi catheter, Martin *et al* found a successful ablation lesion corresponded to ΔLI of 14Ω in the left atrium by using a standard of 50% attenuation in the near field EGM amplitude and the inability to pace capture. This value was similar to that found in the prospective LOCALIZE trial, which examined the ΔLI of individual ablation lesions in WACA lines and compared successful lesions to those adjacent to sites of pulmonary vein reconnection. Patients then went under a repeat procedure at 3 months to examine for any further pulmonary vein reconnections to established values of ΔLI consistent with long-term PVI. The LOCALIZE trial established 16.9Ω (anterior-superior walls) and 14.2Ω (posterior-inferior walls) as ΔLI targets with positive predictive values for transmurality of 97.7% and 96.9% respectively[511].

For the Stablepoint catheter, as LI values are higher than that of MiFi due to the differences in sampling, the results from LOCALIZE cannot be directly applied. To that end, multiple studies using a similar methodology to LOCALIZE have been performed, producing ΔLI values consistent with transmurality acutely, (i.e., at the time of the ablation procedure rather than at follow up procedure). Szegedi *et al* found optimal ΔLI values of 21.8Ω anteriorly and 18.3Ω posteriorly for a successful WACA ablation lesion[416]. Ikenouchi *et al* found a difference between carinal and non-carinal regions of 24Ω and 21Ω respectively[512]. Yasumoto *et al* and Fukaya *et al* found values of 23Ω and 20Ω respectively[504,513], whilst Solimene *et al* established values for posterior wall isolation of 19Ω for the roof line and 18Ω for the floor line[417].

Optimal ΔLI values for an effective lesion to for durable PVI have not yet been published but will be established in the upcoming LOCALIZE-CF trial, (ClinicalTrials.gov Identifier: NCT04740801).

1.11 Formulation of Thesis Studies

AF and VT ablation are procedures which can provide patients with significant relief from symptoms and/or ICD therapies. As clinicians we seek to continually advance these procedures to

improve outcomes. To this end, the advent of ultra-high-density mapping systems and LI provides a potential new step forward in the field of interventional electrophysiology. However, there are multiple gaps in our knowledge from a mapping and ablation perspective which when filled could help improve our understanding of the technology and its application in ablation procedures. Therefore, the objective of this thesis is to explore ultra-high-density mapping, LI, GI, and their relationships with diseased myocardium.

In Chapter 3, the ultra-high-density mapping of Rhythmia is used to challenge the traditional cut-offs for electrically inert and diseased atrial myocardium of 0.05mV and 0.5mV, values which although widely used, were arbitrarily selected. To do this, a simple yet original method is used by examining the pacing thresholds at different sites across the left atrium, and comparing to bipolar, unipolar and LI values. If different cut-offs are found using this method, it would give evidence for electrophysiologists to question and debate whether these held norms should be adjusted.

In Chapter 4, Rhythmia is used to examine if relationships established using lower density systems are still held to be true using modern, ultra-high-density, automated mapping system used today. These relationships include differences in the surface area and bipolar voltage between patients with paroxysmal and persistent AF; between left atrial maps in SR and AF; and novelly, a comparison between left and right atria. The results here provide insight into whether modern electroanatomical maps are able to bridge the gap between those created in SR or AF, and whether they are reasonable representations of each other. Furthermore, they provide insight to whether clinically relevant substrate is present in the under-investigated right atrium.

In Chapter 5, the relationship of CF with baseline LI is studied alongside the effect of atrial rhythm and bipolar voltage. Pre-clinical and clinical studies give different results for the CF-LI relationship, with pre-clinical studies showing a strong positive relationship which is absent clinically. However, their methodologies differ significantly, with no clinical study examining the effect on tissue characteristics, not taking repeat measurements from the same site. Knowledge of this relationship is important as both are known to affect ΔLI and ablation lesion size. Furthermore, the effect of atrial rhythm on CF-LI would be interesting, as if a stronger relationship is seen in AF or SR, it would suggest ablation could be optimised by being performed in that rhythm.

In Chapter 6, the effect of various clinical factors on ΔLI is investigated. In particular, the added effect of CF technology is examined by comparing the ability of the Stablepoint catheter to the MiFi catheter to predict ΔLI in a multivariable analysis. Through data modelling, the most significant clinical factors are highlighted, optimal values suggested and targets for ΔLI presented based upon the LOCALIZE trial.

Finally, in Chapter 7, the biophysical relationships between ΔGI, AI, FTI and ventricular scar are examined in patients undergoing VT ablation. The ability of AI and FTI to predict ΔGI in different levels of scar is established. By providing insight into this area, an average value of AI, FTI and ΔGI can be offered, which could form a guide for electrophysiologists performing the procedure. Furthermore, as a workflow for VT ablation is not clearly established, it presents values that could be used in future research.

The over-arching goal of this thesis is to provide new information concerning these recent technologies in mapping and ablation of the atria and ventricles, to help electrophysiologists optimise their procedures, and ultimately to drive improvement in patient outcomes and care.

Chapter 2 Shared Methods

Common methodology shared between studies is discussed in this chapter below. Specific methods are detailed in each chapter.

2.1 Study Institution

The data for the studies in this thesis were derived from cardiac ablation procedures performed within the cardiac catheter laboratories at University Hospital Southampton NHS Foundation Trust, UK. Procedures from were performed by four consultant cardiac electrophysiologists, Dr Waqas Ullah, Dr Arthur Yue, Dr John Paisey and Professor Paul Roberts, all of whom have extensive experience in using the Rhythmia HDx and CARTO3 mapping systems and their associated catheters. Support for the procedures was provided by specialised cardiac rhythm physiologists at University Hospital Southampton, Boston Scientific (Rhythmia HDx) and Biosense Webster Inc (CARTO3).

2.2 Funding

Funding was provided for the studies in Chapters 3 – 6 by an Investigator Sponsored Research funding agreement with Boston Scientific, (ISRCAR00110, ISRRM12101). Funding was provided for the study in Chapter 7 by an Investigator-Initiated Study funding agreement with Biosense Webster Inc (IIS-484).

2.3 Research and Development, Ethical Approval and Governance

All studies in this thesis achieved the relevant approvals from national and local ethical and research and development boards.

Chapters 3 – 6 are had data collected as part of the 'High Density Scar Guided Atrial Fibrillation Mapping' study (HD-SAGA), which was approved by the South Central – Oxford A Research and Ethics Committee (18/SC/0077), University Hospital Southampton Research and

Development (RHM CAR0523) and University of Southampton (ERGO 53201). The study is registered on clinicaltrials.gov, (Identifier: NCT 03363087).

Chapter 7 had data collected as part of the 'Late Potential and Ablation Index in Ventricular Tachycardia Ablation' study, which was approved by the London - City and East Research and Ethics Committee, (18/LO/0839), University Hospital Southampton Research and Development (RHM CAR0538) and University of Southampton (ERGO 53204). The study is registered on clinicaltrials.gov, (Identifier: NCT 03437408).

Adverse events were recorded and reported to University Hospital Southampton Research and Development as the sponsor and the approving Research and Ethics Committee in line with reporting policy.

2.4 Patient Recruitment

The inclusion criteria for the studies were:

- Clinically listed for AF or VT ablation procedure
- Age > 18 years
- Ability to consent to procedure and research protocol

Exclusion criteria were:

- Inability to take oral anti-coagulation, (Chapters 3 – 6 only)
- Clinical contraindication to ablation procedure (e.g., intra-cardiac thrombus)

Patients meeting criteria for participation in the studies were assessed from procedural waiting lists and clinic records. Confirmation of this was then obtained from their respective consultant electrophysiologist. Patients were approached by telephone where the relevant study was explained to them. A patient information sheet and general data protection regulation form was then forwarded to them by post or secure email. A follow up telephone call to address any questions and obtain a participation decision was conducted at least one week following receipt

of the information to allow a patient time for discussion with family and friends. Written consent for participation in the studies was taken on the day of their procedure. Participation in a study was voluntary.

2.5 Data Handling and Record Keeping

All confidential patient data was accessed and stored consistent with and general data protection regulation, hospital policies and the Data Protection Act 1998. Patient data was accessed using hospital systems. Procedural data used for the studies was exported onto password protected encrypted external hard drives and stored in a secure office on hospital site. Paper records were stored in a site file in a secure office. Study participant data was anonymised via use of a personal code which was stored on the 'Edge' clinical research management system.

2.6 Electroanatomical Mapping Systems

Two electroanatomical mapping systems were used for the studies in this thesis. In chapters 3 – 6, the Rhythmia HDx system (Boston Scientific, Marlborough, MA, USA) was used in conjunction with the Orion mapping catheter in studies related to the atria. In Chapter 7, the CARTO3 system (Biosense Webster Inc., Irvine, CA, USA) was used with the PENTARAY mapping catheter in a study on the left ventricle.

2.6.1 Rhythmia HDx

2.6.1.1 Interface

An example of the Rhythmia interface is shown in Figures 2-1 and 2-2. As an ultra-high-density system, Rhythmia is able to create 3D electroanatomical maps using over 10 000 electrograms in a matter of minutes. Anatomical, electrophysiological and ablation parameters including LI can be displayed on a single screen.

Figure 2-1 *The Rhythmia HDx interface.*

This interface relays real-time anatomical and electrophysiological information to the operator. A = ECG and electrogram recordings; B = Parameters required for acceptance of an electrogram to the electroanatomical map; C = Two views of the electroanatomical map, see Figure 2-2 for details.

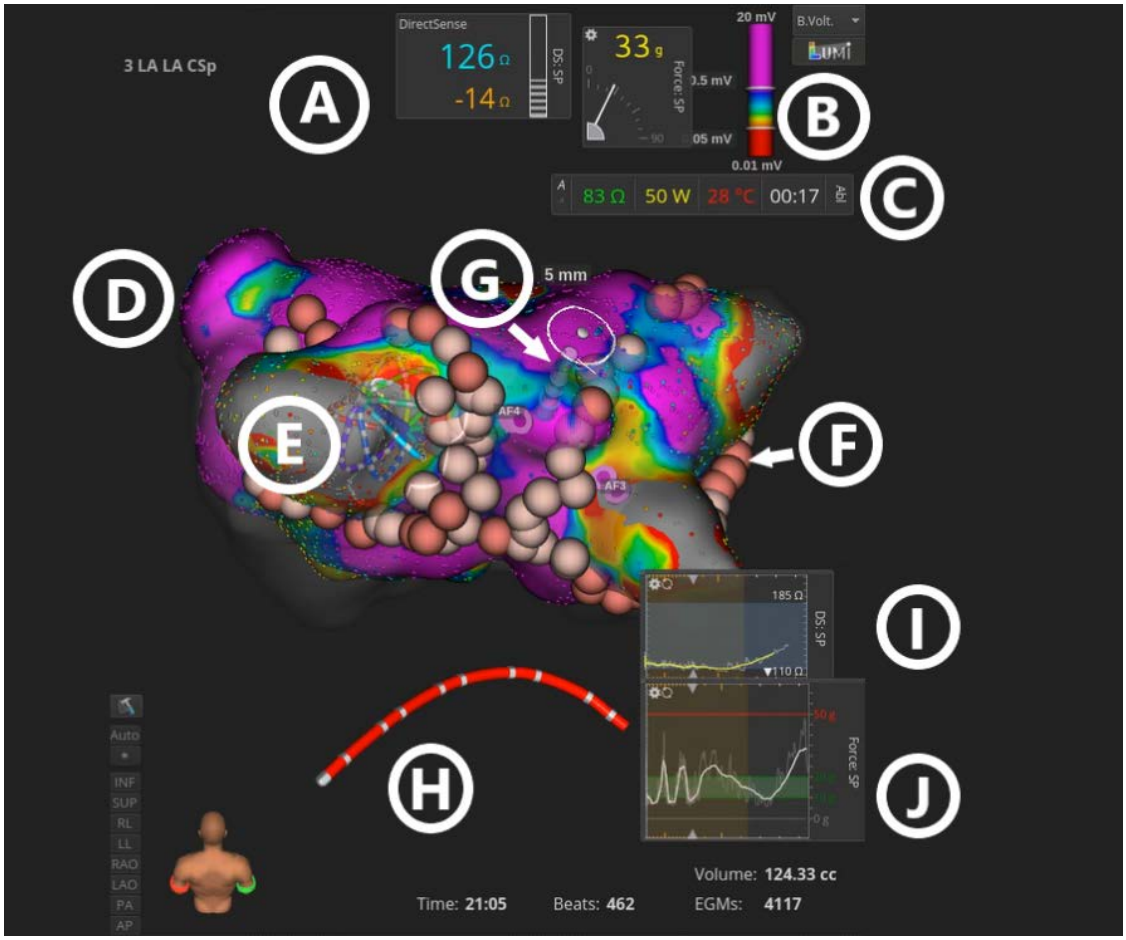

Figure 2-2 *Focussed image of a left atrial electroanatomical map using Rhythmia HDx. A = Local impedance reading (126 Ω), change from baseline (-14 Ω) during an ablation and contact force reading (33g); B = Bipolar voltage values and colour code to delineate dense scar and diseased tissue; C = Ablation information displaying generator impedance, power, catheter tip temperature and duration; D = The 3D anatomical shell coloured as per B; E = Intracardiac position of the Orion catheter; F = Ablation lesion tag; G = Ablation catheter and distance (5mm) to nearest ablation tag; H = Coronary sinus reference catheter; I = Real time local impedance graph; J = Real time contact force graph.*

2.6.1.2 Export

Mapping and ablation data was exported from Rhythmia as MATLAB files (The Mathworks Inc. Natick, MA, USA) where it was processed before re-export for statistical analysis on SPSS Statistics (IBM, Armonk, NY, USA).

The mapping export provides the xyz co-ordinates, local activation time, bipolar and unipolar voltages of accepted electrograms that form the visualised electroanatomical shell. An example of the processed data from the export is shown in Table 2-1. Various arrangements of this data were used depending on the statistical tests used.

Table 2.1 *Example of Processed Data from the Rhythmia Mapping Export. 'Atrium' and 'AF Type' are coded as they are discrete variables*

Point	Patient	Atrium	AF Type	x	y	z	Bipolar	Unipolar
1	1	0	0	34.90	-0.96	-207.62	0.47	0.94
2	1	0	0	36.00	-1.38	-207.85	0.51	0.93
3	1	0	0	37.05	-1.53	-207.94	0.52	0.93
4	1	0	0	38.13	0.18	-207.83	0.58	0.95
5	1	0	0	35.00	-0.33	-208.00	0.48	0.92

Trios of electrograms forming the vertices of a triangle are also provided, which in combination recreate the entire anatomical shell. Using these, the surface area of the shell can be calculated, and then divided up how the user deems appropriate.

Rhythmia also provides a cut-out tool, allowing a user to remove sections of a map they do not wish to be analysed, for example, electrically inert areas such as the pulmonary veins or vena cavae. The export provides co-ordinates of all excluded electrograms using this tool, making their removal from any analysis straightforward.

The ablation export supplies details of every ablation that occurred including duration, average power, average CF, starting LI, minimum LI, maximal LI drop and xyz co-ordinates of the ablation tag placed on the map. Through a research agreement with Boston Scientific, access to higher levels of detail were also made available for analysis, including LI, CF and xyz of the catheter tip position, sampled at 20Hz from approximately 5 seconds prior to ablation to 5 seconds after. LI is provided in both a raw and filtered format. This export provides large levels of detail on electrophysiological parameters and their changes with radiofrequency ablation. It also allows creation of variables such as catheter drift (the maximum distance travelled from the mean

xyz co-ordinates) or contact force variability (the difference between averaged CF peaks and troughs). Also, through combining the ablation and mapping export data, tissue voltages of each ablation can be established by co-locating their xyz co-ordinates. An example of the processed data from the export is shown in Table 2.2

Table 2.2 *Example of Processed Data from the Rhythmia Ablation Export. 'Location' and 'Power' are coded as discrete variables*

Point	Patient	Ablation No	Location	Duration	LI	CF	Power	BiP
1	1	1	2	0.00	101.15	11.15	50	0.47
2	1	1	2	0.05	101.10	11.23	50	0.51
3	1	1	2	0.10	101.03	11.04	50	0.52
4	1	1	2	0.15	100.87	10.98	50	0.58
5	1	1	2	0.20	100.65	10.97	50	0.48

2.6.2 CARTO3

2.6.2.1 Interface

An example of the CARTO3 interface is displayed in Figure 2-3 Anatomical, electrophysiological and ablation parameters are displayed with the cumulative scoring system 'Ablation Index' to guide an operator on how long to administer radiofrequency energy.

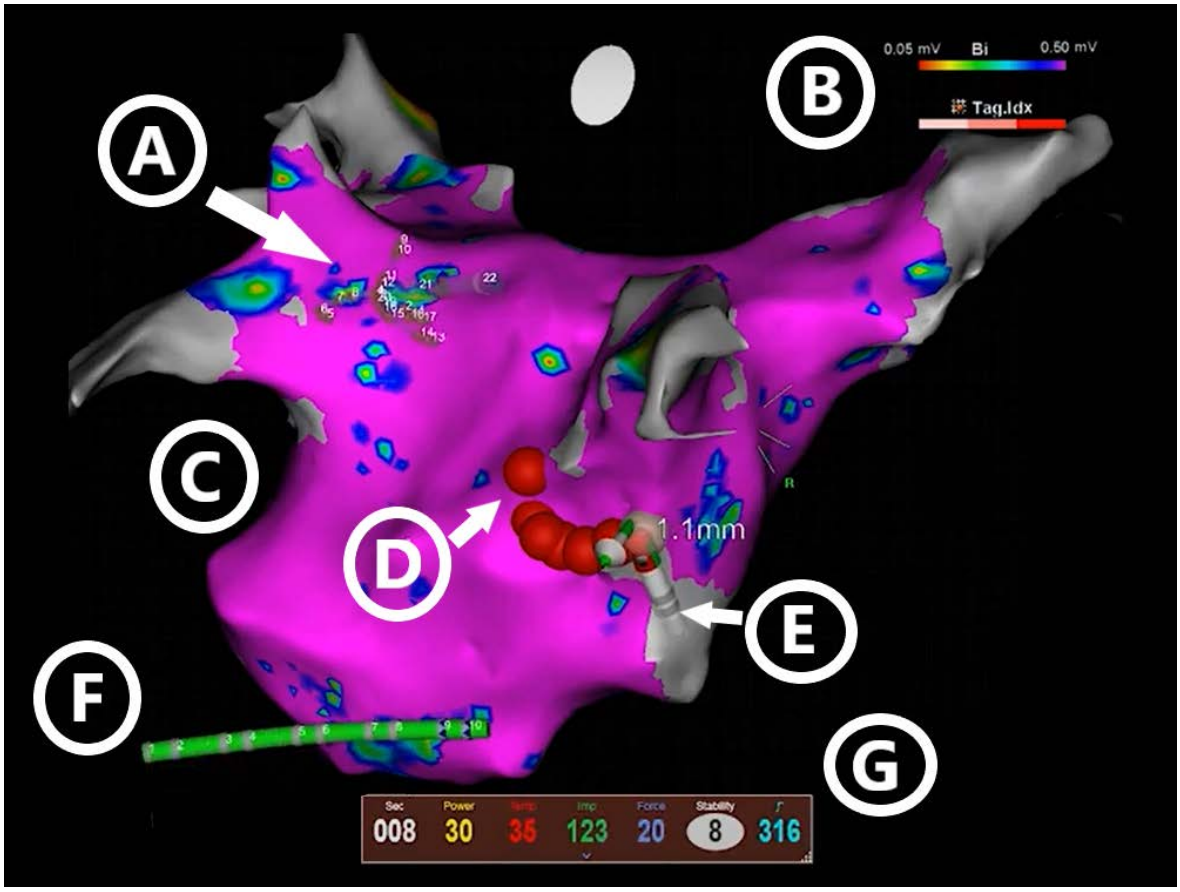

Figure 2-3 *A focussed image of a left atrial electroanatomical map using CARTO3*
This interface relays real-time anatomical and electrophysiological information to the operator. A = Pentaray mapping catheter; B = Bipolar voltage parameters set to delineate healthy (purple) and diseased tissue (rainbow or grey); C = The 3D electroanatomical voltage map; D = An ablation tag; E = The ablation catheter and distance to the last tag (1.1mm); F = Decapolar reference catheter in the coronary sinus; G = Ablation parameters including current ablation duration, power, temperature, generator impedance, contact force, catheter stability and ablation index respectively.

2.6.2.2 Export

The CARTO3 export provides data in thousands of separate .txt files which were imported onto MATLAB and processed accordingly. Ablation data is automatically created by the system for export, and any manual tags that are placed also generate data 2 seconds retrospectively, and 0.5 seconds prospectively. Parameters exported include timestamps, CF, GI, power (sampled at 10Hz), and xyz co-ordinates (50Hz) of catheter electrodes. Similar to the Rhythmia export, as

ablation parameters are linked to time, relevant variables such as catheter drift can be created if required.

Both FTI and AI are provided in the export, but only as the values created by the end of the ablation. To allow for more in-depth analysis in Chapter 7, the FTI and AI were calculated for every available timepoint, thereby generating the cumulative AI and FTI during ablation.

For the FTI, the area under the force – time curve was calculated using trapezoidal integration. Therefore, a cumulative FTI value was created every 100ms that specifically reflected the changes in CF. This was seen as preferable to calculating total FTI using the product of the mean contact force and total ablation duration and then equally distributing FTI values across the ablation.

For AI, a proprietary algorithm is required for calculation. The general formula is published:

$$(k * \int^{T}_{0} CF^{a}(t)\, P^{b}(t)\, \delta t)^{c}$$

CF is contact force, P is power, T is total ablation duration, and other letters being unpublished constants that were kindly provided by Biosense Webster for analyses in Chapter 7. As these variables are provided on the export at 10Hz, a cumulative AI value could be calculated every 100ms.

The GI values exported from CARTO3 are in a raw, unfiltered format which suffer from a lot of noise. Data was smoothed by applying a Savitzky-Golay mathematical filter to allow a greater appreciation of the true signal over the noise. This is a commonly used digital filter which applies a low degree polynomial to successive adjacent data points[514].

2.7 Data Analysis

All exported data was processed into an appropriate format for statistical analysis using MATLAB Version R2020a. Due to the specific nature of the data exports for both Rhythmia and CARTO3, custom MATLAB scripts were written from the ground up by the thesis author. All statistical analyses were performed in SPSS Statistics Version 27 by the thesis author.

2.7.1 MATLAB Coding

Although the exports from both Rhythmia and CARTO3 were highly detailed, they were not in a form that could immediately be used for analysis. Consequently, in order to examine data in a detailed manner, custom MATLAB scripts were used to examine, clean and order the data appropriately so statistical testing could occur.

For Rhythmia HDx, the export generated direct MATLAB files as discussed in Chapter 2.6.1.2. The ablation data export was verified by comparing to manually recorded data that was taken for each ablation. This included the ablation number within the procedure, ablation duration, starting LI, ending LI and generator impedance of every lesion taken. When an ablation was deemed inappropriate for analysis during the procedure, for example, pre-mature curtailment due to macrodisplacement, these ablations were swiftly identified by co-locating the manually recorded data with that on the export. These data could then be deleted from files used for analysis.

For ablation data, a large table was created with columns holding variables of interest during the ablation, for example, time since the beginning of ablation, current LI values, contact force, ablation location and so on. The rows of this table contained data organised in time order, i.e. each subsequent row contained data 50ms later than the previous. This continued until the end of the ablation and the next ablation data would begin. Due to the ablation data being available every 50ms on the export, this generated an eventual table with 1,410,291 rows.

For mapping data, a similar table was created holding the xyz co-ordinates of every electrogram recorded and associated data, for example tissue voltages. This generated a table with 215,930 rows.

For all MATLAB scripts written, they were assembled in blocks, meaning every variable of interest was extracted, its data cleaned and placed into the master table individually. The scripts would function by looping, that is extracting a piece of data before repeating the method to extract the next one. By doing this, it was simple to verify the correct functioning of the script by manually checking the correct data had been extracted after it had run after a single loop. Typically, a script was manually checked 3-5 single loops to ensure correct extraction. After one variable of interest had been completely extracted, it would move onto the next portion of the script and extract another one, which could be verified manually in a similar way. This process would repeat until all cleaned, relevant data for each patient had been extracted.

For CARTO3, the extracted data was cleaned and verified in a similar manner, with manual checks occurring. Likewise, the MATLAB scripts written were checked by running a single loop multiple times to ensure the correct data was extracted into the master table for each variable. However, the extraction process was slightly different requiring the identification of the correct .txt file before its import into MATLAB. This was achieved by running code that identified the files of interest. Specifically, for contact force data, files ending in ***ContactForce.txt, and ablation data ending in ***ContactForceinRF.txt

Chapter 3 Refinement of Voltage-Based Atrial Scar Assessment Using Pacing Thresholds and Local Impedance

3.1 Abstract

Background

Conventional cut-offs for scar (0.05 and 0.5mV) on left atrial 3D electroanatomical mapping have minimal physiological validation.

Objectives

Investigate the relationships between tissue voltages and local impedance with pacing thresholds (PT). Establish cut-offs for electrically inert (EI), partially active (PA) and electrically active (EA) tissue.

Methods

Patients undergoing atrial fibrillation ablation were recruited. Pacing thresholds, tissue voltages and local impedance referenced to blood pool (LIr) were obtained using IntellaNav MiFi and Stablepoint (SP) catheters. EI, PA and EA sites were defined as no pacing capture, a PT of 5-20mA and <5mA respectively.

Results

292 sites (202 MiFi, 90 SP) were recorded in 40 patients. Tissue voltages correlated weakly with PT (Spearman's ρ – Bipolar: -0.35, Unipolar: -0.26, both $p < 0.0005$). LIr correlated moderately with PT (ρ – MiFi = -0.52, SP = -0.57, both $p < 0.0005$).

The lowest values for sites with pacing capture were 0.03mV, and 1Ω (both MiFi and SP). For the PA-EA cut-off, the discriminatory ability for bipolar voltages was fair (AUROC = 0.69, optimal cut-off 1.29mV) and LIr was good, (AUROC - MiFi = 0.82, optimal 12.5Ω, SP = 0.89, optimal 10.5Ω). Using these cut-offs, significant differences were seen for PTs and variance between PA and EA, for bipolar voltage ($p < 0.0005$) and LIr (MiFi: $p = 0.001$, SP: $p < 0.0005$).

Conclusions

PTs suggest conventional voltage cut-offs could be improved. LIr shows potential as a novel parameter in assessing tissue health complimentary to bipolar voltages.

3.2 Introduction

Fibrosis is implicated in the pathophysiology of atrial arrhythmias as a trigger[332] and substrate[333] for atrial fibrillation (AF), alongside acting as an anatomical obstacle for re-entrant tachycardias. An accurate appreciation of atrial substrate is important, as the extent and severity of fibrosis is associated with progression of AF[334,335,378], arrhythmic recurrence post-ablation[377] and can be used to guide ablation[336,345].

Electroanatomical mapping systems display atrial substrate using bipolar voltage as a surrogate for histological fibrosis. Conventionally, healthy tissue is defined as greater than 0.5mV and dense scar less than 0.05mV. These values have not been histologically confirmed, and have only minimal physiological validation using the original CARTO mapping system[401].

A novel marker with the potential to assess atrial substrate is local impedance (LI). Although initial studies have shown LI capable of determining tissue health based on bipolar mapping[500,505], its ability to determine electrically inert from fibrosed to healthy tissue is unknown.

To assess atrial tissue health more physiologically, this study investigated the relationship between tissue voltage, LI, and pacing thresholds (PT). Healthy tissue was hypothesised to have a

low PT with little variance; fibrosis was expected to raise the PT and have a greater variability of measurements. A further objective was to develop cut-off values separating electrically inert (EI), partially active (PA) and electrically active tissue (EA) based on these results.

3.3 Methods

3.3.1 Procedure

Patients scheduled for elective ablation of atrial fibrillation were prospectively enrolled. Procedures were performed under general anaesthetic or local anaesthetic with conscious sedation. The Agilis® steerable sheath (Abbott Laboratories, Chicago, IL, USA) was used for all cases. Mapping was performed with proximal coronary sinus pacing from a decapolar catheter placed in the coronary sinus. Patients in AF at the start of the procedure underwent DC cardioversion to sinus rhythm. For all cases, 3D electroanatomical maps were created using proximal coronary sinus pacing with the 64-electrode IntellaMap Orion™ basket catheter paired with the Rhythmia HDx™ system,

3.3.2 Data Collection and Analysis

PT sites were selected by the operator encompassing a range of locations and voltages as shown by the 3D electroanatomical maps. The specific anatomical locations of PT sites were not pre-determined and could occur anywhere on the left atrial endocardium. However, operators were instructed to select sites surrounded by tissue of a similar voltage as visualised on the 3D map. This was to minimise the recruitment of adjacent healthier tissue when testing diseased tissue and thereby giving a falsely low reading. A minimum of 5 PTs were performed in each patient. PTs were assessed using either the IntellaNav MiFi and Stablepoint (SP) ablation catheters between the tip and first ring electrodes. The MiFi catheter does not possess contact force technology. Consequently, contact was assessed by a combination of proximity to the anatomical shell on the 3D electroanatomical map, presence of electrograms from the catheter tip and tactile feedback. With the SP catheter, since it is able to measure contact force, a contact force of 10g was targeted. PTs were assessed with a 2ms pulse duration commencing at 5mA and moved up or down accordingly. Sites without capture had their PT recorded as the maximum tested 20mA. At PT sites a manual tag was placed to allow for analysis of data following export. Both voltage (bipolar and unipolar) and LI data were recorded at each site.

3.3.3 Local Impedance

LI was measured using methods described in previous studies[375,489]. The MiFi catheter establishes LI by taking the highest of three values sampled between the proximal ring and three miniature tip electrodes. The SP catheter only possesses a single tip electrode due to the presence of CF technology, and therefore samples LI between the tip and the second ring electrode. Due to this, a difference in LI values is seen, and consequently analysis involving LI was performed separately for MiFi and SP. As LI varies with cardiac contraction, the mid-point of measured LI minima and maxima during the PT was recorded. LI was referenced against a blood pool reading (LIr = Recorded LI – Blood Pool LI).

3.3.4 Bipolar and Unipolar Voltage

Voltage data from the 3D electroanatomical maps created with the Orion mapping catheter were exported from Rhythmia and analysed using custom MATLAB scripts. The bipolar and unipolar voltages of the PT sites were determined by co-locating the xyz co-ordinates of the Orion-collected voltage map with those of the manual tags.

3.3.5 Statistical Analysis

IBM SPSS Statistics was used for statistical analysis. A p-value of <0.05 was considered statistically significant. Variables were assessed as parametric or non-parametric by visual inspection of histograms and a Shapiro-Wilks test. Continuous data were expressed as mean ± SD. Count data were expressed as number (%). Bivariate correlations were performed using Spearman's rank correlation. Independent samples were compared using a t-test for continuous data or a chi-squared test for categorical. Levene's Test was used to assess for homogeneity of variances. Receiver operator curves (ROC) were created to assess for the discriminatory ability of continuous variables on a binary outcome and develop optimal cut-off values.

3.4 Results

3.4.1 Patient and Pacing Site Characteristics

Patient and pacing site characteristics are detailed in Tables 3.1 & 3.2.

Table 3.1 *Study Population Characteristics*

Patient Characteristics	Altogether	MiFi	Stablepoint	P-Value
n	36	18	18	--
Female	18 (50%)	7 (38.9%)	11 (61.1%)	0.34
Age, Years	66.5 ± 9.1	66.2 ± 9.1	66.8 ± 9.3	0.84
Body Mass Index (kg/m^2)	31.4 ± 5.4	29.6 ± 5.7	33.2 ± 4.6	0.04
Type of Procedure				
De Novo	18	9	9	1.00
Redo	18	9	9	
Co-Morbidities				
Arterial hypertension	16 (44.4%)	7 (38.9%)	9 (50%)	0.50
Ischaemic heart disease	5 (13.9%)	2 (11.1%)	3 (16.7%)	0.63
Diabetes mellitus	3 (8.3%)	1 (5.6%)	2 (11.1%)	0.55
Stroke	1 (2.8%)	1 (5.6%)	0	0.31
Heart Failure	9 (25%)	3 (16.7%)	4 (22.2%)	0.67
LVEF (%)	57.4 ± 7.9	57.1 ± 10.1	57.8 ± 5.7	0.80
CHA_2DS_2-VASc	2.3 ± 1.3	2.0 ± 1.4	2.6 ± 1.2	0.22
Type of Atrial Fibrillation				
Paroxysmal	9 (25%)	9 (50%)	0	
Persistent	8 (22.2%)	3 (16.7%)	5 (27.8%)	0.002
Chronic persistent	19 (52.8%)	7 (33.3%)	13 (72.2%)	

Displayed as n, (%) or mean ± standard deviation. ACEi: Angiotensin converting enzyme inhibitor; ARB: Angiotensin receptor blocker; ARNI: Angiotensin receptor neprilysin inhibitor; DOAC: Direct oral anti-coagulant; MRA: Mineralocorticoid receptor antagonist; LVEF: Left ventricular ejection fraction

Table 3.2 *Procedural and Pacing Site Characteristics*

Tissue Health Markers	Altogether	MiFi	Stablepoint
Bipolar Voltage	1.58 ± 2.17	1.63 ± 2.28	1.46 ± 1.90
Unipolar Voltage	2.40 ± 2.23	2.42 ± 2.33	2.38 ± 1.98
Blood Pool LI	----	96.5 ± 10.3	145.9 ± 15.0
Tissue LI	----	115.8 ± 18.1	161.6 ± 19.2
Referenced LI	16.2 ± 15.2	18.1 ± 17.0	12.0 ± 8.5
Pacing Site Locations			
Total	292	202	90
Per Patient	8.11 ± 4.01	11.22 ± 3.51	5.00 ± 0.49
Roof	25	15	10
Posterior	67	47	20
Anterior	65	40	25
Inferior	35	26	9
Lateral	52	39	13
Septum	30	22	8
Appendage	18	13	5

Displayed as n (%) or mean ± standard deviation. Local impedance (LI) measured in Ohms. Voltages measured in millivolts.

Across 36 patients, 292 pacing thresholds were checked. LIr correlated weakly with both bipolar and unipolar voltage, (Spearman's ρ – MiFi: Bipolar 0.34, Unipolar 0.25 [$p < 0.0005$ both]; SP: Bipolar 0.22 [$p = 0.02$], Unipolar 0.20 [$p = 0.04$]).

3.4.2 Relationship of Pacing Threshold to Tissue Health

Both bipolar and unipolar voltages correlated weakly with PT (ρ – Bipolar: -0.35, Unipolar: -0.26, both $p < 0.0005$). In contrast, LIr showed moderate correlations with PT for both catheters (ρ – MiFi = 0.52, SP = 0.57, both $p < 0.0005$, Figures 3-1 & 3-2). All methods of assessing tissue health showed a similar negative relationship with PT which plateaued between 2 and 5mA. The variability of PTs observed decreased as tissue health improved, a finding that was more marked for LIr than tissue voltage.

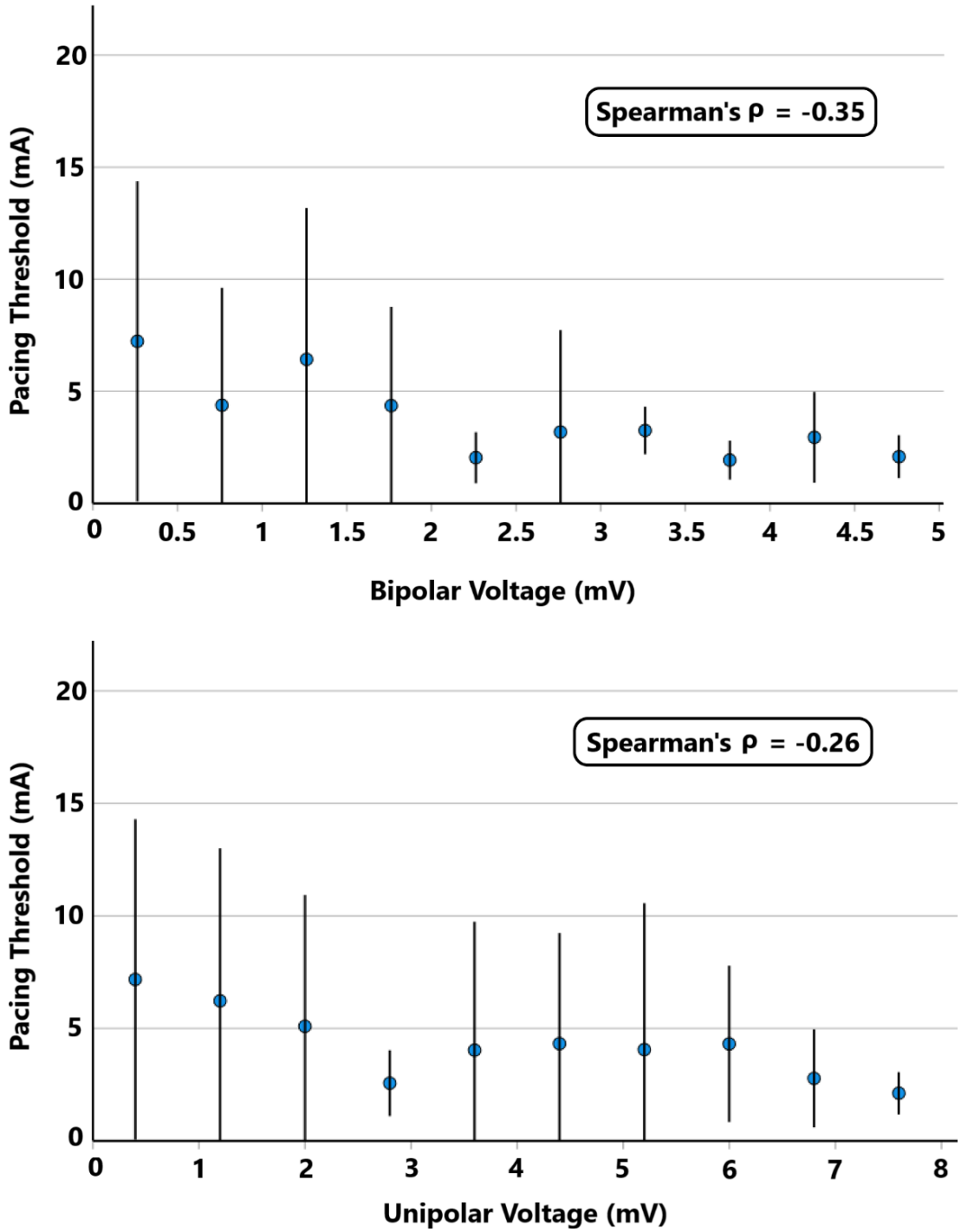

Figure 3-1 *Relationship of tissue voltages with pacing threshold.*
Voltages were placed into deciles every 0.5mV (bipolar) and 0.8mV (unipolar). Each data point is the mean pacing threshold for that decile ± 1 standard deviation and is placed in the mid-point of the voltages it represents. (n = 36)

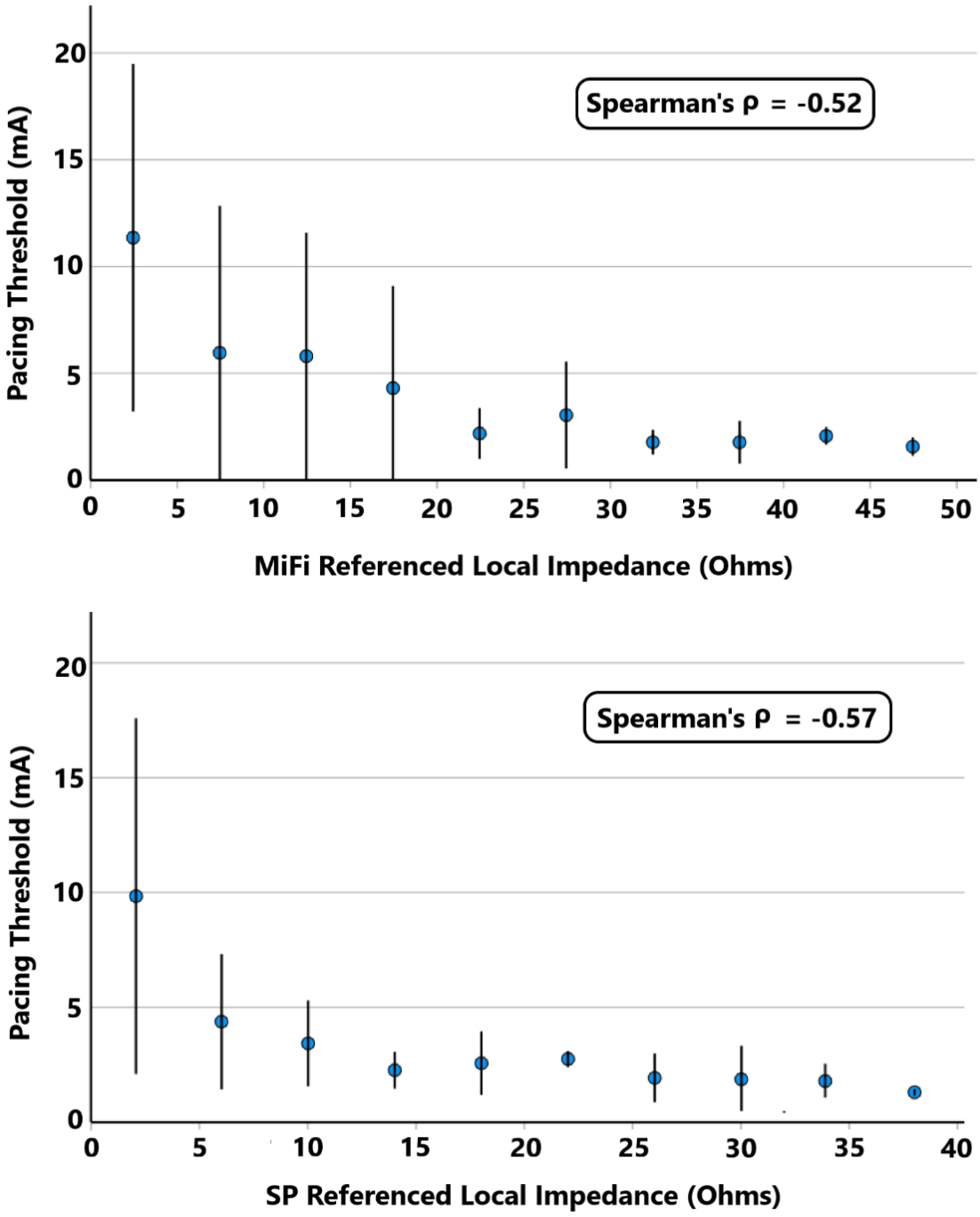

Figure 3-2 *Relationship of referenced local impedance with pacing threshold.*

Local impedance was placed into deciles every 5Ω (MiFi) or 4Ω (SP). Each data point is the mean pacing threshold for that decile ± 1 standard deviation and is placed in the mid-point of the referenced local impedance it represents. SP = Stablepoint. (n = 18 for MiFi and SP)

3.4.3 Optimal Values for Inert Tissue

LIr showed a greater ability to distinguish EI from active tissue than tissue voltages, (AUROC – LIr MiFi: 0.87, LIr SP: 0.90; Bipolar: 0.74, Unipolar: 0.68; Figure 3-3). Optimal cut-off values calculated for LIr were 7.5Ω for MiFi and 8.5Ω for SP (Youden's Index = 0.57 / 0.70). For bipolar voltage the optimal cut-off was 0.12mV and for unipolar voltage 1.33mV, (Youden's Index = 0.29 / 0.32).

However, these values had poor positive predictive values, (LIr – MiFi: 0.52, SP: 0.20; Bipolar: 0.37, Unipolar: 0.28), consequently classifying sites as inert where electrical activity was possible. Due to the clinical importance of knowing when tissue is electrically inert, (for instance, in examining gaps in PVI lines), values with 100% positive predictive value were also sought, (i.e., the lowest recorded tissue parameter with any capture). Both MiFi and SP LIr showed pacing capture at 1Ω, (1.0mA and 1.6mA respectively). The lowest bipolar voltage value with pacing capture was 0.03mV (two instances of capture - 8mA and 9mA) and unipolar voltage 0.31mV (2.0mA).

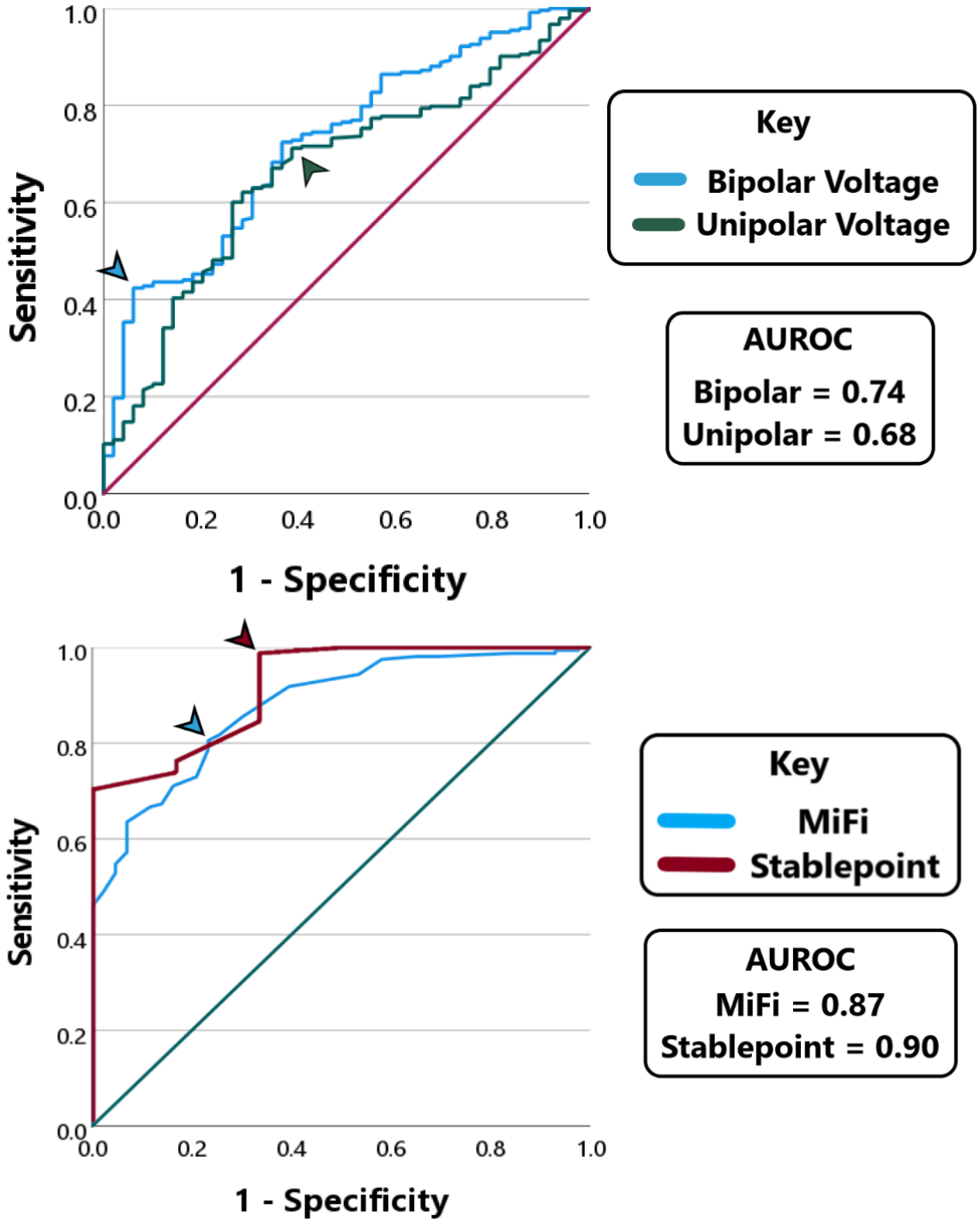

Figure 3-3 *Receiver operator curves to delineate electrically inert from active tissue*

Optimal values using Youden's Index are highlighted (arrowhead). However, as these cut-offs had poor specificity and misclassified active tissue as inert, preference was given to cut-offs with 100% specificity. n = 36 for bipolar and unipolar voltages, n = 18 for each of MiFi and Stablepoint.

3.4.4 Optimal Values for Healthy Tissue

For the purposes of establishing cut-off values between PA and EA tissue, each datapoint required classification as PA or EA based upon their PT. Once this had occurred ROCs could be plotted using tissue voltages and LIr as the discriminating factor and the PT as the 'gold-standard'. As the concept of using PTs to assess the health of atrial tissue has not been performed before, no PT values have been previously validated to assess for this to act as a precedent. Consequently, a cut-off value required selection and based upon our exploratory analysis in Figures 3-1 and 3-2. 5mA was selected in view of the qualitative plateau observed in these plots for the relationships between pacing thresholds and voltage or LIr.

The ability of LIr to distinguish PA from EA tissue was excellent, (AUROC – LIr MiFi: 0.82, LIr SP: 0.89, Figure 4) with optimal cut-off 13Ω for MiFi and 10Ω for SP, (Youden's Index = 0.49 / 0.56). In contrast, tissue voltages had fair discriminatory ability, (AUROC – Bipolar: 0.69, Unipolar: 0.63; Figure 4). Optimal cut offs were 1.29mV and 2.14mV, (Youden's Index = 0.27 and 0.28).

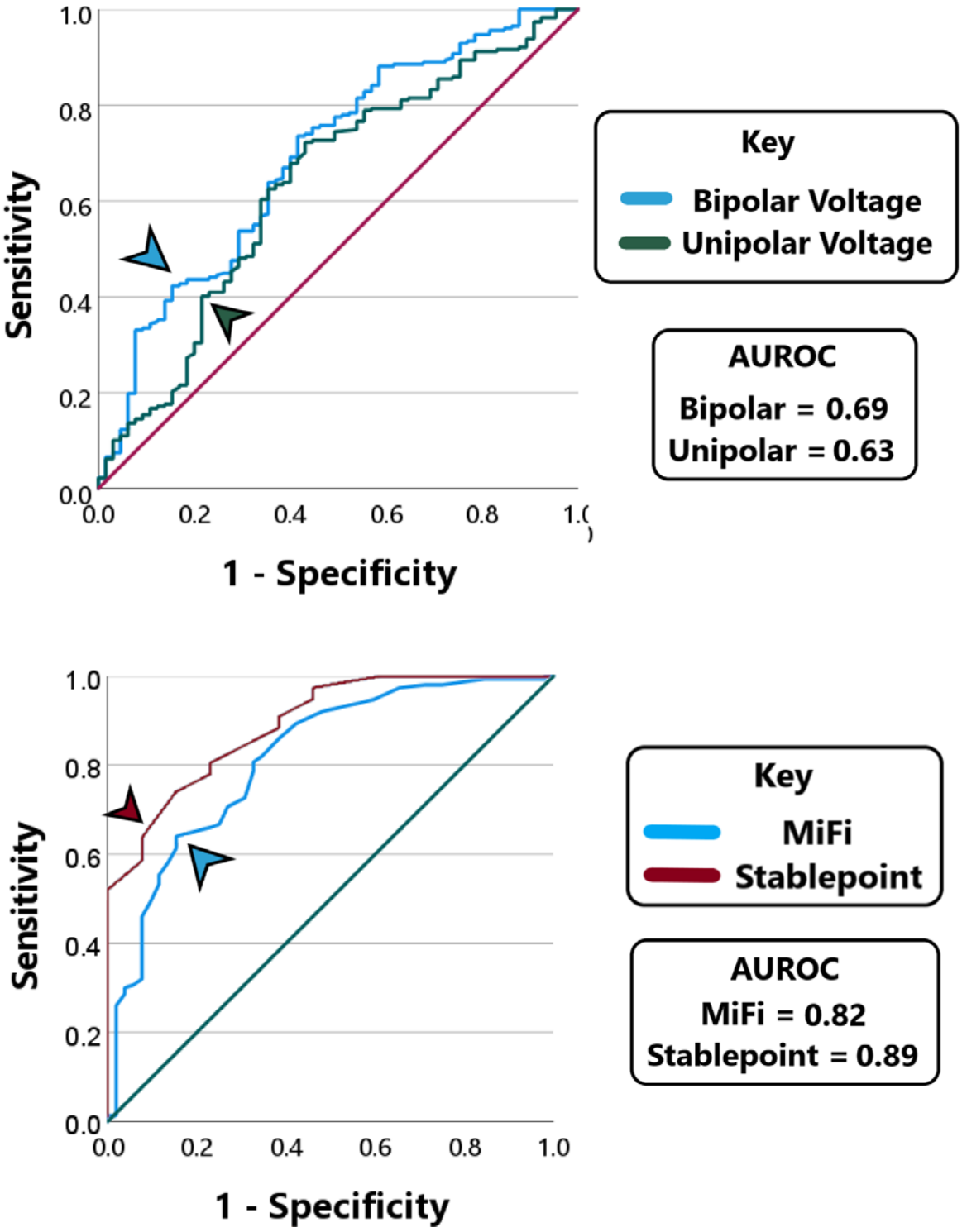

Figure 3-4 *Receiver operator curves to delineate partially active from electrically active tissue Partially active = pacing capture present and threshold >5mA, electrically active = pacing capture present and threshold <5mA. Optimal values using Youden's Index are highlighted (arrowhead). n = 36 for bipolar and unipolar voltages, and n = 18 for each of MiFi and Stablepoint catheters.*

A summary of optimal cut-offs is provided in Table 3.3.

Table 3.3 *Optimal Cut-Off Values*

	Inert	Partially Active	Active
Bipolar (mV)	< 0.03	0.03 – 1.29	> 1.29
Unipolar (mV)	< 0.31	0.31 – 2.14	> 2.14
LIr – MiFi (Ω)	≤ 0	1 – 13	> 13
LIr – SP (Ω)	≤ 0	1 – 10	> 10

LIr: Local Impedance referenced to blood pool, mV: Millivolts

To confirm a difference in PT values and dispersion between PA and EA tissue using these values, a Welch t-test and Levene's Test for equality of variances was undertaken. For the LIr cut-off, both catheters had significantly larger PTs and dispersion in PA than EA tissue, (PT – MiFi: 4.3 ± 3.8mA vs 2.6m ± 2.2mA, p = 0.001, Levene's Test, p < 0.0005; SP: 4.1 ± 2.5mA vs 2.4 ± 1.3mA, p < 0.0005; Levene's Test, p = 0.004, Figure 5). Similarly, tissue voltages also showed significantly larger PTs and dispersion in PA than EA, but the mean difference between PTs were numerically smaller, (PT – Bipolar: 3.7 ± 3.2mA vs 2.6 ± 1.8mA, p < 0.0005, Levene's Test, p = 0.002; Unipolar: 3.6 ± 3.1mA vs 2.7 ± 2.0mA, p = 0.007, Levene's Test, p = 0.017, Figure 5).

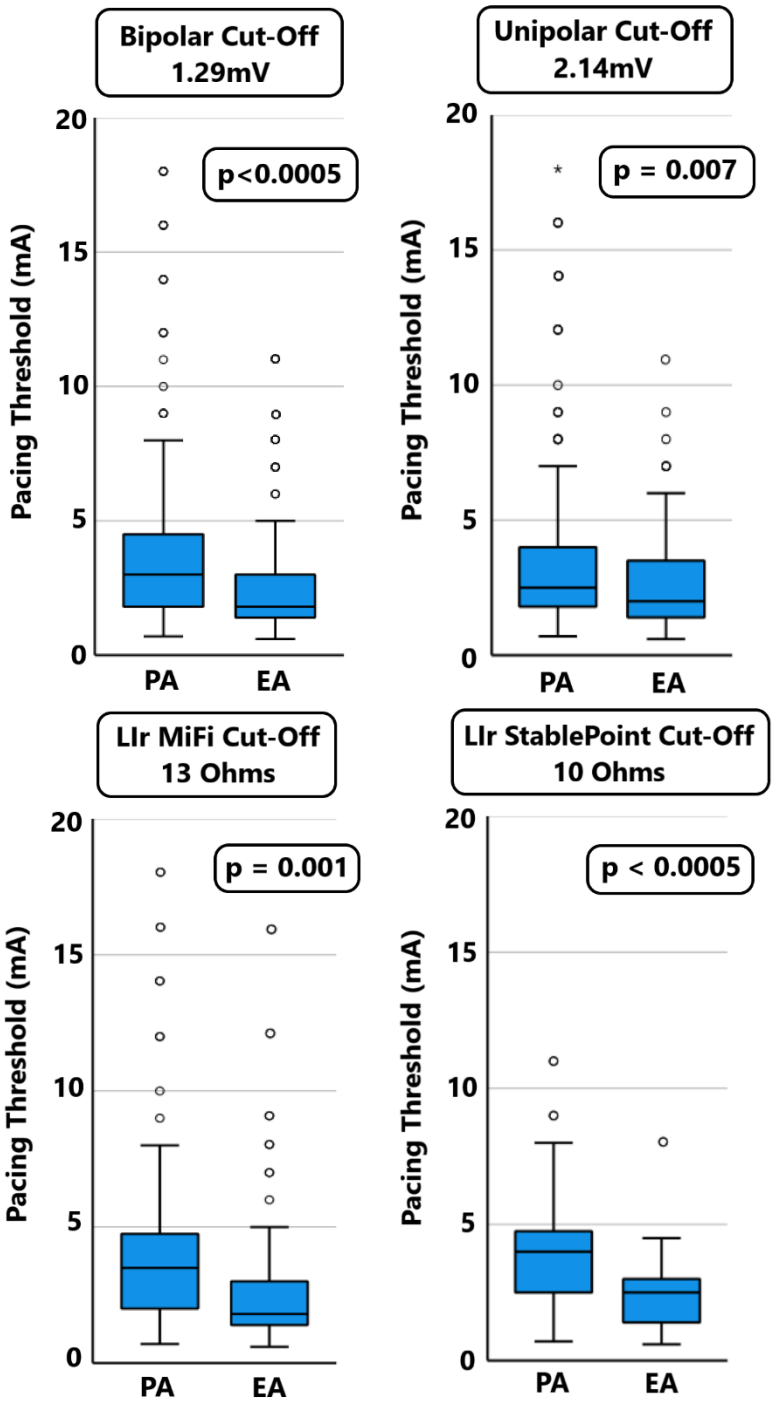

Figure 3-5 *Comparison of pacing thresholds between partially active (PA) and electrically active (EA) tissue based on optimal cut-offs from receiver operator curves.*
Outliers: O = >1.5x interquartile range above 3rd quartile. P-values = Welch t-test for pacing thresholds between PA and EA. n = 36 for bipolar and unipolar voltages, and n = 18 for each of MiFi and Stablepoint

3.5 Discussion

3.5.1 Key Findings

The key results of the study were:

1. There is a negative relationship between tissue health markers (voltage and LIr) and PT.
2. LIr is a stronger correlate to PT than tissue voltages.
3. The variability of PT increases with decreasing tissue health.
4. Pacing capture was present at voltages below current standards used for inert tissue.
5. Lowest values for pacing capture were 0.03mV (bipolar), 0.31mV (unipolar) and 1Ω (LIr).
6. Optimal values to distinguish diseased (PA) and healthy (EA) tissue were 1.29mV (bipolar), 2.14mV (unipolar), 12.5Ω (MiFi) and 10.5Ω (SP).

3.5.2 Pacing Thresholds and Tissue Health

The negative correlation between tissue health markers with PT is an expected finding. As tissue health deteriorates, the PT rises demonstrating the increasing density of electrically inert fibrosis within the myocardium.

The increased variance of PT values in diseased tissue reflects the heterogeneity in tissue structure from site to site. The position of fibrosis within the atrial wall, its presence within a small island or sizable area of scar, and its varied microstructure may explain why some sites showed electrical capture at a lower pacing stimulus than others. As tissue health improved this variability decreased, with easier electrical capture and propagation due to a homogeneous, electrically sensitive atrial tissue structure.

Interestingly, LIr showed a stronger correlation with PT than tissue voltage, suggesting it reflects tissue health more accurately. This may be explained by the reduction in confounding factors when using LIr. When creating a voltage substrate map, sampling of signal occurs which is dependent on numerous factors including the mass of tissue depolarised, the strength of source[390], and the orientation between catheter and activation wavefront[384]. An advantage of

using LIr is its independence from signal, nullifying these confounding factors. Furthermore, sampling can occur at any stage of the cardiac cycle and local influences on the electrical field minimises the effect of other confounders such as the respiratory cycle[415]. Overall, this may allow LIr to better reflect underlying tissue health better than voltage.

Other studies investigating the relationship of atrial fibrosis with tissue voltage have used magnetic resonance imaging with late gadolinium enhancement (LGE). Although LGE is consistently associated with lower bipolar voltages, the mean values associated with LGE have been variable, making selection of a cut off value challenging. Spragg *et al* found a lower bipolar voltage in areas of LGE (0.39 ± 0.61mV vs 1.38 ± 1.23mV) vs areas of non-scar[515]. Malcolme-Lawes *et al* also noted increased intensity of LGE correlated with progressive lower bipolar voltages in paroxysmal AF[516]. However, in examining persistent AF, Jadidi *et al* found a significant but small difference between areas of LGE and not (0.60 ± 0.80mV vs 0.86 ± 0.89mV)[517].

Regrading LI, Unger *et al* noted a fall in LI as a catheter was moved towards a previously established PVI ablation line in a computer modelling study[415]. However, the relationship with LIr to native fibrosis established by histology or MRI remains uninvestigated.

3.5.3 Re-Evaluating Cut-off for Inert Tissue

In the absence of histological validation, a commonly used clinical value for electrically inert scar is 0.05mV, a value based upon the background noise readings from the original CARTO mapping system and an absence of capture at 20mA at 2ms[401]. However, this value has not been reinvestigated since despite improved sensitivity and filtering of modern mapping systems. Electrograms can now be detected at even lower values and our study found capture as low as 0.03mV. This value has clinical significance, as lowering this cut-off could highlight potential connections across PVI lines or alter scar morphology affecting targets for ablation.

We also found capture at LIr values as low as 1Ω, essentially demonstrating electrically inert tissue shows the same LI values as the blood pool. This value is also significant for potential impedance mapping, as it highlights catheter contact with the scarred atrial wall could not be confirmed with changes in LI alone[500]. Similarly, with the absence of CF technology on the MiFi

ablation catheter, tissue contact on scarred atria could only be inferred by correspondence to the anatomical shell on the 3D map, tactile feedback and LI response to ablation.

3.5.4 Re-Evaluating Cut-Off for Atrial Fibrosis

The cut-off to determine the presence of a degree of atrial fibrosis, termed PA in this study, is more challenging. A commonly used convenient value is 0.5mV, however this is not based on histological evidence[390]. Studies taking the bottom 5% of electrogram readings in healthy LA of patients undergoing accessory pathway ablation have shown variable results between 0.4mV to 1.46mV[398-400,518]. Furthermore, Lin *et al* noted 95% of complex fractionated electrograms to be present in areas up 1.3mV[398]. Yagishita *et al* noted greater arrhythmic recurrence in patients with low voltage areas defined as <1.1mV[400]. Consequently, there is already significant evidence that arrhythmogenic substrate is present in the atria at higher voltage values than used in clinical practice.

Our study using a PT of 5mA as a reflection of tissue health suggests a cut-off value of 1.29mV. This value is consistent with some of the studies above, however tissue voltages were also found to have low discriminatory ability in determining PTs at 5mA. Consequently, we feel that this value should be considered additional evidence to raise the cut-off values used currently to determine scar, rather than advocating for the adoption of this voltage cut-off.

Raising this cut-off value also could have significant clinical impact. As scar-based ablation strategies beyond PVI are showing improved clinical outcomes[345], adoption of these techniques has the potential to become widespread. Consequently, the process of defining fibrosis accurately becomes extremely important to guide ablation location and strategy.

Interestingly, LIr for both MiFi and SP catheters was shown to have superior discrimination for PT at 5mA. This may also be explained by LI measurements being signal independent and minimising confounding factors as discussed above, making LI an effective parameter to assess tissue health.

3.5.5 Local Impedance Mapping

The advent of LI technology raises the possibility of signal independent substrate mapping[415]. The weak correlation between tissue voltages and LI readings suggests LI offers complimentary, rather than duplicated information, and is able to assess tissue health in a different manner. Further advantages to LI mapping include being able to map in electrically isolated areas (e.g. behind PVI lines, the posterior wall following isolation), and a decreased sensitivity to changes in conductivity caused by the respiratory cycle[415].

The relationship of LI to confounding factors is still unexplored, including CF, cardiac rhythm, irrigation fluids and devices[415]. Furthermore, LI mapping cannot be performed in a rapid, automated fashion, only on a point-to-point basis. Additional studies investigating these confounders are required to discover its full capabilities.

3.5.6 Limitations

The PT value of 5mA to determine PA from EA tissue was made following exploration of our data. As a novel method of assessing healthy from fibrosed tissue, no value has been validated for this on histological data. CF was not available on the MiFi catheter, and this may have affected the LIr values sampled. No distinction between native scar and that resulting from previous ablation was made in this study. The Orion, MiFi and SP catheters were used in this study paired with Rhythmia HDx. Ablation and mapping catheters often have different electrode configurations, therefore extrapolation of the study results to other catheters or mapping systems should be performed with caution. Patients with PeAF underwent DC cardioversion to restore SR. There is no data examining the consequence of this on electrophysiological parameters, and this may have affected the pacing thresholds taken. Only a single pacing threshold was taken at each site due to time constraints. Repeating this procedure would have ensured greater reproducibility of the results.

3.6 Conclusions

Tissue LIr correlates with PT better than tissue voltages. Commonly used cut-offs for inert and fibrosed atrial tissue should be reconsidered to better reflect the underlying tissue's ability to

be electrically captured and conduct. Values of 0.03mV and 1.29mV are suggested for bipolar mapping, 0.5Ω and 12.5Ω for LIr using the MiFi catheter, and 0.5Ω and 10.5Ω for LIr using Stablepoint.

Chapter 4 Comparison of Voltages Between Atria, Rhythms and Atrial Fibrillation Types: Does Ultra-High-Density Mapping Offer New Insights?

4.1 Abstract

Background

Ultra-high-density mapping systems allow for comparison of atrial electroanatomical maps in unprecedented detail.

Objectives

Assessment of atrial scar determined by voltages and surface area between atria, rhythm, and atrial fibrillation (AF) types.

Methods

Left (LA) and right atrial (RA) maps were created using Rhythmia HDx in patients listed for ablation for paroxysmal (PAF, sinus rhythm [SR] maps only) or persistent AF (PeAF, AF and SR maps). Electrograms on corresponding SR/AF maps were paired for direct comparison. Percentage surface area of scar was assigned low- (LVM, ≤0.05mV) , intermediate- (IVM, 0.05-0.5mV) or normal voltage myocardium, (NVM, >0.5mV).

Results

38 patients were recruited generating 95 maps using 913480 electrograms. Paired SR-AF bipolar electrograms showed moderate correlation in LA (Spearman's ρ = 0.32) and weak correlation in RA (ρ = 0.19) and were significantly higher in SR in both (LA: 0.61mV [0.20 – 1.67] vs 0.31mV [0.10 – 0.74], RA: 0.68mV [0.19 – 1.88] vs 0.47mV [0.14 – 1.07], p <0.0005 both). Voltages were significantly higher in patients with PAF over PeAF, (LA: 1.13mV [0.39 – 2.93] vs

0.52mV [0.16 – 1.49]; RA: 0.93mV [0.24 – 2.46] vs 0.57mV [0.17 – 1.69]). Minimal differences were seen in electrogram voltages between atria.

Significantly more IVM/LVM surface area were seen in AF over SR (LA only, $p < 0005$), and PeAF over PAF (LA: $p = 0.01$, RA: $p = 0.04$). There was minimal difference between atria within patients.

Conclusions

Ultra-high-density mapping confirms atrial voltages and surface area of scar differ between rhythms, and AF types, but are comparable between atria.

4.2 Introduction

Atrial fibrillation (AF) is an arrhythmia associated with progressive mural fibrosis[138]. Atrial fibrosis has been shown to harbour electrical triggers for AF[334], and therefore serves as a target for ablation. Consequently, accurate representation and understanding of atrial substrate on 3D electroanatomical maps (EAM) is vital, particularly as scar guided ablation strategies beyond pulmonary vein isolation (PVI) are showing promise[345].

Atrial fibrosis is depicted on 3D EAMs using bipolar voltage as a surrogate. Studies have investigated the relationships of bipolar voltage with AF progression[334,335,404], and between corresponding SR and AF electrograms[392,393,405,406]. These studies required selection and review of electrograms on a manual basis. However, the advent of new ultra-high-density mapping systems allows for the swift acquisition of thousands of electrograms which can be verified on an automated basis. Consequently, analyses can now be undertaken at an unprecedented level of detail.

In this study, an ultra-high-density mapping system was used to investigate the relationships of electrogram voltage between SR and AF, patients with PAF versus PeAF, and finally between left and right atria.

4.3 Methods

4.3.1 Patient Selection

Patients listed for radiofrequency AF ablation at our centre were prospectively recruited as part of the 'High Density Scar Guided Atrial Fibrillation Mapping' (HD-SAGA, NCT03363087) study. Ethical approval was granted by the UK Research and Ethics Committee, (Reference: 18/SC/0077).

All persistent AF patients were in AF at the time of their procedure.

4.3.2 Procedure

Procedures were performed under general anaesthetic or local anaesthetic with conscious sedation. A decapolar catheter was placed into the coronary sinus as a reference for the creation of 3D electroanatomical maps. Voltage data was collected using the Intellamap Orion catheter with the Rhythmia HDx system.

Additional data collection required in a separate part of the HD-SAGA study meant the mapping protocol was adjusted during recruitment. This was due to procedural time constraints. For the first 19 patients recruited, mapping of both atria occurred whilst the second set only underwent mapping of the LA. The systematic mapping protocol is summarised in Figure 4-1. Maps in SR were collected during proximal coronary sinus pacing.

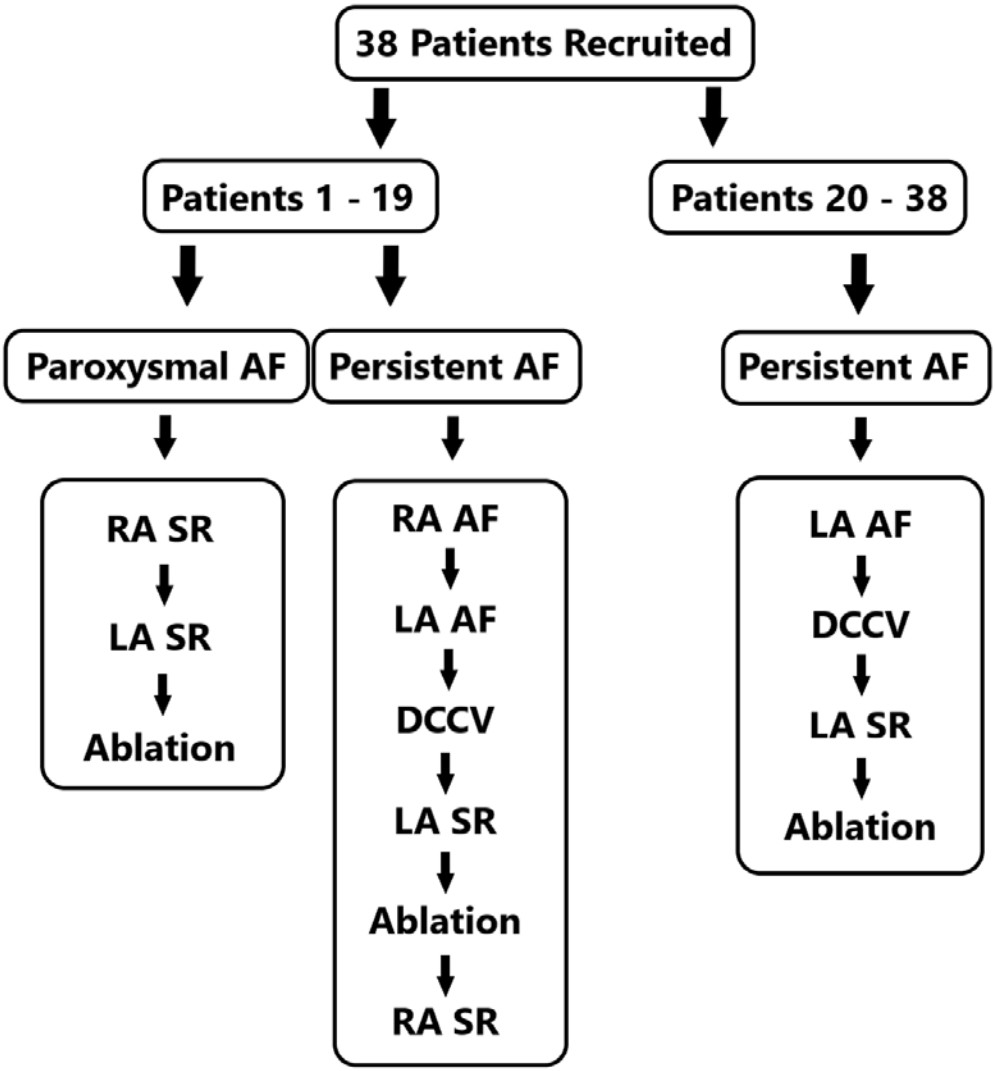

Figure 4-1 *Study mapping protocol.*
AF = Atrial fibrillation; DCCV = Direct current cardioversion; LA = Left atrium; SR = Sinus rhythm; RA = Right atrium.

Mapping points were acquired ensuring all areas of the 3D anatomical shell had bipolar voltage data ascribed, using the automated acceptance criteria of the system. For this purpose, the colour fill threshold was set at 5.0mm and confidence mask of 0.03mV. Electrogram voltages were classified as normal- (NVM, >0.5mV), intermediate- (IVM, 0.05 – 0.5mV) or low voltage myocardium (LVM, ≤0.05mV). In areas where no colour was ascribed, minimal electrical activity was confirmed by real-time manual review of electrograms on the Orion catheter. For AF, accepted electrograms were respiratory gated, with catheter motion <1.0mm. For SR, accepted

electrograms additionally showed timing stability to the proximal coronary sinus reference electrogram, and a cycle length stability, (both <5.0ms).

4.3.3 Data Collection and Analysis

Post-procedure, to ensure only data from the atria were analysed, sites such as the pulmonary veins, vena cavae and value apparatus were excluded from analysis using the Rhythmia cut-out tool. Mapping data were exported from Rhythmia and analysed using custom MATLAB scripts (Mathworks Inc., Natick, MA, USA). Electrogram voltages were co-located with their respective map xyz co-ordinates on the export.

To examine the relationship of voltage amplitude between SR and AF, electrograms on corresponding maps were paired with their nearest counterpart based on their xyz co-ordinates. An electrogram could only be paired once to avoid repeat comparisons. Electrograms without a partner within 2.5mm were excluded, a value based upon the distance between Orion electrodes. To examine the electrogram voltage differences between patients with PAF and PeAF, the global median voltage for each map was calculated and compared between groups. To examine for differences in electrogram voltages between atria, comparisons were made within patients.

To determine the percentage surface area attributed to LVM / IVM / NVM, the mapped area ascribed to each electrogram was calculated. The export connects every mapped electrogram to two neighbours, forming a triangle. Combining these triangles allows for the entire map to be reconstructed. From the xyz co-ordinates of each set of 3 electrograms, the area of a triangle can be calculated. Each triangle was then divided into three equal sections, each being assigned LVM / IVM / NVM based upon the voltages at its vertices.

4.3.4 Statistical Analysis

IBM SPSS Statistics (Version 27, IBM Corp, NY, USA) was used for statistical analysis. A p-value of <0.05 was considered statistically significant. Variables were assessed as parametric or non-parametric by visual inspection of histograms and a Shapiro-Wilks test. Continuous data were expressed as mean ± SD or median [lower quartile, upper quartile]. Count data were

expressed as number (%). Bivariate correlations were performed using Pearson's product moment correlation. Repeated data was analysed using a Wilcoxon signed rank test. Agreement of assignment to categories was assessed by Cohen's Kappa. Linear regression was performed to assess modelling of continuous data. Independent samples were compared using Mann-Whitney U Test for medians. A generalized linear mixed model was used to compare data between atria and within patients (random factor). Comparison of data with multiple dependent variables was performed using a one-way MANOVA where data was independent and a repeated measures MANOVA where it was not.

4.4 Results

4.4.1 Patient and Mapping Characteristics

38 patients were recruited to the study generating 95 maps (LA-SR 38, LA-AF 30, RA-SR 17, RA-AF 10) using a total of 913480 electrograms. Patient details are described in Table 4.1.

Table 4.1 *Study Population Characteristics*

Patient Characteristics	
n	38
Female	18 (47.4%)
Age, years	67.2 ± 8.8
Body mass index (kg/m^2)	31.1 ± 5.1
Co-Morbidities	
Arterial hypertension	18 (47.4%)
Ischaemic heart disease	6 (15.8%)
Diabetes mellitus	3 (7.9%)
Stroke	2 (5.3%)
Heart failure	9 (23.7%)
COPD	1 (2.6%)
LVEF (%)	57.1 ± 8.2
CHA_2DS_2-VASc	2.4 ± 1.5
Type of Atrial Fibrillation	
Paroxysmal	9 (23.7%)
Persistent	8 (21.1%)
Long standing persistent	21 (55.3%)

4.4.2 Sinus Rhythm vs Atrial Fibrillation

There were moderate correlations between paired SR and AF electrogram voltages in the LA, (Pearson's r – 0.32, p <0.0005), but weak correlations in the RA, (r – 0.19, p <0.0005). Linear regression showed LA-SR bipolar voltages could be statistically significantly predicted by their paired AF voltages, but the predictive ability was low (Adjusted R^2 = 0.11, p <0.0005). Similarly, for classifying voltages into LVM, IVM or NVM, there was only fair agreement between LA-SR and LA-AF (Cohen's κ= 0.24, p <0.0005). Bipolar RA-SR and paired RA-AF voltages showed weaker results (Adjusted R^2 = 0.04, Cohen's κ = 0.18, p <0.0005 both).

Paired electrograms were significantly larger in SR than AF in both atria, (p < 0.0005, Figure 4-2A & Table 4.2). In the LA, the percentage surface areas denoted as LVM / IVM / NVM were significantly different between SR and AF, with AF having greater IVM and LVM than SR, (p < 0.0005). In the RA, a trend in this direction was seen but did not reach statistical significance, (p = 0.62, Figure 4-3A & Table 4.2).

Table 4.2 *Comparison of Electrogram Voltages and Mapped Surface Area between Sinus Rhythm vs Atrial Fibrillation*

Paired Voltages (mV)		**Sinus Rhythm**	**Atrial Fibrillation**	**P – Value**
Left Atrium		0.61 [0.20 – 1.67]	0.31 [0.10 – 0.74]	All < 0.0005
Right Atrium		0.68 [0.19 – 1.88]	0.47 [0.14 – 1.07]	
Mapped Surface Area (%)				
Left Atrium	LVM	7.3 ± 6.9	12.2 ± 9.5	< 0.0005
	IVM	41.0 ± 12.1	50.5 ± 10.0	
	NVM	51.7 ± 17.2	37.3 ± 16.1	
Right Atrium	LVM	6.5 ± 5.3	8.4 ± 8.3	0.62
	IVM	42.0 ± 10.1	44.6 ± 6.9	
	NVM	51.5 ± 13.6	47.0 ± 13.8	

Data is mean ± standard deviation or median [lower quartile – upper quartile]. IVM: Intermediate voltage myocardium; LVM: Low voltage myocardium; mV: Millivolts; NVM: Normal voltage myocardium

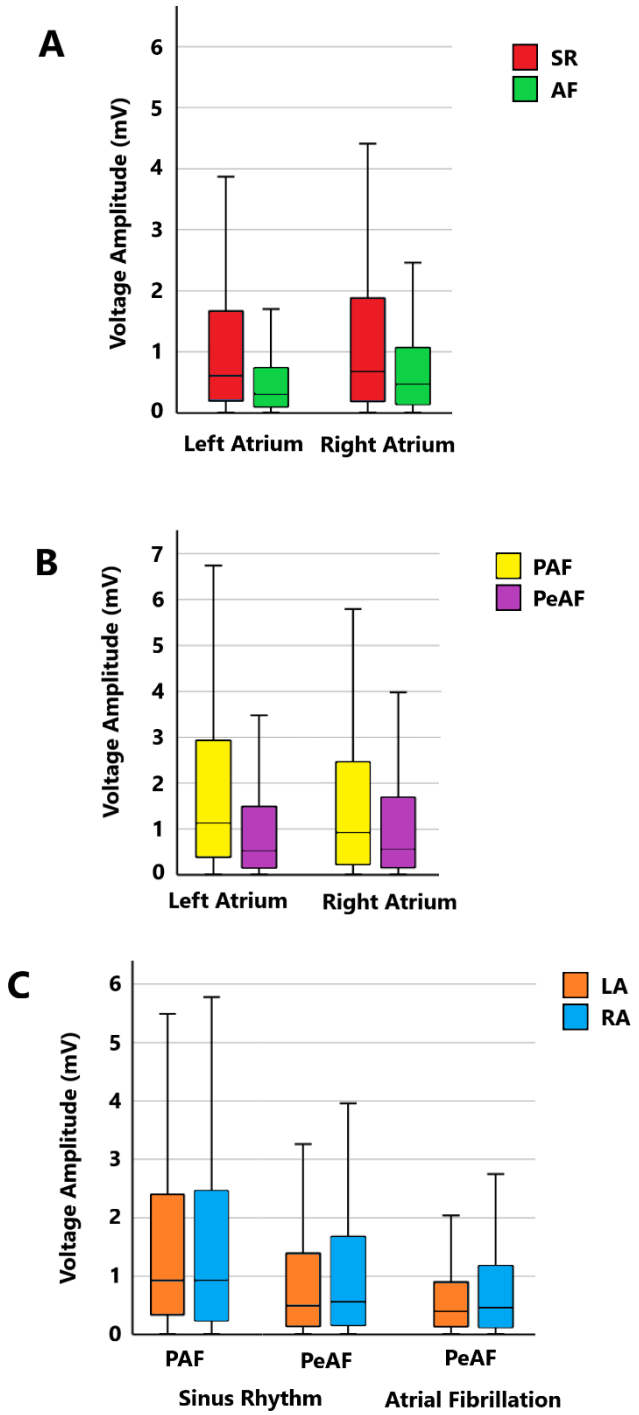

Figure 4-2 *Boxplot comparing electrogram voltage amplitudes.*

A = Between sinus rhythm (SR) and atrial fibrillation (AF) (n = 29); B = Between paroxysmal (PAF, n = 9) and persistent AF (PeAF, n = 29); C = Between left (LA) and right atria (RA) – (PAF, n = 9, PeAF n = 10). Significant differences ($p < 0.0005$) between groups were seen in all circumstances between rhythms (A) and AF types (B) (Tables 4.2 & 4.3). Minimal differences were found between atria on mixed modelling (C) (Table 4.4).

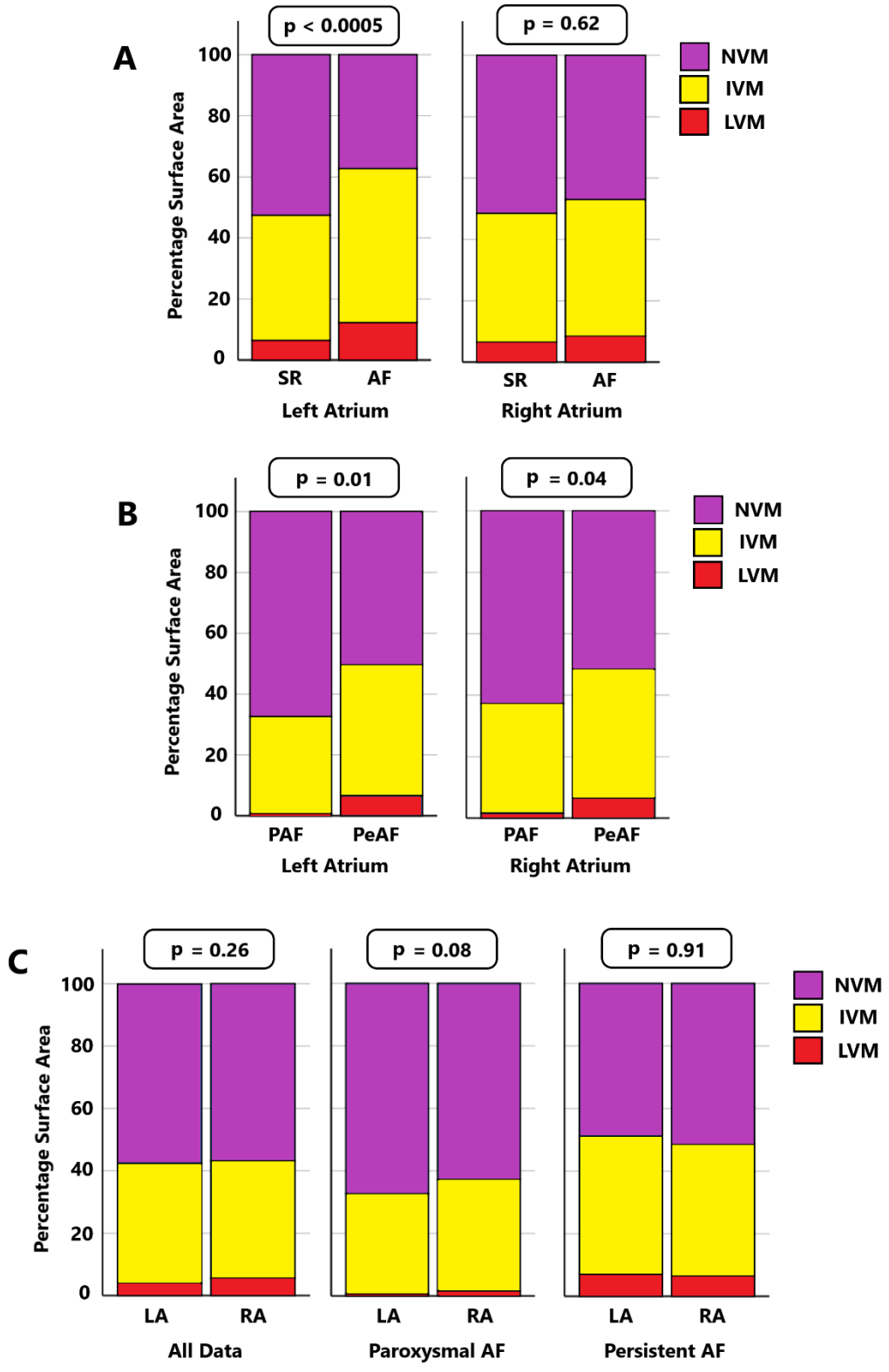

Figure 4-3 *Bar chart comparing the percentage surface area attributed to voltage categories. Low voltage (LVM, ≤ 0.05mV), intermediate voltage (IVM, 0.05 – 0.5mV) and normal voltage myocardium (NVM, > 0.5mV) between: A) Sinus rhythm (SR) and atrial fibrillation (AF) (n = 29); B) Paroxysmal (PAF, n = 9) and persistent AF (PeAF, n = 29); C) Left (LA) and right atria (RA) – (PAF, n = 9, PeAF n = 10).*

Despite these results, a considerable proportion (29.5%) of the paired electrograms had a larger amplitude in AF than SR. Additionally, 11.4% of electrogram pairs had the AF electrogram placed in a healthier category than their SR counterpart, (for example, AF electrogram graded as NVM, whilst SR graded as IVM or LVM).

Typical examples of paired SR and AF maps are displayed in Figure 4-4.

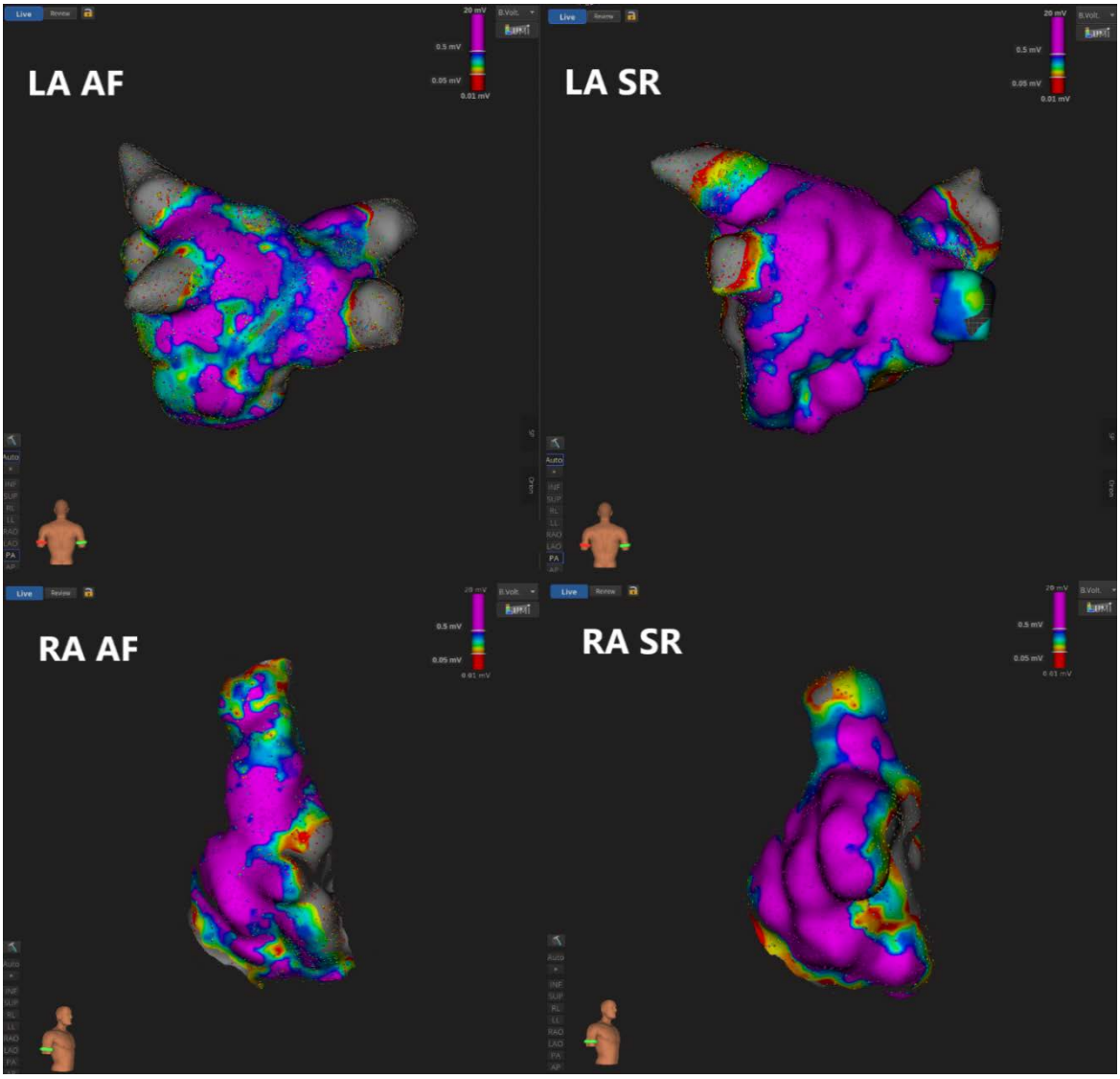

Figure 4-4 *An example of 3D electroanatomical maps of the left (LA) and right (RA) atria between sinus rhythm (SR) and atrial fibrillation (AF) within the same patient*

4.4.3 Paroxysmal vs Persistent Atrial Fibrillation

To compare parameters between patients with PAF or PeAF, maps created in SR were used and a global median voltage for each map calculated.

Global median electrogram voltages were significantly higher in patients with PAF over PeAF for both atria, (LA & RA, both $p < 0.0005$, Figure 4-2B & Table 4.3). The percentage surface area attributed to different voltage categories were also significantly different between patients with PAF and PeAF in both atria. Both LVM and IVM were higher in PeAF than PAF, with NVM correspondingly lower, (Figure 4-3B & Table 4.3).

Table 4.3 *Comparison of Electrogram Voltages and Mapped Surface Area between Paroxysmal and Persistent Atrial Fibrillation*

Global Voltages (mV)		**Paroxysmal**	**Persistent**	**P – Value**
Left Atrium		1.13 [0.39 – 2.93]	0.52 [0.16 – 1.49]	All < 0.0005
Right Atrium		0.93 [0.24 – 2.46]	0.57 [0.17 – 1.69]	
Mapped Surface Area (%)				
Left Atrium	LVM	0.7 ± 0.7	6.6 ± 6.8	0.01
	IVM	32.0 ± 10.6	43.1 ± 11.4	
	NVM	67.3 ± 11.0	50.3 ± 16.4	
Right Atrium	LVM	1.6 ± 1.3	6.5 ± 5.3	0.04
	IVM	35.7 ± 10.1	42.0 ± 10.1	
	NVM	62.7 ± 12.1	51.5 ± 13.6	

Data is mean ± standard deviation or median [lower quartile – upper quartile]. Maps were taken in sinus rhythm with proximal coronary sinus pacing. IVM: Intermediate voltage myocardium; LVM: Low voltage myocardium; mV: Millivolts; NVM: Normal voltage myocardium

Typical examples of PAF and PeAF maps are displayed in Figures 4-5 and 4-6.

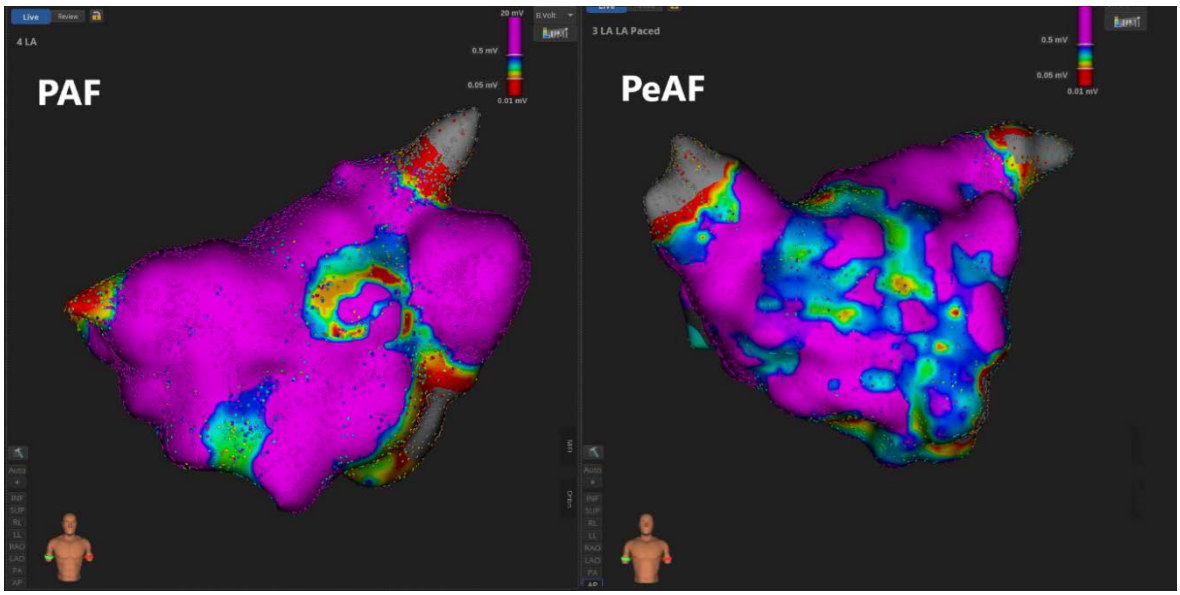

Figure 4-5 *An example of 3D electroanatomical maps of the left atrium in patients with paroxysmal (PAF) and persistent atrial fibrillation (PeAF)*

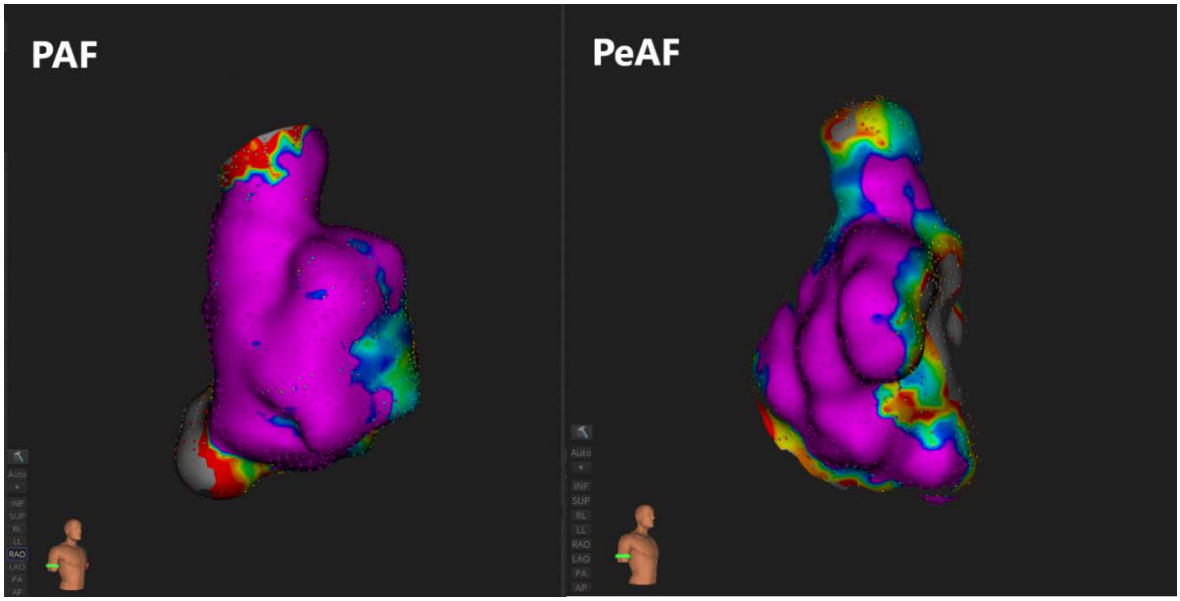

Figure 4-6 *An example of 3D electroanatomical maps of the right atrium in patients with paroxysmal (PAF) and persistent atrial fibrillation (PeAF)*

4.4.4 Left vs Right Atrium

To compare parameters between atria, the data were divided into PAF and PeAF as this was known to significantly affect electrogram voltages. To allow for comparison of data within patients, generalized linear mixed models were performed.

For patients with PAF, there was minimal difference in SR bipolar voltages between atria, (Co-efficient comparing LA/RA – 1.06). For patients with PeAF, bipolar voltages were slightly lower in the LA over the RA for both SR and AF, (Co-efficient LA/RA – SR: 0.78; AF 0.70). In all cases, the random factor (patient) was close to the cut-off for statistical significance, suggesting that that there may be patient to patient variation, (Figure 4-2C & Table 4.4)

Table 4.4 *Comparisons of Electrogram Voltages between Atria using Generalised Linear Mixed Modelling*

Voltages (mV)		Left Atrium	Right Atrium	LA/RA	95% Confidence Interval	Random Factor P-Value
Paroxysmal	SR Bipolar	0.93 [0.34 – 2.40]	0.93 [0.24 – 2.46]	1.06	1.05 – 1.07	0.06
Persistent	SR Bipolar	0.50 [0.15 – 1.40]	0.57 [0.17 – 1.69]	0.78	0.77 – 0.79	0.02
	AF Bipolar	0.40 [0.14 – 0.90]	0.47 [0.13 – 1.18]	0.70	0.69 – 0.71	0.03

Data is median [lower quartile – upper quartile]. Dependent variable = Electrogram amplitude, Fixed Factor = Left atrium referenced to right atrium; Random factor = Patient. The model used a gamma distribution with logarithmic link function. LA/RA is calculated from converting unstandardised β co-efficient

AF: Atrial Fibrillation; LA: Left Atrium; mV: Millivolts; RA: Right Atrium; SR: Sinus Rhythm.

There was no significant difference between atria when comparing percentage surface area attributed to LVM / IVM / NVM, (Figure 4-3C & Table 4.5).

Table 4.5 *Comparison of Mapped Surface Area between Atria*

Mapped Surface Area (%)		Left Atrium	Right Atrium	P-Value
All (n = 17)	LVM	4.0 ± 6.3	5.6 ± 4.6	0.26
	IVM	38.4 ± 14.0	37.6 ± 10.7	
	NVM	57.5 ± 18.4	56.8 ± 13.8	
Paroxysmal (n = 8)	LVM	0.7 ± 0.7	1.6 ± 1.3	0.08
	IVM	32.0 ± 10.6	35.7 ± 10.1	
	NVM	67.3 ± 11.0	62.7 ± 12.1	
Persistent (n = 9)	LVM	7.0 ± 7.6	6.5 ± 5.3	0.91
	IVM	44.1 ± 14.7	42.0 ± 10.1	
	NVM	48.9 ± 19.9	51.5 ± 13.6	

Data is mean ± standard deviation. Maps were taken in sinus rhythm with proximal coronary sinus pacing. IVM: Intermediate voltage myocardium; LVM: Low voltage myocardium; mV: Millivolts; NVM: Normal voltage myocardium

Typical examples of paired LA and RA maps are displayed in Figure 4-4.

4.5 Discussion

4.5.1 Key Findings

This study investigated the differences in quantity and severity of fibrosis between rhythms, AF types and atria using an ultra-high-density mapping system with voltage amplitude as a surrogate. The key results of the study were:

1. Overall, anatomically paired electrograms correlate poorly between SR and AF, and the ability to model each other is low.
2. There is poor agreement between SR and AF electrograms in classification as LVM, IVM or NVM.
3. SR electrograms have a larger amplitude than their corresponding AF counterparts in the same atria - though in a proportion of instances, the converse is also noted

4. The percentage surface area determined as IVM / LVM is greater in AF than SR for the LA, but not the RA.
5. Patients with PeAF have a lower global voltage and more percentage surface area of IVM / LVM than PAF in both atria.
6. Tissue voltages and percentage surface area of IVM / LVM are comparable between atria within a patient.

4.5.2 Correlating Sinus Rhythm and Atrial Fibrillation Electrogram Amplitudes

PVI is the cornerstone of AF ablation[322]. However, patients with PeAF and advanced substrate remodelling have increased arrhythmic recurrence post-ablation[323]. One ablation strategy used to improve outcomes is scar guided ablation, which has shown promise in multiple single centre trials[335,336,338] and a recent prospective randomised trial[345]. By definition, scar guided ablation is dependent on an accurate substrate map, which in all trials were created in SR. In some patients however, a map in SR is not achievable as the atria are highly susceptible to redeveloping AF, even after DC cardioversion and PVI. In these circumstances, it is necessary to map and ablate during AF. It is therefore desirable to know if low voltage areas seen during AF correspond to those in SR. Unfortunately, our data find the correlations between SR and AF electrogram amplitudes is poor, as is the agreement in classification into LVM, IVM or NVM. Therefore, what is determined to be fibrosis in AF will not be in SR and vice versa, hindering a scar-based ablation strategy.

The poor correlation between paired electrograms is reflective of the chaotic nature of AF. During SR, a constant anatomical source initiates a wave of excitation across fully repolarised tissue with a consistent directionality, resulting in electrograms with minimal variation in amplitude. Conversely in AF, multiple wavelets meander through mixed refractory and repolarised atrial tissue in disorganised re-entrant circuits[519]. This results in a constantly changing wavefront directionality, decreased conduction velocities, inconsistent electrogram amplitudes and fractionation.

The results seen contrast with those of previous studies. Yagishita *et al* noted a strong correlation of voltage amplitudes between rhythms of paired bipolar electrograms (Pearson's r = 0.707)[393]. Similarly, Masuda *et al* found a moderate correlation (r = 0.56), whilst importantly

noting the strength of this relationship was dependent on whether SR bipolar electrograms became fractionated during AF, (SR: normal, AF: fractionated, r = 0.29; SR & AF: normal, r = 0.73)[392]. The weak correlations seen in our study may be explained by high levels of fractionation during AF, particularly reflecting the large surface area of IVM-LVM in our cohort (Mean – LA: 48.3%, RA: 48.5%). Alternatively, different sampling methods, (automated in the current study versus manual in prior work), and catheters used may have affected the results. Ideally, our study would have also been able to classify electrograms by levels of fractionation, but this was impractical to perform manually due to the sheer volume of data obtained.

Clinically these findings are pertinent, as they suggest that patients unable to maintain SR for the length of time required to construct a 3D EAM, would be suboptimal candidates for a scar guided strategy. Adoption of such a strategy in this circumstance may result in excess, unnecessary ablation of areas deemed to be scar on an AF voltage map, but which are in fact healthy tissue. In these patients, other ablation strategies such as posterior wall isolation may need to be undertaken, or their scar assessed in an alternative manner, for example late gadolinium enhanced magnetic resonance imaging (LGE-MRI)[520].

4.5.3 Sinus Rhythm vs Atrial Fibrillation Electrogram Amplitudes and Fibrotic Surface Area

Electrogram amplitudes were found to overall be significantly smaller in AF than SR for both atria, a result consistent with previous studies[393,521]. As stated above, the electrically chaotic nature of AF results in varying and reduced electrogram amplitudes explaining this result. From a clinical perspective, the greater electrogram amplitudes seen in SR, and lack of electrogram-to-electrogram variation would suggest it would be a more predictable surrogate for underlying atrial fibrosis than AF. However, whilst this is true generally, a considerable proportion of the paired SR-AF electrograms were higher in AF than SR which in many cases resulted in a healthier tissue categorisation. This may highlight the limitation of direction dependency in bipolar mapping in SR. Although there is the benefit of uniformity in wavefront direction resulting in smaller electrogram amplitude variability, if the alignment of the propagating wavefront is perpendicular to the sampling bipole, the electrogram amplitude could be significantly underestimated. In contrast, the chaotic nature of AF may result in a wavefront propagating towards a bipole in multiple directions in close succession, which could result in a potentially greater reading.

As histological validation of electrogram voltages with fibrosis has not been studied, one non-invasive method of investigating this relationship uses signal intensity of LGE-MRI. A recent meta-analysis noted 19 of 22 studies found a significant correlation between LGE signal intensity and low voltage areas, however the analysis also highlighted a large heterogeneity between studies, hampering interpretation of the results[522]. Curiously however, in the only study comparing 3D EAMs in both SR and AF to LGE-MRI within the same patient, Quereshi *et al* found a significant correlation between LGE signal intensity and bipolar voltages in AF, but not SR[520]. These results suggest greater understanding of the relationships between LGE-MRI and 3D EAMs representation of fibrosis is still required.

Interestingly, despite both atria having lower voltages in AF than SR, the RA did not show significantly more scar (IVM / LVM) between rhythms. This may suggest that the fibrillatory waveforms are more organised and less fractionated in the RA compared to the LA.

4.5.4 Paroxysmal vs Persistent Atrial Fibrillation

The pathological progression of AF from paroxysmal to persistent types has been shown to be consistent with increased mural fibrosis demonstrated on MRI[380], 3D EAM studies[334,335,398], and autopsy[138]. This is logical as increased fibrosis harbours a greater number of triggers for AF[333] and substrate for enhanced anisotropy, and micro re-entry[391]. Our study is consistent with these findings with lower global atrial voltages being found in patients with PeAF than PAF. Logically following from this, an increased surface area of diseased myocardium was also noted in PeAF.

Also of note is the significant quantity of atrium classified as diseased (LVM / IVM) in both PAF (LA: 32.7%; RA: 37.3%) and PeAF (LA: 47.7%, RA: 48.5%), reflecting the widespread nature of the fibrotic pathophysiologic process that characterises AF. These values are higher than comparable studies using other mapping systems[334,398], perhaps due to the ultra-high-density mapping system used in our work or our cohort having an advanced stage of AF.

4.5.5 Left vs Right Atrium

Outside of the pulmonary veins, several sites acting as triggers for AF have been documented[156,334]. In general, non-pulmonary vein trigger sites in the LA are associated with low voltage areas of the LA body (posterior wall, septum). In contrast, in the RA, trigger sites are typically associated with the venous system, (crista terminalis, superior vena cava, coronary sinus)[334,411]. However, 25% of rotational activity has been documented in the RA[162], whilst electrogram fractionation and localised sources detected by automated algorithms have been shown to be equally distributed across atria[412]. Furthermore, low voltage extensions of the crista terminalis have also been shown to be associated with AF[523], all highlighting that the RA possesses the necessary substrate to maintain AF. In our study, minimal differences in electrogram voltages were seen between atria for PAF but were slightly lower in the LA for PeAF. This suggests that AF is a progressive bi-atrial fibrotic disease with a minor predominance for the LA.

Consequently, when performing ablation beyond PVI, mapping the RA may provide significant additional information to guide a scar-based strategy.

4.5.6 Limitations

Due to the sheer volume of data collected, only electrogram amplitude was considered as a marker of tissue health as an exported value. Ideally other indicators such as electrogram fractionation and their changes between SR and AF would have been explored. Conventional cut-offs of 0.05mV and 0.5mV for dense scar and diseased atrial tissue were used, however these values are not histologically validated. Other higher values suggested by other studies, may produce different results[398,400]. This study used the Orion mapping catheter: caution should be used when extrapolating of results to other catheters and mapping systems. Contact is known to affect the size of an electrogram collected[524], as the maps were collected by a non-contact force sensing multipolar catheter, some of the variance observed may have been related to differences in contact. In view of the large amount of data collected per map, and the efforts made as far as possible to generate a complete map, we would hope that this limitation would be minimised for this study. Patients with PeAF underwent DC cardioversion to restore SR before they underwent mapping. DC cardioversion is known to cause a period of myocardial stunning and the effect of this on tissue voltages has not been examined. Due to the length of time required to take additional maps, a single map was taken for each rhythm. Taking multiple maps in the same

rhythm and comparing would be useful for ensuring the reliability and reproducibility of the results.

4.6 Conclusions

Ultra-high-density mapping confirms atrial voltages are lower in PeAF patients compared to PAF, and when mapping in AF over SR. Consequently, the surface area of scar is increased in patients with PeAF and mapping in AF. Tissue voltages and scar surface area are comparable, at the patient level, between right and left atria.

Chapter 5 Determinants of Left Atrial Local Impedance: Relationships with Contact Force, Atrial Fibrosis and Rhythm

5.1 Abstract

Background and Objectives

To investigate the relationships between baseline tissue local impedance (LI), contact force (CF), atrial fibrosis and atrial rhythm (atrial fibrillation [AF] vs sinus rhythm [SR]) which are currently unstudied in a clinical setting.

Methods

Patients undergoing persistent AF ablation were recruited. LI was recorded referenced to patient blood pool, (LIr) and concurrent to changes in CF, with data collected at the same locations in AF and SR.

Results

20 patients were recruited. 109 locations were sampled obtaining 1903 datapoints (SR: 966, AF: 937). CF correlated strongly with LI (repeated measures correlation = 0.64). The relationship between CF and LIr was logarithmic. Rhythm and CF had a significant main (both $p < 0.0005$) and interaction effect ($p = 0.022$) on tissue LI: AF demonstrated higher LIr values than SR for similar CF.

Bipolar voltage had no effect on the relationship of CF to LIr in either rhythm. Assessing fibrosis using LIr showed an interaction effect with CF for LIr in SR and AF, (SR: $p < 0.0005$, AF: $p = 0.01$), with increased fibrosis showing lesser change in LIr per gram of CF.

Conclusions

CF and rhythm significantly affect the measured LIr of LA myocardium. Optimal catheter-tissue coupling may be better achieved with higher levels of CF and in AF rather than SR. Atrial fibrosis as assessed by LIr, but not bipolar voltage, affected the CF-LI relationship.

5.2 Introduction

Local impedance (LI) is a novel parameter which has shown clinical utility in radiofrequency ablation. Drops in LI (ΔLI) correlate with ablation lesion size in pre-clinical studies[375,503,525] and targets consistent with successful achievement of pulmonary vein isolation (PVI) have been developed in clinical trials[506,511]. The greatest correlate of ΔLI prior to ablation is the starting tissue LI[417,504]. Consequently, there is merit in establishing the relationships of factors affecting pre-ablation tissue LI.

In vitro and computer modelling studies have shown that tissue LI is affected by catheter proximity, contact force (CF) and tissue fibrosis[415,489]. However, this has not been established clinically. Furthermore, a clinical study has shown underlying rhythm to affect contact with the atrial wall, and thus may also affect tissue LI[389].

The IntellaNav Stablepoint (SP) is an ablation catheter which combines LI and CF technology, allowing for the relationships of CF, tissue fibrosis and atrial rhythm with tissue LI to be explored in a clinical setting.

5.3 Methods

5.3.1 Patient Selection

Patients listed for radiofrequency ablation for persistent AF at our centre were prospectively recruited for the study. Ethical approval was granted by the UK Research and Ethics Committee, (Reference: 18/SC/0077).

5.3.2 Procedure

Procedures were performed under general anaesthetic or local anaesthetic with conscious sedation. A decapolar catheter was placed into the coronary sinus as a reference for the creation of 3D electroanatomical maps. Mapping was conducted using the INTELLAMAP Orion catheter using the RHYTHMIA HDx system, (Boston Scientific, Marlborough, MA, USA). The Agilis steerable sheath (Abbott Laboratories, Chicago, IL, USA) was used for all cases. Maps were created in AF and then SR (pacing at 600ms from the proximal coronary sinus) following direct current cardioversion.

In order to minimise inter-patient variability, LI values were referenced to a patient's blood pool reading, (LIr). Catheter tip presence in the blood pool was confirmed by position on the map, a 0g CF reading and lack of electrograms on the SP catheter tip electrode. LI and CF were measured using previously described methods[375].

To examine the relationship between CF and LI, the SP catheter was moved to a point on the LA wall selected by the operator. For 30 seconds, the CF was then gently adjusted between 0 – 40g, (Figure 5-1). A manual tag placed at the beginning of this manoeuvre allowed for any macro-displacement to be easily noticed. If macro-displacement did occur, that site was excluded from analysis and a new site found to repeat the manoeuvre. Up to 6 locations were examined per patient. This procedure was initially conducted in AF, and following DC cardioversion, these specific points were then returned to and re-examined in SR. Assistance for this was provided by the Rhythmia tag distance tool, which minimised the distance between evaluated points in SR and AF, (Figure 1). Up to 10 corresponding CF and LI values were manually obtained per manoeuvre. Following export, the distance between xyz co-ordinates of corresponding SR and AF tags was calculated. Any points > 2.5mm (catheter tip width) were excluded from analysis.

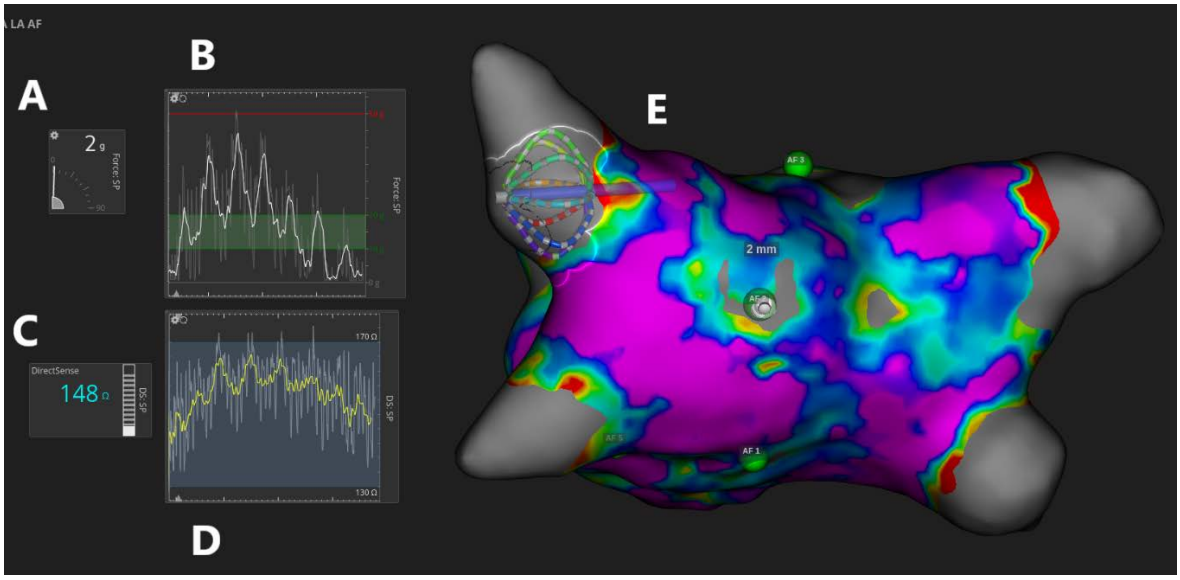

Figure 5-1 *A simplified version of the Rhythmia interface demonstrating response of local impedance (LI) to changes in contact force (CF).*

A = CF reading; B = Real-time graphical representation of changes in CF; C = LI reading; D = Real-time graphical representation of changes in LI, (White = Raw LI reading, Yellow = Filtered LI). Note the peaks and troughs that correspond between CF and LI; E = 3D electroanatomical map of the left atrium in a postero-anterior projection. The tip of the ablation catheter can be seen in the centre of the posterior wall overlying a tag 'AF2'. A distance measurement can be seen above this tag (2mm) and allows for assessment of catheter drift.

To assess the effect of atrial fibrosis on the CF-LI relationship, the commonly used surrogate bipolar voltage was used, alongside the novel parameter LI. Bipolar voltages sampled from the Orion catheter were obtained by co-locating the xyz co-ordinates of the manual tag and the mapping data from the Rhythmia export. This data were processed using custom written MATLAB scripts, (Mathworks Inc., Natick, MA, USA). Bipolar voltages were categorised as normal- (NVM), and intermediate/low voltage myocardium (I-LVM) using 0.5mV as a cut-off. Ideally, a 0.05mV cut-off would have also been used, however, this was merged with <0.5mV due to a paucity of data. A cut-off of 1.29mV was also used based upon the results from Chapter 3 in distinguishing electrically active from partially active tissue based upon response to pacing. As above, LI values were referenced to the blood pool (LIr) and taken at 10g of CF. Locations were then classified as electrically inert (EI), partially active (PA) and electrically active (EA), using cut-offs of < 1Ω and > 10Ω based on the work using pacing thresholds in Chapter 3.

5.3.3 Statistical Analysis

IBM SPSS Statistics (Version 27, IBM Corp, NY, USA) was used for statistical analysis. A p-value of <0.05 was considered statistically significant. Variables were assessed as parametric or non-parametric by visual inspection of histograms and a Shapiro-Wilks test. Continuous data were expressed as mean ± SD. Count data were expressed as number (%). As multiple CF and LIr measurements were taken from each location and patient, repeated measures correlation (RMCorr) was used when data was not independent. The CF-LIr relationship was mathematically modelled. The effects of rhythm, bipolar voltage categories and LIr categories upon the CF-LIr relationship were examined using linear mixed modelling.

5.4 Results

5.4.1 Patient and Datapoint Characteristics

Patient and datapoint characteristics are described in Tables 5.1 & 5.2. From 20 patients, 109 locations were sampled in both SR and AF obtaining a total of 1903 datapoints.

5.4.2 Effect of Rhythm on the Contact Force and Local Impedance Relationship

At an individually sampled location, CF correlates strongly with LIr (RMCorr = 0.64). Linear mixed modelling was used to examine the effects of rhythm and CF on LIr accounting for repeated data at individual locations. Both rhythm and CF had a significant main effect on LIr (both $p < 0.0005$) and interaction effect, ($p = 0.022$). Higher CF values meant higher LI values, with AF demonstrating a higher LIr than SR for the same CF values, (mean difference: 7.5Ω, [95% CI 6.5 – 8.5Ω]).

The relationship between CF and LIr was best fitted by a logarithmic model for both rhythms, (SR: $y = 5.30 \text{ Ln } (x) – 1.75$, $R^2 = 0.13$; AF: $y = 6.11 \text{ Ln } (x) + 1.95$, $R^2 = 0.21$, [Figure 5-2]).

Table 5.1 *Study Population Characteristics*

Patient Characteristics	
n	20
Female	11 (55%)
Age, Years	67.4 ± 9.1
Body Mass Index (kg/m^2)	32.9 ± 4.7
Co-Morbidities	
Arterial hypertension	10 (50%)
Ischaemic heart disease	4 (20%)
Diabetes mellitus	2 (10%)
Heart Failure	5 (25%)
LVEF (%)	57.6 ± 5.7
CHA_2DS_2-VASc	2.5 ± 1.4
Type of Atrial Fibrillation	
Persistent	5 (25%)
Chronic persistent	15 (75%)
Medication	
Beta blocker	15 (75%)
Calcium channel blocker	2 (10%)
Digoxin	4 (20%)
Amiodarone	1 (5%)
Flecainide	1 (5%)
ACEi	8 (40%)
ARB	1 (5%)
MRA	7 (35%)
DOAC	20 (100%)

Displayed as n, (%) or mean ± standard deviation. ACEi: Angiotensin converting enzyme inhibitor; ARB: Angiotensin receptor blocker; DOAC: Direct oral anti-coagulant; MRA: Mineralocorticoid receptor antagonist; LVEF: Left ventricular ejection fraction

Table 5.2 *Datapoint Characteristics*

Location	SR	AF	P-value
Altogether	966	937	–
Roof	180	161	
Posterior	296	270	
Inferior	40	50	
Septum	30	40	
Anterior	250	246	0.37
Lateral	20	30	
Appendage	40	30	
L WACA	40	50	
R WACA	70	60	
Contact Force			
Overall (g)	17.59 ± 10.78	17.77 ± 11.29	0.72
1 – 10g	301 (31.2)	303 (32.3)	
11 – 20g	326 (33.7)	296 (31.6)	
21 – 30g	205 (21.2)	203 (21.7)	0.22
31 – 40g	131 (13.6)	124 (13.2)	
41g +	3 (0.3)	11 (1.2)	
Local Impedance			
Blood Pool (Ω)	148.16 ± 16.32	148.50 ± 16.04	0.98
Electrograms			
Bipolar Voltage (mV)	1.28 ± 1.75	0.62 ± 0.91	<0.0005
L-IVM	415 (43.0)	406 (43.3)	0.98
NVM	551 (57.0)	531 (56.7)	

Displayed as n (%) or mean ± standard deviation. g: grams; L-IVM: Low and intermediate voltage myocardium; NVM: Normal voltage myocardium; mV: Millivolts.

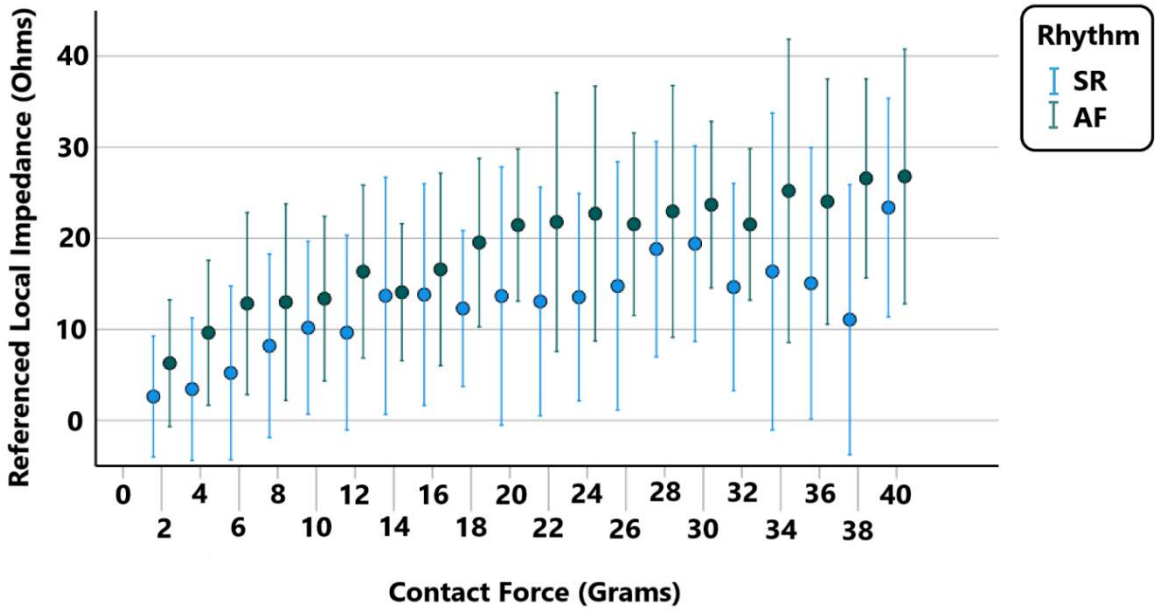

Figure 5-2 *Relationship of contact force vs referenced local impedance for sinus rhythm (SR) and atrial fibrillation (AF).*

Contact force given in 2g categories. Datapoints are mean ± standard deviation for each CF category. R^2 values: SR = 0.13, AF = 0.21. P = 0.022 for interaction effect of rhythm upon the contact force to referenced local impedance relationship. n = 20.

5.4.3 Effect of Atrial Fibrosis on the Contact Force and Local Impedance Relationship

The degree of tissue fibrosis assessed using a cut-off of 0.5mV had no significant main effect on LIr in SR or AF, (p = 0.11 / 0.50) or interaction effect with CF, (p = 0.61 / 0.98, Figure 5-3). When tissue fibrosis was assessed using a cut-off of 1.29mV, a similar result was seen, with no significant main effect was seen on LIr in SR or AF, (p = 0.07 / 0.08) or interaction effect with CF (p = 0.10 / 0.22).

In contrast, when using LIr to assess tissue fibrosis, a significant main effect (p < 0.0005 both) and interaction effect with CF is seen for both SR and AF (p < 0.0005 / 0.01, Figure 5-4), with higher LIr per CF in healthier myocardium.

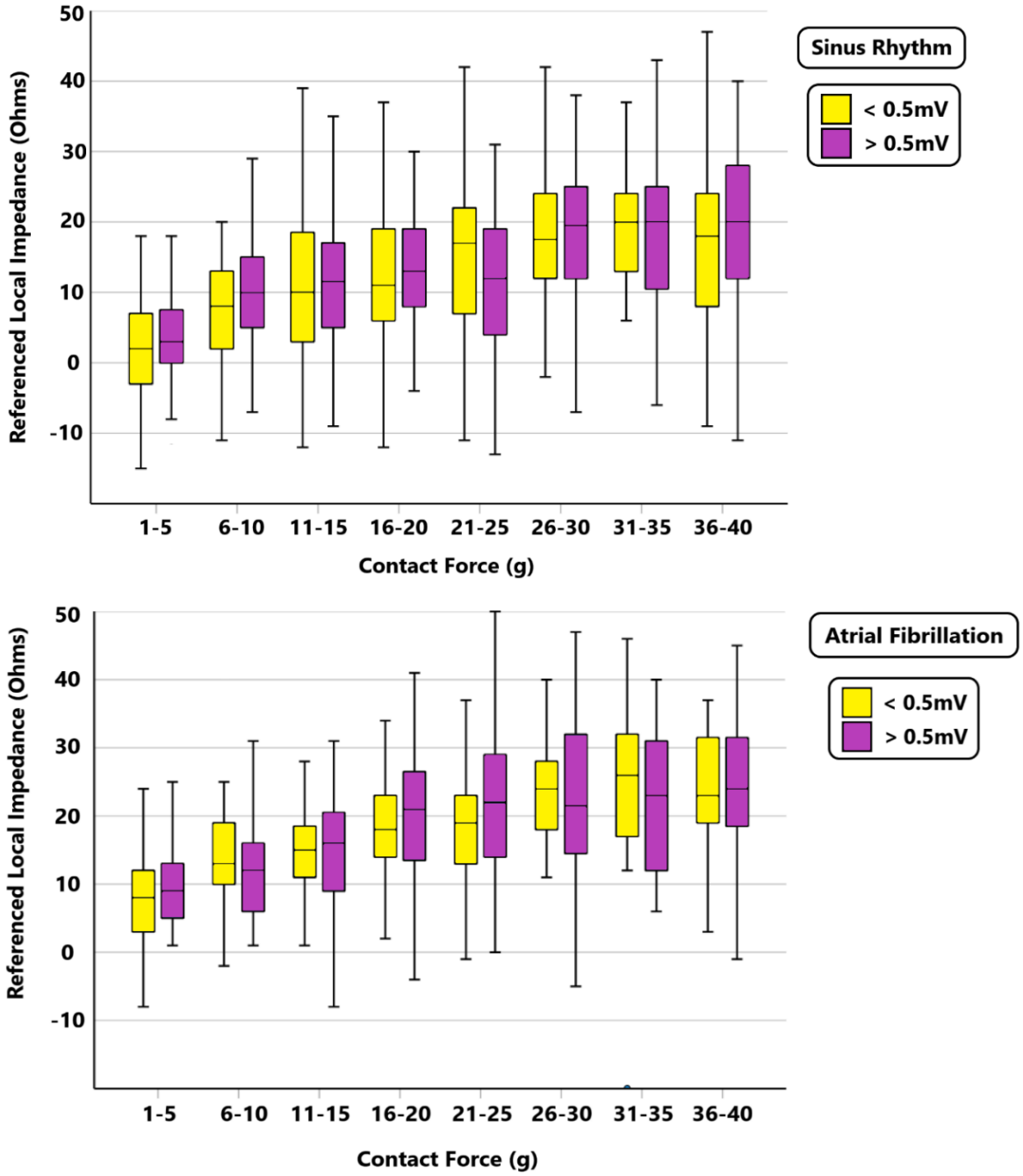

Figure 5-3 *Box plot demonstrating contact force vs referenced local impedance divided by degree of atrial fibrosis assessed by bipolar voltage*

There was no significant interaction effect of bipolar voltage category with contact force on referenced local impedance (Sinus Rhythm: p = 0.61, Atrial Fibrillation: p = 0.98). n = 20.

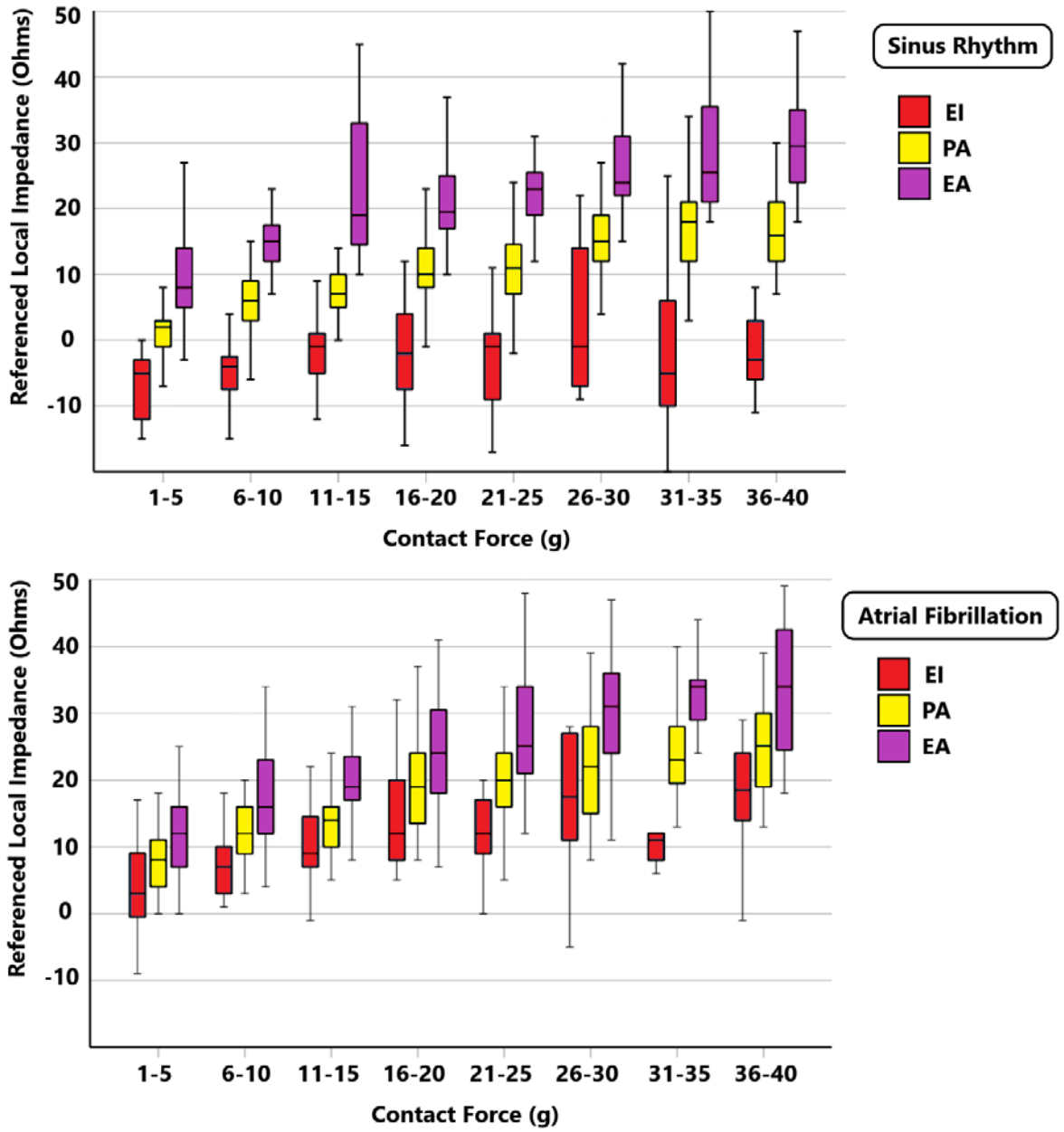

Figure 5-4 *Box plot demonstrating contact force vs referenced local impedance divided by degree of atrial fibrosis assessed as referenced local impedance.*

There was a significant interaction effect between these categories with contact force on referenced local impedance (Sinus Rhythm: $p < 0.0005$, Atrial Fibrillation: $p = 0.01$). EI = Electrically Inert (LIr < 0.5Ω), PA = Partially Active (0.5Ω < LIr < 10.5Ω), EA = Electrically Active (LIr > 10.5Ω). n = 20.

5.5 Discussion

5.5.1 Key Findings

In summary, our clinical study demonstrates a strong correlation between CF and LIr on the left atrial endocardium. The CF-LIr relationship is logarithmic in nature and affected by atrial rhythm. Assessment of atrial fibrosis using bipolar voltage was not shown to affect this relationship, however, an effect was seen if fibrosis was assessed by LIr itself.

5.5.2 Contact Force and Referenced Local Impedance

The biophysical reasoning behind the CF-LIr correlation reflects the improved catheter-tissue coupling offered by greater CF. LI readings are formed from a combination of conductivities at the electrode-tissue and electrode-blood pool interfaces, similar to two resistors in parallel. As CF increases, more of the catheter tip is embedded within the myocardium, decreasing the effect of the higher blood pool conductivity, and raising LI readings. Following on from this, one may anticipate a plateau in this relationship as whilst CF can increase, tissue coupling, and LI would be expected to reach a maximum level. This was not clearly found in our study, perhaps as we limited CF to 40g to minimise the risk of perforation, and to best reflect clinical practice. It may be that at higher levels of CF this relationship is seen, or the tissue properties may change dynamically to alter the nature of the relationship.

The strong correlation between CF and LIr reproduces the results of laboratory models in a clinical setting. Using the same catheter, Unger *et al* demonstrated how both approaching tissue and increasing contact force lead to a rise in LI using an in silico model[376]. Their work produced similar results to Sulkin *et al*, who noted in vitro a non-linear monotonic increase in LI when the IntellaNav MiFi catheter approached tissue, before a linear relationship following tissue contact[489]. Although these studies use catheter displacement in mm rather than measuring contact force in grams, and thus a direct comparison is not possible, the relationship between CF and LIr closely resembles our findings.

Additionally, two studies using ex vivo animal models and the SP catheter have demonstrated increasing LI with CF in clinical ranges. However, the absolute increase in LIr with

CF is much greater than seen in our study. For example, using a porcine model in a saline solution, Matsuura *et al* demonstrated a rise in LI of 60-80Ω at 10g of CF from a baseline of 140Ω depending on catheter orientation[503]. Undertaking a similar experiment, Tsutsui *et al* recorded values of approximately 220Ω at 10g of CF[507]. In comparison, using curves of best fit, our clinical study we obtained values of 10.5Ω (SR) and 16.0Ω (AF). The discrepancy in these results may be explained by the natural variation in conductivity of human tissue, differences in tissue deformation between clinical and in vitro experiments and the thickness of tissue examined (atrial vs ventricular). In contrast, Gutbrod *et al* demonstrated closer absolute results to our study using a left atrial in vivo canine model[502]. This highlights the importance of translating concepts discovered in thoroughly controlled, well designed pre-clinical studies, into the more difficult to control, complex clinical setting.

Interestingly, the correlation between CF and tissue LI has not been shown in other clinical studies. However, the objectives of Solimene *et al* and Yasumoto *et al* were to examine the relationship of CF to LI drop with ablation[417,504]. Consequently, single readings of LI and CF were taken at multiple locations prior to ablation. In contrast, in our study, multiple LI and CF measurements were taken from each location and referenced to the patient blood pool, therefore reflecting the relationship between CF and LI at individual sites more clearly.

5.5.3 The Effect of Rhythm

In the presence of AF, higher LIr readings were seen for corresponding CF values in SR. This finding may be related to improved tissue-catheter coupling in AF, where the atrial wall does not have the rhythmic 'kick' that would be seen in SR. In a previous left atrial study, Ullah *et al* noted greater CF variability, (the difference between peak and trough CF values) using the Thermocool SmartTouch catheter (Biosense Webster Inc.) in SR compared to AF, and this correlated with a comparatively smaller generator impedance drop during ablation[389]. This finding could have particular clinical significance. Pre-ablation LI values have been shown to strongly correlate with LI drop during ablation[375,417,512]. Our study demonstrates that higher LI values can be achieved in AF over SR, suggesting AF may a preferable rhythm to ablate during in order to maximise ablation efficacy. Whether the higher LIr values seen in AF translate to greater LI drop with ablation is unclear and was outside the remit of this study.

5.5.4 The Effect of Fibrosis

In analysing the effect of atrial fibrosis on the CF-LIr relationship, mixed results were obtained. Classifying fibrosis by bipolar voltage demonstrated no interaction on the CF-LIr relationship. In contrast, using LIr to classify atrial fibrosis did reveal a significant effect on the CF-LIr relationship.

In current clinical practice, bipolar voltage amplitude is used as a surrogate for atrial fibrosis. Using modern mapping systems and specialised catheters, thousands of electrograms can be sampled rapidly and automatically verified, creating exquisite ultra-high-density maps familiar to electrophysiologists. However, the cut-off value to delineate fibrosis from healthy tissue (0.5mV) has never been histologically verified. The lack of interaction effect of bipolar voltage categories on CF-LIr could therefore be explained by an inappropriate cut-off to determine fibrosis, or that bipolar voltage is a poor reflection of tissue tensile properties.

Using LI as a mapping parameter to assess tissue fibrosis on a point-by-point basis, has been used in a small study[415], and is capable of finding gaps in PVI lines[414]. The significant interaction effect of tissue fibrosis when classified by LIr (at 10g) on CF-LIr is of clinical use. For example, if a tissue LIr at 10g is classified as EI, one may be tempted to increase CF to improve LIr prior to ablation. However, our data suggests minimal changes in LIr will be seen in exchange for increased risk of perforation or steam pops. In contrast, classifying a point as EA, increasing CF beyond 10g will continue to show increases in LIr which may improve LI drop. These findings suggest that LIr may represent a better reflection of tensile changes secondary to atrial fibrosis affecting catheter tissue-coupling. Furthermore, for a potential LI mapping catheter, it should be considered that the amount of tissue contact made will affect readings considerably, especially in healthier tissue.

5.5.5 Limitations

The measurements made used the IntellaNav Stablepoint catheter. Extrapolation to any future CF and LI equipped catheters should be performed cautiously. Although increasing CF results in greater LI values, it is unclear if this would result in a greater LI drop with ablation. Orientation was not considered in our analysis and may affect LI readings at certain CF levels[503]. Thickness of atrial tissue could not be considered in our analysis and its effect on deformation

may affect the CF-LI relationship. All patients underwent DC cardioversion to restore SR. The effect of this on electrophysiological parameters has not been studied. As an export of data for the corresponding CF-LI measurements is unavailable, they had to be recorded manually. This is likely to affect the reproducibility of the data greater than if recorded by the mapping system.

5.6 Conclusions

CF correlates with LIr in the left atrial endocardium. Rhythm affects this relationship with measurements during AF showing higher LIr values than in SR at the same locations for corresponding CF. Optimal catheter-tissue coupling, as judged by tissue LI may be better achieved in AF than SR. Atrial fibrosis does not affect the CF-LIr relationship when assessed by bipolar voltage but does when assessed by LIr values at 10g.

Chapter 6 Predictors of Local Impedance Drop with Left Atrial Ablation

6.1 Abstract

Background and Objectives

The IntellaNav Stablepoint (SP) catheter combines local impedance (LI) and contact force (CF). Ablation targets, factors affecting LI drop (ΔLI), and the specific effect of adding CF are not well studied. The relationships of ablation parameters with LI between IntellaNav MiFi and SP are investigated.

Methods

Patients undergoing AF ablation were recruited. The ΔLI recorded during ablation was mathematically modelled and compared between catheters. The relationships between starting LI, ΔLI, CF and other variables were explored.

Results

2203 ablations (MiFi: 1082, SP: 1121) were analysed in 40 patients. The maximal ΔLI was significantly higher using SP, (MiFi: 13.3 ± 6.9Ω, SP: 17.8 ± 7.3Ω; p <0.0005). The conversion factor from MiFi to SP was 1.42.

Starting LI correlated with ΔLI at 5 seconds (ΔLI5s) (R – MiFi: 0.37, SP: 0.44, both p <0.0005). Mean CF correlated with ΔLI5s (R = 0.20, p <0.0005) exhibiting a linear relationship up to 10g before plateauing.

Multivariable models examining ΔLI5s fit closer for SP than MiFi, (adjusted R^2: 0.47 vs 0.23, both p <0.0005) with significant variables being starting LI, CF, 50W power and location.

Based on data modelling, for SP, a starting LI of 143 Ω (anterior-superior) and 134 Ω (posterior-inferior) would be predicted to reach targets developed in the LOCALIZE trial for 50W ablations.

Conclusions

SP values of ΔLI are 1.42x MiFi. Target ΔLI suggested for ablation are 20Ω (inferior-posterior) and 24Ω (anterior-superior). ΔLI is more predictable using SP, with higher LI, CF and power key influencing factors.

6.2 Introduction

Pulmonary vein isolation (PVI) is the cornerstone of atrial fibrillation (AF) ablation[322]. To achieve PVI via radiofrequency (RF) ablation, transmurality of each individual lesion is required. As histology is unavailable during the procedure, reliable surrogates of assessing individual lesion efficacy are necessary. One such surrogate previously studied is the change in impedance with ablation[383,493,526].

A novel metric to assess ablation is local impedance (LI), a dynamic biophysical marker that reduces with ablation (ΔLI) and correlates with lesion dimensions[375,489,503]. An advantage of ΔLI is that its dynamic nature allows an operator to curtail ablation when a target has been reached, which can reduce ablation time[525] and minimise risk of steam pops[509]. The LOCALIZE trial established values of 17Ω (antero-superior) and 14Ω (postero-inferior) as reliable ΔLI targets by assessing gaps in PVI lines[506,511]. However, these ΔLI targets were established with the IntellaNav MiFi, an ablation catheter without CF technology. Contact force (CF) is a metric known to correlate with lesion dimensions[510] and durability in creating PVI lines when used optimally, likely via improved catheter-tissue coupling[453,465,527]. The recently released IntellaNav Stablepoint (SP) catheter, integrates CF with ΔLI. However, due to a difference in sampling, LI values are higher, and those established in LOCALIZE cannot now be applied in clinical practice with the new catheter.

Consequently, establishing new ΔLI targets for SP is important to guide ablation procedures, as is understanding the interaction of CF on ΔLI alongside other metrics known to affect ablation lesion dimensions.

In this study, the ΔLI during ablation between the MiFi and SP was compared with the aim of providing extrapolated targets for SP. Furthermore, the influence of CF alongside other variables on ΔLI during ablation was studied.

6.3 Methods

Ethical approval for the study was granted by the UK Research and Ethics Committee, (Reference: 18/SC/0077).

6.3.1 Procedure

40 consecutive patients with AF scheduled for elective ablation were prospectively enrolled. Procedures were performed under general anaesthetic or local anaesthetic with conscious sedation. Unfractionated heparin boluses or infusion were used to achieve a target activated clotting time of >300 seconds. A decapolar catheter was placed via the femoral vein into the coronary sinus and used as a reference for the creation of 3D electroanatomical maps. Maps were created using the INTELLAMAP Orion™ catheter with the RHYTHMIA HDx™ system, (Boston Scientific, USA). The Agilis® steerable sheath (Abbott Laboratories, USA) was used for all cases. *De novo* patients underwent PVI on a point-by-point basis. Redo patients received ablation where necessary to ensure PVI. Ablation beyond PVI was at the discretion of the operator, as were ablation duration and power (30-50W). Operators were not blinded to LI. All ablations were temperature controlled, power limited, static deliveries.

6.3.2 Data Collection and Analysis

Ablation data were exported from Rhythmia and analysed using custom MATLAB scripts (Mathworks Inc., USA). LI (Ω), CF (g), and xyz co-ordinates of the catheter tip were sampled at 20Hz. All LI measurements used system-filtered LI.

6.3.3 Local Impedance

LI was measured using previously described methods[375,489]. To examine the relationship between ablation duration and LI drop (ΔLI), an incremental analysis was undertaken as employed in prior studies[383,493,526]. For this analysis, the largest ΔLI was taken from zero to each time point exported (every 50ms), i.e. the largest ΔLI from 0-50ms, 0-100ms, 0-150ms and so on.

6.3.4 Other Parameters

CF was measured using the SP catheter as described in a previous study[375]. Pre-ablation bipolar voltage was established using the Orion mapping catheter and sampled by co-locating co-ordinates between mapping and ablation exports as described in Chapter 2.6.1.2. Using the xyz co-ordinates supplied within the ablation and mapping exports, data linking the ablation parameters and mapping data could be paired allowing for an in-depth analysis to occur. Ablations were categorised low (LVM: <0.05mV), intermediate (IVM) and normal voltage myocardium (NVM: >0.5mV) based upon commonly used clinical values.

Drift was calculated as the maximum Euclidian distance from the mean co-ordinates during ablation. Ablations with catheter drift greater than the tip width (4mm [MiFi] or 4.5mm [SP]) were excluded, as this was felt to reflect an unacceptable level of catheter instability and inconsistent tissue ablation.

6.3.5 Ablation Location

Ablations were defined on their anatomical side (right vs left) and location (anterior, posterior, inferior or superior) based on Figure 6-1 and previous work[505,506]. Only PVI ablations were considered.

6.3.6 Statistical Analysis

IBM SPSS Statistics (Version 27, IBM Corp, USA) was used for statistical analysis. A p-value of <0.05 was considered significant. Variables were assessed as parametric by inspection of histograms and a Shapiro-Wilks test. Continuous data were expressed as mean ± SD. Count data were expressed as number (%). Bivariate correlations were performed using Pearson's correlation, and repeated measures correlation (RMCorr) when data was not independent. Independent samples were compared using a T-Test or one-way ANOVA with post hoc Tukey's Test for continuous data and a chi-squared test for categorical. Related samples were analysed with a paired T-Test. Multivariable regression was performed to assess the influence of factors on ΔLI.

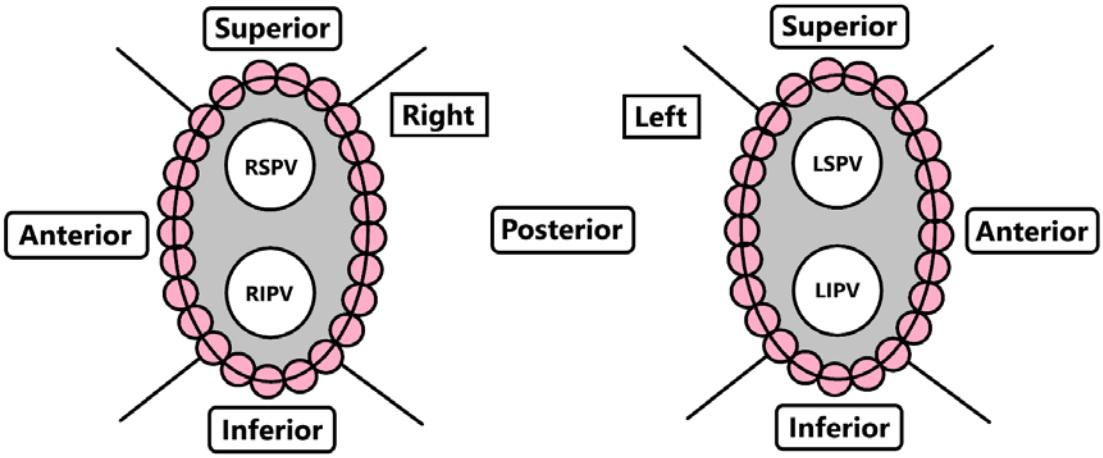

Figure 6-1 *Locations assigned to ablations based on PVI lines*

6.4 Results

6.4.1 Patient and Ablation Characteristics

Patient, procedural and ablation characteristics are detailed in Tables 6.1 & 6.2. 20 patients underwent ablation with each catheter. 3435 ablations were performed, 1232 ablations were excluded (non-PVI, excessive catheter drift), leaving 2203 ablations to proceed to analysis (MiFi: 1082, SP: 1121). One patient experienced tamponade using the MiFi catheter. The suspected ablation lesion responsible was curtailed after 4 seconds following a rapid LI drop (52Ω). No long-term sequelae were experienced.

Table 6.1 *Study Population Characteristics*

Patient Characteristics	MiFi	Stablepoint	P-Value
n	20	20	-
Female	8 (40%)	11 (55%)	0.34
Age, Years	66.1 ± 8.7	67.4 ± 9.1	0.65
Body Mass Index (kg/m^2)	29.8 ± 5.6	32.9 ± 4.7	0.06
Type of Procedure			
General Anaesthetic	19	19	1.00
Conscious Sedation	1	1	
De Novo	10	10	1.00
Redo	10	10	
Co-Morbidities			
Hypertension	9 (45%)	10 (50%)	0.75
Ischaemic heart disease	2 (10%)	4 (20%)	0.38
Diabetes mellitus	1 (5%)	2 (10%)	0.55
Stroke	2 (10%)	0	0.15
Heart Failure	4 (20%)	5 (25%)	0.71
LVEF (%)	56.7 ± 9.9	57.6 ± 5.7	0.74
CHA_2DS_2-VASc	2.2 ± 1.6	2.5 ± 1.4	0.47
Type of Atrial Fibrillation			
Paroxysmal	10 (50%)	0	
Persistent	3 (15%)	5 (25%)	0.001
Chronic persistent	7 (35%)	15 (75%)	
Medication			
Beta blocker	14 (70%)	15 (75%)	0.72
Calcium channel blocker	2 (10%)	2 (10%)	1.00
Digoxin	2 (10%)	4 (20%)	0.38
Amiodarone	1 (5%)	1 (5%)	1.00
Flecainide	3 (15%)	1 (5%)	0.29
ACEi	4 (20%)	8 (40%)	0.17
ARB	2 (10%)	1 (5%)	0.55
MRA	10 (50%)	7 (35%)	0.34
Warfarin	3 (15%)	0	0.07
DOAC	15 (75%)	20 (100%)	0.01

Displayed as n, (%) or mean ± standard deviation. ACEi: Angiotensin converting enzyme inhibitor; ARB: Angiotensin receptor blocker; DOAC: Direct oral anti-coagulant; LVEF: Left ventricular ejection fraction; MRA: Mineralocorticoid receptor antagonist

Table 6.2 *Procedural and Ablation Characteristics*

Procedural Characteristics	MiFi	Stablepoint	P-Value
Procedure Time, Mins	246.0 ± 53.0	223.5 ± 41.1	0.14
Fluoroscopy Time, Mins	11.9 ± 8.2	16.4 ± 14.6	0.24
Ablation Time, Mins,	33.6 ± 20.0	28.6 ± 10.0	0.33
Complications			
Tamponade, n	1	0	0.31
Skin Burn, n	0	1	0.31
Ablation Characteristics			
Number of Valid Ablations	1082	1121	--
Duration, Seconds	19.6 ± 9.7	18.7 ± 9.6	0.13
Power, Watts	44.1 ± 5.5	45.1 ± 5.8	0.09
Contact Force, grams	N/A	17.2 ± 7.5	--
Bipolar Amplitude, mV	1.54 ± 2.11	1.16 ± 1.49	<0.0005
Blood Pool LI, Ω	96.5 ± 10.3	145.9 ± 15.0	<0.0005
Starting LI	101.6 ± 15.0	145.5 ± 18.9	<0.0005
End LI	88.4 ± 13.9	127.8 ± 17.0	<0.0005
LI Drop	13.3 ± 6.9	17.8 ± 7.3	<0.0005
PVI Locations			
Anterior	462 (42.7)	478 (44.2)	0.716
Superior	178 (16.5)	175 (16.2)	
Posterior	301 (27.8)	333 (30.8)	
Inferior	141 (13.0)	135 (12.5)	

Displayed as n (%) or mean ± standard deviation; LI: Local impedance, mV: Millivolts; PVI: Pulmonary vein isolation

6.4.2 Relationship of Local Impedance Drop with Duration

During ablation, ΔLI correlated with time for both catheters, (RMCorr – MiFi: 0.64; SP: 0.68) and demonstrated a logarithmic relationship, (Figure 2). Logarithmic curves of best fit were applied to the ΔLI – time relationship to allow a direct comparison between the MiFi and SP catheters. The equations for these curves of best fit showed ΔLI values for MiFi could be converted to those of SP by multiplying by 1.42. Both catheters showed a rapid linear ΔLI from 0 – 5 seconds before proceeding to plateau.

In contrast, the maximum ΔLI observed during an ablation was negatively correlated with the total ablation duration, (Pearson's r – MiFi: -0.37, SP: -0.33; p <0.0005 both).

Further analyses assessed the effects of ablation parameters on ΔLI. To analyse this, the maximum ΔLI at 5 seconds (ΔLI5s) was used as the dependent variable, as it represented the timepoint after which there was minimal change in ΔLI, being at the beginning of the ablation time–ΔLI plateau (Figure 6.2). This allowed for an analysis of the individual and relative effects of different ablation parameters whilst local impedance is falling, as opposed to when it remains stable during its plateau phase.

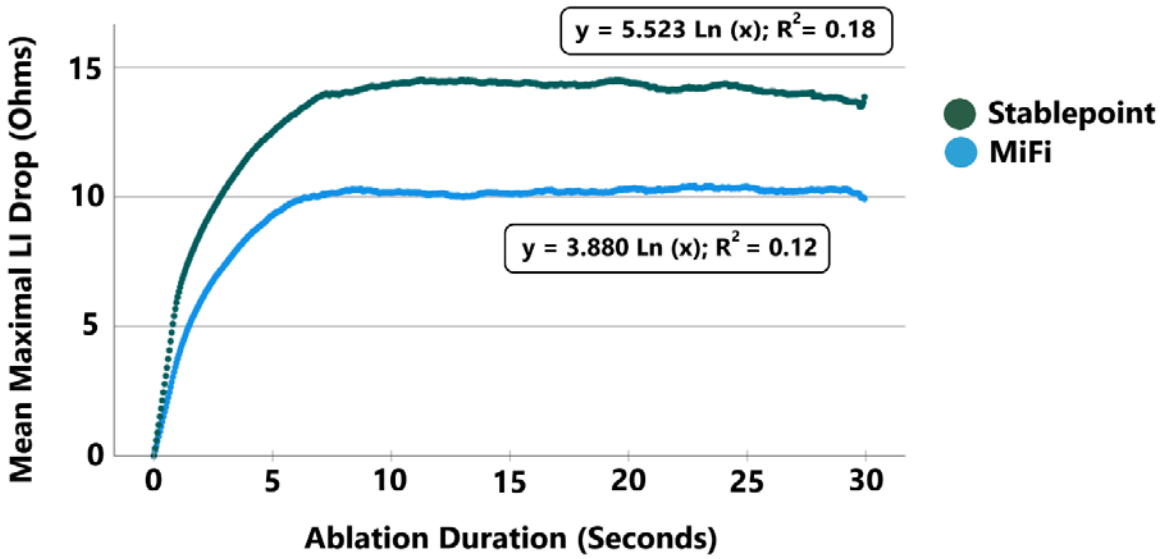

Figure 6-2 *Mean maximal local impedance drop vs ablation duration for MiFi and Stablepoint catheters.*
R^2 values and equations are for curves of best fit for all data. Conversion between the two co-efficients = 1.42

N = 20 for both MiFi and Stablepoint

6.4.3 Individual Relationships of Ablation Parameters on Local Impedance Drop at 5 Seconds

Starting LI correlated moderately with ΔLI5s, (r – MiFi: 0.37, SP: 0.44, both p <0.0005), showing a linear relationship for our dataset (Figure 6.3). In contrast, bipolar voltage correlated

weakly with ΔLI5s (r – MiFi: 0.08, SP: 0.10, p = 0.008 and p <0.0005), and there was no significant difference seen between voltage categories (MiFi: LVM – 10.1 ± 3.7Ω, IVM – 9.2 ± 5.5Ω, NVM – 9.5 ± 5.5Ω, p = 0.53; SP: LVM 13.1 ± 8.0Ω, IVM: 11.9 ± 6.3Ω, NVM: 12.5 ± 6.1Ω, p = 0.07).

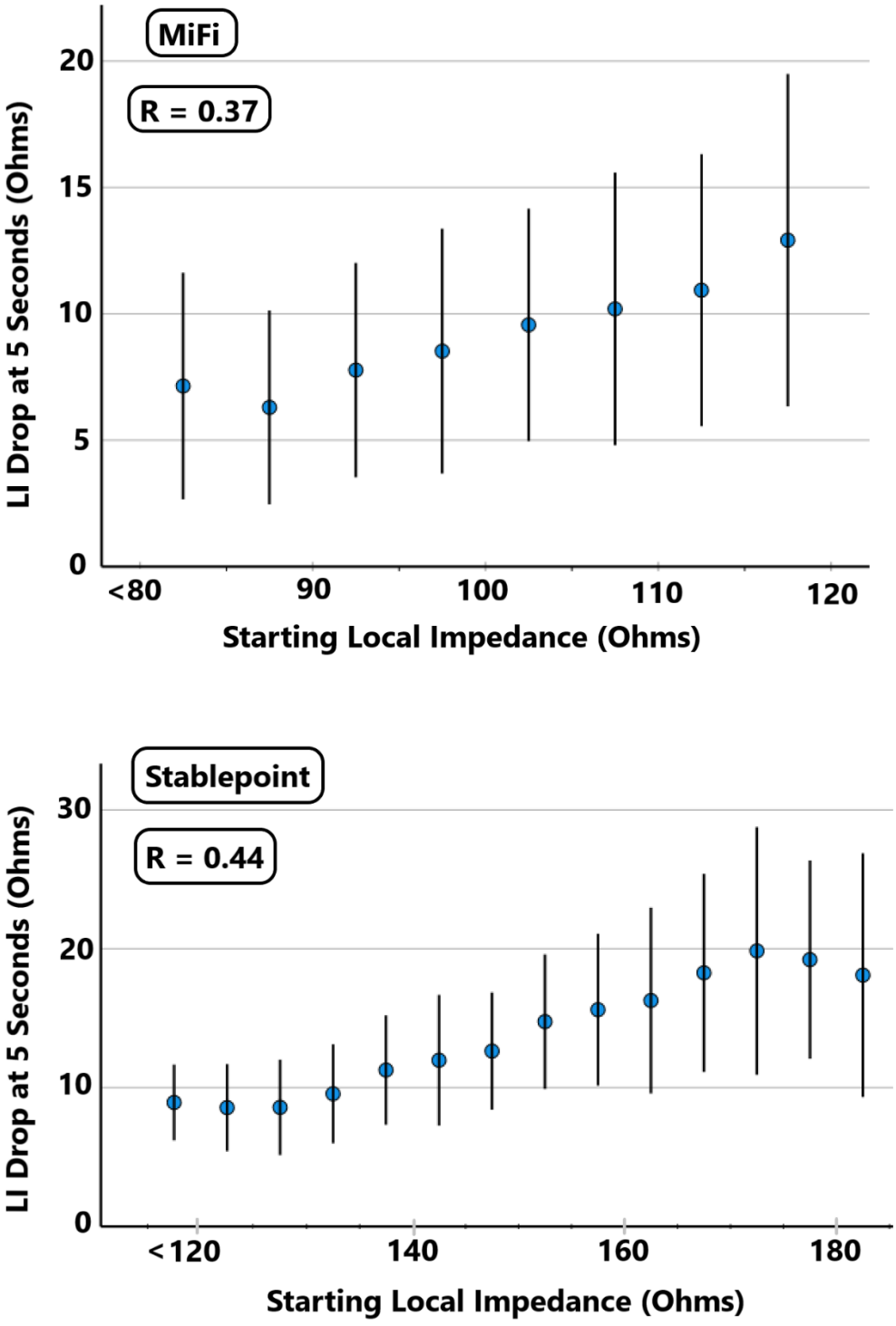

Figure 6-3 *The relationship of starting local impedance to ΔLI5s for MiFi and Stablepoint catheters.*

Datapoint = Mean ± standard deviation for 5Ω categories, n = 20 for both MiFi and Stablepoint

Mean CF correlated with ΔLI5s, (r – SP only: 0.20, p <0.0005), with the most notable increases in ΔLI5s occurring in a linear relationship between 0 – 10 g, (0 – 12Ω). From 10 – 30g, smaller increases in ΔLI5s were seen per unit CF, (12 – 16 Ω , Figure 6.4). Drift negatively correlated with ΔLI5s, (r – MiFi: -0.18, SP: -0.13).

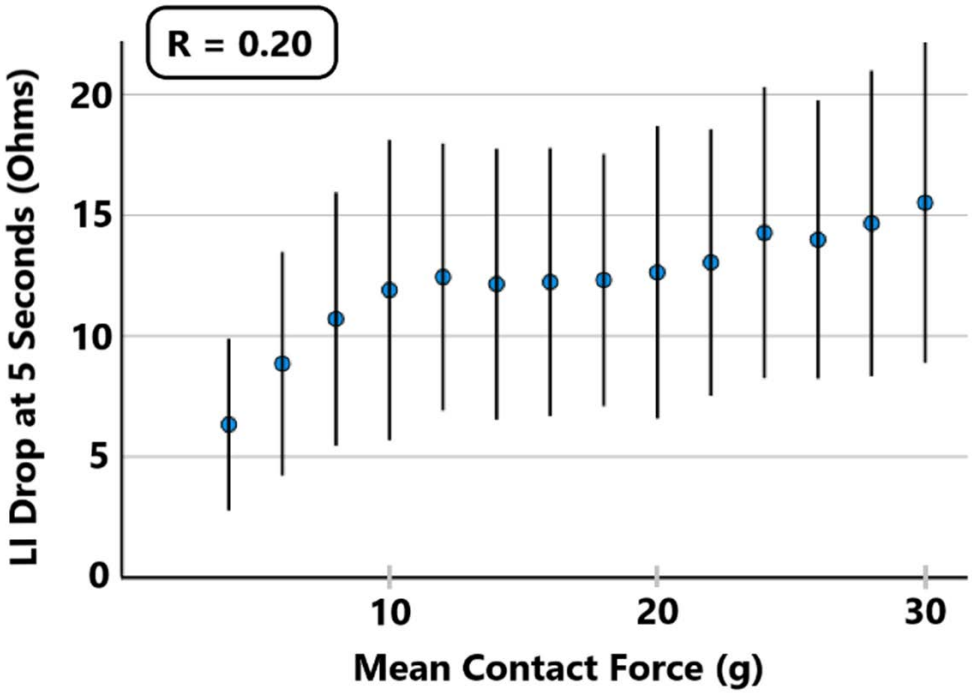

Figure 6-4 *The relationship between mean contact force and ΔLI5s.*

Datapoints are mean ± standard deviation for 2g categories, n = 20 for both MiFi and Stablepoint

6.4.4 Multivariable Relationship of Ablation Parameters with Local Impedance Drop at 5 Seconds

Independent variables were assessed for statistical significance in a univariable model with dependent variable of ΔLI5s, prior to entry into the multivariable analysis. Of particular note, power was found to be non-significant for the MiFi catheter. Multicollinearity was assessed using the variance inflation factor.

The multivariable model was more closely fit for SP than MiFi, (adjusted R^2: 0.47 vs 0.23, both p <0.0005). For MiFi, starting LI, bipolar voltage, drift, ablation side, anterior and superior ablation location were significant, (Table 6.3). Starting LI had the largest effect upon the model as per standardised β. For SP, the same variables were significant in addition to mean CF and 50W power, however, bipolar voltage was not. Similarly, starting LI had the largest effect upon ΔLI5s, followed by 50W and mean CF (Table 6.4).

Table 6.3 *Multivariable Model of Parameters Affecting Local Impedance Drop for MiFi*

Variable	Unstandardised β		Standardised β	P-Value
	β	95% Confidence Interval		
Intercept	-2.895	-5.520 – -0.270	--	--
Starting LI	0.146	0.124 – 0.167	0.401	<0.0005
Bipolar Voltage	0.222	0.069 – 0.374	0.084	0.004
Catheter Drift	-0.736	-1.103 – -0.369	-0.117	<0.0005
Left PVI	0.728	0.080 – 1.376	0.067	0.028
Anterior PVI	1.517	0.431 – 2.603	0.138	0.006
Superior PVI	1.244	0.021 – 2.468	0.088	0.046
Posterior PVI	-0.480	-1.626 – 0.665	-0.039	0.411

Adjusted R^2 = 0.23. Dependent Variable = Maximal local impedance drop at 5 seconds; Reference categories for ablation locations are right PVI (vs left PVI), and inferior PVI (vs anterior, superior, posterior PVI). LI = Local impedance; PVI = Pulmonary vein isolation

Table 6.4 *Multivariable Model of Parameters Affecting Local Impedance Drop for Stablepoint*

Variable	Unstandardised β		Standardised β	P-Value
	β	95% Confidence Interval		
Intercept	-19.142	-22.076 – -16.208	--	<0.0005
Starting LI	0.199	0.183 – 0.215	0.574	<0.0005
Bipolar Voltage	0.150	-0.034 – 0.333	0.038	0.109
Mean Contact Force	0.197	0.161 – 0.234	0.242	<0.0005
Catheter Drift	-0.607	-1.040 – -0.174	-0.064	0.006
40W	0.925	-0.349 – 2.200	0.076	0.155
50W	3.479	2.211 – 4.747	0.287	<0.0005
Left PVI	1.802	1.244 – 2.360	0.147	<0.0005
Anterior PVI	0.910	0.023 – 1.797	0.074	0.044
Superior PVI	1.479	0.432 – 2.527	0.089	0.006
Posterior PVI	-0.869	-1.802 – 0.063	-0.065	0.068

Adjusted R^2 = 0.47. Dependent Variable = Maximal local impedance drop at 5 seconds; Reference categories are right PVI (vs left PVI), inferior PVI (vs anterior, superior, posterior PVI) and 30W. LI = Local impedance; PVI = Pulmonary vein isolation; W = Watts

6.4.5 Individual Relationships of Starting Local Impedance

As the greatest effect on ΔLI5s was shown by starting LI, its relationships with CF and bipolar voltage was explored. Interestingly, starting CF did not correlate with starting LI (r – SP only: 0.05, p = 0.08). Bipolar voltage correlated weakly with starting LI for the SP catheter but not MiFi, (r – MiFi: 0.007, p = 0.82; SP: 0.08, p = 0.004). Similarly, there was a small but significant difference in starting LI between voltage categories for SP but not MiFi, (MiFi – LVM: 104.3 ± 11.3Ω, IVM: 103.0 ± 15.6Ω, NVM: 102.0 ± 14.9Ω, p = 0.09; SP – LVM: 141.3 ± 18.5Ω, IVM: 141.0 ± 18.4Ω, NVM: 145.2 ± 16.6Ω, p = 0.001, Figure 6.5).

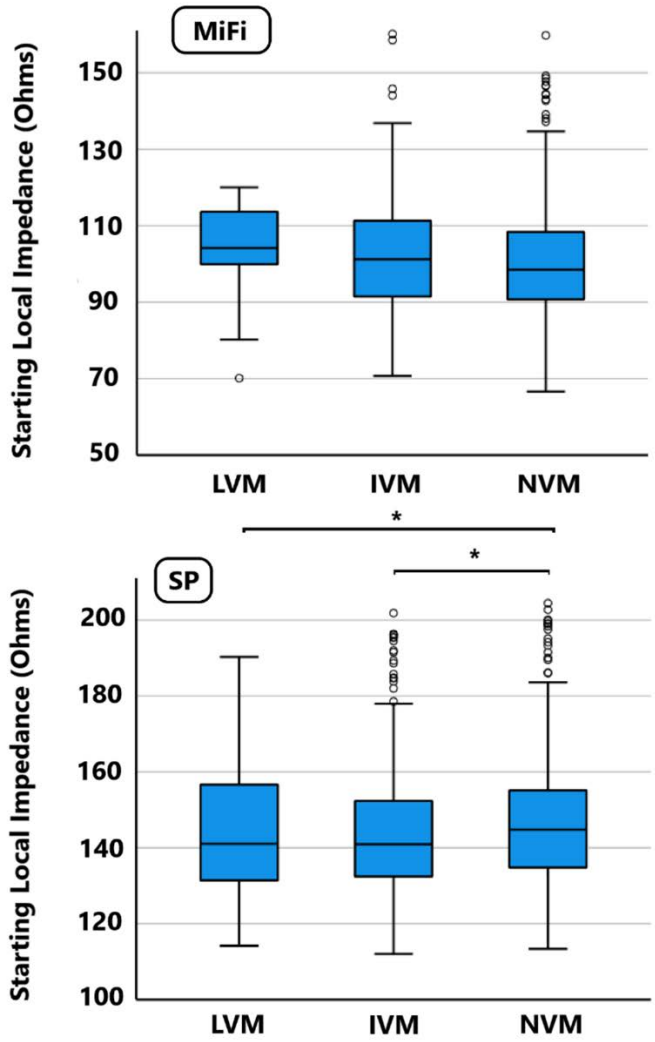

Figure 6-5 *The relationships between starting local impedance and bipolar voltage categories.*

** = Significant p-values (p <0.05) for post-hoc Tukey's test following one-way ANOVA. n = 20 for both MiFi and Stablepoint*

6.4.6 Relationship of Multivariable Analysis to LOCALIZE Local Impedance Drop Targets

Reflecting the importance of starting LI on LI drop, starting LI values projected to reach target ΔLI established using the MiFi catheter in the LOCALIZE[511] trial were sought, (17Ω [anterior-superior], 14Ω [posterior-inferior]). The equations established in the multivariable models were used for this purpose (Table 6.3 & 6.4). As the SP catheter presents higher LI readings than MiFi, and a target ΔLI for SP has not been established in long term studies, values of 24Ω and 20Ω were used, based upon the conversion factor of 1.42 generated earlier. As our multivariable model used ΔLI5s as the dependent variable rather than maximum ΔLI, adjustments to the ΔLI target was made to reflect ΔLI at the 5 second time frame, rather than the end of ablation. For this, 71.3% of the LOCALIZE targets were used, based on a mean of 71.3% of total ΔLI per ablation occurring by 5

seconds, (ΔLI5s used – MiFi: Anterior-superior: 12Ω, Posterior-Inferior 10Ω; SP: Anterior-Superior 17Ω, Posterior-Inferior 14Ω). To use the multivariable model, values for drift, bipolar voltage and contact force also required inputting. For this purpose, mean values for drift (MiFi: 1.7mm, SP: 1.5mm), and bipolar voltage (0.75mV, SP: 0.64mV) from our dataset were entered, whilst CF was set at 10g. Locations of each ablation lesion were combined as anterior-superior or posterior-inferior, and left vs right PVI, similar to the LOCALIZE study.

From this model, for MiFi, starting LI values expected to reach LOCALIZE targets by the end of ablation were 94Ω (posterior-inferior) and 98Ω (anterior-superior). For SP, values ranged from 134Ω (50W, posterior-inferior) to 160Ω (30/40W, anterior-superior). (Table 6.5).

Table 6.5 *Predictions of Starting Local Impedance Values Required to Achieve Target Local Impedance Drops*

Catheter	Location	Power (W)	Starting LI Projected to Achieve LOCALIZE Target (Ω)
MiFi	Anterior-Superior	--	98
	Posterior-Inferior	--	94
Stablepoint	Anterior-Superior	30/40	160
	Posterior-Inferior	30/40	151
	Anterior-Superior	50	143
	Posterior-Inferior	50	134

Predictions based on achievement of 70% of LOCALIZE[511] targets by 5 seconds of ablation – MiFi = 12Ω (Anterior-Superior), 10Ω (Posterior-Inferior); Stablepoint (Using Conversion of 1.42) = 17Ω (Anterior-Superior) and 14Ω (Posterior-Inferior). Values for unlisted significant variables were fixed at mean values, (Drift: MiFi – 1.7, SP – 1.5; Bipolar Voltage: MiFi – 0.75, SP – 0.64; Contact Force: SP only – 10g. LI = Local Impedance

6.5 Discussion

6.5.1 Key Findings

The key results of the study were:

1. The majority of ΔLI occurs within 5 seconds of ablation commencing.
2. ΔLI values for MiFi can be translated to SP by multiplying by 1.42.
3. CF correlates with ΔLI5s with the greatest effect occurring between 0 – 10g.
4. Starting LI has the greatest influence on ΔLI5s.
5. The SP catheter predicts ΔLI5s better than MiFi on multivariable analysis.

6.5.2 Local Impedance Drop Relationship Between MiFi and SP

The logarithmic relationship between ΔLI and ablation duration is a finding shown with generator impedance from the earliest preclinical models[446]. The increase in ΔLI followed by slowing to a plateau reflects the thermodynamic effect on tissue with rapid resistive heating, followed by slower conductive heating. This effect also explains why the majority of ΔLI occurs within 5 seconds of ablation commencing.

A simple multiplicative relationship between SP and MiFi is also expected, reflecting the only difference between the two is the sampling method. For the MiFi catheter, LI is established by taking the largest of 3 values sampled between the 4th ring electrode and each of 3 mini-electrodes in the catheter tip. In SP, due to the absence of the mini-electrodes in place of CF technology, a single reading is taken between the tip and 2nd ring electrode, resulting in a comparatively larger value. Interestingly, the 1.42x difference is similar to a pre-clinical study[376]. Using NaCl solutions of varying concentrations and a phantom model, Unger *et al* found a linear relationship (LI_{SP} = 1.42 * LI_{MiFi} + 8.7Ω), between LI sampled by MiFi or SP.

Although, more sophisticated predictions of ΔLI can be made, the simplicity of this conversion allows electrophysiologists to translate their previous ablation experience with MiFi to SP. Furthermore, it can be extrapolated to results of the LOCALIZE trial[506,511], where results would equate to 20Ω (anterior-superior) and 24Ω (posterior-inferior). Interestingly, similar clinical studies have achieved comparable values. Szegedi *et al* found optimal values of 21.8Ω anteriorly and 18.3Ω posteriorly for capture loss when pacing PVI lines acutely[416]. By examining gaps in PVI lines, Ikenouchi *et al* found ΔLI of 24Ω in carinal regions and 21Ω elsewhere were consistent with acutely successful lesions[512]. Using a similar method, Fukaya *et al* found the optimal ΔLI was

20Ω[513]. Finally, Yasumoto *et al* found blocked PVI segments had a significantly higher ΔLI than those with gaps with an optimal cut-off of 23Ω[504].

6.5.3 Relationship of Local Impedance Drop with Bipolar Voltage

A surprising result was the very weak relationships of bipolar voltage with ΔLI5s. Myocardial scar has been shown to blunt biophysical response to ablation in the left ventricle in both pre-clinical[428] and clinical studies[526]. Consequently, one would hypothesise this would translate to thinner atrial tissue. However, this is an under-investigated area, and currently we are unaware of any pre-clinical studies that assess the effect of atrial fibrosis on the biophysical response to ablation. Despite this, our result is consistent with other studies, Segreti *et al* also found no significant difference in ΔLI between bipolar voltage categories using the MiFi catheter[505]. This lack of influence of bipolar voltage on ΔLI5s implies either the sparse atrial fibrosis seen in AF is not dense enough to affect the biophysical response to ablation, or that bipolar voltage may not be an accurate representation of tissue scarring. A limitation of using bipolar voltage to assess tissue health is underestimating amplitude due to the directionality of wavefront propagation and orientation of the mapping catheter[384], which may explain this result. Baseline LI values are not affected by these two factors, perhaps explaining the poor correlation between the two[417]. In contrast, starting LI had a moderate correlation with ΔLI5s and had the greatest effect in the multivariable analysis. Consequently, baseline LI may reflect tissue health better than bipolar voltage.

6.5.4 Utility of Local Impedance Drop at 5 Seconds to Guide Ablation

Our study analysed ablation parameters that affected ΔLI5s. As the factor with the greatest influence, starting LI values that would achieve target ΔLI developed by the LOCALIZE study are presented in combination with locations and power settings. These starting LI values can be used to guide an operator who may wish to adjust catheter position to optimise starting LI and determine the power and CF they may wish to use. However, it must be emphasised our values are extrapolated from a model designed to determine ΔLI at 5 seconds, therefore they can only serve as an indicative guide.

Using starting LI to predict the potential ΔLI is of particular clinical relevance. For an individual ablation, there is a limit to the ΔLI achievable and it is not always possible to attain set targets. Increased tissue fibrosis, reflected by a low starting LI, is an example of this scenario. It is important to note that LOCALIZE targets were derived in de novo PAF patients with healthy myocardia. In more diseased myocardium, acceptance of a lower ΔLI is pragmatic as may be all that is achievable. Furthermore, excessive ablation to try and reach higher values may offer little additional benefit but increase risk. In this instance the choice is to either stop at a pre-specified ablation time or when the ΔLI curve has plateaued. This illustrates an advantage to using a marker such as ΔLI which gives constant biophysical feedback, and can indicate the likely success of the lesion over using a target such as Ablation Index (Biosense Webster Inc, Irvine, CA, USA), which can always be achieved. ΔLI is consequently a more accurate reflection of the reality of ablation, where the tissue being ablated affects its efficacy and in so doing it may offer more tailored ablation delivery to the individual tissue.

6.5.5 Relationship of Local Impedance Drop with Contac Force and Starting Local Impedance

Pre-clinical studies demonstrate that lesion dimensions correlate with CF[510]. As CF increases, greater catheter-tissue coupling occurs as more tip surface area is embedded. However, there is a point beyond which minimal improvements in coupling would be expected, consistent here with the greatest increases in ΔLI5s occurring from 0 – 10g. This has been shown in previous studies, both pre-clinical[446,447] and clinical[417,508] and reaffirms the notion that having adequate yet reliable contact is as effective as achieving high levels of CF[507].

To gauge tissue contact, the MiFi catheter is reliant upon a rise in LI from the blood pool[489]. However, issues exist with this method as fibrosed tissue shows comparable LI to the blood pool[500] and no standardised values exist for 'effective contact'. The addition of CF in the SP catheter overcomes this and provides reassurance effective coupling has been made prior to ablation. The improved coupling and its effect on ΔLI is reflected in the multivariable model, where ΔLI5s was more reliably predicted with SP than MiFi. By quantifying catheter-tissue coupling with CF, the SP catheter can optimise starting LI and deliver energy more effectively. It may also explain why power was not a significant variable in the MiFi model, as the lack of CF technology may lead to poorer coupling, negating the effect of higher powers on ΔLI with ablation in our dataset.

6.5.6 Relationship of Local Impedance and Ablation Location

The multivariable models note that left-sided, anterior-superior ablations have a greater ΔLI5s. This is consistent with thicker atrial tissue being present in these areas and reaffirms that ΔLI targets for anterior-superior walls ought to be higher than posterior-inferior walls[506,511]. Furthermore, drift was negatively associated with ΔLI5s as expected, likely representing inconsistent tissue heating with excess catheter motion seen in previous left atrial studies[389].

6.5.7 Limitations

Catheter orientation is known to affect ΔLI but was not included in our analysis[417,503]. ΔLI5s was used as a surrogate for maximal ΔLI as operators for reasons discussed above. Although this study compares two catheters, it recruited patients without randomisation and consecutively to MiFi and then SP. As emphasised above, starting LI and ΔLI targets suggested are based purely on data modelling and extrapolation from the LOCALIZE study. . They are intended to be a guide, and confirmation of their clinical utility would require a prospective trial. However, the results are similar to studies using clinical end points. Patients with paroxysmal AF featured in the MiFi group which also had a higher mean bipolar starting voltage. This could have an effect on ΔLI, however the results of our multivariable analysis suggest this would be small. Patients with PeAF underwent DC cardioversion to SR prior to ablation. The effect of this on electrophysiological parameters including tissue voltages and LI has not been studied.

6.6 Conclusions

Values of ΔLI for SP are 1.42x that of MiFi. Target values suggested for ablation are 20Ω (inferior-posterior) and 24Ω (anterior-superior), based on this conversion and the LOCALIZE study[511]. ΔLI is influenced by the starting LI, ablation location, catheter stability, CF and power. The SP catheter exhibits a more predictable relationship with ΔLI than MiFi driven by better tissue coupling aided by the presence of CF technology.

Chapter 7 Radiofrequency Ablation of the Diseased Human Left Ventricle: Biophysical and Electrogram Based Analysis

7.1 Abstract

Background and Objectives

Predictors of effective ablation lesion delivery in the human left ventricle are not established, particularly in scar. Generator impedance drop (ΔGI) and electrogram (EGM) attenuation are potential surrogates to assess this. The objectives of this study are to establish the relationships between Ablation Index (AI) and Force Time Integral (FTI) with ΔGI and EGM attenuation in the human left ventricle.

Methods

Patients undergoing ventricular tachycardia (VT) ablation were recruited. EGMs were collected pre- and post-ablation, with GI, AI and FTI measured during. Based on pre-ablation bipolar voltage, myocardium was adjudged low (LVM, <0.50mV), intermediate (IVM, 0.51–1.50mV) and normal voltage (NVM, >1.50mV). Relationships between these parameters were explored.

Results

402 ablations were analysed in 15 patients. Percentage ΔGI correlated with AI/FTI, ($p < 0.0005$, repeated measures correlation co-efficient [RMCorr] 0.54/0.44), a relationship that became weaker with increased myocardial fibrosis, (RMCorr – NVM/IVM/LVM, AI: 0.67/0.60/0.52; FTI: 0.59/0.51/0.42). The curve between AI/FTI and percentage ΔGI plateaued at 763AI and 713gs, an ΔGI of 7.5%. Shallower curves occurred progressively from NVM to LVM, ($p < 0.0005$). Mixed models demonstrated AI/FTI had greater effect on percentage ΔGI than myocardial fibrosis, drift or orientation, (Standardised $\beta = 0.54/0.48$).

EGMs attenuated with ablation, (29.3% [4.4% – 53.3%], p <0.0005), but attenuation did not correlate with AI or FTI.

Conclusions

On biophysical analysis, ablation beyond AI of 763 and FTI of 713gs offers minimal additional efficacy on average. Fibrosis blunts ablation efficacy. AI is a stronger correlate with percentage ΔGI than FTI. EGM attenuation does not correlate with ablation parameters.

7.2 Introduction

In preclinical radiofrequency ablation studies, several modifiable parameters have been demonstrated to influence the histological lesion produced, including contact force[446,448,490] (CF), power[438,460] and duration[446,460]. Composite scores have also been used to predict this: force-time integral (FTI)[455] was assessed in a bovine skeletal muscle model, while Ablation Index (AI, a non-linear multiple incorporating CF, time and power) was found to be predictive of lesion depth in canine atria[468]and ventricles[469].

Histological lesion parameters are not readily available in humans, and consequently the most commonly used model for assessing clinical ablation efficacy has been investigating gaps in pulmonary vein isolation (PVI) lines during atrial fibrillation (AF) ablation: PVI representing a stereotyped lesion set with a defined end point, lending itself easily to such analysis[465,467]. These data have helped to suggest optimal targets for ablation based on reconnecting segments.

The human ventricle is a more difficult structure in which to analyse the effect of ablation, without an equivalent to PVI lines on which to base an assessment of efficacy clinically. An alternative is to use a variable that changes with ablation such as generator impedance (GI) or electrogram (EGM) amplitude[383,493]. GI drop (ΔGI) correlates with ablation lesion size in preclinical studies[448,490]. GI changes reflect the ongoing thermodynamic effect of ablation on the myocardium, falling with tissue heating before plateauing at a point of equilibrium[446], beyond which further ablation likely has minimal additional efficacy.

The left ventricle (LV) is a thick-walled structure where myocardial fibrosis presents a heterogeneous substrate with uneven thermodynamic properties[428], which is known to affect ablation lesion size in preclinical studies[428,429,528].

In this study, the relationships between ablation delivery indices and biophysical ablation responses (GI and EGM attenuation) are explored in the diseased human left ventricle, including the effect of myocardial scar, with the aim of informing targets for clinical LV ablation.

7.3 Methods

7.3.1 Procedure

Patients listed for ventricular tachycardia (VT) ablation were recruited. Ethical approval was granted by the UK Research and Ethics Committee (Reference: 18/LO/0839). All procedures were performed under general anaesthetic. The ThermoCool® SmartTouch Surround Flow™ ablation catheter, CARTO3 3D mapping system (Biosense Webster Inc., Irvine, CA, USA.) and Agilis® steerable sheath (Abbott Laboratories, Chicago, IL, USA) were used for all cases. The ablation strategy employed, and LV access were left to the discretion of the operator. All ablations were power-controlled, temperature-limited, static deliveries. Only endocardial ablations were included in the study. Catheter irrigation was with heparinised normal saline with manufacturer recommended flow rates during ablation, (7ml/minute for 30W, 17ml/minute for higher powers).

7.3.2 Data Collection and Analysis

Ablation data were exported from CARTO3 for analysis using custom MATLAB scripts, (MathWorks Inc., Natick, MA, USA). CF (g) and catheter angle (degrees) were sampled at 20Hz; GI (Ohms) and power (Watts) at 10Hz.

Bipolar EGM amplitudes were recorded between the tip and first ring electrode. Unipolar EGM amplitudes were referenced to an indifferent electrode in the inferior vena cava. Data was collected from pre- and post-ablation tags that were manually placed on CARTO3. Ablations were discarded if catheter macrodisplacement occurred. Manual tags on CARTO3 record 2.5 seconds of EGM data, 2 seconds retrospectively and 0.5 seconds prospectively. Post-ablation tags were placed at least 3 seconds following ablation termination to avoid artefact. EGM amplitudes were measured automatically by CARTO3 from dominant peak to trough, but also manually verified to ensure accuracy. Where multiple valid EGMs were captured, mean amplitude was taken to improve reliability.

FTI was calculated as the area under the CF – Time curve by trapezoidal integration. AI was calculated from power, CF and timestamp data using a proprietary algorithm provided by the manufacturer (Biosense Webster Inc.). For both FTI and AI, custom written scripts in MATLAB were used to calculate these values from the raw exported CARTO3 data.

GI was measured between the ablation catheter and ground patch placed on a patient's left thigh. GI data were processed through a Savitzky-Golay filter to minimise noise. Analysis was performed on both the absolute filtered GI drop (ΔGI) and the filtered impedance drop as a percentage of the starting impedance for the ablation (Δ%GI). To examine the relationship between AI/FTI and the filtered GI drop, an incremental analysis was undertaken as described in Chapter 2 and used in prior studies[383,389,493], whereby the largest GI drop was taken in increments of 10AI or 10gs for each individual ablation, i.e., the largest drop between 0 and 10AI, 0 and 20AI, 0 and 30AI and so on.

To establish a parameter predicting lesion completion, the point where further ablation provided little change in biophysical measurements as a surrogate for thermodynamic equilibrium was sought, this being the beginning of the plateau in the Δ%GI and AI/FTI relationship. In order to do this qualitatively, the mean Δ%GI was calculated across all ablations for each 10AI or 10gs increment producing a single curve. For quantitative analysis of the relationships, curves of best fit were applied to the entire AI-Δ%GI and FTI-Δ%GI datasets. Plateau points were then determined as a Δ%FI of 0.25% over 100gs/100AI, as calculated from the first derivative of the formulae for the best fit curves.

Ablation catheter drift was calculated as the Euclidian distance between co-ordinates from the pre- and post-ablation tags.

Reflecting the extent of myocardial scar, ablations were divided into low (LVM, <0.50mV), intermediate (IVM, 0.51–1.50mV) and normal voltage (NVM, >1.50mV), based upon pre-ablation bipolar EGM amplitude.

7.3.3 Statistical Analysis

IBM SPSS Statistics (Version 27, IBM Corp, NY, USA) was used for statistical analysis. A p-value of <0.05 was considered statistically significant. Variables were assessed as parametric or non-parametric by visual inspection of histograms and a Shapiro-Wilks test. Continuous data were expressed as mean ± SD or median [interquartile range]. Bivariate correlations were performed using Pearson's product moment correlation. As multiple measures were taken from each patient, repeated measures correlation (RMCorr) was used when data was not independent. Independent samples were compared using a Mann Whitney U Test or Kruskal Wallis H test. Related samples were compared using a Wilcoxon signed rank test.

To assess the relationships between ΔGI and AI/FTI individual generalized linear mixed models were performed using a linear link, also including in the model: catheter drift and orientation (variables known to affect ΔGI in the atrium[389,459]) as well as endocardial scar. Random factors included patient and ablation number. This analysis was performed on the sections of the GI-AI or GI-FTI relationships from the start of Δ%GI (200AI or 0gs) to the calculated plateau point. All variables were checked in an univariable model to ensure significance prior to inclusion.

7.4 Results

7.4.1 Patient and Ablation Characteristics

Patient characteristics are shown in Table 7.1. 15 patients were recruited. No serious procedural complications occurred including no instances of cardiac tamponade nor audible

steam pops. One patient died 11 days following the procedure from refractory ventricular arrhythmias.

402 study ablations were performed, (Table 7.2). There was a significant correlation between starting GI and absolute filtered ΔGI ($p < 0.0005$, Pearson's $R = 0.41$). Therefore, to minimise the influence of initial GI, Δ%GI was used for further analysis. Filtered Δ%GI was found to have a better correlation than absolute filtered ΔGI with AI (RMCorr = 0.54 vs 0.51) and FTI, (RMCorr = 0.44 vs 0.41). When divided into voltage categories, NVM showed the strongest correlation between AI and Δ%GI, a relationship that became progressively weaker with increasing fibrosis, (RMCorr – NVM: 0.67, IVM: 0.60, LVM: 0.52). FTI showed a similar relationship but with weaker correlations comparatively, (RMCorr – NVM: 0.59, IVM: 0.50, LVM: 0.42).

Table 7.1 *Study Population Characteristics*

Patient Characteristics	
n	15
Female	5 (33%)
Age, Years	71.2 ± 10.1
Co-Morbidities	
Arterial hypertension	5 (33%)
Ischaemic heart disease	10 (67%)
Diabetes mellitus	3 (20%)
Dyslipidaemia	11 (73%)
LVEF (%)	30.1 ± 12.7
LVEF ≤ 35%	10 (67%)
Aetiology of VT	
Ischaemic	10 (67%)
Dilated Cardiomyopathy	3 (20%)
Myocarditis	2 (13%)
Medication	
Beta blocker	13 (87%)
Amiodarone	7 (47%)
Sotalol	1 (7%)
ACEi	9 (60%)
ARB	2 (13%)
ARNI	3 (20%)
Statin	11 (73%)
MRA	12 (80%)
Cardiac Device	
ICD	9 (60%)
CRT-D	6 (40%)
Procedural Characteristics	
Procedure Length (Mins)	270 ± 58
Ablation Time (Mins)	26.5 ± 11.7
Fluoroscopy Time (Mins)	15.4 ± 10.5

ACEi: Angiotensin converting enzyme inhibitor; ARB: Angiotensin receptor blocker; ARNI: Angiotensin receptor neprilysin inhibitor; CRT-D: Cardiac resynchronisation therapy with defibrillator; ICD: Implantable cardiac defibrillator; MRA: Mineralocorticoid Receptor Antagonist; LVEF: Left ventricular ejection fraction.

Table 7.2 *Ablation Characteristics*

	Altogether	**LVM**	**IVM**	**NVM**	**P Value**
Definition (mV)	All	≤0.50	0.51 – 1.50	>1.50	
Number of ablations	402	194	157	51	--
Ablation index	803 [712, 859]	803 [662, 856]	806 [717, 866]	790 [728, 848]	0.473
Force time integral (gs)	859 [586, 1147]	858 [518, 1135]	906 [645, 1177]	741 [624, 1043]	0.054
Duration (Seconds)	57.8 [39.7, 69.8]	58.7 [43.1, 69.8]	59.3 [41.1, 68.1]	60.4 [50.8, 75.8]	0.231
Contact force (g)	15.5 [10.4, 22.2]	15.5 [10.4, 23.3]	17.2 [11.3, 22.2]	14.1 [10.7, 19.9]	0.441
Starting impedance (Ω)	112.7 [102.3, 120.9]	111.6 [96.4, 118.5]	112.1 [104.0, 120.8]	120.5 [112.9, 127.9]	< 0.0005
GI drop (Ω)	7.2 [4.6, 11.0]	5.7 [3.4, 8.3]	8.4 [5.7, 11.9]	11.6 [8.5, 15.2]	< 0.0005
Percentage GI drop	6.8 [4.1, 9.3]	5.3 [3.1, 7.4]	7.8 [5.1, 10.4]	9.5 [7.1, 12.8]	< 0.0005

LVM, IVM, NVM = Low, intermediate, normal voltage myocardium; GI = Generator impedance. Values are median [lower quartile, upper quartile]. P-Value = Kruskal Wallis test for medians between LVM / IVM / NVM

7.4.2 Plateau Assessment of Ablation Index and Force Time Integral with Percentage Generator Impedance Drop

Incremental analyses were based upon 224948 individual data points. The relationship curves between AI-Δ%GI and FTI-Δ%GI qualitatively plateaued from 700AI and 700gs respectively, both corresponding to a Δ%GI of 7.5% (Figures 7.1 & 7.2). When subdivided by the three voltage categories, the three resulting curves plateaued in ranges from 700 – 800AI, (Figure 7.3) and 500 – 800gs, (Figure 7.4), with a lesser Δ%GI with increasing myocardial fibrosis, (LVM: 6%, IVM: 8%, NVM: 10%, $p < 0.0005$).

For quantitative assessment, to prevent distortion of the modelling, the lag phase of the AI-Δ%GI data was omitted by removing Δ%GI values equal to zero. Quadratic models fit the AI-

Δ%GI datasets the closest, whilst logarithmic models represented FTI-Δ%GI. The plateaus for these relationships are shown in Figures 7.1 – 7.4. These values fit with the prior qualitative assessment.

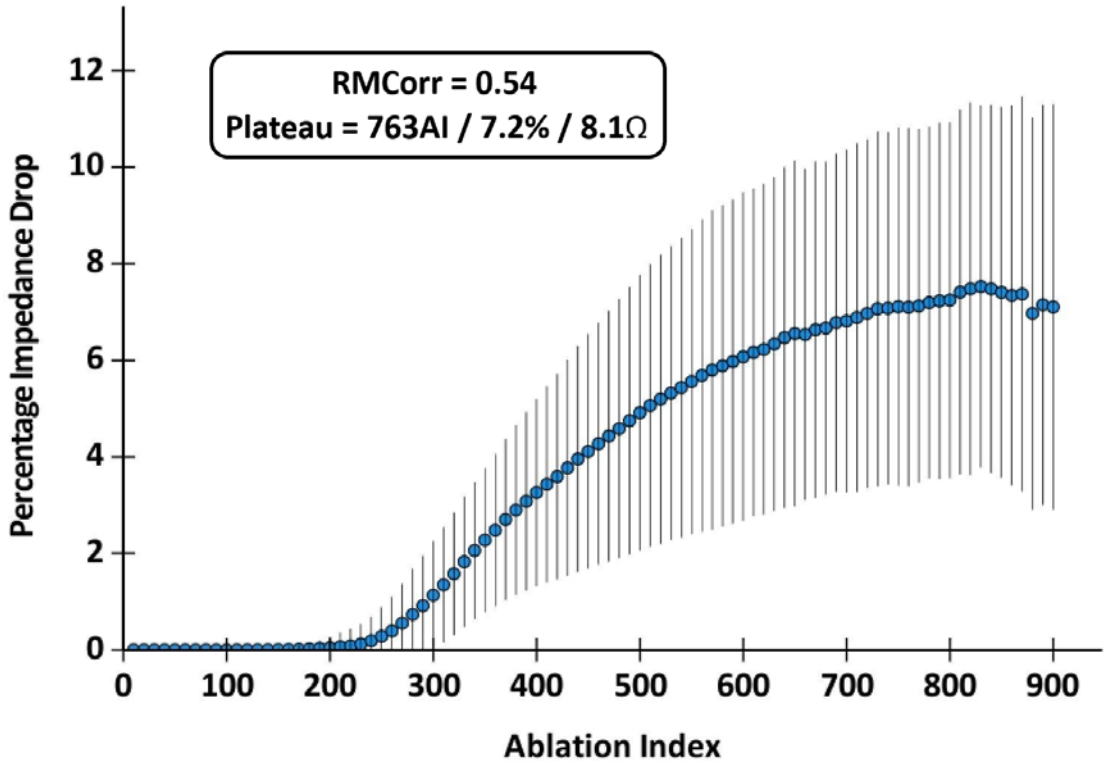

Figure 7-1 *The relationship between Ablation Index and filtered percentage generator impedance drop*

Mean maximal Δ%GI vs incremental AI. Each data point comprises of at least 80% of the total ablations performed. Plateau determined as point at which Δ%GI of 0.25% over 100AI, calculated from the first derivative of the formula for the best fit curve for data. Error bars are ± 1 standard deviation. Chart comprises of 30723 measurements from 15 patients

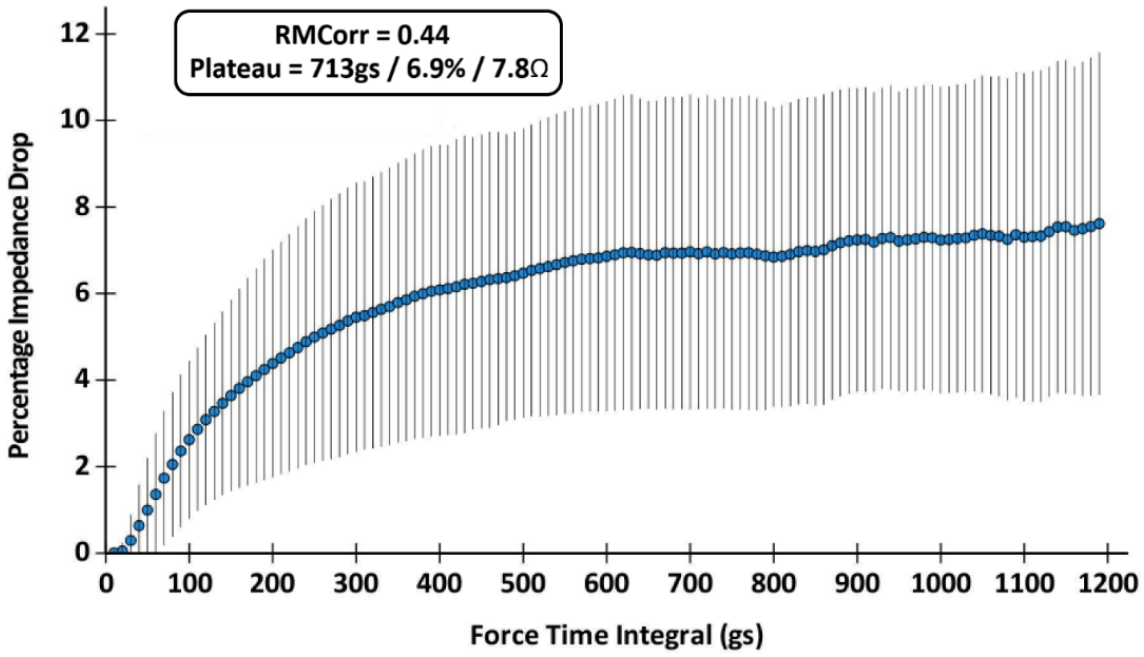

Figure 7-2 *The relationship between force time integral and filtered percentage generator impedance drop*

Mean maximal Δ%GI vs incremental FTI. Plateau determined as point at which Δ%GI of 0.25% over 100gs, calculated from the first derivative of the formula for the best fit curve for data. Each data point comprises at least 80% of ablations. Error bars are ± 1 standard deviation. Chart comprises of 35589 measurements from 15 patients

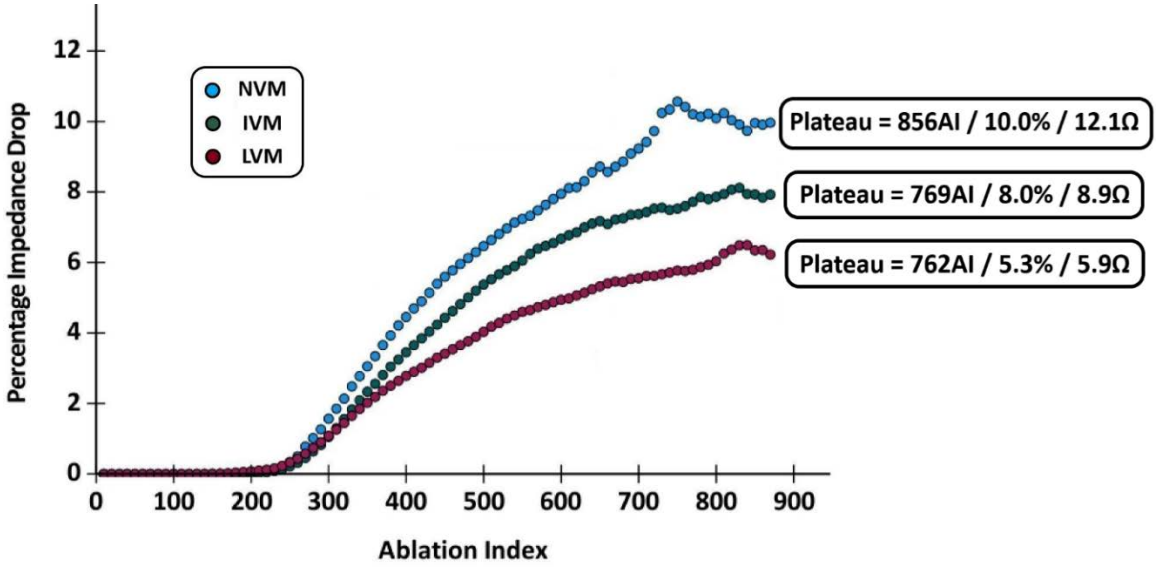

Figure 7-3 *The relationship between Ablation Index and filtered percentage generator impedance drop by voltage class*

Mean maximal Δ%Imp for normal, intermediate, and low voltage myocardium vs AI. Plateau determined as point at which Δ%Imp of 0.25% over 100AI, calculated from the first derivative of the formulae for the best fit curves for data. Each data point comprises at least 80% of ablations for that category. Data from 15 patients.

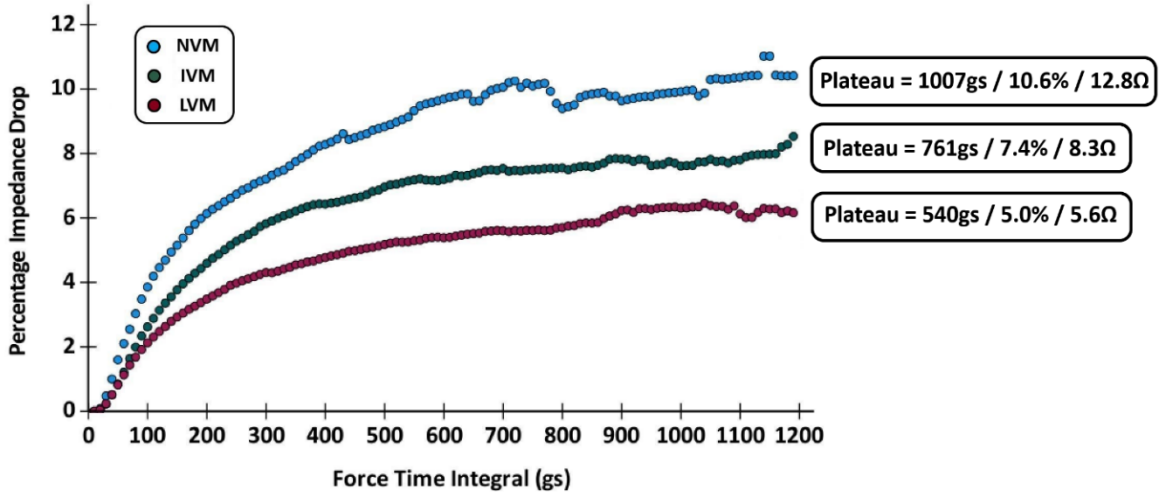

Figure 7-4 *The relationship between force time integral and filtered percentage generator impedance drop by voltage class*

Mean maximal Δ%GI for normal, intermediate, and low voltage myocardium vs FTI. Plateau determined as point at which Δ%GI of 0.25% over 100gs, calculated from the first derivative of the formulae for the best fit curves for data. Each data point comprises at least 80% of ablations for that category. Data from 15 patients.

7.4.3 Generalized Linear Mixed Model

To examine the relationship between AI / FTI with Δ%GI alongside other variables, a generalized linear mixed model was performed using data where both relationships appeared linear, (AI 200 – 763, FTI 0 – 713gs). The mixed model demonstrated all entered variables were significant but both AI and FTI had a considerably larger effect on Δ%GI than orientation or drift as determined by standardised β (Tables 7.3 and 7.4). For example, an AI of 763 would be predicted to achieve a Δ%GI of 7.54%, whilst parallel orientation and a catheter drift of 3mm would only alter Δ%GI by the comparatively small 0.15% and -0.23% respectively.

The random effect (patient) was significant for both AI and FTI ($p = 0.008$ and $p < 0.0005$), suggesting there is considerable variation between subjects.

Table 7.3 *Multivariate Analysis of Factors Affecting Impedance Drop with Ablation in the Left Ventricle with Ablation Index*

Variable	Unstandardised β		Standardised β	P-Value
	β	95% Confidence Interval		
Ln (Ablation Index)	1.63	1.62 – 1.64	0.69	< 0.0005
IVM	0.19	0.19 – 0.20	0.11	< 0.0005
NVM	0.51	0.50 – 0.52	0.20	< 0.0005
Drift	-0.03	-0.04 - -0.03	-0.10	< 0.0005
Parallel Orientation	0.02	0.02 – 0.03	0.01	< 0.0005

Dependent Variable = Square root of percentage impedance drop. Adjusted $R^2 = 0.56$. Reference category for endocardial voltage categories is LVM.

LVM, IVM, NVM = low, intermediate, normal voltage myocardium.

Table 7.4 *Multivariate Analysis of Factors Affecting Impedance Drop with Ablation in the Left Ventricle with Force Time Integral*

Variable	Unstandardised β		Standardised β	P-Value
	β	95% Confidence Interval		
Ln (Force Time Integral)	0.60	0.60 – 0.60	0.61	< 0.0005
IVM	0.25	0.24 – 0.26	0.14	< 0.0005
NVM	0.62	0.61 – 0.63	0.27	< 0.0005
Drift	-0.03	-0.03 – -0.03	-0.09	< 0.0005
Parallel Orientation	0.04	0.03 – 0.04	0.02	< 0.0005

Dependent Variable = Square root of percentage impedance drop. Reference category for endocardial voltage categories is LVM. Adjusted R^2 = 0.46.

LVM, IVM, NVM = Low, intermediate, normal voltage myocardium

7.4.4 Electrogram Analysis

Bipolar analysis consisted of all 402 ablations. Where the protocol specified indifferent electrode was not used in the procedure, ablations were excluded from the unipolar analysis (29 ablations). Ablation resulted in a significant decrease in EGM amplitude, (Bipolar: pre-ablation 0.54mV [IQR 0.29 – 0.98mV], post-ablation 0.37mV [0.20 – 0.56mV], p <0.0005; Unipolar: pre-ablation 3.71mV [2.36 – 5.40mV], post-ablation 3.11mV [2.09 – 4.65mV], p <0.0005). There were strong positive correlations between pre-ablation EGM amplitudes and attenuation (Bipolar: R = 0.871, Unipolar: R = 0.558, both p <0.0005). Consequently, percentage attenuation was used in further analyses to minimise this influence. Median percentage attenuations were bipolar 29.3% [4.4% – 53.3%], and unipolar 9.48% [3.15% – 23.14%]).

Percentage bipolar attenuation correlated weakly with Δ%GI (r = 0.151, p < 0.002) but did not correlate with mean CF or AI/FTI achieved with ablation. Percentage unipolar attenuation did not correlate with Δ%GI, mean CF or AI/FTI achieved.

There was no significant difference in percentage EGM attenuation between ablations reaching the previously established ΔGI plateaus and those that did not. This was the case for both bipolar or unipolar attenuation and AI or FTI plateaus.

7.5 Discussion

7.5.1 Key Findings

The key results of the study were:

1. Δ%GI correlates with AI/FTI achieving a plateau on average at 763AI / 713gs.
2. The degree of underlying myocardial scar significantly affects the relationship between Δ%GI and AI/FTI becoming progressively shallower from NVM to LVM, meaning a lesser Δ%GI for the same AI/FTI.
3. Increasing myocardial scar decreases the correlation of AI / FTI with Δ%GI.
4. AI has a stronger correlation with Δ%GI than FTI.
5. AI / FTI have the greatest effect upon Δ%GI in mixed models including endocardial voltage categories, catheter orientation and drift. EGMs attenuate with ablation, but this attenuation does not correlate with AI or FTI.

7.5.2 Relationship of Percentage Generator Impedance Drop with Ablation Index or Force Time Integral

The correlation between Δ%GI and AI/FTI is expected and consistent with pre-clinical studies[529,530]. Radiofrequency ablation increases tissue temperature which correlates closely with lesion dimensions and is predictable using a mono-exponential model[439]. A mono-exponential model ends with a plateau, representing a point of thermodynamic equilibrium. Beyond this point, there is minimal gain in terms of lesion size from further ablation. As an inverse function of tissue temperature, Δ%GI is a useful clinical surrogate for the former in the absence of direct tissue temperature measurements.

The current study shows a stronger correlation between Δ%GI with AI than FTI. This is likely as the latter only incorporates CF and duration while the former additionally includes power. In so doing, AI incorporates more variables contributing to effective ablation[438,446,448,460].

A recent report by Larsen *et al* demonstrated AI to be a good predictor of both lesion dimensions and ΔGI using a cubic spline model when ablating healthy ex vivo swine ventricular myocardium[529]. Two clinical studies have investigated AI in ablation of the ventricles. Gasperetti *et al* prospectively treated right ventricular idiopathic premature ventricular complexes (PVCs) with AI guided ablation, aiming for 590-610 AI dependent on location and compared to propensity matched non-AI guided cases[474]. Decreased arrhythmic recurrence was seen at 6 months in the AI guided group. Casella *et al* retrospectively investigated 145 patients with either left or right outflow tract PVCs, finding those free from arrhythmia at 6 months also received higher AI ablations with an average AI of 489 vs 372, and an average maximum AI of 630 vs 487[473]. The pathophysiology and arrhythmic mechanisms behind PVCs are different to that of scar mediated VT, as is the myocardium being ablated in those studies, however these studies do demonstrate that AI guided ablation of the ventricle as a concept has the potential to improve outcomes.

The current study is mechanistic in design and presents average AI and FTI values for LV ablation beyond which there are greatly diminished biophysical returns from further ablation. Not every ablation reaching these AI or FTI values will have an adequate impedance drop, nor maximised lesion parameters which may be achieved with prolonged ablation[531,] but it offers a starting point for the electrophysiologist in ventricular ablation and to guide further research. The study does not evaluate long term arrhythmic free outcomes: these would need to be investigated in a prospective trial. However, this is challenging. Previous LA studies have used procedural endpoints (PVI) to determine the effectiveness of AI and FTI targets[466,467,472]. Staged procedures also allow for examination of gaps in PVI lines and thereby analysis of specific lesions. Ideally, one would use a similar method in VT ablation, however, a comparable consistent procedural endpoint does not exist.

7.5.3 The Effect of Tissue Voltage upon the Percentage Impedance Drop – Ablation Index / Force Time Integral Relationship

There was a progressive decrease in Δ%GI plateau from NVM to LVM in the current study. If this plateau is taken as approaching the maximal area of heating delivered by the radiofrequency ablation, then this suggests scarred tissue is increasingly resistant to and may experience less efficacious ablation for the same AI / FTI reached. Moreover, based on the biophysics, there appears to be minimal gain in ablating beyond the plateau point, as presumably the limitations of the radiofrequency ablation set up for that individual ablation are being reached, leaving only the possibility of complications occurring such as steam pops and extra-cardiac damage. Consequently, to derive further incremental ablation benefit in LVM, alternative adjuncts such as half normal saline irrigation or bipolar ablation may be necessary.

The difference in the behaviour of the tissue with respect to scar has biological plausibility. NVM is composed of densely packed healthy cardiomyocytes allowing uniform heat conduction and thermal injury with ablation. Conversely, LVM is heavily scarred featuring interspersed cardiomyocytes, collagen, and adipose tissue which results in uneven resistive heating. Conductive heating is then also reduced due to the heat capacitance of adipose tissue and shunting to blood. The result, as observed in preclinical studies, is a smaller, poorly demarcated ablation lesion and lesser drop in Δ%GI[428,429].

A recent publication by Garg *et al* demonstrated clinical benefit to prolonged ablation of up to 300 seconds in the LV summit[531]. Several differences exist between this study and the current one, including anatomical site of ablation, method of power delivery (static vs incremental) and underlying mechanism of arrhythmia (PVC vs scar-mediated) in the ablated tissue making comparison challenging. However, the work by Garg *et al* highlights that although there are diminishing returns from ablation at high AI/FTI pre-clinically[429,528] and biophysically, prolonged ablation and these small returns maybe necessary in the correct circumstances to disrupt crucial arrhythmic circuitry.

The decreased ability of AI / FTI to predict Δ%GI with progressive fibrosis observed in the current study is also explained by the histological features of LVM, as greater variation in tissue heterogeneity would be expected between lesions within the IVM and LVM categories over NVM[428]. Consequently, estimating the extent of myocardial heating would be inherently more

unpredictable. Barkagan *et al* noted the result of this is a histologically irregular pattern of temperature induced necrosis with islands of affected cardiomyocytes interspersed with strands of viable myocytes[428]. Despite this, the correlation co-efficient of 0.52 suggests AI possesses a moderate relationship with Δ%GI in LVM, suggesting use AI is a reasonable surrogate. Furthermore, the correlation co-efficient of AI for Δ%GI are greater than that of FTI for all endocardial voltage categories, emphasising the importance of incorporating power into lesion indices.

Drift and orientation were also found to have significant effects on Δ%GI in the mixed model alongside AI or FTI. The negative relationship of drift with Δ%GI is expected, and likely to represent inconsistent tissue heating with excess catheter motion as seen in previous clinical studies in the LA[389]. Parallel catheter orientation may improve the surface area of electrode-tissue coupling compared to perpendicular and has also been seen in the LA[389]. However, its relative effect on Δ%GI is minor compared to other factors in the model. Significant subject to subject variability was also seen in the model, most likely explained by non-ablation factors contributing to the circuit forming the impedance reading.

7.5.4 Differences Between Ablation Index and Force Time Integral in their Relationships with Percentage Impedance Drop

A clear difference in the relationship of AI and FTI with impedance drop existed. Whilst FTI-Δ%GI has a logarithmic relationship, AI-Δ%GI has a lag phase, then an almost linear phase before plateauing. These relationships have been noted in previous LA ablation studies[383,493]. However, in comparison with the latter studies, subtle differences exist, including a higher Δ%GI at the plateau point plateau[493] and higher AI/FTI plateau values in the ventricle[493]. This is explained by the increased thickness of the LV compared to the LA. Interestingly, Larsen *et al* noted impedance drop and lesion parameters to plateau at a lower AI of 550 in their ex vivo healthy ventricular swine model, corresponding to an impedance drop of approximately 20Ω. The difference in values can be explained by the more fibrotic, human, ventricle ablated in the current study and factors associated with a beating heart such as catheter instability, and varying CF and orientation[529].

7.5.5 Relationship of Electrogram Attenuation and Ablation Index or Force Time Integral

In this study, both bipolar and unipolar EGM amplitudes attenuated with ablation but did not correlate with AI or FTI. Ideally, EGM attenuation would be assessed dynamically during ablation as with the impedance analysis. However, this is impractical due to artefact affecting the EGM during ablation as well as the increased motion of the ablation in the ventricle compared to the atrium making this more procedurally challenging. Previous studies have noted both bipolar and unipolar EGM attenuation not to be a reliable marker of ablation lesion volume in a pre-clinical swine model[482], nor correlate with pacing threshold clinically[532]. Overall, the lack of consistent correlations between EGM attenuation, generator impedance drop, FTI and AI, and impracticalities in reliably assessing the EGM during ablation suggest that this is a suboptimal surrogate for lesion progression and only serves to confirm lesion delivery.

7.5.6 Limitations

Δ%GI was used as a surrogate for lesion parameters in the absence of anatomical assessment. Options are limited when assessing individual lesion development and completion in scarred myocardium specifically as no clinical parameters have been found to correlate with lesion size[429], histologically lesions can be difficult to find[428], and histology is not available for clinical ablations generally. Consequently, there is not a clear 'gold standard' for measuring ablation lesion size in scarred ventricular tissue, which comprises most of the target in VT ablation. Generator impedance drop at least offers a dynamic assessment of ablation lesion development and thermodynamic equilibrium.

The operators were not blinded to impedance, and this may have influenced their ablations leading to premature curtailment in some applications.

Bipolar voltage may not reflect the transmural scar burden and represents a limitation of the voltage-based subdivisions we have used. Although unipolar voltage could have been used, only endocardial ablations were considered in our analysis and the commonly used division of 8.27mV would only allow consideration of two scar categories[533].

The study was conducted exclusively with surround flow catheters, it is unclear if the findings would be applicable to conventionally irrigated catheters. Further, during the study bipolar ablation and alterations in the ablation catheter irrigant salinity were not used, which would likely alter the relationships observed. Electrogram voltage amplitude was measured manually using CARTO3. This could introduce error based on person-to-person variation when taking measurements and affect result reproducibility.

7.6 Conclusions

During VT ablation, 763AI or a FTI of 713gs are suggested by biophysical analysis as average points where further biophysical response is limited and corresponds to a filtered generator impedance drop of 7.5%. The biophysical response to ablation is influenced by tissue fibrosis, with more scarred tissue demonstrating a lower generator impedance drop and achieving an earlier plateau, suggesting a greater resistance to radiofrequency ablation by scarred myocardium. AI and FTI both correlate significantly with generator impedance drop with AI superior. This relationship becomes weaker with more scarred myocardium. While EGM attenuation occurs with ablation, it is not consistently correlated with any ablation parameter, suggesting it is a less favourable target to guide ablation.

Chapter 8 Conclusions and Future Directions

8.1 Summary of Findings

In this thesis the relationships between myocardial fibrosis, impedance, contact force and other parameters were investigated before and during radiofrequency ablation.

In Chapter 3, the suitability of current values of tissue voltage used as surrogates for atrial myocardial fibrosis were assessed physiologically using pacing thresholds. LI was also investigated as a novel biophysical parameter. It was found that although current values of 0.05mV and 0.5mV could be optimised to 0.03mV and 1.29mV. Furthermore, referenced LI holds promise in assessing health of atrial tissue, being an effective and superior discriminator of electrically active and partially active tissue than bipolar voltage.

In Chapter 4, differences in tissue voltages seen between rhythms and AF types seen on lower density mapping systems were re-investigated using the ultra-high-density Rhythmia mapping system. Uniquely, differences in voltages between left and right atria were also assessed. Ultra high-density mapping confirmed previous findings with lower voltages being seen in AF over SR and PeAF over SR. There was no differences between atria.

In Chapter 5, the relationship of referenced tissue LI with increasing CF on the left atrial wall was investigated in a clinical setting. The effect of rhythm and tissue fibrosis (as assessed by bipolar voltage) was also investigated. A strong positive correlation was seen between CF and LIr with a logarithmic relationship being demonstrated for both AF and SR. Interestingly AF showed higher LIr values for same amount of CF over SR suggesting improved catheter-tissue coupling. Tissue voltages did not affect these relationships.

In Chapter 6, the influence of multiple factors upon ΔLI were assessed, with particular focus on differences between the MiFi and SP catheters, and the introduction of CF technology. A direct multiplicative relationship of 1.42 was found between ΔLI values of MiFi and SP. SP was found to be much more capable of predicting ΔLI at 5 seconds than MiFi, with starting LI, CF, 50W

power and ablation location significant factors. The degree of atrial scarring as assessed by bipolar voltage did not significantly affect ΔLI5s when using the SP catheter.

In Chapter 7, the biophysical effects of radiofrequency ablation on the left ventricular endocardium were studied with focus on the degree of underlying scarring. GI was found to plateau at 763 AI on average. Smaller Δ%GI values were seen per unit AI with increasing grades of scarring. AI had the largest effect on Δ%GI of all variables sampled, however increased scar was shown to decrease the correlation of AI with Δ%GI

8.2 Clinical Implications

The specific clinical implications of the work in this thesis have been explored in their individual chapters, however a collation of these will be discussed below.

Electrically inert and diseased atrial myocardium are currently represented on electroanatomical maps using bipolar voltage values of 0.05mV and 0.5mV respectively. These values are used clinically and are widespread throughout the literature including in trials of scar guided ablation and international guidelines[101]. However, no histological and minimal physiological validation of these values has occurred. By using pacing thresholds to assess the conduction capacity of left atrial tissue of varying degrees of health, optimisation of these cut-offs to 0.03mV and 1.29mV is suggested. Changing the electrically inert value of 0.05mV to 0.03mV is unlikely to cause differences in current procedural practice, however it highlights how even extremely low voltage tissue still possesses the capacity to conduct signal. Consequently, it should not be exempt from ablation, particularly in critical areas, for example in PVI lines. In contrast, altering the diseased tissue value of 0.5mV to 1.29mV could have significant clinical implications as an increased amount of tissue categorised as diseased is displayed on mapping systems. This could alter the ablation strategy of an operator and would likely result in more extensive ablation occurring. The work in this thesis is clearly unable to determine whether this is appropriate to do, as a clinical trial of scar guided ablation based on these tissue voltage levels would be required. However, it raises the question of whether the fundamental values we use in atrial ablation and clinical trials are actually appropriate. Changing them may unveil clinically relevant substrate that affects the strategies used in trials and individual patient procedures and potentially outcomes.

Investigating the differences in voltage mapping between AF types, rhythms and atria with an ultra-high-density mapping system reaffirms widely held knowledge created on lower density systems. Patients with persistent AF do have a lower global voltage across their atria and more surface area of fibrosis than patients with paroxysmal AF; and AF electrograms are generally smaller in amplitude than their SR counterparts. As these findings are previously established, they will not alter clinical practice, but their confirmation on up-to-date technology is reassuring. However, finding that the correlation between paired SR and AF electrogram amplitudes is weak, with poor agreement between their voltage categories does have significant clinical implications. As discussed before, patients with advanced substrate remodelling that could benefit from scar guided ablation strategies may be precluded from this if they cannot maintain SR for the period of time necessary to have a 3D electroanatomical map created. In this scenario, empirical ablation rather than a scar guided strategy may be required using a map developed in AF in an attempt to improve long term arrhythmia free outcomes.

Additionally, new knowledge has been created through investigating fibrosis in the right atrium. The differences seen between AF types and rhythms for the LA were shown to also be present in the RA and there were no differences between atria within patients. This highlights the bi-atrial nature of AF and the potential of the RA to harbour relevant substrate that may require ablation. Whether ablation to the RA occurring beyond that in the LA would confer additional clinical benefit would require a prospective trial.

Optimising ablation lesion creation is important to ensure effective and enduring isolation or destruction of arrhythmogenic tissue. As a more recently developed parameter, our understanding of LI, its interactions with other pre-ablation modifiable factors and its optimal changes with ablation are gradually becoming elucidated. Achieving a larger ΔLI increases the likelihood that transmurality is achieved in the left atrium, and consequently understanding the relative effects of modifiable independent variables that could be manipulated by an operator prior to ablation is important. From this thesis, the starting LI was found to have the largest effect on ΔLI5s than any other independent variable. Consequently, being able to increase the starting LI prior to ablation seems likely to be beneficial. In Chapter 5, it was found that starting LI increased with CF within the clinically used ranges of 0-40g with the largest change from 0-10g. This emphasises the importance of establishing good catheter-tissue coupling before ablation and suggests a CF of at least 10g should be targeted. Interestingly though, establishing contact in AF

was also found to augment the starting LI. In Chapter 6, the relative effects of different parameters on ΔLI5s were established. However, these ablations occurred during SR. Consequently, although the larger starting LI values found in AF would suggest that it would be a preferable rhythm to ablate in, this thesis cannot confirm that would result in a larger LI drop. However, it is certainly hypothesis generating. It also introduces a new argument in answering the question of which rhythm is preferable to ablate in, AF or SR?

In addition to increasing starting LI, CF itself was found to significantly increase ΔLI5s on multivariable analysis. However, when examined by itself, the relationship between CF and ΔLI5s was seen to plateau from approximately 10g. Other factors having an appreciable effect on ΔLI5s were 50W of power (over 30 or 40W), and location of ablation. Interestingly, though bipolar voltage was not seen to have a significant effect on ΔLI5s. Clinically these results would suggest that to optimise an ablation lesion (based on ΔLI5s), one should aim for a CF of at least 10g whilst using a power of 50W. This strategy should not change for different degrees of fibrosis seen on the 3D electroanatomical voltage map, which does not appear to affect the relationship between CF and starting LI, nor the ΔLI5s significantly.

Finally, in Chapter 7, the analysis of the relationships of ventricular endocardial scar with generator impedance allowed for the creation of average values of AI and FTI after which minimal biophysical change was seen during ablation. Due to the thickness of the ventricular myocardium, and the lack of a standardised workflow or endpoint for VT ablation, our knowledge of what composes an effective ablation is much less clear than that of the left atrium. The values established in this thesis for AI, and Δ%GI for different degrees of scar are intended to give electrophysiologists a guide during their procedures, allowing them to reflect if the current ablation lesion is developing well compared to our dataset. One may use this data to judge if there is an adequate Δ%GI by a specific AI they have targeted, or a poor one. Procedurally, this knowledge may give electrophysiologists confidence to ablate for longer periods of time or at higher powers to achieve levels of AI that were achieved in our study. For ablations that do not meet expectations, operators may decide to provide a second 'reinforcement' lesion to the site in question.

8.3 Future Directions

There are numerous extensions to the work in this thesis that could help confirm its findings.

Regarding 3D electroanatomical mapping, the most significant gap in our knowledge is not having histological confirmation of tissue voltages that signify the presence of atrial fibrosis. In this thesis a new value for this cut-off of 1.29mV is suggested. However, confirmation of this (or another) value through a histological study would be ideal. In the absence of this, validating a reliable physiological test as a surrogate to determine fibrosis in the human heart could be developed. For example, validating a pacing threshold value that reliably determines the presence of atrial fibrosis, perhaps in a pre-clinical model would be of great use. That could then be translatable to a repeat clinical study.

The potential of LI as a mapping parameter and the cut-off values (0Ω and 10 / 13Ω), also require further validation. Unfortunately, an automated LI mapping catheter has not been developed that would allow for large amounts of data to be collected in a timely manner that would facilitate this. However, point by point collection (at a defined CF) and histological validation could occur in a pre-clinical model. Another more clinical proposal would be to use LI to map along PVI lines to assess for gaps. Discovering a rise in LI that reliably indicates the presence of a gap would help facilitate further ablation.

Whilst refinement of our definition of atrial fibrosis would be useful in highlighting pathological tissue, what is of greater significance are clinical outcomes. Examining the relationship between recurrence of atrial arrhythmias following AF ablation to surface area of atrial fibrosis shown on 3D electroanatomical mapping defined using a variety of different voltage cut-offs would be of interest. From this information a more precise cut-off of fibrotic surface area indicative of increased likelihood of arrhythmic recurrence could be created. To perform this more accurately, a prospective trial would be preferable using a reliable method of capturing arrhythmic recurrence, perhaps with prolonged ECG monitoring at 6 months, or (more invasively) an implantable loop recorder. If a LI mapping catheter was to be created, a similar study could be performed, investigating the relationships of surface area of map deemed to be fibrotic at a specified LIr cut-off with arrhythmic recurrence.

Redefining atrial scar could have significant effects on scar guided ablation strategies. If values defining fibrosis are raised to 1.29mV, a greater amount of atrial tissue would be subject to isolation. Whether incorporating this tissue into the scar guided strategy is appropriate is unclear. If it was to be found that patients with increased surface area of fibrosis as defined by 1.29mV had increased arrhythmic recurrence, performing a prospective trial of scar guided therapy using 1.29mV as the cut-off over 0.5mV would be of interest.

Determining that LIr rises more with CF in AF than SR is an interesting finding. As starting LI has the largest effect on ΔLI, this raises the question of whether atrial ablation would be better performed in AF over SR. To determine this one could perform a randomised trial comparing PVI performed in SR or AF and examine procedural metrics such as procedure time, ablation time, number of gaps post PVI, ablation parameters such as ΔLI, and clinical metrics such as freedom from arrhythmia and quality of life.

Ablation targets from AF and VT ablation were developed from biophysical information in chapters 6 and 7. For the ΔLI targets for the Stablepoint catheter in AF ablation, these were created using data modelling and extrapolation from the MiFi catheter rather than clinical outcomes. Studies investigating optimal ΔLI values examining PVI and posterior wall isolation gaps have occurred, presenting similar values to those suggested in this thesis. However, long term clinical outcomes have not been studied at this point reflecting the recent availability of the Stablepoint catheter. Establishing favourable clinical outcomes at a prolonged timeframe for patients meeting these ΔLI targets during their ablation procedures would provide further evidence of their validity.

Designing further studies for the AI targets suggested in Chapter 7 is more challenging. VT ablation does not have a well-defined procedural endpoint nor workflow. Ablation strategies can vary from operator to operator in where a set of ablation lesions is placed and how each ablation lesion is delivered. The AI targets developed in Chapter 7 provide a starting point in determining a workflow for VT ablation whereby lesions can be standardised by AI. A study of AI-guided vs non-AI guided ablation with matched ablation strategy (for example, exclusively scar homogenisation) could examine this. As a clear electrophysiological endpoint is not present in VT

ablation (such as PVI in AF ablation), the best (and perhaps more important) parameter to use would be clinical outcomes such as freedom from arrhythmia or ICD therapy.

8.4 Final Remarks

Radiofrequency ablation has been a mainstay of interventional electrophysiological procedures for over two decades, yet it is still being refined to this day. The advent of ever more detailed mapping technology and ablation catheters allows for evolving research which aims to refine our procedural techniques in order to improve our patient's mortality and morbidity.

The aim of this thesis is to contribute new knowledge that plays a part in this procedural refinement. This knowledge has an array of effects including challenging well established threshold values in Chapter 3, reaffirming previous relationships with updated technology in Chapter 4, and providing insights into biophysical relationships before and during ablation in Chapters 5-7.

Despite our advances in ablation technology and procedural workflows over the last twenty years, there are still significant cohorts of patients that have sub-optimal outcomes. Thus, we still need to continuously strive for improvement. I hope this research contributes in a small but meaningful way to the advanced treatment of our patients suffering from cardiac arrhythmias.

Reference List

1. Lip GYH, Beevers DG. ABC of Atrial Fibrillation: HISTORY, EPIDEMIOLOGY, AND IMPORTANCE OF ATRIAL FIBRILLATION. *BMJ* 1995;311(7016):1361.

2. Bedford DE. The ancient art of feeling the pulse. *British heart journal* 1951;13(4):423-37.

3. McMichael J. History of atrial fibrillation 1628-1819 Harvey - de Senac - Laennec. *British heart journal* 1982;48(3):193-7.

4. de Senac J-B. Traits des maladies du coeur. *(Mtquignon l'aine).* 1783.

5. Lewis T. REPORT CXIX. AURICULAR FIBRILLATION: A COMMON CLINICAL CONDITION. *British medical journal* 1909;2(2552):1528-28.

6. Lewis T. Observations upon flutter and fibrillation. Part 9. 'The nature of auricular fibrillation as it occurs in patients.'. *Heart* 1921(8):193.

7. Scherf D, Romano FJ, Terranova R. Experimental studies on auricular flutter and auricular fibrillation. *Am Heart J* 1948;36(2):241-51.

8. Moe GK, Abildskov JA. Atrial fibrillation as a self-sustaining arrhythmia independent of focal discharge. *Am Heart J* 1959;58(1):59-70.

9. Lown B. Electrical reversion of cardiac arrhythmias. *British heart journal* 1967;29(4):469-89.

10. Petersen P, Boysen G, Godtfredsen J, et al. Placebo-controlled, randomised trial of warfarin and aspirin for prevention of thromboembolic complications in chronic atrial fibrillation. The Copenhagen AFASAK study. *Lancet* 1989;1(8631):175-9.

11. Cox JL, Schuessler RB, D'Agostino HJ, Jr., et al. The surgical treatment of atrial fibrillation. III. Development of a definitive surgical procedure. *J Thorac Cardiovasc Surg* 1991;101(4):569-83.

12. Haissaguerre M, Jais P, Shah DC, et al. Spontaneous initiation of atrial fibrillation by ectopic beats originating in the pulmonary veins. *N Engl J Med* 1998;339(10):659-66.

13. Lewis T. SINGLE AND SUCCESSIVE EXTRA-SYSTOLES. *The Lancet* 1909;173(4458):382-85.

14. Alzand BS, Crijns HJ. Diagnostic criteria of broad QRS complex tachycardia: decades of evolution. *Europace* 2011;13(4):465-72.

15. Lewis T. The experimental production of paroxysmal tachycardia and the effects of ligation of the coronary arteries. *Heart* 1909;1(98):10.

16. Robinson G, HERRMAN G. Paroxysmal tachycardia of ventricular origin, and its relation to coronary occlusion. *The American Journal of the Medical Sciences* 1921;162(2).

17. Rosenberg DH. Fusion beats: A report of a clinical instance and an experimental study in the dog. *The Journal of Laboratory and Clinical Medicine* 1940;25(9):919-25.

18. Dressler W, Roesler H. The occurrence in paroxysmal ventricular tachycardia of ventricular complexes transitional in shape to sinoauricular beats: A diagnostic aid. *American heart journal* 1952;44(4):485-93.

19. Scott R. Observations on a case of ventricular tachycardia with retrograde conduction. *Heart* 1922;9(297):1921-22.

20. Beck CS, Mautz FR. The control of the heart beat by the surgeon: with special reference to ventricular fibrillation occurring during operation. *Annals of surgery* 1937;106(4):525.

21. McGovern B, Schoenfeld MH, Ruskin JN, et al. Ventricular tachycardia: historical perspective. *Pacing Clin Electrophysiol* 1986;9(3):449-62.

22. Singh BN. Amiodarone: Historical development and pharmacologic profile. *American heart journal* 1983;106(4, Part 2):788-97.

23. Black JW, Prichard BN. Activation and blockade of beta adrenoceptors in common cardiac disorders. *Br Med Bull* 1973;29(2):163-7.

24. Zoll PM, Linenthal AJ, Gibson W, et al. Termination of ventricular fibrillation in man by externally applied electric countershock. *N Engl J Med* 1956;254(16):727-32.

25. Lown B, Amarasingham R, Neuman J. New method for terminating cardiac arrhythmias. Use of synchronized capacitor discharge. *JAMA* 1962;182:548-55.

26. Lown B, Neuman J, Amarasingham R, et al. Comparison of alternating current with direct electroshock across the closed chest. *Am J Cardiol* 1962;10:223-33.

27. Mirowski M, Reid PR, Mower MM, et al. Termination of malignant ventricular arrhythmias with an implanted automatic defibrillator in human beings. *N Engl J Med* 1980;303(6):322-4.

28. Heiman DF, Helwig J. Suppression of ventricular arrhythmias by transvenous intracardiac pacing. *JAMA* 1966;195(13):1150-53.

29. Sowton E, Leatham A, Carson P. The suppression of arrhythmias by artificial pacemaking. *The Lancet* 1964;284(7369):1098-100.

30. Schwedel JB, Furman S, Escher DJ. Use of an intracardiac pacemaker in the treatment of Stokes-Adams seizures. *Progress in Cardiovascular Diseases* 1960;3(2):170-77.

31. Couch Jr O. Cardiac aneurysm with ventricular tachycardia and subsequent excision of aneurysm: case report. *Circulation* 1959;20(2):251-53.

32. Mason JW, Stinson EB, Winkle RA, et al. Relative efficacy of blind left ventricular aneurysm resection for the treatment of recurrent ventricular tachycardia. *Am J Cardiol* 1982;49(1):241-8.

33. Miller JM, Tyson GS, Hargrove WC, 3rd, et al. Effect of subendocardial resection on sinus rhythm endocardial electrogram abnormalities. *Circulation* 1995;91(9):2385-91.

34. Cronin EM, Bogun FM, Maury P, et al. 2019 HRS/EHRA/APHRS/LAHRS expert consensus statement on catheter ablation of ventricular arrhythmias. *Heart Rhythm* 2020;17(1):e2-e154.

35. Hindricks G, Potpara T, Dagres N, et al. 2020 ESC Guidelines for the diagnosis and management of atrial fibrillation developed in collaboration with the European Association of Cardio-Thoracic Surgery (EACTS). *Eur Heart J* 2020.

36. Calkins H, Brugada J, Packer DL, et al. HRS/EHRA/ECAS expert consensus statement on catheter and surgical ablation of atrial fibrillation: recommendations for personnel, policy, procedures and follow-up. A report of the Heart Rhythm Society (HRS) Task Force on

Catheter and Surgical Ablation of Atrial Fibrillation developed in partnership with the European Heart Rhythm Association (EHRA) and the European Cardiac Arrhythmia Society (ECAS); in collaboration with the American College of Cardiology (ACC), American Heart Association (AHA), and the Society of Thoracic Surgeons (STS). Endorsed and approved by the governing bodies of the American College of Cardiology, the American Heart Association, the European Cardiac Arrhythmia Society, the European Heart Rhythm Association, the Society of Thoracic Surgeons, and the Heart Rhythm Society. *Europace* 2007;9(6):335-79.

37. von Eisenhart Rothe A, Hutt F, Baumert J, et al. Depressed mood amplifies heart-related symptoms in persistent and paroxysmal atrial fibrillation patients: a longitudinal analysis--data from the German Competence Network on Atrial Fibrillation. *Europace* 2015;17(9):1354-62.

38. Peinado R, Arribas F, Ormaetxe JM, et al. Variation in quality of life with type of atrial fibrillation. *Rev Esp Cardiol* 2010;63(12):1402-9.

39. Steg PG, Alam S, Chiang CE, et al. Symptoms, functional status and quality of life in patients with controlled and uncontrolled atrial fibrillation: data from the RealiseAF cross-sectional international registry. *Heart* 2012;98(3):195-201.

40. Dorian P, Jung W, Newman D, et al. The impairment of health-related quality of life in patients with intermittent atrial fibrillation: implications for the assessment of investigational therapy. *J Am Coll Cardiol* 2000;36(4):1303-9.

41. Benjamin EJ, Wolf PA, D'Agostino RB, et al. Impact of atrial fibrillation on the risk of death: the Framingham Heart Study. *Circulation* 1998;98(10):946-52.

42. Andersson T, Magnuson A, Bryngelsson IL, et al. All-cause mortality in 272,186 patients hospitalized with incident atrial fibrillation 1995-2008: a Swedish nationwide long-term case-control study. *Eur Heart J* 2013;34(14):1061-7.

43. Kannel WB, Wolf PA, Benjamin EJ, et al. Prevalence, incidence, prognosis, and predisposing conditions for atrial fibrillation: population-based estimates. *Am J Cardiol* 1998;82(8A):2N-9N.

44. Stewart S, Hart CL, Hole DJ, et al. A population-based study of the long-term risks associated with atrial fibrillation: 20-year follow-up of the Renfrew/Paisley study. *Am J Med* 2002;113(5):359-64.

45. Krahn AD, Manfreda J, Tate RB, et al. The natural history of atrial fibrillation: incidence, risk factors, and prognosis in the Manitoba Follow-Up Study. *Am J Med* 1995;98(5):476-84.

46. Wolf PA, Abbott RD, Kannel WB. Atrial fibrillation as an independent risk factor for stroke: the Framingham Study. *Stroke* 1991;22(8):983-8.

47. Saglietto A, Matta M, Gaita F, et al. Stroke-independent contribution of atrial fibrillation to dementia: a meta-analysis. *Open Heart* 2019;6(1):e000984.

48. Gaita F, Corsinovi L, Anselmino M, et al. Prevalence of silent cerebral ischemia in paroxysmal and persistent atrial fibrillation and correlation with cognitive function. *J Am Coll Cardiol* 2013;62(21):1990-97.

49. Rattanawong P, Upala S, Riangwiwat T, et al. Atrial fibrillation is associated with sudden cardiac death: a systematic review and meta-analysis. *J Interv Card Electrophysiol* 2018;51(2):91-104.

50. Savelieva I, John Camm A. Atrial fibrillation and heart failure: natural history and pharmacological treatment. *Europace* 2004;5 Suppl 1:S5-19.

51. Dries DL, Exner DV, Gersh BJ, et al. Atrial fibrillation is associated with an increased risk for mortality and heart failure progression in patients with asymptomatic and symptomatic left ventricular systolic dysfunction: a retrospective analysis of the SOLVD trials. Studies of Left Ventricular Dysfunction. *J Am Coll Cardiol* 1998;32(3):695-703.

52. Rivero-Ayerza M, Scholte Op Reimer W, Lenzen M, et al. New-onset atrial fibrillation is an independent predictor of in-hospital mortality in hospitalized heart failure patients: results of the EuroHeart Failure Survey. *Eur Heart J* 2008;29(13):1618-24.

53. Wang TJ, Larson MG, Levy D, et al. Temporal relations of atrial fibrillation and congestive heart failure and their joint influence on mortality: the Framingham Heart Study. *Circulation* 2003;107(23):2920-5.

54. Public Health England. *Atrial Fibrillation Prevelance Estimates*. https://www.gov.uk/government/publications/atrial-fibrillation-prevalence-estimates-for-local-populations (accessed 11/01/2021).

55. Zoni-Berisso M, Lercari F, Carazza T, et al. Epidemiology of atrial fibrillation: European perspective. *Clin Epidemiol* 2014;6:213-20.

56. Stewart S, Murphy NF, Walker A, et al. Cost of an emerging epidemic: an economic analysis of atrial fibrillation in the UK. *Heart* 2004;90(3):286-92.

57. Ringborg A, Nieuwlaat R, Lindgren P, et al. Costs of atrial fibrillation in five European countries: results from the Euro Heart Survey on atrial fibrillation. *Europace* 2008;10(4):403-11.

58. Patel AB, Vladislav; King, Derek; Quayyum, Zahidul; Wittenberg, Raphael; Knapp, Martin. *Current, future and avoidable costs of stroke in the UK*. https://www.stroke.org.uk/sites/default/files/costs_of_stroke_in_the_uk_report_-executive_summary_part_2.pdf.

59. Morady F, Shen EN, Bhandari A, et al. Clinical symptoms in patients with sustained ventricular tachycardia. *West J Med* 1985;142(3):341-4.

60. Koplan BA, Stevenson WG. Ventricular tachycardia and sudden cardiac death. *Mayo Clin Proc* 2009;84(3):289-97.

61. Gula LJ, Doucette S, Leong-Sit P, et al. Quality of life with ablation or medical therapy for ventricular arrhythmias: A substudy of VANISH. *J Cardiovasc Electrophysiol* 2018;29(3):421-34.

62. Kuck KH, Tilz RR, Deneke T, et al. Impact of Substrate Modification by Catheter Ablation on Implantable Cardioverter-Defibrillator Interventions in Patients With Unstable Ventricular Arrhythmias and Coronary Artery Disease: Results From the Multicenter Randomized Controlled SMS (Substrate Modification Study). *Circ Arrhythm Electrophysiol* 2017;10(3).

63. Janssen B, Szende A. Population Norms for the EQ-5D. In: Szende A, Janssen B, Cabases J (eds.) *Self-Reported Population Health: An International Perspective based on EQ-5D*. Dordrecht (NL); 2014 p19-30.

64. Tomzik J, Koltermann KC, Zabel M, et al. Quality of Life in Patients with an Implantable Cardioverter Defibrillator: A Systematic Review. *Frontiers in Cardiovascular Medicine* 2015;2.

65. Chugh SS, Jui J, Gunson K, et al. Current burden of sudden cardiac death: multiple source surveillance versus retrospective death certificate-based review in a large U.S. community. *J Am Coll Cardiol* 2004;44(6):1268-75.

66. de Vreede-Swagemakers JJ, Gorgels AP, Dubois-Arbouw WI, et al. Out-of-hospital cardiac arrest in the 1990's: a population-based study in the Maastricht area on incidence, characteristics and survival. *J Am Coll Cardiol* 1997;30(6):1500-5.

67. Vaillancourt C, Stiell IG, Canadian Cardiovascular Outcomes Research T. Cardiac arrest care and emergency medical services in Canada. *Can J Cardiol* 2004;20(11):1081-90.

68. Eckart RE, Shry EA, Burke AP, et al. Sudden death in young adults: an autopsy-based series of a population undergoing active surveillance. *J Am Coll Cardiol* 2011;58(12):1254-61.

69. Asif IM, Harmon KG. Incidence and Etiology of Sudden Cardiac Death: New Updates for Athletic Departments. *Sports Health* 2017;9(3):268-79.

70. Risgaard B. Sudden cardiac death: a nationwide cohort study among the young. *Dan Med J* 2016;63(12).

71. Anastasakis A, Papatheodorou E, Ritsatos K, et al. Sudden unexplained death in the young: epidemiology, aetiology and value of the clinically guided genetic screening. *Europace* 2018;20(3):472-80.

72. Solomon SD, Zelenkofske S, McMurray JJ, et al. Sudden death in patients with myocardial infarction and left ventricular dysfunction, heart failure, or both. *N Engl J Med* 2005;352(25):2581-8.

73. Camm J, Klein H, Nisam S. The cost of implantable defibrillators: perceptions and reality. *Eur Heart J* 2007;28(4):392-7.

74. Garcia-Perez L, Pinilla-Dominguez P, Garcia-Quintana A, et al. Economic evaluations of implantable cardioverter defibrillators: a systematic review. *Eur J Health Econ* 2015;16(8):879-93.

75. Caro JJ, Ward A, Deniz HB, et al. Cost-benefit analysis of preventing sudden cardiac deaths with an implantable cardioverter defibrillator versus amiodarone. *Value Health* 2007;10(1):13-22.

76. Coyle K, Coyle D, Nault I, et al. Cost Effectiveness of Ventricular Tachycardia Ablation Versus Escalation of Antiarrhythmic Drug Therapy: The VANISH Trial. *JACC Clin Electrophysiol* 2018;4(5):660-68.

77. Giusca S, Jurcut R, Ginghina C, et al. The right ventricle: anatomy, physiology and functional assessment. *Acta Cardiol* 2010;65(1):67-77.

78. Ho SY. Anatomy and myoarchitecture of the left ventricular wall in normal and in disease. *Eur J Echocardiogr* 2009;10(8):iii3-7.

79. Monfredi O, Dobrzynski H, Mondal T, et al. The anatomy and physiology of the sinoatrial node--a contemporary review. *Pacing Clin Electrophysiol* 2010;33(11):1392-406.

80. Ho SY, Anderson RH, Sanchez-Quintana D. Gross structure of the atriums: more than an anatomic curiosity? *Pacing Clin Electrophysiol* 2002;25(3):342-50.

81. Yu W-C, Chen S-A, Lee S-H, et al. Tachycardia-Induced Change of Atrial Refractory Period in Humans. *Circulation* 1998;97(23):2331-37.

82. Guss S, Kastor J, Josephson M, et al. Human ventricular refractoriness. Effects of cycle length, pacing site and atropine. *Circulation* 1976;53(3):450-55.

83. Antzelevitch C, Antzelevitch C, Burashnikov A. Overview of Basic Mechanisms of Cardiac Arrhythmia. *Cardiac electrophysiology clinics* 2011;3(1):23-45.

84. January CT, Chau V, Makielski JC. Triggered activity in the heart: cellular mechanisms of early after-depolarizations. *Eur Heart J* 1991;12 Suppl F:4-9.

85. Cranefield PF. Action potentials, afterpotentials, and arrhythmias. *Circ Res* 1977;41(4):415-23.

86. Tse G. Mechanisms of cardiac arrhythmias. *Journal of Arrhythmia* 2016;32(2):75-81.

87. January CT, Riddle JM. Early afterdepolarizations: mechanism of induction and block. A role for L-type Ca2+ current. *Circ Res* 1989;64(5):977-90.

88. Szabo B, Sweidan R, Rajagopalan CV, et al. Role of Na+:Ca2+ exchange current in Cs(+)-induced early afterdepolarizations in Purkinje fibers. *J Cardiovasc Electrophysiol* 1994;5(11):933-44.

89. Anumonwo JM, Pandit SV. Ionic mechanisms of arrhythmogenesis. *Trends Cardiovasc Med* 2015;25(6):487-96.

90. Cerrone M, Noujaim SF, Tolkacheva EG, et al. Arrhythmogenic mechanisms in a mouse model of catecholaminergic polymorphic ventricular tachycardia. *Circ Res* 2007;101(10):1039-48.

91. Ferrier GR, Saunders JH, Mendez C. A cellular mechanism for the generation of ventricular arrhythmias by acetylstrophanthidin. *Circ Res* 1973;32(5):600-9.

92. Lehnart SE, Wehrens XH, Laitinen PiJ, et al. Sudden death in familial polymorphic ventricular tachycardia associated with calcium release channel (ryanodine receptor) leak. *Circulation* 2004;109(25):3208-14.

93. Aronson RS. Afterpotentials and triggered activity in hypertrophied myocardium from rats with renal hypertension. *Circ Res* 1981;48(5):720-7.

94. Vermeulen JT, McGuire MA, Opthof T, et al. Triggered activity and automaticity in ventricular trabeculae of failing human and rabbit hearts. *Cardiovasc Res* 1994;28(10):1547-54.

95. Lazzara R, el-Sherif N, Scherlag BJ. Electrophysiological properties of canine Purkinje cells in one-day-old myocardial infarction. *Circ Res* 1973;33(6):722-34.

96. Gaztanaga L, Marchlinski FE, Betensky BP. Mechanisms of cardiac arrhythmias. *Rev Esp Cardiol (Engl Ed)* 2012;65(2):174-85.

97. Waks JW, Josephson ME. Mechanisms of Atrial Fibrillation - Reentry, Rotors and Reality. *Arrhythm Electrophysiol Rev* 2014;3(2):90-100.

98. Allessie MA, Bonke FI, Schopman FJ. Circus movement in rabbit atrial muscle as a mechanism of tachycardia. III. The "leading circle" concept: a new model of circus movement in cardiac tissue without the involvement of an anatomical obstacle. *Circ Res* 1977;41(1):9-18.

99. Allessie MA, Bonke FI, Schopman FJ. Circus movement in rabbit atrial muscle as a mechanism of trachycardia. *Circ Res* 1973;33(1):54-62.

100. Wiener N, Rosenblueth A. The mathematical formulation of the problem of conduction of impulses in a network of connected excitable elements, specifically in cardiac muscle. *Arch Inst Cardiol Mex* 1946;16(3):205-65.

101. Calkins H, Hindricks G, Cappato R, et al. 2017 HRS/EHRA/ECAS/APHRS/SOLAECE expert consensus statement on catheter and surgical ablation of atrial fibrillation: Executive summary. *Heart Rhythm* 2017;14(10):e445-e94.

102. Winfree AT. Varieties of spiral wave behavior: An experimentalist's approach to the theory of excitable media. *Chaos* 1991;1(3):303-34.

103. Pertsov AM, Davidenko JM, Salomonsz R, et al. Spiral waves of excitation underlie reentrant activity in isolated cardiac muscle. *Circ Res* 1993;72(3):631-50.

104. Narayan SM, Krummen DE, Clopton P, et al. Direct or coincidental elimination of stable rotors or focal sources may explain successful atrial fibrillation ablation: on-treatment analysis of the CONFIRM trial (Conventional ablation for AF with or without focal impulse and rotor modulation). *J Am Coll Cardiol* 2013;62(2):138-47.

105. Sommer P, Kircher S, Rolf S, et al. Successful Repeat Catheter Ablation of Recurrent Longstanding Persistent Atrial Fibrillation With Rotor Elimination as the Procedural Endpoint: A Case Series. *J Cardiovasc Electrophysiol* 2016;27(3):274-80.

106. Antzelevitch C, Jalife J, Moe GK. Characteristics of reflection as a mechanism of reentrant arrhythmias and its relationship to parasystole. *Circulation* 1980;61(1):182-91.

107. Di Diego JM, Antzelevitch C. Pinacidil-induced electrical heterogeneity and extrasystolic activity in canine ventricular tissues. Does activation of ATP-regulated potassium current promote phase 2 reentry? *Circulation* 1993;88(3):1177-89.

108. Lukas A, Antzelevitch C. Phase 2 reentry as a mechanism of initiation of circus movement reentry in canine epicardium exposed to simulated ischemia. *Cardiovasc Res* 1996;32(3):593-603.

109. Antzelevitch C. Brugada syndrome. *Pacing Clin Electrophysiol* 2006;29(10):1130-59.

110. Kalsto SM, Siland JE, Rienstra M, et al. Atrial Fibrillation Genetics Update: Toward Clinical Implementation. *Front Cardiovasc Med* 2019;6:127.

111. Chen YH, Xu SJ, Bendahhou S, et al. KCNQ1 gain-of-function mutation in familial atrial fibrillation. *Science* 2003;299(5604):251-4.

112. Landstrom AP, Dobrev D, Wehrens XH. Calcium signaling and cardiac arrhythmias. *Circulation research* 2017;120(12):1969-93.

113. Voigt N, Li N, Wang Q, et al. Enhanced sarcoplasmic reticulum Ca2+ leak and increased Na+-Ca2+ exchanger function underlie delayed afterdepolarizations in patients with chronic atrial fibrillation. *Circulation* 2012;125(17):2059-70.

114. Neef S, Dybkova N, Sossalla S, et al. CaMKII-dependent diastolic SR Ca2+ leak and elevated diastolic Ca2+ levels in right atrial myocardium of patients with atrial fibrillation. *Circ Res* 2010;106(6):1134-44.

115. Kazemian P, Gollob MH, Pantano A, et al. A novel mutation in the RYR2 gene leading to catecholaminergic polymorphic ventricular tachycardia and paroxysmal atrial fibrillation: dose-dependent arrhythmia-event suppression by beta-blocker therapy. *Can J Cardiol* 2011;27(6):870 e7-10.

116. Yue L, Feng J, Gaspo R, et al. Ionic remodeling underlying action potential changes in a canine model of atrial fibrillation. *Circ Res* 1997;81(4):512-25.

117. Christ T, Boknik P, Wohrl S, et al. L-type Ca2+ current downregulation in chronic human atrial fibrillation is associated with increased activity of protein phosphatases. *Circulation* 2004;110(17):2651-7.

118. Luo X, Pan Z, Shan H, et al. MicroRNA-26 governs profibrillatory inward-rectifier potassium current changes in atrial fibrillation. *The Journal of clinical investigation* 2013;123(5):1939-51.

119. Girmatsion Z, Biliczki P, Bonauer A, et al. Changes in microRNA-1 expression and IK1 up-regulation in human atrial fibrillation. *Heart Rhythm* 2009;6(12):1802-09.

120. Girmatsion Z, Biliczki P, Bonauer A, et al. Changes in microRNA-1 expression and IK1 up-regulation in human atrial fibrillation. *Heart Rhythm* 2009;6(12):1802-9.

121. Makary S, Voigt N, Maguy A, et al. Differential protein kinase C isoform regulation and increased constitutive activity of acetylcholine-regulated potassium channels in atrial remodeling. *Circ Res* 2011;109(9):1031-43.

122. Cha TJ, Ehrlich JR, Chartier D, et al. Kir3-based inward rectifier potassium current: potential role in atrial tachycardia remodeling effects on atrial repolarization and arrhythmias. *Circulation* 2006;113(14):1730-7.

123. Qi X-Y, Diness JG, Brundel BJ, et al. Role of small-conductance calcium-activated potassium channels in atrial electrophysiology and fibrillation in the dog. *Circulation* 2014;129(4):430-40.

124. Kato T, Iwasaki YK, Nattel S. Connexins and atrial fibrillation: filling in the gaps. *Circulation* 2012;125(2):203-6.

125. Polontchouk L, Haefliger JA, Ebelt B, et al. Effects of chronic atrial fibrillation on gap junction distribution in human and rat atria. *J Am Coll Cardiol* 2001;38(3):883-91.

126. Kostin S, Klein G, Szalay Z, et al. Structural correlate of atrial fibrillation in human patients. *Cardiovasc Res* 2002;54(2):361-79.

127. Olshansky B, Heller EN, Mitchell LB, et al. Are transthoracic echocardiographic parameters associated with atrial fibrillation recurrence or stroke? Results from the Atrial Fibrillation Follow-Up Investigation of Rhythm Management (AFFIRM) study. *J Am Coll Cardiol* 2005;45(12):2026-33.

128. Nattel S, Harada M. Atrial remodeling and atrial fibrillation: recent advances and translational perspectives. *J Am Coll Cardiol* 2014;63(22):2335-45.

129. Ramires FJ, Sun Y, Weber KT. Myocardial fibrosis associated with aldosterone or angiotensin II administration: attenuation by calcium channel blockade. *J Mol Cell Cardiol* 1998;30(3):475-83.

130. Lau DH, Mackenzie L, Kelly DJ, et al. Hypertension and atrial fibrillation: evidence of progressive atrial remodeling with electrostructural correlate in a conscious chronically instrumented ovine model. *Heart Rhythm* 2010;7(9):1282-90.

131. Abed HS, Samuel CS, Lau DH, et al. Obesity results in progressive atrial structural and electrical remodeling: implications for atrial fibrillation. *Heart Rhythm* 2013;10(1):90-100.

132. Iwasaki YK, Shi Y, Benito B, et al. Determinants of atrial fibrillation in an animal model of obesity and acute obstructive sleep apnea. *Heart Rhythm* 2012;9(9):1409-16 e1.

133. Iwasaki YK, Kato T, Xiong F, et al. Atrial fibrillation promotion with long-term repetitive obstructive sleep apnea in a rat model. *J Am Coll Cardiol* 2014;64(19):2013-23.

134. Kato T, Yamashita T, Sekiguchi A, et al. AGEs-RAGE system mediates atrial structural remodeling in the diabetic rat. *J Cardiovasc Electrophysiol* 2008;19(4):415-20.

135. Li D, Fareh S, Leung TK, et al. Promotion of atrial fibrillation by heart failure in dogs: atrial remodeling of a different sort. *Circulation* 1999;100(1):87-95.

136. Andrade J, Khairy P, Dobrev D, et al. The clinical profile and pathophysiology of atrial fibrillation: relationships among clinical features, epidemiology, and mechanisms. *Circ Res* 2014;114(9):1453-68.

137. Mahnkopf C, Badger TJ, Burgon NS, et al. Evaluation of the left atrial substrate in patients with lone atrial fibrillation using delayed-enhanced MRI: implications for disease progression and response to catheter ablation. *Heart Rhythm* 2010;7(10):1475-81.

138. Platonov PG, Mitrofanova LB, Orshanskaya V, et al. Structural abnormalities in atrial walls are associated with presence and persistency of atrial fibrillation but not with age. *J Am Coll Cardiol* 2011;58(21):2225-32.

139. John B, Stiles MK, Kuklik P, et al. Reverse remodeling of the atria after treatment of chronic stretch in humans: implications for the atrial fibrillation substrate. *J Am Coll Cardiol* 2010;55(12):1217-26.

140. Teh AW, Kistler PM, Lee G, et al. Long-term effects of catheter ablation for lone atrial fibrillation: progressive atrial electroanatomic substrate remodeling despite successful ablation. *Heart Rhythm* 2012;9(4):473-80.

141. Kottkamp H. Human atrial fibrillation substrate: towards a specific fibrotic atrial cardiomyopathy. *Eur Heart J* 2013;34(35):2731-8.

142. Kottkamp H. Fibrotic atrial cardiomyopathy: a specific disease/syndrome supplying substrates for atrial fibrillation, atrial tachycardia, sinus node disease, AV node disease, and thromboembolic complications. *J Cardiovasc Electrophysiol* 2012;23(7):797-9.

143. Akoum N, McGann C, Vergara G, et al. Atrial fibrosis quantified using late gadolinium enhancement MRI is associated with sinus node dysfunction requiring pacemaker implant. *J Cardiovasc Electrophysiol* 2012;23(1):44-50.

144. Chen PS, Chen LS, Fishbein MC, et al. Role of the autonomic nervous system in atrial fibrillation: pathophysiology and therapy. *Circ Res* 2014;114(9):1500-15.

145. Ng J, Villuendas R, Cokic I, et al. Autonomic remodeling in the left atrium and pulmonary veins in heart failure: creation of a dynamic substrate for atrial fibrillation. *Circ Arrhythm Electrophysiol* 2011;4(3):388-96.

146. Chang CM, Wu TJ, Zhou S, et al. Nerve sprouting and sympathetic hyperinnervation in a canine model of atrial fibrillation produced by prolonged right atrial pacing. *Circulation* 2001;103(1):22-5.

147. Jayachandran JV, Sih HJ, Winkle W, et al. Atrial fibrillation produced by prolonged rapid atrial pacing is associated with heterogeneous changes in atrial sympathetic innervation. *Circulation* 2000;101(10):1185-91.

148. Nguyen BL, Fishbein MC, Chen LS, et al. Histopathological substrate for chronic atrial fibrillation in humans. *Heart Rhythm* 2009;6(4):454-60.

149. Gould PA, Yii M, McLean C, et al. Evidence for increased atrial sympathetic innervation in persistent human atrial fibrillation. *Pacing Clin Electrophysiol* 2006;29(8):821-9.

150. Sharifov OF, Fedorov VV, Beloshapko GG, et al. Roles of adrenergic and cholinergic stimulation in spontaneous atrial fibrillation in dogs. *J Am Coll Cardiol* 2004;43(3):483-90.

151. Tan AY, Zhou S, Ogawa M, et al. Neural mechanisms of paroxysmal atrial fibrillation and paroxysmal atrial tachycardia in ambulatory canines. *Circulation* 2008;118(9):916-25.

152. Po SS, Nakagawa H, Jackman WM. Localization of left atrial ganglionated plexi in patients with atrial fibrillation. *J Cardiovasc Electrophysiol* 2009;20(10):1186-9.

153. Po SS, Scherlag BJ, Yamanashi WS, et al. Experimental model for paroxysmal atrial fibrillation arising at the pulmonary vein-atrial junctions. *Heart Rhythm* 2006;3(2):201-8.

154. Choi EK, Zhao Y, Everett THt, et al. Ganglionated plexi as neuromodulation targets for atrial fibrillation. *J Cardiovasc Electrophysiol* 2017;28(12):1485-91.

155. Pappone C, Rosanio S, Oreto G, et al. Circumferential radiofrequency ablation of pulmonary vein ostia: A new anatomic approach for curing atrial fibrillation. *Circulation* 2000;102(21):2619-28.

156. Santangeli P, Zado ES, Hutchinson MD, et al. Prevalence and distribution of focal triggers in persistent and long-standing persistent atrial fibrillation. *Heart Rhythm* 2016;13(2):374-82.

157. Garrey WE. The nature of fibrillary contraction of the heart.—Its relation to tissue mass and form. *American Journal of Physiology-Legacy Content* 1914;33(3):397-414.

158. Moe GK, Rheinboldt WC, Abildskov JA. A Computer Model of Atrial Fibrillation. *Am Heart J* 1964;67:200-20.

159. Cox JL, Canavan TE, Schuessler RB, et al. The surgical treatment of atrial fibrillation. II. Intraoperative electrophysiologic mapping and description of the electrophysiologic basis of atrial flutter and atrial fibrillation. *J Thorac Cardiovasc Surg* 1991;101(3):406-26.

160. Konings KT, Kirchhof CJ, Smeets JR, et al. High-density mapping of electrically induced atrial fibrillation in humans. *Circulation* 1994;89(4):1665-80.

161. Winfree A. Vortex action potentials in normal ventricular muscle. *Annals of the New York Academy of Sciences* 1990;591:190.

162. Narayan SM, Krummen DE, Rappel WJ. Clinical mapping approach to diagnose electrical rotors and focal impulse sources for human atrial fibrillation. *J Cardiovasc Electrophysiol* 2012;23(5):447-54.

163. Haissaguerre M, Hocini M, Denis A, et al. Driver domains in persistent atrial fibrillation. *Circulation* 2014;130(7):530-8.

164. Jalife J, Berenfeld O, Mansour M. Mother rotors and fibrillatory conduction: a mechanism of atrial fibrillation. *Cardiovasc Res* 2002;54(2):204-16.

165. Pathik B, Lee G, Sacher F, et al. Epicardial-endocardial breakthrough during stable atrial macroreentry: Evidence from ultra-high-resolution 3-dimensional mapping. *Heart Rhythm* 2017;14(8):1200-07.

166. de Groot N, van der Does L, Yaksh A, et al. Direct Proof of Endo-Epicardial Asynchrony of the Atrial Wall During Atrial Fibrillation in Humans. *Circ Arrhythm Electrophysiol* 2016;9(5).

167. de Groot NM, Houben RP, Smeets JL, et al. Electropathological substrate of longstanding persistent atrial fibrillation in patients with structural heart disease: epicardial breakthrough. *Circulation* 2010;122(17):1674-82.

168. Lee S, Sahadevan J, Khrestian CM, et al. Simultaneous Biatrial High-Density (510-512 Electrodes) Epicardial Mapping of Persistent and Long-Standing Persistent Atrial Fibrillation in Patients: New Insights Into the Mechanism of Its Maintenance. *Circulation* 2015;132(22):2108-17.

169. Kapplinger JD, Tester DJ, Alders M, et al. An international compendium of mutations in the SCN5A-encoded cardiac sodium channel in patients referred for Brugada syndrome genetic testing. *Heart Rhythm* 2010;7(1):33-46.

170. Pilichou K, Thiene G, Bauce B, et al. Arrhythmogenic cardiomyopathy. *Orphanet J Rare Dis* 2016;11:33.

171. Wieneke H, Svendsen JH, Lande J, et al. Polymorphisms in the GNAS Gene as Predictors of Ventricular Tachyarrhythmias and Sudden Cardiac Death: Results From the DISCOVERY Trial and Oregon Sudden Unexpected Death Study. *J Am Heart Assoc* 2016;5(12).

172. Landstrom AP, Dobrev D, Wehrens XHT. Calcium Signaling and Cardiac Arrhythmias. *Circ Res* 2017;120(12):1969-93.

173. Napolitano C, Antzelevitch C. Phenotypical manifestations of mutations in the genes encoding subunits of the cardiac voltage-dependent L-type calcium channel. *Circ Res* 2011;108(5):607-18.

174. Pogwizd SM, Qi M, Yuan W, et al. Upregulation of Na(+)/Ca(2+) exchanger expression and function in an arrhythmogenic rabbit model of heart failure. *Circ Res* 1999;85(11):1009-19.

175. Pogwizd SM, Schlotthauer K, Li L, et al. Arrhythmogenesis and contractile dysfunction in heart failure: Roles of sodium-calcium exchange, inward rectifier potassium current, and residual beta-adrenergic responsiveness. *Circ Res* 2001;88(11):1159-67.

176. Bers DM, Pogwizd SM, Schlotthauer K. Upregulated Na/Ca exchange is involved in both contractile dysfunction and arrhythmogenesis in heart failure. *Basic Res Cardiol* 2002;97 Suppl 1:I36-42.

177. Nattel S, Maguy A, Le Bouter S, et al. Arrhythmogenic ion-channel remodeling in the heart: heart failure, myocardial infarction, and atrial fibrillation. *Physiol Rev* 2007;87(2):425-56.

178. Gupta RC, Mishra S, Rastogi S, et al. Cardiac SR-coupled PP1 activity and expression are increased and inhibitor 1 protein expression is decreased in failing hearts. *Am J Physiol Heart Circ Physiol* 2003;285(6):H2373-81.

179. Zhang T, Maier LS, Dalton ND, et al. The deltaC isoform of CaMKII is activated in cardiac hypertrophy and induces dilated cardiomyopathy and heart failure. *Circ Res* 2003;92(8):912-9.

180. Hayashi M, Shimizu W, Albert CM. The spectrum of epidemiology underlying sudden cardiac death. *Circ Res* 2015;116(12):1887-906.

181. Carmeliet E. Cardiac ionic currents and acute ischemia: from channels to arrhythmias. *Physiol Rev* 1999;79(3):917-1017.

182. Rodriguez B, Trayanova N, Noble D. Modeling cardiac ischemia. *Ann N Y Acad Sci* 2006;1080:395-414.

183. Mendonca Costa C, Plank G, Rinaldi CA, et al. Modeling the Electrophysiological Properties of the Infarct Border Zone. *Front Physiol* 2018;9:356.

184. Antzelevitch C, Nesterenko V, Shryock JC, et al. The role of late I Na in development of cardiac arrhythmias. *Handb Exp Pharmacol* 2014;221:137-68.

185. Watson CL, Gold MR. Effect of intracellular and extracellular acidosis on sodium current in ventricular myocytes. *Am J Physiol* 1995;268(4 Pt 2):H1749-56.

186. Verkerk AO, Veldkamp MW, van Ginneken AC, et al. Biphasic response of action potential duration to metabolic inhibition in rabbit and human ventricular myocytes: role of transient outward current and ATP-regulated potassium current. *J Mol Cell Cardiol* 1996;28(12):2443-56.

187. Liang JJ, Prasad A, Cha YM. Temporal evolution and implications of ventricular arrhythmias associated with acute myocardial infarction. *Cardiol Rev* 2013;21(6):289-94.

188. Lee YS, Chang PC, Hsueh CH, et al. Apamin-sensitive calcium-activated potassium currents in rabbit ventricles with chronic myocardial infarction. *J Cardiovasc Electrophysiol* 2013;24(10):1144-53.

189. Dun W, Baba S, Yagi T, et al. Dynamic remodeling of K+ and Ca2+ currents in cells that survived in the epicardial border zone of canine healed infarcted heart. *Am J Physiol Heart Circ Physiol* 2004;287(3):H1046-54.

190. Litwin SE, Bridge JH. Enhanced Na(+)-Ca2+ exchange in the infarcted heart. Implications for excitation-contraction coupling. *Circ Res* 1997;81(6):1083-93.

191. Pinto JM, Yuan F, Wasserlauf BJ, et al. Regional gradation of L-type calcium currents in the feline heart with a healed myocardial infarct. *J Cardiovasc Electrophysiol* 1997;8(5):548-60.

192. Ursell PC, Gardner PI, Albala A, et al. Structural and electrophysiological changes in the epicardial border zone of canine myocardial infarcts during infarct healing. *Circ Res* 1985;56(3):436-51.

193. Sah R, Ramirez RJ, Oudit GY, et al. Regulation of cardiac excitation-contraction coupling by action potential repolarization: role of the transient outward potassium current (I(to)). *J Physiol* 2003;546(Pt 1):5-18.

194. Cutler MJ, Jeyaraj D, Rosenbaum DS. Cardiac electrical remodeling in health and disease. *Trends Pharmacol Sci* 2011;32(3):174-80.

195. Valdivia CR, Chu WW, Pu J, et al. Increased late sodium current in myocytes from a canine heart failure model and from failing human heart. *J Mol Cell Cardiol* 2005;38(3):475-83.

196. Chen X, Piacentino V, 3rd, Furukawa S, et al. L-type Ca2+ channel density and regulation are altered in failing human ventricular myocytes and recover after support with mechanical assist devices. *Circ Res* 2002;91(6):517-24.

197. Schroder F, Handrock R, Beuckelmann DJ, et al. Increased availability and open probability of single L-type calcium channels from failing compared with nonfailing human ventricle. *Circulation* 1998;98(10):969-76.

198. Kääb S, Nuss HB, Chiamvimonvat N, et al. Ionic Mechanism of Action Potential Prolongation in Ventricular Myocytes From Dogs With Pacing-Induced Heart Failure. *Circulation research* 1996;78(2):262-73.

199. Akar FG, Rosenbaum DS. Transmural electrophysiological heterogeneities underlying arrhythmogenesis in heart failure. *Circ Res* 2003;93(7):638-45.

200. Wiegerinck RF, Verkerk AO, Belterman CN, et al. Larger cell size in rabbits with heart failure increases myocardial conduction velocity and QRS duration. *Circulation* 2006;113(6):806-13.

201. Poelzing S, Rosenbaum DS. Altered connexin43 expression produces arrhythmia substrate in heart failure. *Am J Physiol Heart Circ Physiol* 2004;287(4):H1762-70.

202. Peters NS. Myocardial gap junction organization in ischemia and infarction. *Microsc Res Tech* 1995;31(5):375-86.

203. Ai X, Pogwizd SM. Connexin 43 downregulation and dephosphorylation in nonischemic heart failure is associated with enhanced colocalized protein phosphatase type 2A. *Circ Res* 2005;96(1):54-63.

204. Peters NS, Wit AL. Myocardial architecture and ventricular arrhythmogenesis. *Circulation* 1998;97(17):1746-54.

205. Peters NS, Green CR, Poole-Wilson PA, et al. Reduced content of connexin43 gap junctions in ventricular myocardium from hypertrophied and ischemic human hearts. *Circulation* 1993;88(3):864-75.

206. Smith JH, Green CR, Peters NS, et al. Altered patterns of gap junction distribution in ischemic heart disease. An immunohistochemical study of human myocardium using laser scanning confocal microscopy. *Am J Pathol* 1991;139(4):801-21.

207. Yao JA, Hussain W, Patel P, et al. Remodeling of gap junctional channel function in epicardial border zone of healing canine infarcts. *Circ Res* 2003;92(4):437-43.

208. Peters NS, Coromilas J, Severs NJ, et al. Disturbed connexin43 gap junction distribution correlates with the location of reentrant circuits in the epicardial border zone of healing canine infarcts that cause ventricular tachycardia. *Circulation* 1997;95(4):988-96.

209. Talman V, Ruskoaho H. Cardiac fibrosis in myocardial infarction-from repair and remodeling to regeneration. *Cell Tissue Res* 2016;365(3):563-81.

210. Lopez EM, Malhotra R. Ventricular Tachycardia in Structural Heart Disease. *J Innov Card Rhythm Manag* 2019;10(8):3762-73.

211. de Bakker JM, van Capelle FJ, Janse MJ, et al. Slow conduction in the infarcted human heart. 'Zigzag' course of activation. *Circulation* 1993;88(3):915-26.

212. Mahida S, Sacher F, Dubois R, et al. Cardiac Imaging in Patients With Ventricular Tachycardia. *Circulation* 2017;136(25):2491-507.

213. Chan RH, Maron BJ, Olivotto I, et al. Prognostic value of quantitative contrast-enhanced cardiovascular magnetic resonance for the evaluation of sudden death risk in patients with hypertrophic cardiomyopathy. *Circulation* 2014;130(6):484-95.

214. Gulati A, Jabbour A, Ismail TF, et al. Association of fibrosis with mortality and sudden cardiac death in patients with nonischemic dilated cardiomyopathy. *JAMA* 2013;309(9):896-908.

215. Dawson DK, Hawlisch K, Prescott G, et al. Prognostic role of CMR in patients presenting with ventricular arrhythmias. *JACC Cardiovasc Imaging* 2013;6(3):335-44.

216. de Haan S, Meijers TA, Knaapen P, et al. Scar size and characteristics assessed by CMR predict ventricular arrhythmias in ischaemic cardiomyopathy: comparison of previously validated models. *Heart* 2011;97(23):1951-6.

217. Roes SD, Borleffs CJ, van der Geest RJ, et al. Infarct tissue heterogeneity assessed with contrast-enhanced MRI predicts spontaneous ventricular arrhythmia in patients with ischemic cardiomyopathy and implantable cardioverter-defibrillator. *Circ Cardiovasc Imaging* 2009;2(3):183-90.

218. Shen MJ, Zipes DP. Role of the autonomic nervous system in modulating cardiac arrhythmias. *Circ Res* 2014;114(6):1004-21.

219. Schomig A, Haass M, Richardt G. Catecholamine release and arrhythmias in acute myocardial ischaemia. *Eur Heart J* 1991;12 Suppl F:38-47.

220. Schomig A. Adrenergic mechanisms in myocardial infarction: cardiac and systemic catecholamine release. *J Cardiovasc Pharmacol* 1988;12 Suppl 1:S1-7.

221. Vaseghi M, Lux RL, Mahajan A, et al. Sympathetic stimulation increases dispersion of repolarization in humans with myocardial infarction. *Am J Physiol Heart Circ Physiol* 2012;302(9):H1838-46.

222. Barber MJ, Mueller TM, Henry DP, et al. Transmural myocardial infarction in the dog produces sympathectomy in noninfarcted myocardium. *Circulation* 1983;67(4):787-96.

223. Kammerling JJ, Green FJ, Watanabe AM, et al. Denervation supersensitivity of refractoriness in noninfarcted areas apical to transmural myocardial infarction. *Circulation* 1987;76(2):383-93.

224. Vaseghi M, Barwad P, Malavassi Corrales FJ, et al. Cardiac Sympathetic Denervation for Refractory Ventricular Arrhythmias. *J Am Coll Cardiol* 2017;69(25):3070-80.

225. Fallavollita JA, Heavey BM, Luisi AJ, Jr., et al. Regional myocardial sympathetic denervation predicts the risk of sudden cardiac arrest in ischemic cardiomyopathy. *J Am Coll Cardiol* 2014;63(2):141-9.

226. Cao JM, Fishbein MC, Han JB, et al. Relationship between regional cardiac hyperinnervation and ventricular arrhythmia. *Circulation* 2000;101(16):1960-9.

227. Cao JM, Chen LS, KenKnight BH, et al. Nerve sprouting and sudden cardiac death. *Circ Res* 2000;86(7):816-21.

228. Ajijola OA, Yagishita D, Reddy NK, et al. Remodeling of stellate ganglion neurons after spatially targeted myocardial infarction: Neuropeptide and morphologic changes. *Heart Rhythm* 2015;12(5):1027-35.

229. Meredith IT, Eisenhofer G, Lambert GW, et al. Cardiac sympathetic nervous activity in congestive heart failure. Evidence for increased neuronal norepinephrine release and preserved neuronal uptake. *Circulation* 1993;88(1):136-45.

230. Meredith IT, Broughton A, Jennings GL, et al. Evidence of a selective increase in cardiac sympathetic activity in patients with sustained ventricular arrhythmias. *N Engl J Med* 1991;325(9):618-24.

231. Akiyama T, Yamazaki T. Adrenergic inhibition of endogenous acetylcholine release on postganglionic cardiac vagal nerve terminals. *Cardiovasc Res* 2000;46(3):531-8.

232. Aggarwal A, Esler MD, Socratous F, et al. Evidence for functional presynaptic alpha-2 adrenoceptors and their down-regulation in human heart failure. *J Am Coll Cardiol* 2001;37(5):1246-51.

233. De Ferrari GM, Sanzo A, Bertoletti A, et al. Baroreflex sensitivity predicts long-term cardiovascular mortality after myocardial infarction even in patients with preserved left ventricular function. *J Am Coll Cardiol* 2007;50(24):2285-90.

234. Clemson B, Gaul L, Gubin SS, et al. Prejunctional angiotensin II receptors. Facilitation of norepinephrine release in the human forearm. *J Clin Invest* 1994;93(2):684-91.

235. Gerling IC, Sun Y, Ahokas RA, et al. Aldosteronism: an immunostimulatory state precedes proinflammatory/fibrogenic cardiac phenotype. *Am J Physiol Heart Circ Physiol* 2003;285(2):H813-21.

236. Rodeheffer RJ, Lerman A, Heublein DM, et al. Increased plasma concentrations of endothelin in congestive heart failure in humans. *Mayo Clin Proc* 1992;67(8):719-24.

237. Szabo T, Geller L, Merkely B, et al. Investigating the dual nature of endothelin-1: ischemia or direct arrhythmogenic effect? *Life Sci* 2000;66(26):2527-41.

238. Yorikane R, Shiga H, Miyake S, et al. Evidence for direct arrhythmogenic action of endothelin. *Biochem Biophys Res Commun* 1990;173(1):457-62.

239. Hart RG, Pearce LA, Aguilar MI. Meta-analysis: antithrombotic therapy to prevent stroke in patients who have nonvalvular atrial fibrillation. *Ann Intern Med* 2007;146(12):857-67.

240. Hart RG, Benavente O, McBride R, et al. Antithrombotic therapy to prevent stroke in patients with atrial fibrillation: a meta-analysis. *Ann Intern Med* 1999;131(7):492-501.

241. EBM DataLab. *Direct Oral Anticoagulants (DOACs)*. https://openprescribing.net/measure/doacs/national/england.

242. Giugliano RP, Ruff CT, Braunwald E, et al. Edoxaban versus warfarin in patients with atrial fibrillation. *N Engl J Med* 2013;369(22):2093-104.

243. Granger CB, Alexander JH, McMurray JJ, et al. Apixaban versus warfarin in patients with atrial fibrillation. *N Engl J Med* 2011;365(11):981-92.

244. Connolly SJ, Ezekowitz MD, Yusuf S, et al. Dabigatran versus warfarin in patients with atrial fibrillation. *N Engl J Med* 2009;361(12):1139-51.

245. Patel MR, Mahaffey KW, Garg J, et al. Rivaroxaban versus warfarin in nonvalvular atrial fibrillation. *N Engl J Med* 2011;365(10):883-91.

246. Lip GY, Nieuwlaat R, Pisters R, et al. Refining clinical risk stratification for predicting stroke and thromboembolism in atrial fibrillation using a novel risk factor-based approach: the euro heart survey on atrial fibrillation. *Chest* 2010;137(2):263-72.

247. Pisters R, Lane DA, Nieuwlaat R, et al. A novel user-friendly score (HAS-BLED) to assess 1-year risk of major bleeding in patients with atrial fibrillation: the Euro Heart Survey. *Chest* 2010;138(5):1093-100.

248. Chung MK, Eckhardt LL, Chen LY, et al. Lifestyle and Risk Factor Modification for Reduction of Atrial Fibrillation: A Scientific Statement From the American Heart Association. *Circulation* 2020;141(16):e750-e72.

249. Van Gelder IC, Groenveld HF, Crijns HJ, et al. Lenient versus strict rate control in patients with atrial fibrillation. *N Engl J Med* 2010;362(15):1363-73.

250. Lei M, Wu L, Terrar DA, et al. Modernized Classification of Cardiac Antiarrhythmic Drugs. *Circulation* 2018;138(17):1879-96.

251. Ruaengsri C, Schill MR, Khiabani AJ, et al. The Cox-maze IV procedure in its second decade: still the gold standard? *European Journal of Cardio-Thoracic Surgery* 2018;53(suppl_1):i19-i25.

252. Lall SC, Melby SJ, Voeller RK, et al. The effect of ablation technology on surgical outcomes after the Cox-maze procedure: A propensity analysis. *The Journal of Thoracic and Cardiovascular Surgery* 2007;133(2):389-96.

253. Opolski G, Torbicki A, Kosior DA, et al. Rate control vs rhythm control in patients with nonvalvular persistent atrial fibrillation: the results of the Polish How to Treat Chronic Atrial Fibrillation (HOT CAFE) Study. *Chest* 2004;126(2):476-86.

254. Hagens VE, Van Gelder IC, Crijns HJ, et al. The RACE study in perspective of randomized studies on management of persistent atrial fibrillation. *Card Electrophysiol Rev* 2003;7(2):118-21.

255. Carlsson J, Miketic S, Windeler J, et al. Randomized trial of rate-control versus rhythm-control in persistent atrial fibrillation: the Strategies of Treatment of Atrial Fibrillation (STAF) study. *J Am Coll Cardiol* 2003;41(10):1690-6.

256. Hohnloser SH, Kuck KH, Lilienthal J. Rhythm or rate control in atrial fibrillation--Pharmacological Intervention in Atrial Fibrillation (PIAF): a randomised trial. *Lancet* 2000;356(9244):1789-94.

257. Wyse DG, Waldo AL, DiMarco JP, et al. A comparison of rate control and rhythm control in patients with atrial fibrillation. *N Engl J Med* 2002;347(23):1825-33.

258. Jenkins LS, Brodsky M, Schron E, et al. Quality of life in atrial fibrillation: the Atrial Fibrillation Follow-up Investigation of Rhythm Management (AFFIRM) study. *Am Heart J* 2005;149(1):112-20.

259. Corley SD, Epstein AE, DiMarco JP, et al. Relationships between sinus rhythm, treatment, and survival in the Atrial Fibrillation Follow-Up Investigation of Rhythm Management (AFFIRM) Study. *Circulation* 2004;109(12):1509-13.

260. Pedersen OD, Brendorp B, Elming H, et al. Does conversion and prevention of atrial fibrillation enhance survival in patients with left ventricular dysfunction? Evidence from the Danish Investigations of Arrhythmia and Mortality ON Dofetilide/(DIAMOND) study. *Card Electrophysiol Rev* 2003;7(3):220-4.

261. Pedersen OD, Bagger H, Keller N, et al. Efficacy of dofetilide in the treatment of atrial fibrillation-flutter in patients with reduced left ventricular function: a Danish investigations of arrhythmia and mortality on dofetilide (diamond) substudy. *Circulation* 2001;104(3):292-6.

262. Deedwania PC, Singh BN, Ellenbogen K, et al. Spontaneous conversion and maintenance of sinus rhythm by amiodarone in patients with heart failure and atrial fibrillation: observations from the veterans affairs congestive heart failure survival trial of

antiarrhythmic therapy (CHF-STAT). The Department of Veterans Affairs CHF-STAT Investigators. *Circulation* 1998;98(23):2574-9.

263. Kirchhof P, Camm AJ, Goette A, et al. Early Rhythm-Control Therapy in Patients with Atrial Fibrillation. *N Engl J Med* 2020;383(14):1305-16.

264. Packer DL, Mark DB, Robb RA, et al. Effect of Catheter Ablation vs Antiarrhythmic Drug Therapy on Mortality, Stroke, Bleeding, and Cardiac Arrest Among Patients With Atrial Fibrillation: The CABANA Randomized Clinical Trial. *JAMA* 2019;321(13):1261-74.

265. Mark DB, Anstrom KJ, Sheng S, et al. Effect of Catheter Ablation vs Medical Therapy on Quality of Life Among Patients With Atrial Fibrillation: The CABANA Randomized Clinical Trial. *JAMA* 2019;321(13):1275-85.

266. Blomstrom-Lundqvist C, Gizurarson S, Schwieler J, et al. Effect of Catheter Ablation vs Antiarrhythmic Medication on Quality of Life in Patients With Atrial Fibrillation: The CAPTAF Randomized Clinical Trial. *JAMA* 2019;321(11):1059-68.

267. Marrouche NF, Brachmann J, Andresen D, et al. Catheter Ablation for Atrial Fibrillation with Heart Failure. *N Engl J Med* 2018;378(5):417-27.

268. Antiarrhythmics versus Implantable Defibrillators (AVID) Investigators. A comparison of antiarrhythmic-drug therapy with implantable defibrillators in patients resuscitated from near-fatal ventricular arrhythmias. *N Engl J Med* 1997;337(22):1576-83.

269. Connolly SJ, Gent M, Roberts RS, et al. Canadian implantable defibrillator study (CIDS) : a randomized trial of the implantable cardioverter defibrillator against amiodarone. *Circulation* 2000;101(11):1297-302.

270. Kuck KH, Cappato R, Siebels J, et al. Randomized comparison of antiarrhythmic drug therapy with implantable defibrillators in patients resuscitated from cardiac arrest : the Cardiac Arrest Study Hamburg (CASH). *Circulation* 2000;102(7):748-54.

271. Connolly SJ, Hallstrom AP, Cappato R, et al. Meta-analysis of the implantable cardioverter defibrillator secondary prevention trials. AVID, CASH and CIDS studies. Antiarrhythmics vs Implantable Defibrillator study. Cardiac Arrest Study Hamburg . Canadian Implantable Defibrillator Study. *Eur Heart J* 2000;21(24):2071-8.

272. Bardy GH, Lee KL, Mark DB, et al. Amiodarone or an implantable cardioverter-defibrillator for congestive heart failure. *N Engl J Med* 2005;352(3):225-37.

273. Moss AJ, Zareba W, Hall WJ, et al. Prophylactic implantation of a defibrillator in patients with myocardial infarction and reduced ejection fraction. *N Engl J Med* 2002;346(12):877-83.

274. Kadish A, Dyer A, Daubert JP, et al. Prophylactic defibrillator implantation in patients with nonischemic dilated cardiomyopathy. *N Engl J Med* 2004;350(21):2151-8.

275. Køber L, Thune JJ, Nielsen JC, et al. Defibrillator Implantation in Patients with Nonischemic Systolic Heart Failure. *New England Journal of Medicine* 2016;375(13):1221-30.

276. van der Heijden AC, Borleffs CJ, Buiten MS, et al. The clinical course of patients with implantable cardioverter-defibrillators: Extended experience on clinical outcome, device replacements, and device-related complications. *Heart Rhythm* 2015;12(6):1169-76.

277. Schulz SM, Massa C, Grzbiela A, et al. Implantable cardioverter defibrillator shocks are prospective predictors of anxiety. *Heart Lung* 2013;42(2):105-11.

278. Mark DB, Anstrom KJ, Sun JL, et al. Quality of life with defibrillator therapy or amiodarone in heart failure. *N Engl J Med* 2008;359(10):999-1008.

279. Proietti R, Labos C, Davis M, et al. A systematic review and meta-analysis of the association between implantable cardioverter-defibrillator shocks and long-term mortality. *Can J Cardiol* 2015;31(3):270-7.

280. Biton Y, Daimee UA, Baman JR, et al. Prognostic Importance of Defibrillator-Appropriate Shocks and Antitachycardia Pacing in Patients With Mild Heart Failure. *J Am Heart Assoc* 2019;8(6):e010346.

281. Norwegian Multicenter Study Group. Timolol-induced reduction in mortality and reinfarction in patients surviving acute myocardial infarction. *N Engl J Med* 1981;304(14):801-7.

282. A randomized trial of propranolol in patients with acute myocardial infarction. I. Mortality results. *JAMA* 1982;247(12):1707-14.

283. Randomised trial of intravenous atenolol among 16 027 cases of suspected acute myocardial infarction: ISIS-1. First International Study of Infarct Survival Collaborative Group. *Lancet* 1986;2(8498):57-66.

284. CIBIS II Investigators. The Cardiac Insufficiency Bisoprolol Study II (CIBIS-II): a randomised trial. *Lancet* 1999;353(9146):9-13.

285. Packer M, Fowler MB, Roecker EB, et al. Effect of carvedilol on the morbidity of patients with severe chronic heart failure: results of the carvedilol prospective randomized cumulative survival (COPERNICUS) study. *Circulation* 2002;106(17):2194-9.

286. Effect of metoprolol CR/XL in chronic heart failure: Metoprolol CR/XL Randomised Intervention Trial in-Congestive Heart Failure (MERIT-HF). *The Lancet* 1999;353(9169):2001-07.

287. A comparison of antiarrhythmic-drug therapy with implantable defibrillators in patients resuscitated from near-fatal ventricular arrhythmias. *N Engl J Med* 1997;337(22):1576-83.

288. Connolly SJ, Dorian P, Roberts RS, et al. Comparison of beta-blockers, amiodarone plus beta-blockers, or sotalol for prevention of shocks from implantable cardioverter defibrillators: the OPTIC Study: a randomized trial. *JAMA* 2006;295(2):165-71.

289. Pacifico A, Hohnloser SH, Williams JH, et al. Prevention of implantable-defibrillator shocks by treatment with sotalol. d,l-Sotalol Implantable Cardioverter-Defibrillator Study Group. *N Engl J Med* 1999;340(24):1855-62.

290. Waldo AL, Camm AJ, deRuyter H, et al. Effect of d-sotalol on mortality in patients with left ventricular dysfunction after recent and remote myocardial infarction. The SWORD Investigators. Survival With Oral d-Sotalol. *Lancet* 1996;348(9019):7-12.

291. Reddy VY, Reynolds MR, Neuzil P, et al. Prophylactic catheter ablation for the prevention of defibrillator therapy. *N Engl J Med* 2007;357(26):2657-65.

292. Sapp JL, Wells GA, Parkash R, et al. Ventricular Tachycardia Ablation versus Escalation of Antiarrhythmic Drugs. *N Engl J Med* 2016;375(2):111-21.

293. Kuck KH, Schaumann A, Eckardt L, et al. Catheter ablation of stable ventricular tachycardia before defibrillator implantation in patients with coronary heart disease (VTACH): a multicentre randomised controlled trial. *Lancet* 2010;375(9708):31-40.

294. Kuck K-H, Tilz RR, Deneke T, et al. Impact of substrate modification by catheter ablation on implantable cardioverter–defibrillator interventions in patients with unstable ventricular arrhythmias and coronary artery disease: results from the multicenter randomized controlled SMS (Substrate Modification Study). *Circulation: Arrhythmia and Electrophysiology* 2017;10(3):e004422.

295. Bella PD, Baratto F, Vergara P, et al. Does Timing of Ventricular Tachycardia Ablation Affect Prognosis in Patients With an Implantable Cardioverter Defibrillator? Results From the Multicenter Randomized PARTITA Trial. *Circulation* 2022;145(25):1829-38.

296. Priori SG, Blomström-Lundqvist C, Mazzanti A, et al. 2015 ESC Guidelines for the management of patients with ventricular arrhythmias and the prevention of sudden cardiac death: The Task Force for the Management of Patients with Ventricular Arrhythmias and the Prevention of Sudden Cardiac Death of the European Society of Cardiology (ESC)Endorsed by: Association for European Paediatric and Congenital Cardiology (AEPC). *European Heart Journal* 2015;36(41):2793-867.

297. Joseph JP, Rajappan K. Radiofrequency ablation of cardiac arrhythmias: past, present and future. *QJM* 2012;105(4):303-14.

298. Jackman WM, Wang XZ, Friday KJ, et al. Catheter ablation of accessory atrioventricular pathways (Wolff-Parkinson-White syndrome) by radiofrequency current. *N Engl J Med* 1991;324(23):1605-11.

299. Kay GN, Epstein AE, Dailey SM, et al. Role of radiofrequency ablation in the management of supraventricular arrhythmias: experience in 760 consecutive patients. *J Cardiovasc Electrophysiol* 1993;4(4):371-89.

300. Barkagan M, Rottmann M, Leshem E, et al. Effect of Baseline Impedance on Ablation Lesion Dimensions: A Multimodality Concept Validation From Physics to Clinical Experience. *Circ Arrhythm Electrophysiol* 2018;11(10):e006690.

301. Nath S, Lynch C, 3rd, Whayne JG, et al. Cellular electrophysiological effects of hyperthermia on isolated guinea pig papillary muscle. Implications for catheter ablation. *Circulation* 1993;88(4 Pt 1):1826-31.

302. Nath S, Redick JA, Whayne JG, et al. Ultrastructural observations in the myocardium beyond the region of acute coagulation necrosis following radiofrequency catheter ablation. *J Cardiovasc Electrophysiol* 1994;5(10):838-45.

303. Huang SK, Bharati S, Graham AR, et al. Closed chest catheter desiccation of the atrioventricular junction using radiofrequency energy--a new method of catheter ablation. *J Am Coll Cardiol* 1987;9(2):349-58.

304. Huang SK, Graham AR, Wharton K. Radiofrequency catheter ablation of the left and right ventricles: anatomic and electrophysiologic observations. *Pacing Clin Electrophysiol* 1988;11(4):449-59.

305. Koruth JS, Dukkipati S, Miller MA, et al. Bipolar irrigated radiofrequency ablation: a therapeutic option for refractory intramural atrial and ventricular tachycardia circuits. *Heart Rhythm* 2012;9(12):1932-41.

306. Sapp JL, Beeckler C, Pike R, et al. Initial human feasibility of infusion needle catheter ablation for refractory ventricular tachycardia. *Circulation* 2013;128(21):2289-95.

307. Kuck K-H, Brugada J, Fürnkranz A, et al. Cryoballoon or Radiofrequency Ablation for Paroxysmal Atrial Fibrillation. *New England Journal of Medicine* 2016;374(23):2235-45.

308. Andrade JG, Champagne J, Dubuc M, et al. Cryoballoon or Radiofrequency Ablation for Atrial Fibrillation Assessed by Continuous Monitoring. *Circulation* 2019;140(22):1779-88.

309. Andrade JG, Dubuc M, Guerra PG, et al. The Biophysics and Biomechanics of Cryoballoon Ablation. *Pacing and Clinical Electrophysiology* 2012;35(9):1162-68.

310. Assaf A, Bhagwandien R, Szili-Torok T, et al. Comparison of procedural efficacy, balloon nadir temperature, and incidence of phrenic nerve palsy between two cryoballoon technologies for pulmonary vein isolation: A systematic review and meta-analysis. *J Cardiovasc Electrophysiol* 2021;32(9):2424-31.

311. Chun JKR, Bordignon S, Last J, et al. Cryoballoon Versus Laserballoon: Insights From the First Prospective Randomized Balloon Trial in Catheter Ablation of Atrial Fibrillation. *Circ Arrhythm Electrophysiol* 2021;14(2):e009294.

312. Boersma L. New energy sources and technologies for atrial fibrillation catheter ablation. *EP Europace* 2022;24(Supplement_2):ii44-ii51.

313. Koruth JS, Kuroki K, Kawamura I, et al. Pulsed Field Ablation Versus Radiofrequency Ablation. *Circulation: Arrhythmia and Electrophysiology* 2020;13(3):e008303.

314. Reddy VY, Neuzil P, Koruth JS, et al. Pulsed Field Ablation for Pulmonary Vein Isolation in Atrial Fibrillation. *J Am Coll Cardiol* 2019;74(3):315-26.

315. Reddy VY, Dukkipati SR, Neuzil P, et al. Pulsed Field Ablation of Paroxysmal Atrial Fibrillation: 1-Year Outcomes of IMPULSE, PEFCAT, and PEFCAT II. *JACC Clin Electrophysiol* 2021;7(5):614-27.

316. Chen SA, Hsieh MH, Tai CT, et al. Initiation of atrial fibrillation by ectopic beats originating from the pulmonary veins: electrophysiological characteristics, pharmacological responses, and effects of radiofrequency ablation. *Circulation* 1999;100(18):1879-86.

317. Mangrum JM, Mounsey JP, Kok LC, et al. Intracardiac echocardiography-guided, anatomically based radiofrequency ablation of focal atrial fibrillation originating from pulmonary veins. *J Am Coll Cardiol* 2002;39(12):1964-72.

318. Robbins IM, Colvin EV, Doyle TP, et al. Pulmonary vein stenosis after catheter ablation of atrial fibrillation. *Circulation* 1998;98(17):1769-75.

319. Sanders P, Morton JB, Deen VR, et al. Immediate and long-term results of radiofrequency ablation of pulmonary vein ectopy for cure of paroxysmal atrial fibrillation using a focal approach. *Intern Med J* 2002;32(5-6):202-7.

320. Gerstenfeld EP, Guerra P, Sparks PB, et al. Clinical outcome after radiofrequency catheter ablation of focal atrial fibrillation triggers. *J Cardiovasc Electrophysiol* 2001;12(8):900-8.

321. Arentz T, Jander N, von Rosenthal J, et al. Incidence of pulmonary vein stenosis 2 years after radiofrequency catheter ablation of refractory atrial fibrillation. *Eur Heart J* 2003;24(10):963-9.

322. Sau A, Howard JP, Al-Aidarous S, et al. Meta-Analysis of Randomized Controlled Trials of Atrial Fibrillation Ablation With Pulmonary Vein Isolation Versus Without. *JACC Clin Electrophysiol* 2019;5(8):968-76.

323. Arbelo E, Brugada J, Hindricks G, et al. The atrial fibrillation ablation pilot study: a European Survey on Methodology and results of catheter ablation for atrial fibrillation conducted by the European Heart Rhythm Association. *Eur Heart J* 2014;35(22):1466-78.

324. Chen C, Zhou X, Zhu M, et al. Catheter ablation versus medical therapy for patients with persistent atrial fibrillation: a systematic review and meta-analysis of evidence from randomized controlled trials. *J Interv Card Electrophysiol* 2018;52(1):9-18.

325. Nademanee K, McKenzie J, Kosar E, et al. A new approach for catheter ablation of atrial fibrillation: mapping of the electrophysiologic substrate. *J Am Coll Cardiol* 2004;43(11):2044-53.

326. Verma A, Jiang CY, Betts TR, et al. Approaches to catheter ablation for persistent atrial fibrillation. *N Engl J Med* 2015;372(19):1812-22.

327. Dixit S, Marchlinski FE, Lin D, et al. Randomized ablation strategies for the treatment of persistent atrial fibrillation: RASTA study. *Circ Arrhythm Electrophysiol* 2012;5(2):287-94.

328. Vogler J, Willems S, Sultan A, et al. Pulmonary Vein Isolation Versus Defragmentation: The CHASE-AF Clinical Trial. *J Am Coll Cardiol* 2015;66(24):2743-52.

329. Mohanty S, Mohanty P, Trivedi C, et al. Long-Term Outcome of Pulmonary Vein Isolation With and Without Focal Impulse and Rotor Modulation Mapping: Insights From a Meta-Analysis. *Circ Arrhythm Electrophysiol* 2018;11(3):e005789.

330. Spitzer SG, Miller JM, Sommer P, et al. Randomized evaluation of redo ablation procedures of atrial fibrillation with focal impulse and rotor modulation-guided procedures: the REDO-FIRM study. *EP Europace* 2022.

331. Zlochiver S, Munoz V, Vikstrom KL, et al. Electrotonic myofibroblast-to-myocyte coupling increases propensity to reentrant arrhythmias in two-dimensional cardiac monolayers. *Biophys J* 2008;95(9):4469-80.

332. Yue L, Xie J, Nattel S. Molecular determinants of cardiac fibroblast electrical function and therapeutic implications for atrial fibrillation. *Cardiovasc Res* 2011;89(4):744-53.

333. Miragoli M, Salvarani N, Rohr S. Myofibroblasts induce ectopic activity in cardiac tissue. *Circ Res* 2007;101(8):755-8.

334. Kawai S, Mukai Y, Inoue S, et al. Non-Pulmonary Vein Triggers of Atrial Fibrillation Are Likely to Arise from Low-Voltage Areas in the Left Atrium. *Sci Rep* 2019;9(1):12271.

335. Rolf S, Kircher S, Arya A, et al. Tailored atrial substrate modification based on low-voltage areas in catheter ablation of atrial fibrillation. *Circ Arrhythm Electrophysiol* 2014;7(5):825-33.

336. Kottkamp H, Berg J, Bender R, et al. Box Isolation of Fibrotic Areas (BIFA): A Patient-Tailored Substrate Modification Approach for Ablation of Atrial Fibrillation. *J Cardiovasc Electrophysiol* 2016;27(1):22-30.

337. Blandino A, Bianchi F, Grossi S, et al. Left Atrial Substrate Modification Targeting Low-Voltage Areas for Catheter Ablation of Atrial Fibrillation: A Systematic Review and Meta-Analysis. *Pacing Clin Electrophysiol* 2017;40(2):199-212.

338. Kircher S, Arya A, Altmann D, et al. Individually tailored vs. standardized substrate modification during radiofrequency catheter ablation for atrial fibrillation: a randomized study. *Europace* 2018;20(11):1766-75.

339. Yamaguchi T, Tsuchiya T, Nakahara S, et al. Efficacy of Left Atrial Voltage-Based Catheter Ablation of Persistent Atrial Fibrillation. *J Cardiovasc Electrophysiol* 2016;27(9):1055-63.

340. Kumagai K, Toyama H, Zhang B. Effects of additional ablation of low-voltage areas after Box isolation for persistent atrial fibrillation. *Journal of Arrhythmia* 2019;35(2):197-204.

341. Huang D, Li J-b, Zghaib T, et al. The Extent of Left Atrial Low-Voltage Areas Included in Pulmonary Vein Isolation Is Associated With Freedom from Recurrent Atrial Arrhythmia. *Canadian Journal of Cardiology* 2018;34(1):73-79.

342. Efremidis M, Vlachos K, Letsas KP, et al. Targeted ablation of specific electrogram patterns in low-voltage areas after pulmonary vein antral isolation in persistent atrial fibrillation: Termination to an organized rhythm reduces atrial fibrillation recurrence. *Journal of Cardiovascular Electrophysiology* 2019;30(1):47-57.

343. Jadidi AS, Lehrmann H, Keyl C, et al. Ablation of Persistent Atrial Fibrillation Targeting Low-Voltage Areas With Selective Activation Characteristics. *Circulation: Arrhythmia and Electrophysiology* 2016;9(3):e002962.

344. Nery PB, Alqarawi W, Nair GM, et al. Catheter Ablation of Low-Voltage Areas for Persistent Atrial Fibrillation: Procedural Outcomes Using High-Density Voltage Mapping. *Canadian Journal of Cardiology* 2020;36(12):1956-64.

345. Huo Y, Gaspar T, Schönbauer R, et al. Low-Voltage Myocardium-Guided Ablation Trial of Persistent Atrial Fibrillation. *NEJM Evidence* 2022;0(0):EVIDoa2200141.

346. Josephson ME, Harken AH, Horowitz LN. Endocardial excision: a new surgical technique for the treatment of recurrent ventricular tachycardia. *Circulation* 1979;60(7):1430-39.

347. Guandalini GS, Liang JJ, Marchlinski FE. Ventricular Tachycardia Ablation: Past, Present, and Future Perspectives. *JACC: Clinical Electrophysiology* 2019;5(12):1363-83.

348. Morady F, Harvey M, Kalbfleisch SJ, et al. Radiofrequency catheter ablation of ventricular tachycardia in patients with coronary artery disease. *Circulation* 1993;87(2):363-72.

349. Stevenson WG, Khan H, Sager P, et al. Identification of reentry circuit sites during catheter mapping and radiofrequency ablation of ventricular tachycardia late after myocardial infarction. *Circulation* 1993;88(4 Pt 1):1647-70.

350. Gepstein L, Hayam G, Ben-Haim SA. A novel method for nonfluoroscopic catheter-based electroanatomical mapping of the heart. In vitro and in vivo accuracy results. *Circulation* 1997;95(6):1611-22.

351. Kumar S, Tedrow UB, Stevenson WG. Entrainment Mapping. *Card Electrophysiol Clin* 2017;9(1):55-69.

352. Fernandez-Armenta J, Penela D, Acosta J, et al. Substrate modification or ventricular tachycardia induction, mapping, and ablation as the first step? A randomized study. *Heart Rhythm* 2016;13(8):1589-95.

353. Di Biase L, Burkhardt JD, Lakkireddy D, et al. Ablation of Stable VTs Versus Substrate Ablation in Ischemic Cardiomyopathy: The VISTA Randomized Multicenter Trial. *J Am Coll Cardiol* 2015;66(25):2872-82.

354. Briceno DF, Romero J, Villablanca PA, et al. Long-term outcomes of different ablation strategies for ventricular tachycardia in patients with structural heart disease: systematic review and meta-analysis. *Europace* 2018;20(1):104-15.

355. Marchlinski FE, Callans DJ, Gottlieb CD, et al. Linear ablation lesions for control of unmappable ventricular tachycardia in patients with ischemic and nonischemic cardiomyopathy. *Circulation* 2000;101(11):1288-96.

356. Di Biase L, Santangeli P, Burkhardt DJ, et al. Endo-epicardial homogenization of the scar versus limited substrate ablation for the treatment of electrical storms in patients with ischemic cardiomyopathy. *J Am Coll Cardiol* 2012;60(2):132-41.

357. Berruezo A, Fernandez-Armenta J, Andreu D, et al. Scar dechanneling: new method for scar-related left ventricular tachycardia substrate ablation. *Circ Arrhythm Electrophysiol* 2015;8(2):326-36.

358. Arenal A, Glez-Torrecilla E, Ortiz M, et al. Ablation of electrograms with an isolated, delayed component as treatment of unmappable monomorphic ventricular tachycardias in patients with structural heart disease. *J Am Coll Cardiol* 2003;41(1):81-92.

359. Vergara P, Trevisi N, Ricco A, et al. Late potentials abolition as an additional technique for reduction of arrhythmia recurrence in scar related ventricular tachycardia ablation. *J Cardiovasc Electrophysiol* 2012;23(6):621-7.

360. Jaïs P, Maury P, Khairy P, et al. Elimination of local abnormal ventricular activities: a new end point for substrate modification in patients with scar-related ventricular tachycardia. *Circulation* 2012;125(18):2184-96.

361. Tzou WS, Frankel DS, Hegeman T, et al. Core Isolation of Critical Arrhythmia Elements for Treatment of Multiple Scar-Based Ventricular Tachycardias. *Circulation: Arrhythmia and Electrophysiology* 2015;8(2):353-61.

362. Khongphatthanayothin A, Kosar E, Nademanee K. Nonfluoroscopic three-dimensional mapping for arrhythmia ablation: tool or toy? *J Cardiovasc Electrophysiol* 2000;11(3):239-43.

363. Rotter M, Takahashi Y, Sanders P, et al. Reduction of fluoroscopy exposure and procedure duration during ablation of atrial fibrillation using a novel anatomical navigation system. *Eur Heart J* 2005;26(14):1415-21.

364. Ben-Haim SA, Osadchy D, Scnuster I, et al. Nonfluoroscopic, in vivo navigation and mapping technology. *Nature Medicine* 1996;2(12):1393-95.

365. Shpun S, Gepstein L, Hayam G, et al. Guidance of radiofrequency endocardial ablation with real-time three-dimensional magnetic navigation system. *Circulation* 1997;96(6):2016-21.

366. Gepstein L, Wolf T, Hayam G, et al. Accurate linear radiofrequency lesions guided by a nonfluoroscopic electroanatomic mapping method during atrial fibrillation. *Pacing Clin Electrophysiol* 2001;24(11):1672-8.

367. Smeets JL, Ben-Haim SA, Rodriguez LM, et al. New method for nonfluoroscopic endocardial mapping in humans: accuracy assessment and first clinical results. *Circulation* 1998;97(24):2426-32.

368. Kabra R, Singh J. Recent trends in imaging for atrial fibrillation ablation. *Indian Pacing Electrophysiol J* 2010;10(5):215-27.

369. Bourier F, Fahrig R, Wang P, et al. Accuracy assessment of catheter guidance technology in electrophysiology procedures: a comparison of a new 3D-based fluoroscopy navigation system to current electroanatomic mapping systems. *J Cardiovasc Electrophysiol* 2014;25(1):74-83.

370. Chen CF, Gao XF, Liu MJ, et al. Safety and efficacy of the ThermoCool SmartTouch SurroundFlow catheter for atrial fibrillation ablation: A meta-analysis. *Clin Cardiol* 2020;43(3):267-74.

371. Page SP, Dhinoja M. SmartTouch - The Emerging Role of Contact Force Technology in Complex Catheter Ablation. *Arrhythm Electrophysiol Rev* 2012;1(1):59-62.

372. Mantziari L, Butcher C, Kontogeorgis A, et al. Utility of a Novel Rapid High-Resolution Mapping System in the Catheter Ablation of Arrhythmias: An Initial Human Experience of Mapping the Atria and the Left Ventricle. *JACC Clin Electrophysiol* 2015;1(5):411-20.

373. Ptaszek LM, Chalhoub F, Perna F, et al. Rapid acquisition of high-resolution electroanatomical maps using a novel multielectrode mapping system. *J Interv Card Electrophysiol* 2013;36(3):233-42.

374. Nakagawa H, Ikeda A, Sharma T, et al. Rapid high resolution electroanatomical mapping: evaluation of a new system in a canine atrial linear lesion model. *Circ Arrhythm Electrophysiol* 2012;5(2):417-24.

375. Garrott K, Laughner J, Gutbrod S, et al. Combined local impedance and contact force for radiofrequency ablation assessment. *Heart Rhythm* 2020;17(8):1371-80.

376. Unger LA, Anton CM, Stritt M, et al. In Silico Study of Local Electrical Impedance Measurements in the Atria - Towards Understanding and Quantifying Dependencies in Human. *IEEE Trans Biomed Eng* 2022;Pp.

377. Verma A, Wazni OM, Marrouche NF, et al. Pre-existent left atrial scarring in patients undergoing pulmonary vein antrum isolation: an independent predictor of procedural failure. *J Am Coll Cardiol* 2005;45(2):285-92.

378. Marrouche NF, Wilber D, Hindricks G, et al. Association of atrial tissue fibrosis identified by delayed enhancement MRI and atrial fibrillation catheter ablation: the DECAAF study. *JAMA* 2014;311(5):498-506.

379. Oakes RS, Badger TJ, Kholmovski EG, et al. Detection and quantification of left atrial structural remodeling with delayed-enhancement magnetic resonance imaging in patients with atrial fibrillation. *Circulation* 2009;119(13):1758-67.

380. Kuppahally SS, Akoum N, Burgon NS, et al. Left atrial strain and strain rate in patients with paroxysmal and persistent atrial fibrillation: relationship to left atrial structural remodeling detected by delayed-enhancement MRI. *Circ Cardiovasc Imaging* 2010;3(3):231-9.

381. Sasaki N, Okumura Y, Watanabe I, et al. Relations between contact force, bipolar voltage amplitude, and mapping point distance from the left atrial surfaces of 3D ultrasound– and merged 3D CT–derived images: Implication for atrial fibrillation mapping and ablation. *Heart Rhythm* 2015;12(1):36-43.

382. Kumar S, Chan M, Lee J, et al. Catheter-tissue contact force determines atrial electrogram characteristics before and lesion efficacy after antral pulmonary vein isolation in humans. *J Cardiovasc Electrophysiol* 2014;25(2):122-9.

383. Ullah W, Hunter RJ, Baker V, et al. Target indices for clinical ablation in atrial fibrillation: insights from contact force, electrogram, and biophysical parameter analysis. *Circ Arrhythm Electrophysiol* 2014;7(1):63-8.

384. Blauer JJ, Swenson D, Higuchi K, et al. Sensitivity and specificity of substrate mapping: an in silico framework for the evaluation of electroanatomical substrate mapping strategies. *J Cardiovasc Electrophysiol* 2014;25(7):774-80.

385. Anter E, Tschabrunn CM, Josephson ME. High-Resolution Mapping of Scar-Related Atrial Arrhythmias Using Smaller Electrodes With Closer Interelectrode Spacing. *Circulation: Arrhythmia and Electrophysiology* 2015;8(3):537-45.

386. Beheshti M, Magtibay K, Masse S, et al. Determinants of atrial bipolar voltage: Inter electrode distance and wavefront angle. *Comput Biol Med* 2018;102:449-57.

387. Marcus GM, Yang Y, Varosy PD, et al. Regional left atrial voltage in patients with atrial fibrillation. *Heart Rhythm* 2007;4(2):138-44.

388. LIN Y-J, TAI C-T, LO L-W, et al. Optimal Electrogram Voltage Recording Technique for Detecting the Acute Ablative Tissue Injury in the Human Right Atrium. *Journal of Cardiovascular Electrophysiology* 2007;18(6):617-22.

389. Ullah W, Hunter RJ, Baker V, et al. Factors affecting catheter contact in the human left atrium and their impact on ablation efficacy. *J Cardiovasc Electrophysiol* 2015;26(2):129-36.

390. Sim I, Bishop M, O'Neill M, et al. Left atrial voltage mapping: defining and targeting the atrial fibrillation substrate. *J Interv Card Electrophysiol* 2019;56(3):213-27.

391. de Bakker JM, Wittkampf FH. The pathophysiologic basis of fractionated and complex electrograms and the impact of recording techniques on their detection and interpretation. *Circ Arrhythm Electrophysiol* 2010;3(2):204-13.

392. Masuda M, Fujita M, Iida O, et al. Comparison of Left Atrial Voltage between Sinus Rhythm and Atrial Fibrillation in Association with Electrogram Waveform. *Pacing Clin Electrophysiol* 2017;40(5):559-67.

393. Yagishita A, S DEO, Cakulev I, et al. Correlation of Left Atrial Voltage Distribution Between Sinus Rhythm and Atrial Fibrillation: Identifying Structural Remodeling by 3-D Electroanatomic Mapping Irrespective of the Rhythm. *J Cardiovasc Electrophysiol* 2016;27(8):905-12.

394. Cutler MJ, Johnson J, Abozguia K, et al. Impact of Voltage Mapping to Guide Whether to Perform Ablation of the Posterior Wall in Patients With Persistent Atrial Fibrillation. *J Cardiovasc Electrophysiol* 2016;27(1):13-21.

395. Sanders P, Morton JB, Kistler PM, et al. Electrophysiological and electroanatomic characterization of the atria in sinus node disease: evidence of diffuse atrial remodeling. *Circulation* 2004;109(12):1514-22.

396. Sanders P, Morton JB, Davidson NC, et al. Electrical remodeling of the atria in congestive heart failure: electrophysiological and electroanatomic mapping in humans. *Circulation* 2003;108(12):1461-8.

397. Harrison JL, Jensen HK, Peel SA, et al. Cardiac magnetic resonance and electroanatomical mapping of acute and chronic atrial ablation injury: a histological validation study. *Eur Heart J* 2014;35(22):1486-95.

398. Lin Y, Yang B, Garcia FC, et al. Comparison of left atrial electrophysiologic abnormalities during sinus rhythm in patients with different type of atrial fibrillation. *J Interv Card Electrophysiol* 2014;39(1):57-67.

399. Saghy L, Callans DJ, Garcia F, et al. Is there a relationship between complex fractionated atrial electrograms recorded during atrial fibrillation and sinus rhythm fractionation? *Heart Rhythm* 2012;9(2):181-88.

400. Yagishita A, Sparano D, Cakulev I, et al. Identification and electrophysiological characterization of early left atrial structural remodeling as a predictor for atrial fibrillation recurrence after pulmonary vein isolation. *J Cardiovasc Electrophysiol* 2017;28(6):642-50.

401. Jais P, Shah DC, Haissaguerre M, et al. Mapping and ablation of left atrial flutters. *Circulation* 2000;101(25):2928-34.

402. Kogawa R, Okumura Y, Watanabe I, et al. Left atrial remodeling: Regional differences between paroxysmal and persistent atrial fibrillation. *J Arrhythm* 2017;33(5):483-87.

403. Jadidi AS, Duncan E, Miyazaki S, et al. Functional nature of electrogram fractionation demonstrated by left atrial high-density mapping. *Circ Arrhythm Electrophysiol* 2012;5(1):32-42.

404. Teh AW, Kistler PM, Lee G, et al. Electroanatomic remodeling of the left atrium in paroxysmal and persistent atrial fibrillation patients without structural heart disease. *J Cardiovasc Electrophysiol* 2012;23(3):232-8.

405. Teh AW, Kistler PM, Lee G, et al. The relationship between complex fractionated electrograms and atrial low-voltage zones during atrial fibrillation and paced rhythm. *Europace* 2011;13(12):1709-16.

406. Ndrepepa G, Schneider MA, Karch MR, et al. Impact of atrial fibrillation on the voltage of bipolar signals acquired from the left and right atria. *Pacing Clin Electrophysiol* 2003;26(4 Pt 1):862-9.

407. Katritsis D, Sougiannis D, Giazitzoglou E, et al. Regional endocardial left atrial voltage and electrogram fractionation in patients with atrial fibrillation. *J Cardiovasc Electrophysiol* 2008;19(12):1254-8.

408. Calo L, Lamberti F, Loricchio ML, et al. Long-term follow-up of right atrial ablation in patients with atrial fibrillation. *J Cardiovasc Electrophysiol* 2004;15(1):37-43.

409. Garg A, Finneran W, Mollerus M, et al. Right atrial compartmentalization using radiofrequency catheter ablation for management of patients with refractory atrial fibrillation. *J Cardiovasc Electrophysiol* 1999;10(6):763-71.

410. Haissaguerre M, Jais P, Shah DC, et al. Right and left atrial radiofrequency catheter therapy of paroxysmal atrial fibrillation. *J Cardiovasc Electrophysiol* 1996;7(12):1132-44.

411. Higa S, Lo LW, Chen SA. Catheter Ablation of Paroxysmal Atrial Fibrillation Originating from Non-pulmonary Vein Areas. *Arrhythm Electrophysiol Rev* 2018;7(4):273-81.

412. Nagase T, Kato R, Asano S, et al. Spatial relationship of localized sources of persistent atrial fibrillation identified by a unipolar-based automated algorithm to complex fractionated atrial electrocardiograms and atrial low voltage areas. *Journal of Cardiovascular Electrophysiology* 2022;n/a(n/a).

413. Huang S-Y, Lin Y-J, Tsao H-M, et al. The biatrial substrate properties in different types of paroxysmal atrial fibrillation. *Heart Rhythm* 2011;8(7):961-67.

414. Solimene F, Maddaluno F, Malacrida M, et al. How to leverage local impedance to guide effective ablation strategy: A case series. *HeartRhythm Case Reports* 2021;7(2):65-68.

415. Unger LA, Schicketanz L, Oesterlein T, et al. Local Electrical Impedance Mapping of the Atria: Conclusions on Substrate Properties and Confounding Factors. *Frontiers in Physiology* 2022;12.

416. Szegedi N, Salló Z, Perge P, et al. The role of local impedance drop in the acute lesion efficacy during pulmonary vein isolation performed with a new contact force sensing catheter—A pilot study. *PLoS One* 2021;16(9):e0257050.

417. Solimene F, Schillaci V, Stabile G, et al. Prospective evaluation of local impedance drop to guide left atrial posterior wall ablation with high power. *Journal of Interventional Cardiac Electrophysiology* 2022.

418. Wellens HJ, Duren DR, Lie KI. Observations on mechanisms of ventricular tachycardia in man. *Circulation* 1976;54(2):237-44.

419. Ciaccio EJ, Coromilas J, Wit AL, et al. Formation of Functional Conduction Block During the Onset of Reentrant Ventricular Tachycardia. *Circ Arrhythm Electrophysiol* 2016;9(12).

420. Haqqani HM, Tschabrunn CM, Tzou WS, et al. Isolated septal substrate for ventricular tachycardia in nonischemic dilated cardiomyopathy: incidence, characterization, and implications. *Heart Rhythm* 2011;8(8):1169-76.

421. Nazarian S, Bluemke DA, Lardo AC, et al. Magnetic resonance assessment of the substrate for inducible ventricular tachycardia in nonischemic cardiomyopathy. *Circulation* 2005;112(18):2821-5.

422. Soejima K, Stevenson WG, Sapp JL, et al. Endocardial and epicardial radiofrequency ablation of ventricular tachycardia associated with dilated cardiomyopathy: the importance of low-voltage scars. *J Am Coll Cardiol* 2004;43(10):1834-42.

423. Mattfeldt T, Schwarz F, Schuler G, et al. Necropsy evaluation in seven patients with evolving acute myocardial infarction treated with thrombolytic therapy. *Am J Cardiol* 1984;54(6):530-4.

424. Wijnmaalen AP, Schalij MJ, von der Thusen JH, et al. Early reperfusion during acute myocardial infarction affects ventricular tachycardia characteristics and the chronic electroanatomic and histological substrate. *Circulation* 2010;121(17):1887-95.

425. O'Hanlon R, Grasso A, Roughton M, et al. Prognostic significance of myocardial fibrosis in hypertrophic cardiomyopathy. *J Am Coll Cardiol* 2010;56(11):867-74.

426. Maron BJ. Hypertrophic cardiomyopathy: a systematic review. *JAMA* 2002;287(10):1308-20.

427. Herren T, Gerber PA, Duru F. Arrhythmogenic right ventricular cardiomyopathy/dysplasia: a not so rare "disease of the desmosome" with multiple clinical presentations. *Clin Res Cardiol* 2009;98(3):141-58.

428. Barkagan M, Leshem E, Shapira-Daniels A, et al. Histopathological Characterization of Radiofrequency Ablation in Ventricular Scar Tissue. *JACC Clin Electrophysiol* 2019;5(8):920-31.

429. Tofig BJ, Lukac P, Nielsen JM, et al. Radiofrequency ablation lesions in low-, intermediate-, and normal-voltage myocardium: an in vivo study in a porcine heart model. *Europace* 2019;21(12):1919-27.

430. Josephson ME, Horowitz LN, Farshidi A. Continuous local electrical activity. A mechanism of recurrent ventricular tachycardia. *Circulation* 1978;57(4):659-65.

431. Deneke T, Muller KM, Lemke B, et al. Human histopathology of electroanatomic mapping after cooled-tip radiofrequency ablation to treat ventricular tachycardia in remote myocardial infarction. *J Cardiovasc Electrophysiol* 2005;16(11):1246-51.

432. Callans DJ, Ren JF, Michele J, et al. Electroanatomic left ventricular mapping in the porcine model of healed anterior myocardial infarction. Correlation with intracardiac echocardiography and pathological analysis. *Circulation* 1999;100(16):1744-50.

433. de Riva M, Naruse Y, Ebert M, et al. Targeting the Hidden Substrate Unmasked by Right Ventricular Extrastimulation Improves Ventricular Tachycardia Ablation Outcome After Myocardial Infarction. *JACC Clin Electrophysiol* 2018;4(3):316-27.

434. Wolf M, Sacher F, Cochet H, et al. Long-Term Outcome of Substrate Modification in Ablation of Post-Myocardial Infarction Ventricular Tachycardia. *Circ Arrhythm Electrophysiol* 2018;11(2):e005635.

435. Silberbauer J, Oloriz T, Maccabelli G, et al. Noninducibility and late potential abolition: a novel combined prognostic procedural end point for catheter ablation of postinfarction ventricular tachycardia. *Circ Arrhythm Electrophysiol* 2014;7(3):424-35.

436. Yang F, Yu Y, Lei Q, et al. Lobaplatin arrests cell cycle progression, induces apoptosis and impairs migration and invasion in B16-F10 melanoma cell line in vitro. *Biomed Pharmacother* 2015;69:402-8.

437. Tilz RR, Makimoto H, Lin T, et al. Electrical isolation of a substrate after myocardial infarction: a novel ablation strategy for unmappable ventricular tachycardias--feasibility and clinical outcome. *Europace* 2014;16(7):1040-52.

438. Haines DE, Watson DD. Tissue heating during radiofrequency catheter ablation: a thermodynamic model and observations in isolated perfused and superfused canine right ventricular free wall. *Pacing Clin Electrophysiol* 1989;12(6):962-76.

439. Haines DE, Verow AF. Observations on electrode-tissue interface temperature and effect on electrical impedance during radiofrequency ablation of ventricular myocardium. *Circulation* 1990;82(3):1034-8.

440. Nakagawa H, Yamanashi WS, Pitha JV, et al. Comparison of in vivo tissue temperature profile and lesion geometry for radiofrequency ablation with a saline-irrigated electrode versus temperature control in a canine thigh muscle preparation. *Circulation* 1995;91(8):2264-73.

441. Dorwarth U, Fiek M, Remp T, et al. Radiofrequency catheter ablation: different cooled and noncooled electrode systems induce specific lesion geometries and adverse effects profiles. *Pacing Clin Electrophysiol* 2003;26(7 Pt 1):1438-45.

442. Weiss C, Antz M, Eick O, et al. Radiofrequency catheter ablation using cooled electrodes: impact of irrigation flow rate and catheter contact pressure on lesion dimensions. *Pacing Clin Electrophysiol* 2002;25(4 Pt 1):463-9.

443. Kotadia ID, Williams SE, O'Neill M. High-power, Short-duration Radiofrequency Ablation for the Treatment of AF. *Arrhythm Electrophysiol Rev* 2020;8(4):265-72.

444. Gupta D, Calvert P. Very high power very short duration ablation for atrial fibrillation: With great power comes great responsibility. *Journal of Cardiovascular Electrophysiology* 2022;33(5):928-31.

445. Nath S, DiMarco JP, Haines DE. Basic aspects of radiofrequency catheter ablation. *J Cardiovasc Electrophysiol* 1994;5(10):863-76.

446. Haines DE. Determinants of Lesion Size During Radiofrequency Catheter Ablation: The Role of Electrode-Tissue Contact Pressure and Duration of Energy Delivery. *Journal of Cardiovascular Electrophysiology* 1991;2(6):509-15.

447. Petersen HH, Chen X, Pietersen A, et al. Temperature-controlled radiofrequency ablation of cardiac tissue: an in vitro study of the impact of electrode orientation, electrode tissue contact pressure and external convective cooling. *J Interv Card Electrophysiol* 1999;3(3):257-62.

448. Avitall B, Mughal K, Hare J, et al. The effects of electrode-tissue contact on radiofrequency lesion generation. *Pacing Clin Electrophysiol* 1997;20(12 Pt 1):2899-910.

449. Okumura Y, Johnson SB, Bunch TJ, et al. A systematical analysis of in vivo contact forces on virtual catheter tip/tissue surface contact during cardiac mapping and intervention. *J Cardiovasc Electrophysiol* 2008;19(6):632-40.

450. Di Biase L, Natale A, Barrett C, et al. Relationship between catheter forces, lesion characteristics, "popping," and char formation: experience with robotic navigation system. *J Cardiovasc Electrophysiol* 2009;20(4):436-40.

451. Yokoyama K, Nakagawa H, Shah DC, et al. Novel contact force sensor incorporated in irrigated radiofrequency ablation catheter predicts lesion size and incidence of steam pop and thrombus. *Circ Arrhythm Electrophysiol* 2008;1(5):354-62.

452. Shurrab M, Di Biase L, Briceno DF, et al. Impact of Contact Force Technology on Atrial Fibrillation Ablation: A Meta-Analysis. *J Am Heart Assoc* 2015;4(9):e002476.

453. Reddy VY, Dukkipati SR, Neuzil P, et al. Randomized, Controlled Trial of the Safety and Effectiveness of a Contact Force-Sensing Irrigated Catheter for Ablation of Paroxysmal Atrial Fibrillation: Results of the TactiCath Contact Force Ablation Catheter Study for Atrial Fibrillation (TOCCASTAR) Study. *Circulation* 2015;132(10):907-15.

454. Matsuda H, Parwani AS, Attanasio P, et al. Atrial rhythm influences catheter tissue contact during radiofrequency catheter ablation of atrial fibrillation: comparison of contact force between sinus rhythm and atrial fibrillation. *Heart Vessels* 2016;31(9):1544-52.

455. Shah DC, Lambert H, Nakagawa H, et al. Area under the real-time contact force curve (force-time integral) predicts radiofrequency lesion size in an in vitro contractile model. *J Cardiovasc Electrophysiol* 2010;21(9):1038-43.

456. Haines DE, Watson DD, Verow AF. Electrode radius predicts lesion radius during radiofrequency energy heating. Validation of a proposed thermodynamic model. *Circ Res* 1990;67(1):124-9.

457. Nakagawa H, Wittkampf FH, Yamanashi WS, et al. Inverse relationship between electrode size and lesion size during radiofrequency ablation with active electrode cooling. *Circulation* 1998;98(5):458-65.

458. Wittkampf FH, Nakagawa H. RF catheter ablation: Lessons on lesions. *Pacing Clin Electrophysiol* 2006;29(11):1285-97.

459. Wood MA, Goldberg SM, Parvez B, et al. Effect of electrode orientation on lesion sizes produced by irrigated radiofrequency ablation catheters. *J Cardiovasc Electrophysiol* 2009;20(11):1262-8.

460. Borne RT, Sauer WH, Zipse MM, et al. Longer Duration Versus Increasing Power During Radiofrequency Ablation Yields Different Ablation Lesion Characteristics. *JACC Clin Electrophysiol* 2018;4(7):902-08.

461. An HL, Saksena S, Janssen M, et al. Radiofrequency ablation of ventricular myocardium using active fixation and passive contact catheter delivery systems. *Am Heart J* 1989;118(1):69-77.

462. . *Journal of the American College of Cardiology*: ELSEVIER SCIENCE INC 655 AVENUE OF THE AMERICAS, NEW YORK, NY 10010.

463. Squara F, Latcu DG, Massaad Y, et al. Contact force and force-time integral in atrial radiofrequency ablation predict transmurality of lesions. *Europace* 2014;16(5):660-7.

464. Neuzil P, Reddy VY, Kautzner J, et al. Electrical reconnection after pulmonary vein isolation is contingent on contact force during initial treatment: results from the EFFICAS I study. *Circ Arrhythm Electrophysiol* 2013;6(2):327-33.

465. Kautzner J, Neuzil P, Lambert H, et al. EFFICAS II: optimization of catheter contact force improves outcome of pulmonary vein isolation for paroxysmal atrial fibrillation. *Europace* 2015;17(8):1229-35.

466. le Polain de Waroux JB, Weerasooriya R, Anvardeen K, et al. Low contact force and force-time integral predict early recovery and dormant conduction revealed by adenosine after pulmonary vein isolation. *Europace* 2015;17(6):877-83.

467. Das M, Loveday JJ, Wynn GJ, et al. Ablation index, a novel marker of ablation lesion quality: prediction of pulmonary vein reconnection at repeat electrophysiology study and regional differences in target values. *Europace* 2017;19(5):775-83.

468. Nakagawa H, Ikeda A, Govari A, et al. Abstract 12104: Prospective Study Using a New Formula Incorporating Contact Force, Radiofrequency Power and Application Time (Force-Power-Time Index) for Quantifying Lesion Formation to Guide Long Continuous Atrial lesions in the Beating Canine Heart. *Circulation* 2013;128(suppl_22):A12104-A04.

469. Nakagawa H, Ikeda A, Govari A, et al. Prospective study to test the ability to create RF lesions at predicted depths of 3, 5, 7 and 9 mm using a new formula incorporating contact force, radiofrequency power and application time (Force-Power-Time Index) in the beating canine heart. *Heart Rhythm* 2013;10(5):S475-S86.

470. Hussein A, Das M, Chaturvedi V, et al. Prospective use of Ablation Index targets improves clinical outcomes following ablation for atrial fibrillation. *J Cardiovasc Electrophysiol* 2017;28(9):1037-47.

471. Pranata R, Vania R, Huang I. Ablation-index guided versus conventional contact-force guided ablation in pulmonary vein isolation - Systematic review and meta-analysis. *Indian Pacing Electrophysiol J* 2019;19(4):155-60.

472. Hussein A, Das M, Riva S, et al. Use of Ablation Index-Guided Ablation Results in High Rates of Durable Pulmonary Vein Isolation and Freedom From Arrhythmia in Persistent Atrial Fibrillation Patients: The PRAISE Study Results. *Circ Arrhythm Electrophysiol* 2018;11(9):e006576.

473. Casella M, Gasperetti A, Gianni C, et al. Ablation Index as a predictor of long-term efficacy in premature ventricular complex ablation: A regional target value analysis. *Heart Rhythm* 2019;16(6):888-95.

474. Gasperetti A, Sicuso R, Dello Russo A, et al. Prospective use of ablation index for the ablation of right ventricle outflow tract premature ventricular contractions: a proof of concept study. *Europace* 2020.

475. Otomo K, Uno K, Fujiwara H, et al. Local unipolar and bipolar electrogram criteria for evaluating the transmurality of atrial ablation lesions at different catheter orientations relative to the endocardial surface. *Heart Rhythm* 2010;7(9):1291-300.

476. Gepstein L, Hayam G, Shpun S, et al. Atrial linear ablations in pigs. Chronic effects on atrial electrophysiology and pathology. *Circulation* 1999;100(4):419-26.

477. Kosmidou I, Houde-Walter H, Foley L, et al. Loss of pace capture after radiofrequency application predicts the formation of uniform transmural lesions. *Europace* 2013;15(4):601-6.

478. Steven D, Reddy VY, Inada K, et al. Loss of pace capture on the ablation line: a new marker for complete radiofrequency lesions to achieve pulmonary vein isolation. *Heart Rhythm* 2010;7(3):323-30.

479. Moser J, Sultan A, Luker J, et al. 5-Year Outcome of Pulmonary Vein Isolation by Loss of Pace Capture on the Ablation Line Versus Electrical Circumferential Pulmonary Vein Isolation. *JACC Clin Electrophysiol* 2017;3(11):1262-71.

480. Andrade JG, Pollak SJ, Monir G, et al. Pulmonary vein isolation using a pace-capture-guided versus an adenosine-guided approach: effect on dormant conduction and long-term freedom from recurrent atrial fibrillation--a prospective study. *Circ Arrhythm Electrophysiol* 2013;6(6):1103-8.

481. Steven D, Sultan A, Reddy V, et al. Benefit of pulmonary vein isolation guided by loss of pace capture on the ablation line: results from a prospective 2-center randomized trial. *J Am Coll Cardiol* 2013;62(1):44-50.

482. Sapp JL, Soejima K, Cooper JM, et al. Ablation lesion size correlates with pacing threshold: a physiological basis for use of pacing to assess ablation lesions. *Pacing Clin Electrophysiol* 2004;27(7):933-7.

483. Cronin EM, Bogun FM, Maury P, et al. 2019 HRS/EHRA/APHRS/LAHRS expert consensus statement on catheter ablation of ventricular arrhythmias. *J Interv Card Electrophysiol* 2020;59(1):145-298.

484. Ghanbari H, Baser K, Yokokawa M, et al. Noninducibility in postinfarction ventricular tachycardia as an end point for ventricular tachycardia ablation and its effects on outcomes: a meta-analysis. *Circ Arrhythm Electrophysiol* 2014;7(4):677-83.

485. Berjano E, d'Avila A. Lumped Element Electrical Model based on Three Resistors for Electrical Impedance in Radiofrequency Cardiac Ablation: Estimations from Analytical Calculations and Clinical Data. *Open Biomed Eng J* 2013;7:62-70.

486. Reichlin T, Lane C, Nagashima K, et al. Feasibility, efficacy, and safety of radiofrequency ablation of atrial fibrillation guided by monitoring of the initial impedance decrease as a surrogate of catheter contact. *J Cardiovasc Electrophysiol* 2015;26(4):390-96.

487. Chinitz JS, Kapur S, Barbhaiya C, et al. Sites With Small Impedance Decrease During Catheter Ablation for Atrial Fibrillation Are Associated With Recovery of Pulmonary Vein Conduction. *J Cardiovasc Electrophysiol* 2016;27(12):1390-98.

488. De Bortoli A, Sun LZ, Solheim E, et al. Ablation effect indicated by impedance fall is correlated with contact force level during ablation for atrial fibrillation. *J Cardiovasc Electrophysiol* 2013;24(11):1210-5.

489. Sulkin MS, Laughner JI, Hilbert S, et al. Novel Measure of Local Impedance Predicts Catheter-Tissue Contact and Lesion Formation. *Circ Arrhythm Electrophysiol* 2018;11(4):e005831.

490. Ikeda A, Nakagawa H, Lambert H, et al. Relationship between catheter contact force and radiofrequency lesion size and incidence of steam pop in the beating canine heart: electrogram amplitude, impedance, and electrode temperature are poor predictors of electrode-tissue contact force and lesion size. *Circ Arrhythm Electrophysiol* 2014;7(6):1174-80.

491. Thiagalingam A, D'Avila A, Foley L, et al. Importance of catheter contact force during irrigated radiofrequency ablation: evaluation in a porcine ex vivo model using a force-sensing catheter. *J Cardiovasc Electrophysiol* 2010;21(7):806-11.

492. Kumar S, Haqqani HM, Chan M, et al. Predictive value of impedance changes for real-time contact force measurements during catheter ablation of atrial arrhythmias in humans. *Heart Rhythm* 2013;10(7):962-9.

493. Ullah W, Hunter RJ, Finlay MC, et al. Ablation Index and Surround Flow Catheter Irrigation: Impedance-Based Appraisal in Clinical Ablation. *JACC Clin Electrophysiol* 2017;3(10):1080-88.

494. Thiagalingam A, D'Avila A, McPherson C, et al. Impedance and temperature monitoring improve the safety of closed-loop irrigated-tip radiofrequency ablation. *J Cardiovasc Electrophysiol* 2007;18(3):318-25.

495. Harvey M, Kim YN, Sousa J, et al. Impedance monitoring during radiofrequency catheter ablation in humans. *Pacing Clin Electrophysiol* 1992;15(1):22-7.

496. Bourke T, Buch E, Mathuria N, et al. Biophysical parameters during radiofrequency catheter ablation of scar-mediated ventricular tachycardia: epicardial and endocardial applications via manual and magnetic navigation. *J Cardiovasc Electrophysiol* 2014;25(11):1165-73.

497. Fallert MA, Mirotznik MS, Downing SW, et al. Myocardial electrical impedance mapping of ischemic sheep hearts and healing aneurysms. *Circulation* 1993;87(1):199-207.

498. Amorós-Figueras G, Jorge E, García-Sánchez T, et al. Recognition of Fibrotic Infarct Density by the Pattern of Local Systolic-Diastolic Myocardial Electrical Impedance. *Front Physiol* 2016;7:389.

499. Schwartzman D, Chang I, Michele JJ, et al. Electrical impedance properties of normal and chronically infarcted left ventricular myocardium. *J Interv Card Electrophysiol* 1999;3(3):213-24.

500. Martin CA, Martin R, Gajendragadkar PR, et al. First clinical use of novel ablation catheter incorporating local impedance data. *J Cardiovasc Electrophysiol* 2018;29(9):1197-206.

501. Gunawardene M, Munkler P, Eickholt C, et al. A novel assessment of local impedance during catheter ablation: initial experience in humans comparing local and generator measurements. *Europace* 2019;21(Supplement_1):i34-i42.

502. Gutbrod SR, Shuros A, Koya V, et al. Improved Ablation Efficiency in PVI Guided by Contact Force and Local Impedance: Chronic Canine Model. *Frontiers in Physiology* 2022;12.

503. Matsuura G, Fukaya H, Ogawa E, et al. Catheter contact angle influences local impedance drop during radiofrequency catheter ablation: Insight from a porcine experimental study with 2 different LI-sensing catheters. *Journal of Cardiovascular Electrophysiology* 2022;33(3):380-88.

504. Yasumoto K, Egami Y, Kawanami S, et al. The correlation between local impedance drop and catheter contact in clinical pulmonary vein isolation use. *Pacing and Clinical Electrophysiology* 2022;45(8):984-92.

505. Segreti L, De Simone A, Schillaci V, et al. A novel local impedance algorithm to guide effective pulmonary vein isolation in atrial fibrillation patients: Preliminary experience across different ablation sites from the CHARISMA pilot study. *J Cardiovasc Electrophysiol* 2020.

506. Das M, Luik A, Shepherd E, et al. Local catheter impedance drop during pulmonary vein isolation predicts acute conduction block in patients with paroxysmal atrial fibrillation: initial results of the LOCALIZE clinical trial. *EP Europace* 2021;23(7):1042-51.

507. Tsutsui K, Kawano D, Mori H, et al. Characteristics and optimal ablation settings of a novel, contact-force sensing and local impedance-enabled catheter in an ex vivo perfused swine ventricle model. *Journal of Cardiovascular Electrophysiology* 2021;32(12):3187-94.

508. Solimene F, De Sanctis V, Maggio R, et al. When local impedance meets contact force: preliminary experience from the CHARISMA registry. *J Interv Card Electrophysiol* 2022.

509. Amemiya M, Takigawa M, Goya M, et al. Comparison of two catheters measuring local impedance: local impedance variation vs lesion characteristics and steam pops. *Journal of Interventional Cardiac Electrophysiology* 2022.

510. Kawano D, Mori H, Kato R, et al. The optimal ablation setting for a local impedance guided catheter in an in vitro experimental model. *Journal of Cardiovascular Electrophysiology* 2021;32(8):2069-76.

511. García-Bolao I, Ramos P, Luik A, et al. Local Impedance Drop Predicts Durable Conduction Block in Patients With Paroxysmal Atrial Fibrillation. *JACC: Clinical Electrophysiology* 2022;8(5):595-604.

512. Ikenouchi T, Takigawa M, Goya M, et al. Requirement of larger local impedance reduction for successful lesion formation at carinal area during pulmonary vein isolation. *Journal of Interventional Cardiac Electrophysiology* 2022.

513. Fukaya H, Mori H, Oikawa J, et al. Optimal local impedance parameters for successful pulmonary vein isolation in patients with atrial fibrillation. *Journal of Cardiovascular Electrophysiology* 2022;n/a(n/a).

514. Savitzky A, Golay MJE. Smoothing and Differentiation of Data by Simplified Least Squares Procedures. *Analytical Chemistry* 1964;36(8):1627-39.

515. Spragg DD, Khurram I, Zimmerman SL, et al. Initial experience with magnetic resonance imaging of atrial scar and co-registration with electroanatomic voltage mapping during atrial fibrillation: Success and limitations. *Heart Rhythm* 2012;9(12):2003-09.

516. Malcolme-Lawes LC, Juli C, Karim R, et al. Automated analysis of atrial late gadolinium enhancement imaging that correlates with endocardial voltage and clinical outcomes: A 2-center study. *Heart Rhythm* 2013;10(8):1184-91.

517. Jadidi AS, Cochet H, Shah AJ, et al. Inverse Relationship Between Fractionated Electrograms and Atrial Fibrosis in Persistent Atrial Fibrillation: Combined Magnetic Resonance Imaging and High-Density Mapping. *Journal of the American College of Cardiology* 2013;62(9):802-12.

518. Kapa S, Desjardins B, Callans DJ, et al. Contact Electroanatomic Mapping Derived Voltage Criteria for Characterizing Left Atrial Scar in Patients Undergoing Ablation for Atrial Fibrillation. *Journal of Cardiovascular Electrophysiology* 2014;25(10):1044-52.

519. Bakker JMTd, Wittkampf FHM. The Pathophysiologic Basis of Fractionated and Complex Electrograms and the Impact of Recording Techniques on Their Detection and Interpretation. *Circulation: Arrhythmia and Electrophysiology* 2010;3(2):204-13.

520. Qureshi NA, Kim SJ, Cantwell CD, et al. Voltage during atrial fibrillation is superior to voltage during sinus rhythm in localizing areas of delayed enhancement on magnetic resonance imaging: An assessment of the posterior left atrium in patients with persistent atrial fibrillation. *Heart Rhythm* 2019;16(9):1357-67.

521. Masuda M, Kanda T, Kurata N, et al. Clinical utility of local impedance monitoring during pulmonary vein isolation. *Journal of Cardiovascular Electrophysiology* 2020;31(10):2584-91.

522. Bijvoet GP, Nies HMJM, Holtackers RJ, et al. Correlation between Cardiac MRI and Voltage Mapping in Evaluating Atrial Fibrosis: A Systematic Review. *Radiology. Cardiothoracic imaging* 2022;4(5):e220061. https://doi.org/10.1148/ryct.220061. doi: 10.1148/ryct.220061.

523. Lin Y-J, Higa S, Tai C-T, et al. Role of the right atrial substrate in different types of atrial arrhythmias. *Heart Rhythm* 2009;6(5):592-98.

524. Ullah W, Hunter RJ, Baker V, et al. Impact of Catheter Contact Force on Human Left Atrial Electrogram Characteristics in Sinus Rhythm and Atrial Fibrillation. *Circ Arrhythm Electrophysiol* 2015;8(5):1030-9.

525. Osei K, Sulkin MS, Hamann JJ, et al. Local impedance-guided radiofrequency ablation with standard and high power: Results of a preclinical investigation. *Journal of Cardiovascular Electrophysiology* 2021;32(8):2060-68.

526. Bates A, Paisey J, Yue A, et al. Radiofrequency Ablation of the Diseased Human Left Ventricle: Biophysical and Electrogram Based Analysis. *JACC: Clinical Electrophysiology*;0(0).

527. Natale A, Reddy VY, Monir G, et al. Paroxysmal AF catheter ablation with a contact force sensing catheter: results of the prospective, multicenter SMART-AF trial. *J Am Coll Cardiol* 2014;64(7):647-56.

528. Zilberman I, Younis A, Yavin H, et al. CA-530-04 UTILITY OF ABLATION INDEX FOR GUIDING ABLATION IN VENTRICULAR TISSUE. *Heart Rhythm* 2022;19(5):S26.

529. Larsen T, Du-Fay-de-Lavallaz JM, Winterfield JR, et al. Comparison of Ablation Index versus Time-Guided Radiofrequency Energy Dosing using Normal and Half-normal Saline Irrigation in a Porcine Left Ventricular Model. *J Cardiovasc Electrophysiol* 2022.

530. Mori H, Kato R, Sumitomo N, et al. Relationship between the ablation index, lesion formation, and incidence of steam pops. *J Arrhythm* 2019;35(4):636-44.

531. Garg L, Daubert T, Lin A, et al. Utility of Prolonged Duration Endocardial Ablation for Ventricular Arrhythmias Originating From the Left Ventricular Summit. *JACC Clin Electrophysiol* 2022;8(4):465-76.

532. Delacretaz E, Soejima K, Brunckhorst CB, et al. Assessment of radiofrequency ablation effect from unipolar pacing threshold. *Pacing Clin Electrophysiol* 2003;26(10):1993-6.

533. Hutchinson MD, Gerstenfeld EP, Desjardins B, et al. Endocardial unipolar voltage mapping to detect epicardial ventricular tachycardia substrate in patients with nonischemic left ventricular cardiomyopathy. *Circ Arrhythm Electrophysiol* 2011;4(1):49-55.